EBERHARD KARLS
UNIVERSITÄT
TÜBINGEN

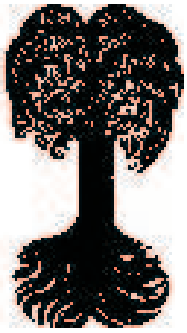

Zentrum für Angewandte Geowissenschaften (ZAG)

TÜBINGER GEOWISSENSCHAFTLICHE ARBEITEN (TGA)

Reihe C: Hydro-, Ingenieur- und Umweltgeologie

Schriftleitung: P. Grathwohl, G. Teutsch

Steffen Birk

Characterisation of Karst Systems by Simulating Aquifer Genesis and Spring Responses: Model Development and Application to Gypsum Karst

TGA, C60, 2002

Characterisation of Karst Systems by Simulating Aquifer Genesis and Spring Responses: Model Development and Application to Gypsum Karst

Steffen Birk

Lehrstuhl für Angewandte Geologie
Institut für Geologie und Paläontologie
Eberhard–Karls–Universität Tübingen
Sigwartstraße 10
72076 Tübingen
Germany

Herausgeber: Institut für Geowissenschaften der Universität Tübingen
Sigwartstraße 10, D-72076 Tübingen

Schriftleitung der Reihe C: Zentrum für Angewandte Geowissenschaften (ZAG)
Lehrstuhl für Angewandte Geologie
Prof. Dr. Peter Grathwohl & Prof. Dr. Georg Teutsch

Redaktion: Dipl.-Geol. Björn Sack-Kühner

ISSN 0935-4948 (Print)
ISSN 1610-4706 (Internet)

TGA	Reihe C	Nr. 60	122 S., 105 Abbildungen, 8 Tabellen	Tübingen, Januar 2002

Characterisation of Karst Systems by Simulating Aquifer Genesis and Spring Responses: Model Development and Application to Gypsum Karst

Steffen Birk [1]

Abstract: Karst aquifers are important groundwater resources, which are highly vulnerable to contamination due to fast transport in solutionally enlarged conduits. Management and protection of karst water resources require an adequate aquifer characterisation at the catchment scale. Due to the heterogeneity and complexity of karst systems, this is not easily achieved by standard investigation techniques such as pumping tests. Therefore, a process-based numerical modelling tool is developed, designed to support the karst aquifer characterisation using two complementary approaches: Firstly, the simulation of conduit enlargement, which aims at predicting aquifer properties by forward modelling of long-term karst genesis; secondly, the simulation of heat and solute transport processes, which aims at inferring aquifer properties from short-term karst spring response after recharge events.

Karst genesis modelling is applied to a conceptual setting based on field observations from the Western Ukraine, where the major part of known gypsum caves is found. Gypsum layers are typically supplied by artesian flow of aggressive water from insoluble aquifers underneath. Processes and parameters, controlling solutional enlargement of single conduits under artesian conditions, are identified in detailed sensitivity analyses. The development of conduit networks is examined in parameter studies, suggesting that the evolution of maze caves is predetermined by structural preferences such as laterally extended fissure networks beneath a horizon less prone to karstification. Without any structural preferences vertical shafts rather than maze caves are predicted to develop. The structure of the mature conduit system is found to be determined during early karstification, which is characterised by high hydraulic gradients and low flow rates in the gypsum layer.

Short-term karst spring response after recharge events is firstly examined in parameter studies by forward modelling. The numerical simulations reveal that different controlling processes of heat and solute transport account for the different behaviour of water temperature and solute concentration frequently observed at karst springs. It is demonstrated that these differences may be employed to reduce the ambiguity in the aquifer characterisation.

In order to test the feasibility of the corresponding inverse approach, which aims at inferring aquifer properties from the karst spring response, the model is applied to a field site in Southern Germany (*Urenbrunnen* spring, Vöhringen). Data input is provided by both literature and own field work. Several models, which reproduce the results of a combined tracer and recharge test, are calibrated to spring discharges and solute concentrations measured after a recharge event. In order to validate the calibrated models, the measured spring water temperatures are simulated by heat transport modelling. The model application yields information on aquifer properties as well as flow and transport processes at the field site. Advection is identified as the dominant transport process, whereas the dissolution reaction of gypsum is found to be insignificant in this case.

The application to gypsum aquifers demonstrates that both suggested approaches are suitable for the characterisation of karst systems. Model results, however, are highly sensitive to several input parameters, in particular in karst genesis modelling. Therefore, extensive field work is required to provide reliable data for site-specific model applications. In order to account for uncertainties, it is recommended to conduct parameter studies covering possible ranges of the most influential parameters.

[1] Dissertation at the Geowissenschaftliche Fakultät, Universität Tübingen
Author's address: Center for Applied Geoscience, Sigwartstr. 10, 72076 Tübingen, Germany

Charakterisierung von Karstsystemen durch Simulation der Aquifergenese und der Reaktionen von Quellen: Modellentwicklung und Anwendung auf Gipskarst

Kurzfassung: Karstgrundwasserleiter sind wichtige Grundwasserressourcen, die aufgrund des schnellen Transports in durch Auslaugung erweiterten Röhren sehr verwundbar in Bezug auf Kontamination sind. Verwaltung und Schutz von Karstwasserressourcen erfordern eine hinreichende Charakterisierung der Grundwasserleiter auf der Skala des Einzugsgebietes. Aufgrund der Heterogenität und Komplexität der Karstsysteme kann dies nicht einfach mittels Standard-Erkundungsmethoden wie Pumpversuchen erreicht werden. Daher wird ein prozess-basiertes numerisches Modellwerkzeug entwickelt, welches die Charakterisierung der Grundwasserleiter mittels zweier sich ergänzender Ansätze unterstützt. Zum einen erfolgt die Simulation der Röhrenaufweitung mit dem Ziel, Eigenschaften der Grundwasserleiter durch Vorwärtsmodellierung der über lange Zeiträume ablaufenden Karstgenese vorherzusagen. Der zweite Ansatz beinhaltet die Simulation von Wärme- und Stofftransportprozessen, welche die Ableitung von Eigenschaften der Grundwasserleiter aus kurzzeitigen Reaktionen von Karstquellen nach Neubildungsereignissen bezweckt.

Die Modellierung der Karstgenese wird auf einen konzeptionellen Standorttyp angewendet, welcher auf Geländebefunden aus der West-Ukraine basiert, wo sich der überwiegende Teil der bekannten Gipshöhlen befindet. Die Gipsschichten werden typischerweise durch artesiche Strömung aus liegenden, unlöslichen Grundwasserleitern mit aggressivem Wasser versorgt. Prozesse und Parameter, welche die Aufweitung von Einzelröhren durch Auslaugung unter artesischen Bedingungen kontrollieren, werden in detaillierten Sensitivitätsanalysen identifiziert. Die Entwicklung von Röhrennetzwerken wird in Parameterstudien untersucht, welche nahe legen, dass strukturelle Präferenzen, wie lateral ausgedehnte Kluftnetzwerke unter einem Horizont, der weniger zur Verkarstung neigt, die Entwicklung von Netzhöhlen vorherbestimmen. Ohne strukturelle Präferenzen wird vorhergesagt, dass sich eher vertikale Schächte als Netzhöhlen entwickeln. Die Struktur des reifen Röhrensystems erweist sich als bereits in der frühen Verkarstungsperiode festgelegt, welche durch hohe hydraulische Gradienten und niedrige Durchflussraten in der Gipsschicht gekennzeichnet ist.

Die kurzzeitige Reaktion von Karstquellen auf Neubildungsereignisse wird zunäst mittels Vorwärtsmodellierung anhand von Parameterstudien untersucht. Die numerischen Simulationen zeigen, dass die unterschiedlichen kontrollierenden Prozesse des Wärme- und Stofftransports die oftmals beobachteten Unterschiede im Verhalten der Wassertemperatur und der Stoffkonzentration an Karstquellen erklären können. Es wird gezeigt, dass diese Unterschiede dazu beitragen, Mehrdeutigkeiten bei der Charakterisierung des Grundwasserleiters zu verringern.

Um die Durchführbarkeit des zugehörigen inversen Ansatzes zu testen, welcher die Ableitung von Eigenschaften der Grundwasserleiter aus der Reaktion von Karstquellen bezweckt, wird das Modell auf einen Feldstandort in Süddeutschland (*Urenbrunnen*-Quelle, Vöhringen) angewendet. Eingabedaten werden sowohl aus der Literatur als auch durch eigene Geländearbeiten bereit gestellt. Verschiedene Modelle, welche die Ergebnisse eines kombinierten Markierungs- und Schluckversuchs nachbilden, werden auf die nach einem Neubildungsereignis gemessenen Quellschüttungen und Stoffkonzentrationen kalibriert. Um die kalibrierten Modelle zu validieren, werden die Quellwassertemperaturen mittels Wärmetransportmodellierung simuliert. Die Modellanwendung liefert Informationen über Eigenschaften des Grundwasserleiters sowie über Strömungs- und Transportprozesse am Feldstandort. Advektion wird als der dominierende Transportprozess identifiziert, während sich die Lösungsreaktion von Gips hier als unbedeutend erweist.

Die Anwendung auf Gipsgrundwasserleiter zeigt, dass sich beide vorgeschlagenen Ansätze zur Charakterisierung von Karstsystemen eignen. Die Modellergebnisse sind jedoch insbesondere bei der Karstgenesemodellierung sehr sensitiv bezüglich mehrerer Eingabeparameter. Deshalb sind umfassende Geländearbeiten erforderlich, um zuverlässige Daten für standortbezogene Modellanwendungen bereit zu stellen. Um Unsicherheiten Rechnung zu tragen, wird die Durchführung von Parameterstudien empfohlen, die den möglichen Schwankungsbereich der einflussreichsten Parameter abdecken.

Acknowledgments

I would like to thank my advisors PD Dr. Rudolf Liedl and Prof. Dr. Martin Sauter for their guidance and examination of this thesis. Both of them stimulated my work by many valuable suggestions and interesting discussions.

Prof. Dr. Paul Younger acted as an external reviewer. I am grateful to him for reading and evaluating this thesis.

Likewise I feel obliged to Prof. Dr. Georg Teutsch for his continuous support.

I am very much indebted to Sebastian Bauer for his cooperation in model development and for many critical remarks and discussions. He and Dr. Ralf Klingbeil deserve special thanks for reading and commenting the manuscript of this thesis.

Part of this work was funded by the European Commission Framework IV Programme (Contract number ENV4-CT97-0603). I appreciate very much the inspiring discussions about gypsum dissolution and speleogenesis within the EU-project ROSES (Risk of Subsidence due to Evaporite Solution).

I am very grateful to my Diplom-student Barbara Vierneisel for reliably conducting laboratory investigations into gypsum dissolution in pipe flow, which proved helpful for model development.

Though focusing on model development and application, this thesis includes the results of field work at the *Urenbrunnen* spring, Vöhringen, which required the help of many persons. Matthias Flegr deserves thanks for his valuable advice at the beginning of the work and for his continuing interest later on. I am also very grateful to Mr. Treinen, City of Vöhringen for his support. For technical help I would like to thank Klaus Faiß and Wolfgang Kürner. The former deserves my special thanks for his interest in my work and his always exceptional ideas. I am further indebted to Ralph Schleifenheimer. Only with his help it was possible to obtain continuous measurements at the *Urenbrunnen* spring. I am particularly grateful to all colleagues who showed their interest in my work by supporting the tracer and recharge test conducted near the spring. Hydrochemical analyses of water samples were conducted by Renate Riehle and Anne Hartmann-Renz, for which I am grateful to them. The *Deutscher Wetterdienst* supported the work by provision of rainfall data.

Many friends and colleagues participated at my work by helpful comments and interesting discussions. I am particular indebted to those who encouraged me to start with this work and even more to those who pushed me to complete it eventually.

Finally, I would like to thank Birgit for her patience whenever I was lost in thoughts about karst and groundwater.

Contents

List of Figures

List of Tables

List of Abbreviations

A	[m^2]	Flow cross-section
$A_{i,j}$	[m^2]	Cylindrical surface area associated with node (i, j) perpendicular to the direction of heat conduction
A, B	[-]	Constants in section 2.3.1
a	[m]	Diameter of a conduit or pipe
a_i	[m]	Diameter of pipe segment i
c	[mol m^{-3}]	Solute concentration (calcium or sulfate)
c_b	[mol m^{-3}]	Solute concentration in the bulk solution
c_{eq}	[mol m^{-3}]	Equilibrium concentration of calcium or sulfate with respect to gypsum
c_i	[mol m^{-3}]	Solute concentration in pipe segment i,
c_i	[mol l^{-1}]	Concentration of ionic species i (section 2.3.1)
c_{in}	[mol m^{-3}]	Solute concentration of inflow
c_{ini}	[mol m^{-3}]	Initial solute concentration
c_{imp}	[mol m^{-3}]	Solute concentration of direct recharge
c_{norm}	[-]	Normalised solute concentration
c_{out}	[mol m^{-3}]	Solute concentration of outflow
c_r	[J kg^{-1} K^{-1}]	Specific heat of rock
c_w	[J kg^{-1} K^{-1}]	Specific heat of water
$\Delta c_{adv,i}$	[mol m^{-3}]	Change of concentration due to advection in pipe segment i
D	[m^2 s^{-1}]	Diffusion coeffcient
D_{dis}	[m^2 s^{-1}]	Dispersion coefficient
F_h	[J m^{-2} s^{-1}]	Heat flux per unit area and time
F_m	[mol m^{-2} s^{-1}]	(Molar) mass flux per unit area and time
f	[-]	Friction factor
g	[m s^{-2}]	Gravitational acceleration
ΔH	[J mol^{-1}]	Reaction enthalpy
h	[J s^{-1} m^{-2} K^{-1}]	Heat transfer coefficient
h_c	[m]	Hydraulic head of the conduit system
h_f	[m]	Hydraulic head of the fissured system

$\overline{h}_i$	[J s^{-1} m^{-2} K^{-1}]	Mean heat transfer coefficient for pipe segment i
I	[mol l^{-1}]	Ionic strength
$K_{CaSO_4^0}$	[-]	Dissociation constant of $CaSO_4^0$
K_g	[-]	Solubility product of gypsum
k	[m s^{-1}]	Mass transfer coefficient
k_c	[m]	Roughness length of conduit walls
k_s	[m s^{-1}]	Rate constant of first-order surface reaction
l	[m]	Length of a conduit or pipe
m	[mol]	Molar mass
$\Delta m_{adv,i}$	[mol]	Change of mass due to advection in pipe segment i
Δm_i	[mol]	Change of mass due to dissolution in pipe segment i
N_{Bi}	[-]	Biot number
N_{Co}	[-]	Courant number
N_{Fo}	[-]	Fourier number
N_{Re}	[-]	Reynolds number
N_{Pr}	[-]	Prandtl number
N_{Sc}	[-]	Schmidt number
N_{Sh}	[-]	Sherwood number
$\overline{N}_{Sh,i}$	[-]	Mean Sherwood number for pipe segment i
Q	[m^3 s^{-1}]	Discharge through conduits or pipes
Q_b	[m^3 s^{-1}]	Rate of flow from head-dependent boundaries into the fissured system
R	[J mol^{-1} K^{-1}]	Gas constant (8.314 J mol^{-1} K^{-1})
R_c	[m^3 s^{-1}]	Rate of flow into the conduit system via sources (or sinks)
r	[m]	Spatial coordinate perpendicular to the surface (cylindrical coordinates in the case of circular conduits)
r_f	[m s^{-1}]	Volumetric rate of flow per unit area into the fissured system via sources (or sinks)
r_i	[Å]	Ionic radius of species i
r_j	[m]	Distance of nodes (i, j) from conduit axis
Δr	[m]	Thickness of cylindrical volume element surrounding a pipe
S_c	[mol m^{-3} s^{-1}]	Source term accounting for an increase of solute concentration due to dissolution reaction
S_T	[K s^{-1}]	Source term accounting for a change of temperature due to heat transfer between conduit wall and water
S_f	[-]	Specific yield (unconfined aquifers) or storage coefficient (confined aquifers) of the fissured system
T	[K]	Water temperature
T_b	[K]	Temperature of the bulk water
T_f	[m^2 s^{-1}]	Transmissivity of the fissured system

$T_{i,b}$	[K]	Bulk water temperature in pipe segment i
$T_{i,j}$	[K]	Rock temperature at node (i, j)
T_{ini}	[K]	Initial water temperature
T_{imp}	[K]	Temperature of direct recharge
T_{norm}	[K]	Normalised water temperature
T_r	[K]	Rock temperature
T_s	[K]	Temperature of the rock surface
t	[s]	Time
Δt	[s]	Time step length
v	[m s^{-1}]	Flow velocity
v_i	[m s^{-1}]	Flow velocity in pipe segment i
x, y	[m]	Cartesian coordinates
z	[m]	Distance along a conduit or pipe
z_i	[-]	Charge number of a ionic species i (section 2.3.1)
Δz_i	[m]	Length of pipe segment i
α	[m^2 s^{-1}]	Exchange coefficient for fluid transfer between conduit system and fissured system
Γ	[m^3 s^{-1}]	Rate of flow from the conduit system to the fissured system
γ	[m s^{-1}]	Volumetric rate of flow per unit area from the conduit system to the fissured system
γ_i	[-]	Activity coefficient of ionic species i
ε_m	[m]	Thickness of diffusion boundary layer
ε_h	[m]	Thickness of thermal boundary layer
η_w	[N s m^{-2}]	Dynamic viscosity of water
κ_r	[m^2 s^{-1}]	Thermal diffusivity of rock
κ_w	[m^2 s^{-1}]	Thermal diffusivity of water
λ_r	[J s^{-1} m^{-1} K^{-1}]	Thermal conductivity of rock
λ_w	[J s^{-1} m^{-1} K^{-1}]	Thermal conductivity of water
ν_w	[m^2 s^{-1}]	Kinematic viscosity of water
ρ_g	[mol m^{-3}]	Molar density of gypsum
ρ_r	[kg m^{-3}]	Density of rock
ρ_w	[kg m^{-3}]	Density of water
ϑ	[°C]	Temperature

Chapter 1

Introduction

1.1 General

Karst aquifers develop where solutional enlargement of joints and bedding planes creates highly permeable conduits in the subsurface. Together with the surrounding rock these conduits form a complex and heterogeneous flow system, which is determined by the interaction of two complementary components. On the one hand, flow is focused to the highly permeable pathways, i.e. the conduit system. On the other hand, the conduit system constitutes only a small part of the aquifer storage, whereas the low permeable fissured system of the surrounding rock provides a much higher storage.

About 25% of the global population is largely or entirely supplied by karst waters (Ford and Williams, 1989). These important groundwater resources are highly vulnerable with respect to contamination due to the fast and unretarded transport of pollutants in the karst conduits. Management and protection of karst water resources, therefore, require an adequate hydrogeological characterisation of the fast conduit flow system at the catchment scale. Due to the heterogeneity and complexity of karst systems this is not easily achieved by standard investigation techniques such as pumping tests. Liedl and Sauter (1998, 2000) suggest to support the characterisation of the karst conduit system by an integrated approach combining modelling of long-term aquifer genesis and short-term heat transfer processes. The first method aims at providing information about present properties of the aquifer by simulating the evolution of karst conduits over geological periods, whereas the second method is based on the simulation of temperature variations at karst springs, which are believed to reflect geometrical properties of the karst conduits.

Although the two methods appear to be generally applicable to karst aquifers, the examples presented and quoted by Liedl and Sauter (1998, 2000) deal with carbonate aquifers only. Karst aquifers, however, may also develop in evaporitic rocks such as gypsum. Due to their high mineralisation the use of these groundwater resources is often limited. Nevertheless, gypsum karst aquifers are of regional importance, e.g. in Germany at the southern flank of the Harz Mountains, where the Rhume Spring is employed for public water supply (Liersch, 1987). The vulnerability of gypsum aquifers is illustrated by the contamination of a water supply well in this area, which was caused by the spilling of hydrocarbons and their rapid spreading through karst conduits (Hartmann, 1998). Even where gypsum aquifers are not employed for water supply purposes, solutional enlargement of conduits can result in severe environmental problems such as leaking dams (James, 1992; Wittke and Hermening, 1997), land subsidence and collapses (Benito et al., 1998; Cooper, 1986, 1988; Gutiérrez, 1996; Ströbel, 1973). Klimchouk and Andrejchuk (1996) provide a summary of environmental problems encountered in gypsum karst terrains. Evidently, these problems are mainly related to solutionally enlarged karst conduits.

Aim of this thesis is to develop and apply a process-based modelling tool, which is de-

signed to support the aforementioned integrated approach for the characterisation of highly complex karst flow systems. Gypsum aquifers provide an excellent example of such flow systems. The high solubility and the fast dissolution process of gypsum suggest that effects caused by the dissolution of rock are more pronounced in gypsum than in carbonates. The hydraulic properties of gypsum aquifers, therefore, are probably even more determined by the solutional enlargement of conduits than those of carbonate aquifers. Thus, forward modelling of conduit development appears to be a promising method for the characterisation of gypsum aquifers. Moreover, the chemical contrast between groundwater and recharge water is much higher in gypsum aquifers than in carbonate aquifers. Dilution of gypsum waters by low mineralised recharge can cause marked hydrochemical variations at gypsum karst springs after precipitation events. In addition to temperature variations, these hydrochemical signals can be used to infer properties of the karst aquifer.

1.2 Previous related work

The difficulty of characterising karst flow system is illustrated by the scientific disputes among karst researchers in the early twentieth century. At that time two conflicting models began to evolve. Whereas Grund (1903) divided karst aquifers into two zones above and below a water table, Katzer (1909) rejected the existence of a zone of saturation. Thus, according to Katzer there was no water table within a karst aquifer, but the water flowed along open cave passages, which were independent of each other. Both of these concepts found support in karst research. For instance, Cvijić (1918) upheld the water table hypothesis, whereas Martel's (1921) work was supportive of Katzer's viewpoint. Lowe (1992, 2000) gives more details about this historic karst hydrologic controversy.

Nowadays, the two conflicting theories have been reconciled in integrative conceptual models of karst aquifers. Within the wide variety of possible flow systems Shuster and White (1971) distinguish two major types, realising that both of them exist side by side in a complex karst aquifer. On the one hand, *diffuse flow* along small interconnected openings such as fissures and bedding planes tends to behave similar to laminar flow in porous media. Due to the high degree of interconnectivity the water table is usually well defined and discharge is through a large number of springs in this type of aquifer. On the other hand, the localisation of groundwater flow paths by solutional modification leads to *conduit flow* systems, which are characterised by fast and often turbulent flow through an irregular network of solution passages. In this type of aquifer a few major conduits may drain large catchment areas through a single large spring. This concept can be of great use in groundwater risk assessment, because conduit flow systems are much more vulnerable with respect to contamination than diffuse flow systems.

A similar but more detailed classification of flow types was provided by White (1969). The great achievement of White's classification is that it relates each flow type to a particular hydrogeologic environment exhibiting a characteristic cave pattern. A particular aquifer may be classified into one of these types based on observed hydrogeological conditions such as structural and lithologic controls or the position of the base level. Evaluation of the hydrogeological conditions may not always be unambiguous, since the classification of flow types is based on qualitative rather than on quantitative criteria. Moreover, different flow mechanisms may exist in the same hydrogeologic environment as pointed out by Shuster and White (1971). Thus, even if the hydrogeologic conditions are well defined the flow system is not easily characterised by this classification scheme. Modern karst hydrologic research aims to develop *quantitative* methods for the investigation of karst aquifers. Within the scope of this work two different approaches are of importance. Firstly, mathematical models of karst genesis are employed to examine the relation between hydrogeologi-

cal environment and properties of the conduit system more quantitatively than the above mentioned conceptual models. Secondly, the behaviour of karst springs, i.e. variation of discharge and physico-chemical parameters, is taken as quantitative characteristic of the flow system and used to infer aquifer properties.

1.2.1 Modelling of karst genesis

Karst genesis is governed by a positive feedback mechanism based on the mutual enhancement of flow rate and solutional conduit enlargement. By coupling flow and dissolution processes in a mathematical model the solutional enlargement of flow paths can be simulated as demonstrated by Dreybrodt (1990, 1992, 1996), Groves and Howard (1994b) and Palmer (1988, 1991, 1998) for single conduits and fractures in limestone. Although these *one-dimensional* models provided a quantitative method for the investigation of processes involved in karst genesis, the characterisation of karst conduit systems at the *catchment* scale requires more complex models. Groves and Howard (1994a) presented such a model simulating the development of two-dimensional fracture networks under laminar flow conditions. Using the same modelling tool Howard and Groves (1995) examined the evolution of fracture networks under turbulent flow conditions. The evolution of two-dimensional networks was further studied by Gabrovšek and Dreybrodt (2000), Kaufmann and Braun (1999), Qingchun et al. (1999), and Siemers and Dreybrodt (1998). Using network models it was possible to examine the relation between the geometry of the conduit system and hydrogeologic conditions such as the initial aperture width or the recharge mode. Comparing these mathematical models with the above mentioned conceptual model suggested by Shuster and White (1971), it is evident that the network models represent only one of the two flow types of a karst aquifer, i.e. the localised conduit flow. In order to provide a better representation of the karst flow system, Clemens (1998) and Hückinghaus (1998) coupled a continuum model, which simulated diffuse flow in the fissured system of the rock, to a discrete pipe network simulating conduit flow. Coupling a limestone dissolution module to the pipe network model yielded the karst genesis model CAVE (Carbonate Aquifer Void Evolution), which was employed to simulate conduit development in carbonate aquifers at a catchment scale (Clemens et al., 1996, 1997a, 1997b, 1998, 1999). The karst genesis model presented by Kaufmann and Braun (2000), which was based on a finite-element approach, also included diffuse and conduit flow. Considering the coupling of the two flow systems their method might be advantageous as compared to the CAVE model. However, it is restricted to laminar flow conditions, whereas CAVE is capable of simulating laminar as well as turbulent conduit flow.

The aforementioned models simulated the solutional enlargement of conduits in limestone aquifers. The underlying modelling approaches, therefore, were based on experimental results, which had shown that the dissolution rate of limestone follows a linear first-order rate law as long as the solution is strongly undersaturated, but switches to a non-linear higher-order kinetics close to chemical equilibrium (Palmer, 1991; Svensson and Dreybrodt, 1992). Dissolution experiments with gypsum, however, yielded a first-order rate law only, while a kinetic switch was not observed (Barton and Wilde, 1971; Christofferson and Christofferson, 1976; James and Lupton, 1978; Kemper et al., 1975; Lebedev and Lekhov, 1990; Liu and Nancollas, 1971; Liu and Dreybrodt, 1997; Opdyke et al., 1997). In contrast, Raines and Dewers (1997) concluded from their experiments a non-linear rate law for a surface reaction controlled dissolution process under turbulent flow conditions. Dreybrodt and Gabrovšek (2000) showed that this interpretation was not unambiguous, because experimental data were not sufficiently reliable to draw conclusions on the surface reaction rate laws of gypsum dissolu-

tion. Jeschke et al. (2001) recently observed a kinetic switch from a linear to a non-linear rate law at a high saturation state of about 95% in dissolution experiments with natural gypsum. To resolve the kinetics more precisely, gypsum dissolution kinetics deserves further investigation.

Based on a first-order rate law James and Lupton (1978) derived a theoretical model for the solutional enlargement of a single conduit in gypsum. Using a measured rate coefficient their model successfully predicted the shape of a pipe, which was solutionally enlarged under laminar flow conditions in a laboratory experiment. A channel network model, which was also based on first-order dissolution kinetics, was employed by Lauritzen et al. (1992) to simulate the dissolution patterns they had observed in laboratory experiments with plaster of Paris. These models simulated the development of conduit systems in gypsum at a laboratory scale only. A conceptual model of gypsum karst genesis at a regional scale was developed by Klimchouk (1996c, 1997a, 2000a, 2000c). His concept of a transverse artesian speleogenesis, which was mainly based on field observations in the Western Ukraine (Klimchouk, 1992, 1996b, 1997b, 2000b), attributed the evolution of maze caves to distributed artesian flow from beneath a gypsum layer. Although Cooper's (1995, 1998) work about gypsum karst in England indicates that this conceptual model is not restricted to the Western Ukraine only, it has never been translated into a mathematical model of gypsum karst genesis.

1.2.2 Analysis of karst spring response

In their work about limestone springs Shuster and White (1971) showed that diffuse and conduit flow systems in the same hydrogeologic environment can be distinguished by analysing *seasonal* fluctuations of spring water temperature and chemistry. However, their method was not suited to predict the properties of the conduit system quantitatively. Ashton (1966) was one of the first, who suggested to characterise karst drainage systems by analysis of *short-term* fluctuations at the spring. His method uses the time lag usually observed between the increase in flow and the change of physico-chemical parameters at a spring after a flood. It was applied, for instance, by Atkinson (1977) and Sauter (1992) to estimate the volumes of conduit water in regional carbonate aquifers.

Dreiss (1989a) used short-term fluctuations in spring water chemistry to quantify the fast flow component after storm events. She further derived linear kernel functions describing these fluctuations and applied time moment analysis to them (Dreiss, 1989b). In earlier work Dreiss (1982, 1983) used linear kernel functions for the analysis of karst spring hydrographs. This method aims at inferring the properties of a karst aquifer from its global response to input events expressed in a spring hydrograph or physico-chemical fluctuations. Another example of such a "global method" (Eisenlohr et al., 1997b) is the analysis of the recession curve of spring hydrographs (e.g. Padilla et al., 1994). Jeannin and Sauter (1998) give a critical overview of global approaches for the analysis of karst spring hydrographs. They conclude that the common methods although helpful in extrapolating discharge in time are not very efficient to infer the structure of the flow system. Eisenlohr et al. (1997a, 1997b) reached the same conclusion by applying global methods to time series generated by a deterministic numerical groundwater model, which included well-defined karst structures.

A main drawback of the common global methods is that they do not include physical processes linking the time response of the karst spring to the spatial heterogeneous flow system (Jeannin and Sauter, 1998). A step towards the incorporation of physical processes into the analysis of the global response of karst aquifers was made by Benderitter and Roy (1993), who employed the simulation of heat transport in a single conduit for the

interpretation of spring water temperatures. Process-based modelling of heat transport in a single fracture (Renner, 1996; Renner and Sauter, 1997; Liedl et al., 1998) revealed that the temperature variations at the outlet depend on the fracture geometry if the discharge is time-variant. More importantly, these simulations yielded information about properties of a regional karst aquifer, such as the total fracture volume. In order to examine the relation between conduit geometry and solution content of spring water Grasso (1998) simulated carbonate dissolution and transport in conduits under steady-state flow conditions. Based on these simulations and on additional field observations he concluded that site-specific relations of spring discharge and solute concentration characterise the geometric properties of karst conduit systems. Hückinghaus (1998) implemented a numerical heat transport module in the CAVE model (see section 1.2.1) and studied heat transport processes in conduit networks. His simulations incorporated more complex conduit flow systems than the aforementioned models, but the hydraulic interaction between the fissured (i.e. diffuse) system and the conduit system was still not considered.

Using a numerical model of flow and heat transport in porous media Bundschuh (1991, 1993) simulated seasonal variations of spring water temperatures in order to characterise gypsum aquifers. Since this modelling approach did not incorporate a fast conduit flow system, however, it is unsuitable for the simulation of short-term fluctuations and their interpretation with respect to the geometric properties of the conduit system.

1.3 Objectives and methodology of this work

The purpose of this work is to support the characterisation of karst systems by an integrated modelling approach combining simulations of both long-term karst genesis and short-term transport processes, as outlined by Liedl and Sauter (1998, 2000) (see also section 1.1). The study includes the development of a process-based numerical modelling tool and its exemplary application to gypsum karst aquifers.

As shown in the previous section karst modelling is widely applied but rather focused to limestone aquifers. The hydraulic behaviour of a karst flow system, however, is likely to be similar in both gypsum and limestone. Therefore, the general modelling approaches applied for limestone aquifers appear to be suitable for the simulation of flow in gypsum karst aquifers. In the present study the coupled continuum-pipe flow model incorporated in the carbonate karst genesis model CAVE (see section 1.2.1) has been chosen to simulate flow. However, the limestone dissolution module of the CAVE model had to be exchanged by a gypsum dissolution module to account for the different type of dissolution kinetics. Since gypsum dissolution kinetics is still controversially discussed (see section 1.2.1), further laboratory experiments were conducted investigating the dissolution process in laminar and turbulent pipe flow (Vierneisel, 2000). Moreover, new solute and heat transport modules had to be developed, in order to be able to simulate short-term fluctuations of spring water chemistry and temperature using a process-based model of flow and transport in a *regional* karst aquifer.

In order to characterise the *early* development of gypsum karst aquifers, the conceptual model suggested by Klimchouk (1996c, 1997a, 2000a, 2000c; see also section 1.2.1) was translated into a numerical model of karst genesis. The objectives of this modelling study were

- to understand the processes involved in the genesis of gypsum aquifers,
- to identify parameters controlling the development of the conduit system,
- to explain the resulting structure of the conduit system,

- to examine the predictive capability of karst genesis modelling with respect to the characterisation of gypsum aquifers.

Whereas the early development of karst aquifers appears to be well suited to karst genesis modelling, short-term fluctuations of spring water chemistry and temperature are more likely to occur in a *mature* karst system with surface karst features such as sinkholes, which rapidly transmit the recharge water to a well developed conduit system and eventually to a karst spring. The solute and heat transport models, therefore, were applied to this type of gypsum aquifer. The objectives of the transport simulations were

- to identify processes which cause fluctuations in spring water chemistry and temperature,
- to identify parameters controlling solute and heat transport in karst aquifers,
- to investigate how far spring water signals can be interpreted in terms of physical parameters characterising the conduit system,
- to examine whether an integrated approach combining solute and heat transport simulations reduces the ambiguity in the interpretation of aquifer flow and transport properties,
- to examine whether the model is suited to reproduce field data from a gypsum karst spring under realistic conditions.

1.4 Format of the thesis

This thesis describes both development and application of a process-based numerical modelling tool supporting the characterisation of karst aquifers. Chapter 2 presents processes governing long-term karst genesis as well as short-term karst spring response. These include flow (section 2.1), solute transport (section 2.2), dissolution reaction (section 2.3) and heat transfer (section 2.4). Chapter 3 describes how these processes were implemented into a numerical modelling tool (section 3.1) and how the modelling tool was verified (section 3.2). The major part of this thesis is devoted to the application of the model. Chapter 4 presents simulations of long-term karst genesis. These are based on speleogenetic concepts (section 4.1) which were transferred into a numerical model (section 4.2). The numerical model is used to examine both single conduit development (section 4.3) and development of conduit networks (section 4.4). Results of karst genesis modelling are discussed in section 4.5. Chapter 5 deals with simulations of karst spring response to recharge events. The suggested approach (section 5.1) includes parameter studies, in which forward modelling is used to examine how conduit geometry influences karst spring signals (section 5.2), and field application of the model, which aims at inferring aquifer properties from measured karst spring responses. Results of these simulations are discussed in section 5.4. Chapter 6 presents conclusions and suggestions for future work.

It is intended to provide a comprehensive and detailed description in particular of model application. Hopefully, this makes it possible to judge critically the results of this work and to proceed further towards the utilisation of modelling approaches for the characterisation of karst systems.

Chapter 2

Processes

This chapter describes processes involved in the evolution of gypsum karst aquifers and in short-term transport of solutes and heat. A conceptual model of karst aquifers is outlined. At the same time a mathematical model is presented, i.e. the processes are quantitatively described.

2.1 Flow

The previous chapter introduced a conceptual model of karst flow systems, which distinguishes between two components, namely diffuse flow and conduit flow (White, 1969; Shuster and White, 1971; Atkinson, 1977). Following Sauter and Liedl (2000) the "diffuse flow system" is termed as "fissured system" within this work. It represents the mass of the fractured rock, which is much less permeable than the highly conductive solution conduits. Compared to the conduit system, which represents only a small percentage of the total rock volume, storage is high in the fissured system. This is illustrated, for instance, by investigations of the carbonate karst system of the Swabian Alb in Southern Germany, which yielded only about 0.01% to 0.03% of the total rock volume for the conduit system, whereas the storage of the fissured system ranged between 0.8% and 2.5% (Sauter, 1992). Fig. 2.1 depicts the basic features of a karst aquifer schematically.

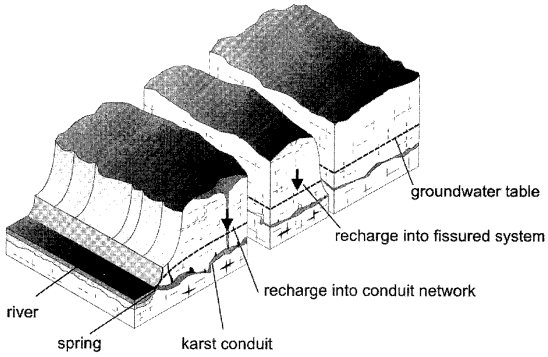

Figure 2.1: Schematic diagram of a karst aquifer (modified from Sauter and Liedl, 2000)

According to Kiraly (1998) the dualistic nature of a karst aquifer includes

- the duality of the infiltration processes, i.e. slow diffuse recharge into the fissured system and rapid localised recharge into the conduit system,
- the duality of the groundwater flow field, i.e. low flow velocities in the fissured system and high flow velocities in the conduit system,
- the duality of the discharge, i.e. diffuse seepage from the fissured system and concentrated discharge from the conduit system through karst springs.

The following sections describe the processes governing flow in and between the two systems.

2.1.1 Flow in the fissured system

Flow in the fissured system is along small openings such as joints and bedding planes,

which are highly interconnected. Therefore, it exhibits a similar behaviour as laminar flow in porous media (Shuster and White, 1971). Hence, it can be treated as a continuous flow field governed by Darcy's law, which states that flow is proportional to the hydraulic gradient, and can be expressed in form of a continuity equation, which is a statement of conservation of mass (White, 1988). Combining these two principles and assuming that the fissured system is isotropic, the vertically integrated equation of flow can be written as (Huyakorn et al., 1983)

$$\frac{\partial}{\partial x}\left(T_f\frac{\partial h_f}{\partial x}\right)+\frac{\partial}{\partial y}\left(T_f\frac{\partial h_f}{\partial y}\right)=S_f\frac{\partial h_f}{\partial t}-\gamma-r_f \tag{2.1}$$

where x and y are Cartesian coordinates [m], t is time [s], h_f is hydraulic head of the fissured system [m], T_f is transmissivity of the fissured system [$m^2\ s^{-1}$], S_f is storage coefficient (for confined aquifers) or specific yield (for unconfined aquifers) [-], γ is the volumetric rate of fluid transfer from the conduit system to the fissured system per unit area [$m\ s^{-1}$], and r_f is the volumetric rate of fluid flow per unit area via sources ($r_f > 0$), e.g. groundwater recharge, or sinks ($r_f < 0$) [$m\ s^{-1}$]. Anisotropy can be taken into account by using different values for the transmissivity in the two terms on the left hand side of eq. (2.1).

2.1.2 Flow in the conduit system

Flow in the conduit system is not continuous but spatially localised to solutionally enlarged flow paths, i.e. the conduits. In the conduits laminar and turbulent flow conditions may occur depending on the flow velocities. A criterion to decide whether flow is laminar or turbulent is given by the dimensionless Reynolds number (e.g. Dreybrodt, 1988)

$$N_{Re}=\frac{v\cdot a}{\nu_w} \tag{2.2}$$

where v is a characteristic velocity [$m\ s^{-1}$], i.e. the average flow velocity in the conduit, a is a characteristic length [m], i.e. the diameter of the conduit, and ν_w is the kinematic viscosity of water [$m^2\ s^{-1}$]:

$$\nu_w=\frac{\eta_w}{\rho_w} \tag{2.3}$$

η_w is the dynamic viscosity of water [$N\ s\ m^{-2}$] and ρ_w is the density of water [$kg\ m^{-3}$], both of which are given by Weast (1979) as functions of temperature. In smooth pipes the transition between laminar and turbulent flow occurs at Reynolds numbers of about 2000 (Dreybrodt, 1988). In rough pipes, e.g. solution conduits, turbulence sets in at lower Reynolds numbers (White, 1988).

Under laminar flow conditions the discharge Q through a circular conduit [$m^3\ s^{-1}$] depends linearly on the hydraulic gradient $\Delta h_c/l$ along the conduit as described by the Hagen-Poiseuille equation (White, 1988).

$$Q=\frac{\pi a^4 g}{128\nu_w}\frac{\Delta h_c}{l} \tag{2.4}$$

where Δh_c is the absolute value of frictional head loss [m] along a conduit of length l [m], and g is the gravitational acceleration [$m\ s^{-2}$].

For turbulent flow the Darcy-Weisbach equation states that the head loss is proportional to the square of the average flow velocity (White, 1988)

$$\Delta h_c=\frac{f l}{2ga}v^2 \tag{2.5}$$

The friction factor f is given by the empirical Colebrook-White formula (Dreybrodt, 1988)

$$\frac{1}{\sqrt{f}}=-2\log\left(\frac{k_c}{3.71a}+\frac{2.51}{N_{Re}\sqrt{f}}\right) \tag{2.6}$$

where k_c is the roughness length of the conduit wall [m].

Combining the Darcy-Weisbach equation (2.5) and the Colebrook-White formula (2.6) yields an explicit expression for the flow rate through a conduit under turbulent flow conditions (Horlacher and Lüdecke, 1992; Hückinghaus, 1998)

$$Q=-2Y\log\left(\frac{k_c}{3.71a}+\frac{2.51\pi\nu_w a}{4Y}\right) \tag{2.7}$$

with

$$Y^2 = \frac{\Delta h_c g a^5 \pi^2}{8l} \tag{2.8}$$

Equations (2.4) and (2.7) provide a quantitative description of laminar and turbulent flow in single conduits. Karst aquifers, however, frequently contain several conduits, forming networks. In such conduit networks total inflow and total outflow have to balance at each node (i.e. at each intersection of conduits) as stated by Kirchhoff's law (Clemens, 1998; Horlacher and Lüdecke, 1992)

$$\sum_{i=1}^{n} Q_i - \Gamma + R_c = 0 \tag{2.9}$$

where n is the number of conduits linked together at a specific node, Q_i are the rates of inflow ($Q_i > 0$) and outflow ($Q_i < 0$) via conduits [$m^3\ s^{-1}$] as given by eqs. (2.4) or (2.7), Γ is the rate of fluid transfer from the conduit system to the fissured system [$m^3\ s^{-1}$], and R_c is the rate of flow via sources ($R_c > 0$), e.g. localised recharge into the conduit system, or sinks ($R_c < 0$), e.g. pumping wells [$m^3\ s^{-1}$].

2.1.3 Flow between the fissured system and the conduit system

Flow between the fissured system and the conduit system is assumed to be controlled by the hydraulic head difference between the two systems. The simplest quantitative description of this process was introduced by Barenblatt et al. (1960), who assumed that the flow rate Γ between the two systems [$m^3\ s^{-1}$] is linearly related to the hydraulic head difference via an exchange coefficient α [$m^2\ s^{-1}$]

$$\Gamma = \alpha\,(h_c - h_f) \tag{2.10}$$

Summarising several approaches for the quantification of exchange flow, Bauer et al. (2000) conclude that the exchange coefficient is generally considered to depend on the hydraulic conductivity of the fissured system, the exchange surface between conduit system and fissured system, and a factor determined by the conduit geometry. The geometry of conduits and inter-conduit blocks is usually unknown. However, the hydraulic conductivity of the fissured system determines the order of magnitude for the exchange coefficient (Bauer et al., 2000).

2.2 Solute transport

Solute transport in karst aquifers is influenced by the dualistic nature of the flow system described in the previous section. On the one hand, flow velocities in conduits are usually found to be in the range from 0.01 to 1 m s^{-1} (Gale, 1984), i.e. solutes are rapidly transported in the conduit system. On the other hand, flow in the low permeable fissured system is much slower. This is illustrated, for instance, by tracer experiments in a limestone karst terrain, which yielded high velocities of between 50 and 100 m h^{-1} when the tracer was directly injected into the conduit system via sinks, whereas an injection into the fissured system via boreholes resulted in low velocities between only 1 and 2 m d^{-1} (Teutsch, 1988). Hence, time scales relevant to solute transport considerably differ between conduit system and fissured system.

The chemical composition of karst spring waters reflects the mixing of the two flow components. At a time scale of hours or days, transport of solutes by flow in the fissured system is negligible. Short-term fluctuations in the chemical composition of the spring water are determined by the fast transport in conduits, e.g. after a direct infiltration of recharge into the conduit system. The fissured system, however, determines the long-term behaviour of spring water chemistry, i.e. the background concentration, because the main portion of the spring flow usually originates from this part of the aquifer.

As will be seen in section 2.3, transport in the fissured system of gypsum aquifers can be neglected not only when short-term processes

are considered, but also in studies of long-term gypsum dissolution and transport. The following sections, therefore, deal with transport processes in the conduit system only.

2.2.1 Advection

The main mechanism of solute transport in conduits is advection. Solutes are transported with the average flow velocity

$$v = \frac{Q}{A} \tag{2.11}$$

where Q is the flow rate [$m^3\ s^{-1}$] given by equation (2.4) or (2.7) depending on the flow conditions, and A is the cross-sectional area of flow, i.e. $A = \frac{\pi}{4}a^2$ in circular conduits.

The governing equation of one-dimensional advection in a conduit is derived from the principle of conservation of mass, which states that the mass accumulation in a volume element is balanced by the mass transport across the faces of the volume element (Clark, 1996):

$$\frac{\partial c}{\partial t} = -v\frac{\partial c}{\partial z} \tag{2.12}$$

where c is solute concentration [mol m^{-3}], t is time [s], and z is spatial coordinate along the conduit [m].

In a conduit network conservation of mass requires that the mass flow rates balance at each intersection of conduits, thus

$$\sum Q_{in}c_{in} = \sum Q_{out}c_{out} \tag{2.13}$$

where Q_{in} are the absolute rates of inflow from conduits, fissured system and other sources such as recharge [$m^3\ s^{-1}$], Q_{out} are the absolute rates of outflow from the intersection into conduits, fissured system and other sinks [$m^3\ s^{-1}$], and c_{in} and c_{out} are the corresponding solute concentrations [mol m^{-3}].

The mass inflow rates to the conduit intersections can be calculated if flow rates and corresponding concentrations are known. However, the distribution of the total mass inflow to the outflow via conduits, fissured system and other sinks depends on the mixing process at the conduit intersection. Under idealised laminar flow conditions streamlines do not intersect. Mixing at conduit intersections is generally not complete under these conditions (Berkowitz et al., 1994), although different concentrations assimilate to a certain degree due to diffusion perpendicular to the streamlines (see also sections 2.2.2 and 2.3). According to Siemers (1998), however, the assumption of complete mixing is reasonable under natural conditions, which include high wall roughness and non-rectangular conduit intersections. Assuming complete mixing, the solute concentration of the outflow from a conduit intersection is given by

$$c_{out} = \frac{\sum Q_{in}c_{in}}{\sum Q_{out}} \tag{2.14}$$

2.2.2 Dispersion

In addition to transport by advection, there is a tendency for the solute to spread out from the bulk motion of the groundwater. This spreading effect is termed (hydrodynamic) dispersion (Freeze and Cherry, 1979). It causes a dilution of the solute.

In laminar flow through a single conduit dispersion is caused by the parabolic velocity profile, i.e. flow velocities are higher in the pipe centre than near the pipe wall. Depending on the distance from the pipe wall, therefore, solute transport may be faster or slower than the average flow velocity. Thus, certain portions of the solute mass arrive earlier and later at the outlet compared to what would be expected if only advection was considered. The effect of the parabolic velocity distribution, however, is modified by diffusive mass transfer reducing concentration gradients perpendicular to the flow direction. The above mentioned dispersion process in laminar pipe flow is often referred to as "Taylor-Aris-dispersion" (Clark, 1996), because Taylor (1953) and Aris (1956) developed mathematical models for it. Dispersion due to mixing processes in turbulent

pipe flow was quantitatively described by Taylor (1954). In both laminar and turbulent flow the one-dimensional advection-dispersion equation applies (Clark, 1996):

$$\frac{\partial c}{\partial t} = -v\frac{\partial c}{\partial z} + D_{dis}\frac{\partial^2 c}{\partial z^2} \qquad (2.15)$$

where D_{dis} is the dispersion coefficient [m^2 s^{-1}]. The dispersion coefficient depends on the flow conditions (e.g. flow velocity and conduit diameter).

In karst aquifers, the one-dimensional dispersion model (eq. 2.15) frequently fails to describe measured tracer breakthrough curves, which are often strongly asymmetric (Field, 1999) and may show several peaks (Werner et al., 1997, 1998). To account for dispersion in karst aquifers, further processes have to be considered, such as diffusion and interaction of the solute with the rock matrix (Neretnieks, 1983; Moreno et al., 1985; de Marsily, 1986), solute storage in immobile fluid zones (Raven et al., 1988), mixing processes in pools, i.e. in conduit enlargements (Hauns et al., 1998, 2001), and different flow paths along multiple conduits (Maloszewski et al., 1992). Although several or all of these processes may be involved in generating dispersion, the latter appears to be the most important process at a catchment scale, since it is likely that flow in regional karst aquifers occurs along networks of multiple conduits, and tracer travel times may be expected to differ significantly between separate conduits. In this work, therefore, dispersion in single conduits is neglected, i.e. transport of non-reactive solutes is described by eq. (2.12) and dispersion results from the mixing of waters at conduit intersections only.

2.2.3 Reaction

Transport by advection and dispersion does not change the total solute mass dissolved in the conduit water. However, the solute mass may change due to reactive processes such as ion exchange, radioactive decay, biodegradation and others (Singhal and Gupta, 1999). In comparison with porous media residence time in the conduits is quite short and the area of rock exposed to water is relatively small. Hence, reactive processes limited by slow kinetics are generally much less important in karst aquifers than in porous media.

This work focuses on the increase of the solute mass due to the dissolution reaction of gypsum (section 2.3). Thus, considering the advective transport of dissolved gypsum (i.e. calcium and sulfate ions) the one-dimensional advection equation (2.12) has to be expanded by a source term $S_c(z,t,c)$, which describes the increase in concentration due to gypsum dissolution [mol m^{-3} s^{-1}]:

$$\frac{\partial c}{\partial t} = -v\frac{\partial c}{\partial z} + S_c(z,t,c) \qquad (2.16)$$

In this general formulation the source term is assumed to be a function of space, time and solute concentration. The following section examines the dissolution reaction of gypsum in more detail.

2.3 Gypsum dissolution

Gypsum dissolution is an important process considering both long-term conduit development in gypsum karst aquifers and short-term fluctuations of water chemistry at gypsum karst springs. The dissolution of gypsum in a hydrogeological setting requires (Lamont-Black et al., 1999):

- Presence of gypsum
- Water undersaturated with respect to gypsum
- Energy to drive the water through the gypsum
- An outlet for the water

If these conditions are fulfilled conduits are enlarged by the dissolution of gypsum. The increasing permeability of the conduits then attracts more water to the pathway, thus enhancing the dissolution process. This positive feedback mechanism results in a localisation of flow to the solutionally enlarged pathways, i.e. the conduits. In the low permeable zones (i.e. the fissured system) of a gypsum aquifer, water is usually not aggressive with respect to gypsum, because it reaches saturation either during the slow diffuse infiltration of recharge or after a short travel distance within the aquifer. Thus, gypsum dissolution in the fissured system can be neglected.

2.3.1 Chemical equilibrium

Gypsum ($CaSO_4 \cdot 2H_2O$) dissolves in water by dissociation to calcium (Ca^{2+}) and sulfate (SO_4^{2-}) ions and water (H_2O) (e.g. Wigley, 1973):

$$CaSO_4 \cdot 2H_2O \rightleftharpoons Ca^{2+} + SO_4^{2-} + 2H_2O \tag{2.17}$$

The equilibrium constant (i.e. the solubility product) is defined as

$$K_g = \gamma_{Ca}\gamma_{SO_4}\left[Ca^{2+}\right]\left[SO_4^{2-}\right] \tag{2.18}$$

where γ_{Ca} and γ_{SO_4} are the activity coefficients and the terms in brackets are the concentrations [mol m^{-3}] of calcium and sulfate, respectively.

The activity coefficients depend on the ionic strength of the solution, which is defined by the concentrations c_i of all ionic species (in mol l^{-1}) and their charge z_i (Appelo and Postma, 1993):

$$I = \frac{1}{2}\sum_i c_i z_i^2 \tag{2.19}$$

Using the extended Debye-Hückel equation the activity coefficient γ_i of a ionic species i can be calculated if the ionic strength (in mol l^{-1}) is known (Dreybrodt, 1988):

$$-\log\gamma_i = Az_i^2 I^{1/2}\left(1 + r_i B I^{1/2}\right)^{-1} \tag{2.20}$$

where r_i is the ionic radius of the species in Å (10^{-10} m), and the values A and B are related to the temperature ϑ in °C ($A = 0.4883 + 8.074 \cdot 10^{-4}\vartheta$, $B = 0.3241 + 1.6 \cdot 10^{-4}\vartheta$).

Values for the equilibrium constant K_g are usually given at a temperature of 25 °C. However, groundwater temperatures are commonly found to be lower. Values of K_g can be extended to other temperatures by use of the van't Hoff equation (Krauskopf, 1982)

$$-\log\frac{K_g(T_1)}{K_g(T_2)} = \frac{\Delta H}{2.303R}\left(\frac{1}{T_1 - T_2}\right) \tag{2.21}$$

where R is the gas constant (8.314 J mol^{-1} K^{-1}), and T_1 and T_2 are temperatures in K. In this equation the change of the reaction enthalpy ΔH [J mol^{-1}] is assumed to remain constant as temperature changes. However, ΔH varies with temperature. Therefore, Wigley (1973) suggests the use of an equation, which resulted from a quadratic fit to experimental data between $\vartheta = 0.5$ °C and $\vartheta = 45$ °C:

$$-\log K_g = 4.6535 - 0.004545\vartheta + 0.000101\vartheta^2 \tag{2.22}$$

If gypsum dissolves in pure water the molar concentrations of calcium and sulfate are equal according to eq. (2.17). Knowing the activity coefficients and the equilibrium constant K_g the concentrations of calcium and sulfate ions at chemical equilibrium can be calculated by use of eq. (2.18):

$$\left[Ca^{2+}\right] = \left[SO_4^{2+}\right] = \sqrt{\frac{K_g}{\gamma_{Ca}\gamma_{SO_4}}} \tag{2.23}$$

The solubility of gypsum is enhanced by the association of calcium and sulfate ions to the uncharged ion pair $CaSO_4^0$ according to the following equilibrium reaction (Wigley, 1973):

$$CaSO_4^0 \rightleftharpoons Ca^{2+} + SO_4^{2-} \tag{2.24}$$

Since the activity coefficient of the uncharged species is supposed to be unity (Wigley, 1973),

the equilibrium constant (i.e. the dissociation constant) for this reaction is given by

$$K_{CaSO_4^0} = \frac{\gamma_{Ca}\gamma_{SO_4}\left[Ca^{2+}\right]\left[SO_4^{2-}\right]}{\left[CaSO_4^0\right]} \quad (2.25)$$

Again the van't Hoff equation (2.21) may be used for temperature corrections of $K_{CaSO_4^0}$.

Combining eq. (2.18) and eq. (2.25) yields the concentration of $CaSO_4^0$ at chemical equilibrium

$$\left[CaSO_4^0\right] = \frac{K_g}{K_{CaSO_4^0}} \quad (2.26)$$

Thus, the total amount of gypsum, which dissolves at chemical equilibrium with pure water, i.e. the equilibrium concentration c_{eq} [mol m^{-3}], is the sum of the concentrations of the ionic species as given by eq. (2.23) and the associated ion pair as given by eq. (2.26):

$$c_{eq} = \sqrt{\frac{K_g}{\gamma_{Ca}\gamma_{SO_4}}} + \frac{K_g}{K_{CaSO_4^0}} \quad (2.27)$$

2.3.2 Dissolution kinetics

If water is at chemical equilibrium with a solid gypsum phase it is not able to dissolve any further gypsum. Thus, in order to maintain the dissolution process a mechanism is needed, which disturbs the chemical equilibrium by removing the dissolved calcium and sulfate ions. Figure 2.2 shows the processes involved in gypsum dissolution and transport of the dissolved calcium and sulfate in a conduit. Firstly, gypsum dissolves at the rock surface, i.e. gypsum molecules dissociate according to eq. (2.17). Secondly, calcium and sulfate are removed from the rock surface by diffusion through a boundary layer into the conduit water if there is a concentration gradient driving the diffusion process (i.e. if the conduit water is undersaturated with respect to gypsum). Thirdly, the solutes are transported by advection along the conduit (see section 2.2.1).

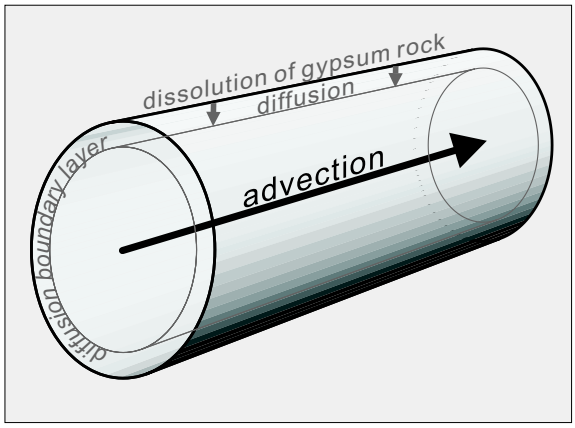

Figure 2.2: Gypsum dissolution and transport processes in a circular conduit.

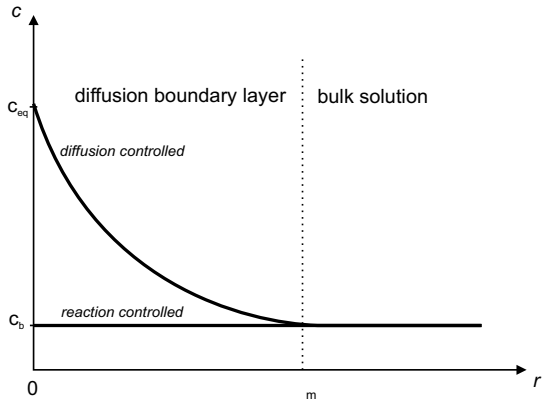

Figure 2.3: Concentration profiles across a diffusion boundary layer.

Gypsum dissolution is governed by the slowest step of the dissolution process. Thus, the dissolution rate may be limited either by the dissociation of gypsum molecules releasing calcium and sulfate at the rock surface or by the diffusion process, which removes the calcium and sulfate from the rock surface. Figure 2.3 shows the concentration profiles across a diffusion boundary layer of thickness ε_m in both cases. If, on the one hand, the dissolution is controlled by a slow diffusion process the calcium and sulfate ions removed from the rock surface are immediately replaced by newly dissociated gypsum molecules. At the rock surface ($r = 0$), hence, the solution is always at chemical equilibrium, i.e. the concentration equals the equilibrium concentration c_{eq}. On the other hand, if dissolution is controlled by a slow surface reaction the calcium and sulfate

ions are almost immediately transported into the bulk solution. Hence, the concentration at the rock surface and the concentration of the bulk solution c_b are nearly identical. The intermediate case of a mixed diffusion/reaction control occurs if neither of the two processes is considerably slower than the other. This case is not of importance within the scope of this work, since it does not occur under conditions considered here. See Dreybrodt (1988) for details about mixed kinetics of dissolution processes.

2.3.2.1 Diffusion controlled kinetics

The mass flux F_m [mol m^{-2} s $^{-1}$] crossing a surface is given by Fick's first law of diffusion (Dreybrodt, 1988)

$$F_m = -D\frac{\partial c(r)}{\partial r} \tag{2.28}$$

where D is the diffusion coefficient [m^2 s^{-1}], r is the spatial coordinate perpendicular to the surface [m], and $c(r)$ is the concentration [mol m^{-3}]. Thus, the mass flux is proportional to the concentration gradient.

If the rock surface is separated from the bulk solution of concentration c_b [mol m^{-3}] by a diffusion boundary layer of thickness ε_m [m] (see Fig. 2.3) the diffusion mass flux across the boundary layer is given by the integrated form of eq. (2.28)

$$F_m = k\,(c_{eq} - c_b) \tag{2.29}$$

where k is the mass transfer coefficient [m s^{-1}]

$$k = \frac{D}{\varepsilon_m} \tag{2.30}$$

Thus, the diffusive mass flux depends linearly on the difference between equilibrium concentration and concentration of the bulk solution, i.e. the dissolution rate follows a linear first-order rate law. Calculation of diffusion controlled dissolution rates requires values for the diffusion coefficient and for the boundary layer thickness.

Diffusion coefficients of calcium and sulfate are given for several temperatures by Dreybrodt (1988). Generally, the diffusion coefficients for various temperatures may be estimated using the Einstein-Nernst-Eyring relation (Beek and Muttzall, 1975)

$$\frac{D\eta_w}{T} = constant \tag{2.31}$$

where T is temperature in K, and η_w is the dynamic viscosity of water [N s m^{-2}]. Although the diffusion coefficients of calcium and sulfate ions are different, the motion of the two ions is tied together due to their opposite charge. The joint coefficient of diffusion is given by Dreybrodt (1988) as

$$D = \frac{(z_+ + z_-)\,D_+ D_-}{z_+ D_+ + z_- D_-} \tag{2.32}$$

where z_- and D_- denote the charge and the diffusion coefficient of the anion (i.e. sulfate) and z_+ and D_+ charge and diffusion coefficient of the cation (i.e. calcium), respectively.

The thickness of the diffusion boundary layer is usually expressed by a dimensionless number, the Sherwood number N_{Sh}, i.e. the ratio between the conduit diameter a and the boundary layer thickness ε_m (Beek and Muttzall, 1975)

$$N_{Sh} = \frac{a}{\varepsilon_m} = k\frac{a}{D} \tag{2.33}$$

Thus, the mass transfer coefficient in eq. (2.29) is given by

$$k = N_{Sh}\frac{D}{a} \tag{2.34}$$

In laminar flow through circular conduits the Sherwood number is constant if the diffusion boundary layer is fully developed, i.e. far from the conduit entrance. If the concentration at the rock surface is constant the Sherwood number is (Beek and Muttzall, 1975)

$$N_{Sh} = 3.66 \quad ; \quad \frac{zD}{va^2} > 0.1 \tag{2.35}$$

where z is the distance from the conduit entrance [m]. Near the conduit entrance the local Sherwood number at the distance z from

the conduit entrance can be approximated by (Beek and Muttzall, 1975)

$$N_{Sh} = 1.08 \left(\frac{zD}{va^2}\right)^{-1/3} \quad ; \quad \frac{zD}{va^2} < 0.05 \tag{2.36}$$

The exact but more complex solution for this problem is given by Skelland (1974).

Several empirical correlations exist for the Sherwood number in fully turbulent flow through smooth pipes. A relative simple expression is given by Beek and Muttzall (1975):

$$N_{Sh} = 0.027 N_{Re}^{4/5} N_{Sc}^{1/3} \tag{2.37}$$

where $N_{Sc} = \nu_w / D$ is the Schmidt number. According to Incropera and DeWitt (1996), however, errors as large as 25% may result from the use of eq. (2.37). If a high level of accuracy is needed they suggest the use of more complex equations such as (Gnielinski, 1976)

$$N_{Sh} = \frac{(f/8)\,(N_{Re} - 1000)\,N_{Sc}}{1 + 12.7\,(f/8)^{1/2}\left(N_{Sc}^{2/3} - 1\right)} \tag{2.38}$$

In this equation the Sherwood number is correlated to the friction factor f given by eq. (2.6). An increasing surface roughness results in higher Sherwood numbers, i.e. higher dissolution rates. Although eq. (2.38) was developed for fully turbulent flow conditions ($N_{Re} > 10000$) in smooth pipes, it may be used as a first approximation at smaller Reynolds numbers and for rough pipes (Incropera and DeWitt, 1996).

The outlined approach is well established for the quantification of diffusive mass transfer in pipe flow. However, it has never been validated with respect to gypsum dissolution. Therefore, laboratory experiments were conducted (Vierneisel, 2000) using samples of natural gypsum from the Permian Zechstein (Niederellenbach, Germany) and the Triassic Keuper (Wittershausen, Germany) formations. In these experiments water was circulated through holes, which were axially drilled into cores of gypsum rock. In both laminar and turbulent flow conditions (up to Reynolds numbers of about 10000) it was found that gypsum dissolution follows a first-order rate law. For the Zechstein samples, which contained about 98% of gypsum, the mass transfer coefficient k calculated by use of eq. (2.33) fitted the experimental data reasonably well if the Sherwood number was taken according to eq. (2.36) in laminar flow and eq. (2.37) or eq. (2.38) in turbulent flow. For some samples turbulent flow conditions had to be assumed at Reynolds numbers as low as 1500. This, however, is reasonable considering the explanations about the transition from laminar to turbulent flow given in section 2.1.2. An important result of the experiments refers to the Keuper samples, which contained only 79% of gypsum. Dissolution rates measured at these samples were significantly lower than expected. Satisfactory fits were obtained when the calculated dissolution rates were reduced to the percentage of gypsum contained in the sample. This is reasonable, because reducing the dissolution rate (i.e. the mass flux per unit area and time) is equivalent to reducing the area of gypsum exposed to water, and it can be expected that this area corresponds to the gypsum content of the rock.

The mass flux F_m refers to a unit area of the rock surface [mol m^{-2} s^{-1}]. For use in the advection equation (2.16), however, a source term $S_c(z,t,c)$ is needed, which refers to a unit volume of the solution [mol m^{-3} s^{-1}]. The mass flux F_m, therefore, has to be multiplied by the ratio of the area of rock exposed to water and the volume of the solution. For a circular conduit this ratio is $4/a$. Thus, the source term in eq. (2.16) is given by

$$S_c(z,t,c) = \frac{4}{a} F_m = \frac{4k(z,t)}{a}\,(c_{eq} - c) \tag{2.39}$$

Note that the source term is a function of the gypsum concentration of the solution, but depends further on the mass transfer coefficient and the conduit diameter, both of which may vary in space and time.

2.3.2.2 Surface reaction controlled kinetics

The mass flux F_m per unit area and time [mol m^{-2} s^{-1}] of a surface reaction controlled dissolution process is usually expressed by empirical rate laws (Dreybrodt, 1988):

$$F_m = k_s(c_{eq} - c_b)^n \tag{2.40}$$

where n is a positive number, and k_s is the dissolution rate constant, i.e. the rate constant of the surface reaction. Note that the unit of k_s depends on the reaction-order n.

An important difference between a diffusion controlled and a reaction controlled dissolution process is that the latter does not depend on the thickness of the diffusion boundary layer, i.e. it is independent of the hydrodynamic conditions. In most of the gypsum dissolution experiments mentioned in section 1.2.1 the dissolution rates were influenced by hydrodynamic conditions such as stirring rates or flow velocities. Thus, in these experiments gypsum dissolution was found to be diffusion controlled. However, Lebedev and Lekhov (1990) increased the mixing rates of a solution in contact with solid gypsum until the dissolution rate became independent of the stirring rate. Under these conditions the dissolution process is believed to be entirely controlled by the surface reaction. The measured dissolution rates followed a first-order rate law ($n = 1$), and the dissolution rate constant k_s was found to be in the order of 10^{-4} m s^{-1}. Only recently, experiments conducted by Jeschke et al. (2001) yielded very similar values for the rate constant of the surface reaction. However, a switch of the reaction-order from $n = 1$ to $n \approx 4.5$ was observed for samples of natural gypsum at high saturation stages ($c \geq 0.95 c_{eq}$). Such a kinetic switch causes a drop of dissolution rates close to chemical equilibrium. Since this was not observed in our experiments (Vierneisel, 2000), it is assumed that the dissolution reaction of gypsum follows a first-order rate law. In order to decide whether the dissolution process is diffusion or reaction controlled, it is sufficient then to compare the values of the mass transfer coefficient k with that of the surface reaction rate constant k_s. In the modelling studies presented in this work k is always much lower than 10^{-4} m s^{-1}, thus justifying the assumption of a diffusion controlled dissolution process.

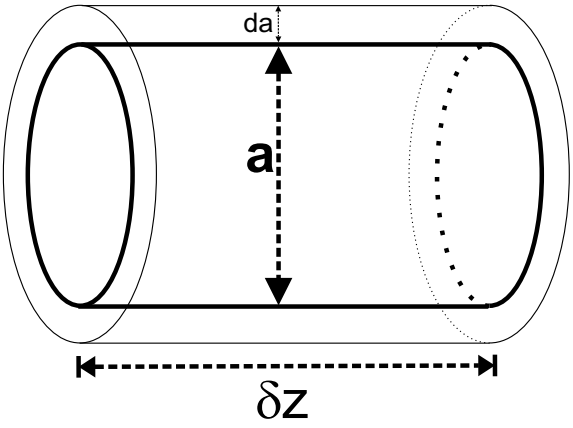

Figure 2.4: Enlargement of a conduit segment of length δz and diameter a.

2.3.3 Conduit enlargement

The dissolution of gypsum causes the enlargement of conduits in the subsurface. In a circular conduit (Fig. 2.4) the rate of gypsum mass loss dm/dt [mol s^{-1}] along a small distance δz depends on the dissolution rate F_m and the area of rock exposed to water ($\pi a \delta z$):

$$\frac{dm}{dt} = F_m \pi a \delta z \tag{2.41}$$

Further, the mass loss rate is related to the volume ($\pi/4 a^2 \delta z$) via the (molar) density of gypsum ρ_g [mol m^{-3}]:

$$\frac{dm}{dt} = \frac{d}{dt}\left(\rho_g \frac{\pi}{4} \delta z a^2\right) = \frac{\pi}{2} \rho \delta z a \frac{da}{dt} \tag{2.42}$$

Combining these equations and solving for the increase of the conduit diameter yields

$$\frac{da}{dt} = \frac{2}{\rho_g} F_m \tag{2.43}$$

Thus, the increase of the conduit diameter is proportional to the dissolution rate. However, gypsum dissolution rates depend on the

solute concentrations and (if the dissolution process is diffusion controlled) on the hydrodynamic conditions, i.e. they are usually not constant in time. Prediction of the rate of conduit enlargement, therefore, requires the quantification of flow and transport processes in the conduit system.

2.4 Heat transfer

The dualistic nature of karst flow systems has similar consequences for heat transfer in karst aquifers as previously described for solute transport (section 2.2). Due to the low flow velocities heat transport by the bulk motion of water, i.e convection, is negligible in the fissured system. Water flowing from the fissured system into conduits has been stored in the aquifer over a long period. Thus, its temperature is about the same as the temperature of the rock. Without any fast infiltration of recharge water into the conduit system the water temperature at a karst spring is determined by the rock temperature. Direct infiltration into the conduit system may cause short-term temperature fluctuations at a spring if the temperature of the recharge water differs from that of the pre-event water stored in the aquifer.

2.4.1 Heat transfer in conduit flow

Figure 2.5 shows the processes determining heat transfer in flow through a conduit. The main mechanism of heat transport along the conduit is convection due to which heat is transported at the average flow velocity v (eq. 2.11). Between conduit wall and bulk water heat is transported by conduction across a thermal boundary layer. Conduction denotes the energy transfer in the presence of a temperature gradient due to the random motion of the molecules. Thus, convection and conduction correspond to advection and diffusion in mass transfer (Beek and Muttzall, 1975).

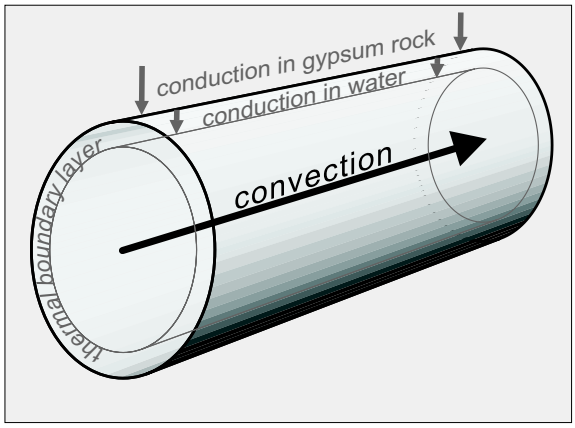

Figure 2.5: Heat transfer processes in circular conduits and the sourrounding rock.

Heat transfer in flow through circular conduits can be described by a one-dimensional convection equation similar to eq. (2.16):

$$\frac{\partial T}{\partial t} = -v\frac{\partial T}{\partial z} + S_T(z,t,T) \qquad (2.44)$$

where T is water temperature [K], and $S_T(z,t,T)$ is a source term [K s^{-1}] accounting for the change in temperature due to heat transfer across the boundary layer between conduit wall and bulk water.

The heat flux F_h [J m^{-2} s^{-1}] across a thermal boundary layer of thickness ε_h is (analogous to section 2.3.2.1) given by

$$F_h = h\,(T_s - T_b) \qquad (2.45)$$

where h is the heat transfer coefficient [J s^{-1} m^{-2} K^{-1}], T_s is temperature of the rock surface [K], and T_b is temperature of the bulk water [K]. The heat transfer coefficient is related to the dimensionless Nusselt number N_{Nu} by (Beek and Muttzall, 1975)

$$h = \frac{\lambda_w}{\varepsilon_h} = N_{Nu}\frac{\lambda_w}{a} \qquad (2.46)$$

where λ_w is the thermal conductivity of water [J s^{-1} m^{-1} K^{-1}]. The Nusselt number corresponds to the Sherwood number in mass transfer analysis. Thus, in laminar flow through a pipe with a constant wall temperature it is given by (Beek and Muttzall, 1975)

$$N_{Nu} = 3.66 \quad ; \quad \frac{z\kappa_w}{va^2} > 0.1 \qquad (2.47)$$

and

$$N_{Nu} = 1.08 \left(\frac{z\kappa_w}{va^2} \right)^{-1/3} \quad ; \quad \frac{z\kappa_w}{va^2} < 0.05 \tag{2.48}$$

where the thermal diffusivity of water [$m^2\ s^{-1}$] is given by

$$\kappa_w = \frac{\lambda_w}{\rho_w c_w} \tag{2.49}$$

c_w is the specific heat of water [J kg^{-1} K^{-1}]. The above equations are usually applied as reasonable approximations for the Nusselt number even if the requirement of a constant temperature along the conduit wall is not met (Whitaker, 1977).

In turbulent flow through a circular conduit the Nusselt number is given by Beek and Muttzall (1975) as

$$N_{Nu} = 0.027 N_{Re}^{4/5} N_{Pr}^{1/3} \tag{2.50}$$

or more accurately by Gnielinski (1976) as

$$N_{Nu} = \frac{(f/8)\,(N_{Re} - 1000)\,N_{Pr}}{1 + 12.7\,(f/8)^{1/2}\left(N_{Pr}^{2/3} - 1\right)} \tag{2.51}$$

where $N_{Pr} = \nu_w/\kappa_w$ is the Prandtl number.

For use in the convection equation (2.44) the heat flux per unit area and time F_h has to be transformed to a rate of temperature change $S_T(z,t,T)$. Multiplying F_h with the factor $4/a$ (i.e. the ratio of the area of the rock surface and the volume for a circular conduit) yields the heat flux per unit volume and time, which is transformed into a rate of temperature change via the specific heat and the density of water:

$$S_T(z,t,T) = \frac{F_h \cdot 4/a}{c_w \rho_w} = \frac{h(z,t) \cdot 4/a}{c_w \rho_w} (T_s - T) \tag{2.52}$$

In a network of conduits the heat fluxes balance at each intersection of conduits. Thus, assuming complete mixing, the temperatures at an intersection (i.e. the temperature of outflow from the intersection) are given analogous to eq. (2.14) by[1]

$$T_{out} = \frac{\sum Q_{in} T_{in}}{\sum Q_{out}} \tag{2.53}$$

[1]It is further assumed that density and specific heat of water are constant within the flow system

where Q_{in} are the absolute rates of inflow from conduits, fissured system and other sources such as recharge [$m^3\ s^{-1}$], Q_{out} are the absolute rates of outflow from the intersection into conduits, fissured system and other sinks [$m^3\ s^{-1}$], and T_{in} and T_{out} are the corresponding water temperatures [K].

2.4.2 Heat transfer in the rock

Heat transfer processes in conduit flow are similar to the mass transport processes described in section 2.3.2.1. However, an important difference concerns the boundary conditions at the conduit wall, i.e. the gypsum concentration and the temperature at the rock surface. On the one hand, the gypsum concentration at the rock surface equals the equilibrium concentration and thus is constant, provided the dissolution process is diffusion controlled. On the other hand, the temperature at the rock surface is unlikely to be constant, because heat conduction in the rock is usually slower than heat transfer in conduit flow. If the heat transfer is limited by conduction in the rock the wall temperature will approach the water temperature as time proceeds (Fig. 2.6). Thus, the heat flux between rock surface and conduit water is reduced, i.e. the water temperature is influenced by heat conduction in the rock.

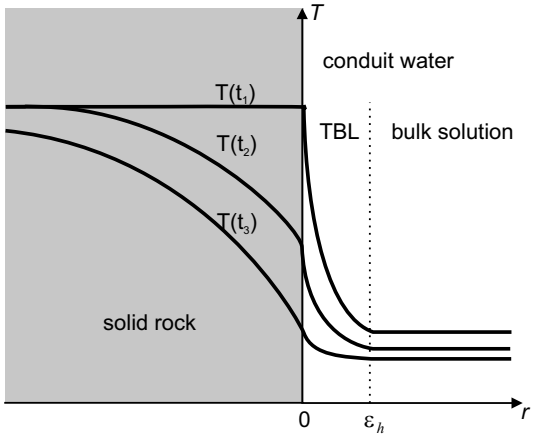

Figure 2.6: Schematized temperature profiles in solid rock and conduit water at time $t_1 < t_2 < t_3$ (TBL = thermal boundary layer).

In order to predict water temperatures in the conduits, heat conduction in the rock surrounding the conduits has to be taken into account. Neglecting conduction along the axis of the conduit (i.e. the z-axis) and assuming isotropy in the rock, the governing equation of conduction in cylindrical coordinates is given by Carslaw and Jaeger (1959) as

$$\frac{\partial T_r}{\partial t} = \kappa_r \left(\frac{\partial^2 T_r}{\partial r^2} + \frac{1}{r} \frac{\partial T_r}{\partial r} \right) \tag{2.54}$$

where T_r is rock temperature [K], κ_r is the thermal diffusivity of the rock [m^2 s^{-1}], and r denotes the cylindrical coordinate [m]. The boundary condition at the conduit wall couples conduction in the rock to heat transfer processes in the conduit system described by eq. (2.44) and eq. (2.52):

$$T_r(r = 0) = T_s \tag{2.55}$$

where T_s is the temperature at the rock surface.

Chapter 3

Model development

The conceptual and mathematical model presented in the previous chapter includes processes, which are mutually coupled to each other. Thus, a numerical model is usually required to solve the governing equations. This chapter describes the development of a numerical modelling tool, designed to simulate long-term conduit development and short-term solute and heat transport processes in gypsum aquifers.

3.1 Implementation

The development of a numerical modelling tool for gypsum aquifers was based on the carbonate karst genesis model CAVE (Carbonate Aquifer Void Evolution), which had been developed earlier by Clemens (1998) and Hückinghaus (1998) (see section 1.2.1). However, only the flow module included in CAVE turned out to be suitable for the purposes of this work. The flow module, therefore, was only slightly modified, whereas a solute transport module, a gypsum dissolution module, and a heat transfer module had to be newly developed and implemented into the CAVE code.

3.1.1 Flow module

In section 2.1 the karst flow system was conceptualised as consisting of a fissured system and a conduit system (Fig. 3.1). CAVE simulates flow in the fissured system using the continuum flow model MODFLOW, which solves the flow equation (2.1) by a finite difference method (McDonald and Harbaugh, 1988). In this work the MODFLOW-88 code originally implemented in CAVE was replaced by the updated MODFLOW-96 code (Harbaugh and McDonald, 1996). The updated code includes, for instance, a more accurate water budget and is more convenient to use.

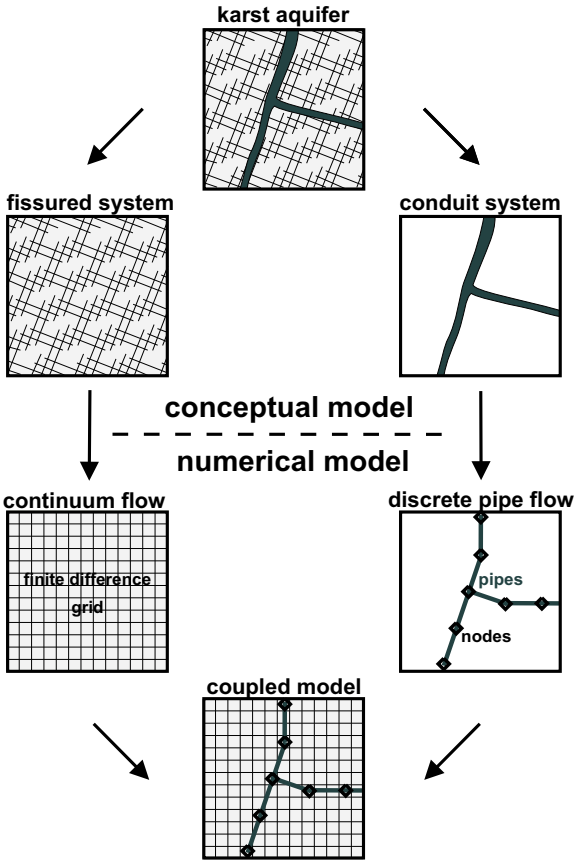

Figure 3.1: Conceptualisation of flow in a karst aquifer and translation into a numerical model.

Flow in the conduit system is modelled by the discrete pipe flow module CONDUIT (Hück-

inghaus, 1998). CONDUIT simulates flow in a pipe network based on the equations listed in section 2.1.2. For each pipe of the network flow conditions may be laminar or turbulent depending on the Reynolds number. In order to deal with the non-linearities occurring for turbulent flow conditions the iterative Newton-Raphson method (Press et al., 1986) is applied. During the iteration flow conditions switch from laminar to turbulent at a Reynolds number (e.g. 3000) which is higher than that for the transition from turbulent to laminar flow (e.g. 1000). If only one Reynolds number was used to decide whether flow is turbulent or laminar the iteration might oscillate, because under a given hydraulic head gradient the flow rate and thus the Reynolds number is found to be lower for turbulent than for laminar flow conditions.

The hydraulic heads of the two systems depend on each other via a linear exchange term as given by eq. (2.10). After each iteration step in MODFLOW the CONDUIT module, therefore, updates the exchange term by computation of the flow field in the pipe network.

In order to solve the flow equations, boundary conditions have to be defined. In both MODFLOW and CONDUIT known hydraulic heads or flow rates (e.g. recharge) can be chosen as boundary conditions. In addition, MODFLOW contains modules such as the General Head Boundary (GHB) and the RIVER package, which simulate boundaries with head-dependent flow rates

$$Q_b = L\,(h_b - h_f) \tag{3.1}$$

where Q_b is the flow rate into the aquifer [$m^3\ s^{-1}$], h_b is the head at the boundary (e.g. in the river) [m], h_f is the head in the fissured system [m], and L is a leakage factor [$m^2\ s^{-1}$], which describes the hydraulic conductance at the boundary (e.g. of the river-aquifer interconnection). This equation looks similar to the expression for the exchange term eq. (2.10). Note that h_b in eq. (3.1) is given as a boundary condition, i.e. it is specified by the user, whereas h_c in eq. (2.10) is calculated for each time step by the CONDUIT module.

Further, initial conditions have to be specified if the simulation is transient. It is sufficient to define initial heads of the fissured system as starting values for the calculation.

3.1.2 Solute transport module

Advective solute transport in conduits (section 2.2) has been implemented in the MTM (Mass Transport Module) package added on the CAVE code. The one-dimensional advection equation (2.12) is solved using an upwind finite difference scheme (Fig. 3.2). Each pipe of the network is subdivided into n segments of length Δz_i, where the subscript $i = 1, ..., n$ denotes the number of the segment.

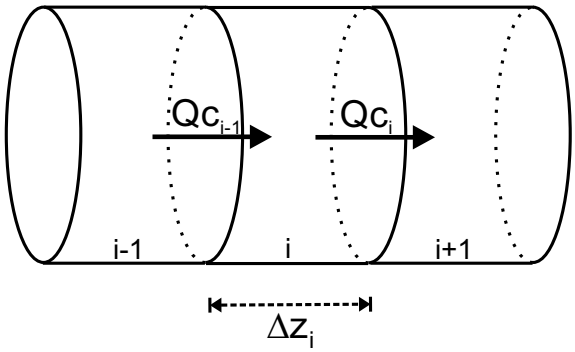

Figure 3.2: Mass fluxes between pipe segments.

The change of mass $\Delta m_{adv,i}$ [mol] within a segment during a time step Δt [s] is given by

$$\Delta m_{adv,i} = Q\,(c_{i-1} - c_i)\,\Delta t \tag{3.2}$$

where Q is the flow rate in the pipe [$m^3\ s^{-1}$], and c_i and c_{i-1} denote the solute concentrations in the segment and the upstream segment, respectively [mol m^{-3}]. This equation is equivalent to the advection equation (2.12) as can be shown by replacing the flow rate $Q = v_i A_i$ in eq. (3.2) by the flow velocity v_i and the cross-sectional area A_i, and setting $\Delta m_{adv,i} = \Delta c_{adv,i} \Delta z_i A_i$, which yields

$$\frac{\Delta c_{adv,i}}{\Delta t} = -v_i \frac{c_i - c_{i-1}}{\Delta z_i} \tag{3.3}$$

where $\Delta c_{adv,i}$ is the change of concentration during the time step due to advective transport.

Adding the change of mass as given by eq. (3.2) to the solute mass previously stored in the pipe segment yields the new solute mass after the time step. The new solute concentration is obtained by dividing the solute mass through the volume of the pipe segment.

The computation of solute mass or concentration at time $t + \Delta t$ is based on the solute concentrations $c_i = c_i(t)$ and $c_{i-1} = c_{i-1}(t)$ of the previous time step, i.e. an explicit finite difference scheme is employed. This numerical method is found to be stable if the Courant criterion is met (Kinzelbach, 1992)

$$N_{Co} = \left| \frac{v_i \Delta t}{\Delta z_i} \right| \leq 1 \tag{3.4}$$

where N_{Co} denotes the Courant number. MTM calculates the length of the transport time steps Δt according to the flow velocities and the spatial discretisation, so that the Courant criterion is met for each pipe segment.

At the nodes of the pipe network concentrations are calculated using eq. (2.14), i.e. average concentrations are calculated using weighting factors proportional to the flow rates. Concentrations of flow from pipes into a node are taken from the previous transport time step. Concentrations of external inflow (i.e. direct recharge or flow from the fissured system) have to be specified as boundary conditions. Alternatively, fixed concentrations may be assigned to the nodes of the pipe network. Furthermore, initial solute concentrations of the conduit water are required to start a transient simulation.

In order to satisfy the Courant criterion, the above outlined approach requires small transport time steps, which are often found to be in the order of seconds. Because of the high computational effort required the method is not suited for long-term simulations over periods of several months or years. Thus, a second method has been implemented for long-term simulations of solute transport in the pipe network, which may be applied if short-term fluctuations of solute concentrations are considered to be unimportant with respect to the given problem, and thus the concentration boundary conditions can be kept constant over long periods of time. Provided that changes of the flow field take place at a time scale, which is large compared to the residence time of water in the conduit system, the transport calculation can be simplified by neglecting the time-dependent term in the advection equation. Thus, after each time step of the flow calculation a steady-state concentration field is computed using a backtracking algorithm developed by Hückinghaus (1998). The computation starts at pipes which are supplied only by external inflow of known concentration from recharge or from the fissured system. Once the concentrations are calculated for these pipe segments, the concentrations of the downstream pipes are calculated. The calculation proceeds further downstream until the concentrations are known in the entire pipe network.

3.1.3 Gypsum dissolution module

The solute mass transport module MTM is supplemented by the gypsum dissolution module EDI (Evaporite Dissolution), which calculates the increase of the solute concentration due to the dissolution of gypsum. Moreover, new diameters of the solutionally enlarged pipe segments are calculated and transformed into a single diameter for each pipe.

3.1.3.1 Computation of concentrations

Calculation of the increase of solute mass due to gypsum dissolution is based on an analytical solution for the outflow concentration of a pipe segment. The analytical solution is derived by considering the mass balance of a volume element of water in the pipe. In a volume element the amount of gypsum dissolved from the pipe wall equals the amount of gypsum removed by the flow:

$$\pi a F_m dz = Q dc \tag{3.5}$$

where dc is the increase of concentration [mol m^{-3}], and dz is the infinitesimal length of the volume element along the pipe axis [m]. The diffusion controlled dissolution rate of gypsum is given by eq. (2.29) and eq. (2.33):

$$F_m = N_{Sh}\frac{D}{a}\left(c_{eq} - c\right) \tag{3.6}$$

Inserting this expression, eq. (3.5) can be rearranged yielding

$$\frac{dc}{c_{eq} - c} = \frac{\pi D}{Q} N_{Sh} dz \tag{3.7}$$

This equation can be integrated from the entrance $z_{in,i}$ to the outlet $z_{out,i}$ of a pipe segment yielding

$$\int_{c_{in,i}}^{c_{out,i}} \frac{dc}{c_{eq} - c} = \frac{\pi D}{Q} \int_{z_{in,i}}^{z_{out,i}} N_{Sh} dz \tag{3.8}$$

where $c_{in,i}$ is the concentration of the inflow to the segment, and $c_{out,i}$ the concentration of the outflow. Solving this equation for the outflow concentration yields

$$c_{out,i} = c_{eq} - (c_{eq} - c_{in,i}) \exp\left(-\overline{N}_{Sh,i} D \frac{\pi \Delta z_i}{Q}\right) \tag{3.9}$$

where the mean Sherwood number for the pipe segment of length $\Delta z_i = z_{out,i} - z_{in,i}$ is given by

$$\overline{N}_{Sh,i} = \frac{1}{\Delta z_i} \int_{z_{in,i}}^{z_{out,i}} N_{Sh} dz \tag{3.10}$$

The inflow concentration in eq. (3.9) is given as the concentration resulting from the computation of advective transport for the segment. The flow rate Q is given as an output of the flow model, and the diffusion coefficient is calculated as described in section 2.3.2.1. The equilibrium concentration of gypsum c_{eq} is calculated iteratively using eq. (2.27), eq. (2.19), and eq. (2.20). The equilibrium concentration may also be specified by the user. For turbulent flow, the local Sherwood number is given either by eq. (2.37) or by eq. (2.38). In both of these empirical equations the Sherwood number is independent of the coordinate z along the pipe axis. Thus, the mean Sherwood number in turbulent flow is simply $\overline{N}_{Sh,i} = N_{Sh}$. In laminar flow with a fully developed diffusion boundary layer the Sherwood number is a constant, thus $\overline{N}_{Sh,i} = 3.66$. However, in the entrance region the local Sherwood number is a function of the distance from the entrance. Inserting eq. (2.36) into eq. (3.10) and replacing the velocity by the flow rate yields the mean Sherwood number for the pipe segments near the entrance

$$\overline{N}_{Sh,i} = 1.75 \left(\frac{Q}{D}\right)^{1/3} \frac{z_{out,i}^{2/3} - z_{in,i}^{2/3}}{\Delta z_i} \tag{3.11}$$

3.1.3.2 Computation of pipe diameters

Replacing the dissolution rate in eq. (2.43) by

$$F_{m,i} = \frac{1}{\pi a_i \Delta z_i} \frac{dm_i}{dt} \tag{3.12}$$

and integrating from t to $t + \Delta t$ yields an expression for the new diameter of the pipe segment after the time step Δt:

$$a_i(t + \Delta t) = \sqrt{a_i^2(t) + \frac{4\Delta m_i}{\rho_g \pi \Delta z_i}} \tag{3.13}$$

where the mass loss due to gypsum dissolution within a pipe segment is given by

$$\Delta m_i = Q\left(c_{out,i} - c_{in,i}\right)\Delta t \tag{3.14}$$

New diameters are calculated for each pipe segment. The computation of the flow field of the next time step, however, requires a single diameter for each pipe of the network. Therefore, an equivalent hydraulic diameter is calculated, i.e. a diameter which causes the same pressure drop along the whole pipe as the series of individual pipe segments (Groves and Howard, 1994a; Clemens, 1998).

3.1.4 Heat transport module

Hückinghaus (1998) implemented heat transport processes in the CAVE code by coupling finite-difference schemes for the calculation of convection along conduits and conduction in the rock. However, applying the code to a single conduit, it was observed that results were dependent on the spatial discretisation of the rock matrix, and the code did not work reliably. Therefore, the Heat Transport Module HTM was newly developed. Conceptually, the most important difference between the former implementation of heat transport processes and HTM is the way of coupling convection and conduction. In the former code it was assumed that the temperature of the conduit wall and the water temperature were identical, i.e. convection along the conduit was directly coupled to conduction in the rock. HTM includes a thermal boundary layer for the coupling, i.e. convection along the conduit and conduction in the rock are connected by heat transfer across a thermal boundary layer separating conduit wall and bulk water (compare section 2.4.1).

HTM solves the governing equations (2.44), (2.52) and (2.45) using an explicit finite-difference scheme. An upwind finite-difference scheme, which calculates convection along the conduit, is coupled to a central finite-difference scheme, which calculates conduction in the rock and heat transfer between conduit wall and water. The latter is based on a method for the calculation of one-dimensional transient conduction described by Incropera and DeWitt (1996), which was adapted to cylindrical coordinates. Fig. 3.3 shows how the conduit and the surrounding rock matrix are discretised. To determine the surface temperature more accurately the volume elements associated with the surface node have been assigned only one-half of the thickness of the other volume elements in the rock matrix. Note that conduction in the rock is radial to the conduit axis. Therefore, the surface area and the volume of the discrete elements in the rock increase with increasing distance from the conduit.

Each pipe of the network is subdivided into n segments of length Δz_i, where the subscript $i = 1, ..., n$ denotes the number of a segment. The diameter $a = 2r_0$ of the pipe segments is constant along a pipe, because conduit enlargement is switched off if HTM is used. Combining the discrete forms of eq. (2.44) and eq. (2.52) yields the change of the bulk water temperature in a pipe segment $\Delta T_{i,b}$ during a time step Δt

$$\frac{\Delta T_{i,b}}{\Delta t} = -v\frac{T_{i,b} - T_{i-1,b}}{\Delta z_i} + \frac{4\overline{h}_i}{\rho_w c_w a}\left(T_{i,0} - T_{i,b}\right) \tag{3.15}$$

This equation may be also derived by setting up an energy balance for a pipe segment similar to the derivation of the discrete form of the advection equation in section 3.1.2 which was based on a mass balance for a segment.

The mean heat transfer coefficient $\overline{h}_i$ for the pipe segment is calculated by eq. (2.46), which requires the determination of a mean Nusselt number. The mean Nusselt number for a pipe segment is calculated analogously as described in section 3.1.3 for the mean Sherwood number.

The explicit scheme evaluates the temperatures in the finite-difference approximation at the previous time $t = p\Delta t$, where p is a positive integer. Solving eq. (3.15) for the new temperature of the bulk water at time $t = (p+1)\Delta t$ therefore yields

$$T_{i,b}^{p+1} = \frac{v\Delta t}{\Delta z_i}T_{i-1,b}^{p} + \frac{4\overline{h}_i\Delta t}{\rho_w c_w a}T_{i,0}^{p} + \left(1 - \frac{v\Delta t}{\Delta z_i} - \frac{4\overline{h}_i\Delta t}{\rho_w c_w a}\right)T_{i,b}^{p} \tag{3.16}$$

where the superscripts denote the time level. The explicit solution scheme is stable if the "coefficient associated with the node of interest at the previous time is greater than or equal to zero" (Incropera and DeWitt, 1996). Thus, the stability criterion is found to be

$$\left(\frac{v}{\Delta z_i} + \frac{4\overline{h}_i}{\rho_w c_w a}\right)\Delta t \leq 1 \tag{3.17}$$

Note that this equation is equivalent to the Courant criterion (eq. 3.4) if the first term in

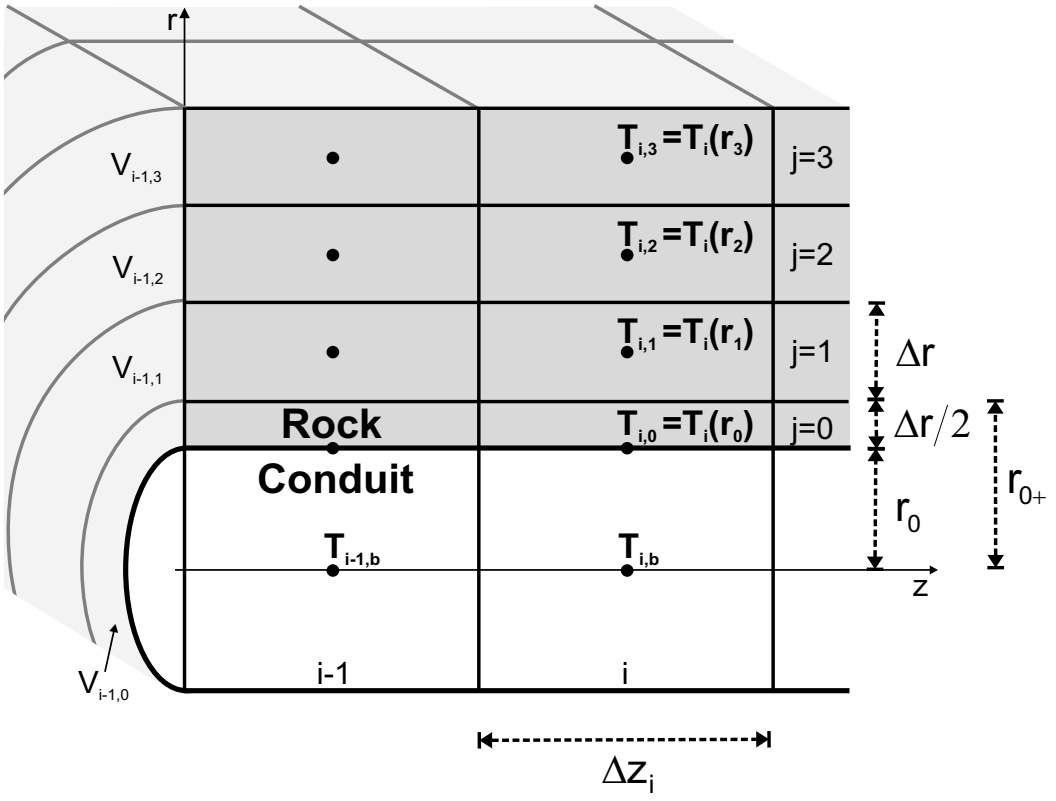

Figure 3.3: Discretisation of a conduit and the surrounding rock matrix (cross-section along and perpendicular to the conduit).

the parenthesis on the left hand side is much greater than the second.

In order to calculate the temperature at the pipe wall eq. (2.52) and eq. (2.54) have to be combined. The explicit formulation of the finite-difference approximation is obtained by considering the energy balance for the discrete rock volume element $V_{i,0} = \pi \Delta z_i (r_{0_+}^2 - r_0^2)$ associated with the surface node $(i, 0)$ (see Fig. 3.3):

$$\rho_r c_r V_{i,0} \frac{T_{i,0}^{p+1} - T_{i,0}^{p}}{\Delta t} = \overline{h}_i A_{i,0} \left(T_{i,b}^{p} - T_{i,0}^{p} \right) + \lambda_r A_{i,0_+} \frac{T_{i,1}^{p} - T_{i,0}^{p}}{\Delta r} \tag{3.18}$$

where ρ_r denotes the density [kg m^{-3}], c_r the specific heat [J kg^{-1} K^{-1}], and λ_r the thermal conductivity of the rock [J m^{-1} K^{-1}], $A_{i,0} = 2\pi \Delta z_i r_0$ and $A_{i,0_+} = 2\pi \Delta z_i r_{0_+}$ are the inner and outer surface areas perpendicular to the direction of conductive heat flow and $r_{0_+} = r_0 + \Delta r/2$. The left hand side of eq. (3.18) represents the change of energy in the volume element. The first term on the right hand side describes heat transfer between pipe wall and water, whilst the second represents conduction in the rock. Solving the equation for the new wall temperature yields

$$T_{i,0}^{p+1} = \frac{2\overline{h}_i r_0 \Delta t}{\rho_r c_r (r_{0_+}^2 - r_0^2)} (T_{i,b}^{p} - T_{i,0}^{p}) + \frac{2\kappa_r r_{0_+} \Delta t}{\Delta r (r_{0_+}^2 - r_0^2)} (T_{i,1}^{p} - T_{i,0}^{p}) + T_{i,0}^{p} \tag{3.19}$$

In order to derive a stability criterion the equation has to be rearranged:

$$T_{i,0}^{p+1} = \frac{4 N_{Fo} N_{Bi} r_0}{r_{0_+} + r_0} T_{i,b}^{p} + \frac{4 N_{Fo} r_{0_+}}{r_{0_+} + r_0} T_{i,1} + \left(1 - \frac{4 N_{Fo}}{r_{0_+} + r_0} \left(r_0 N_{Bi} + r_{0_+} \right) \right) T_{i,1}^{p} \tag{3.20}$$

where a finite-difference form of the Fourier number is given by

$$N_{Fo} = \frac{\kappa_r \Delta t}{(\Delta r)^2} \tag{3.21}$$

and a finite-difference form of the Biot number is

$$N_{Bi} = \frac{\overline{h}_i \Delta r}{\lambda_r} \tag{3.22}$$

The explicit solution scheme is stable if the coefficients associated with the temperatures are greater than or equal to zero, thus

$$N_{Fo} \leq \frac{r_{0_+} + r_0}{4(r_0 N_{Bi} + r_{0_+})} \tag{3.23}$$

Likewise the finite-difference approximation for the rock temperature is derived by considering the energy balance of a volume element $V_{i,j} = \pi \Delta z_i (r_{j_+}^2 - r_{j_-}^2)$, where $r_{j_+} = r_j + \Delta r/2$ and $r_{j_-} = r_j - \Delta r/2$. At an inner node of the rock matrix conservation of energy requires that

$$\rho_r c_r V_{i,0} \frac{T_{i,j}^{p+1} - T_{i,j}^{p}}{\Delta t} = \lambda_r A_{i,j_-} \frac{T_{i,j-1}^{p} - T_{i,j}^{p}}{\Delta r} + \lambda_r A_{i,j_+} \frac{T_{i,j+1}^{p} - T_{i,j}^{p}}{\Delta r} \tag{3.24}$$

where $A_{i,j_-} = 2\pi \Delta z_i r_{j_-}$ and $A_{i,j_+} = 2\pi \Delta z_i r_{j_+}$ are the inner and outer surface areas perpendicular to the direction of conductive heat flow. Solving for the new temperature yields

$$T_{i,j}^{p+1} = N_{Fo} \frac{r_{j_-} T_{i,j-1}^{p} + r_{j_+} T_{i,j+1}^{p}}{r_j} + (1 - 2N_{Fo}) T_{i,j}^{p} \tag{3.25}$$

The corresponding stability criterion reads

$$N_{Fo} \leq \frac{1}{2} \tag{3.26}$$

Each of the three stability criteria given by eq. (3.17), eq. (3.23) and eq. (3.26) has to be satisfied by the coupled solution scheme. Since $N_{Bi} \geq 0$ and $r_{0_+} \geq r_0$, the third criterion (eq. 3.26) is always met if the second (eq. 3.23) is fulfilled. Therefore, a time step length is calculated which satisfies both eq. (3.17) and eq. (3.23).

In order to solve the above equations the initial temperatures of rock and water have to be defined. The initial temperature of the rock is also chosen as a fixed temperature boundary condition for the rock matrix at a "large" distance from the conduit. It is important to set up this boundary at a distance from the conduit large enough to keep the heat flux at the boundary negligible. Moreover, the temperatures of the inflow to the pipes have to be known. Therefore, a mixing temperature is calculated at each node of the pipe network according to eq. (2.53), where the temperatures of inflow from external sources (i.e. recharge and flow from the fissured system) are required as boundary conditions.

3.2 Verification

3.2.1 Flow

Flow in the fissured system is simulated using the finite-difference code MODFLOW (see section 3.1.1). Since "MODFLOW is probably the most widely used, tested and verified model today" (Krešić, 1997), there is no need for further verification.

Hückinghaus (1998) verified the pipe network module CONDUIT (see section 3.1.1), which is coupled to MODFLOW. Using the CONDUIT module and the program STRO (Horlacher and Lüdecke, 1992) he computed hydraulic heads and flow rates for single conduits as well as for pipe networks. The results obtained by the two programs agreed very well for both laminar and turbulent flow conditions. Further, comparing flow rates calculated by the CONDUIT module and the finite-element code ROCKFLOW (Wollrath and Helmig, 1992) yielded deviations of less than 1.5% (Clemens, 1998).

3.2.2 Solute Transport

In order to verify the implementation of advective transport in the solute mass transport module MTM, the pipe network shown in Fig. 3.4 is used.

In a single conduit of constant diameter the residence time (i.e. the travel time, tracer

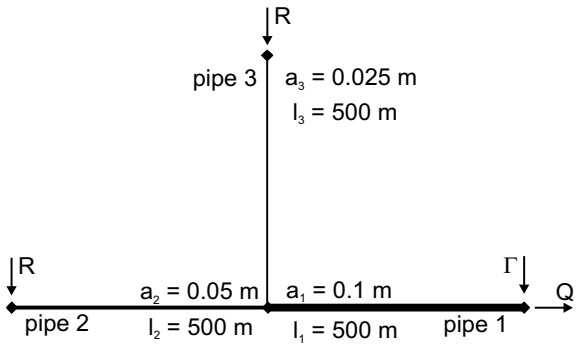

Figure 3.4: Pipe network for the verification of the solute transport module.

breakthrough time) t_r of a tracer which is transported by advection under steady-state flow conditions through a conduit of length l equals

$$t_r = \frac{l}{v} = \frac{\pi a^2 l}{4Q} \tag{3.27}$$

where the velocity v is given by eq. (2.11). Eq. (3.27) is applied for the analytical calculation of the residence time of water in the pipe network.

Pipe 2 and pipe 3 are supplied by a recharge of $R = 0.3142$ l s^{-1} yielding a flow velocity of 0.16 m s^{-1} in pipe 2 and of 0.32 m s^{-1} in pipe 3. Water from pipe 2 and pipe 3 flows into pipe 1. Therefore, the flow rate in pipe 1 is $2R = 0.6284$ l s^{-1}, and the velocity is 0.08 m s^{-1}. In order to check the mixing of waters from the fissured system and the conduit system, fixed heads are assigned to both the continuum flow model and the pipe flow model at the outflow from the pipe network, so that the head difference between the two flow systems amounts to 1 m. The exchange coefficient at this node is set to 0.0001 m^2 s^{-1} yielding a flow rate of $\Gamma = 0.1$ l s^{-1} from the fissured system to the conduit system, and thus a total outflow rate of $Q = 0.7284$ l s^{-1}. At the other nodes the exchange between fissured system and conduit system is switched off.

For convenience, dimensionless concentrations are used in this chapter. This will be especially helpful in comparing results of solute transport calculations to heat transport calculations. Normalised concentrations are defined as

$$c_{norm}(t) = \frac{c(t) - c_{imp}}{c_{ini} - c_{imp}} \tag{3.28}$$

where $c_{norm}(t)$ is the dimensionless normalised concentration, $c(t)$ is solute concentration [mol m^{-3}] at time t, c_{ini} is initial solute concentration of water in the conduits [mol m^{-3}], and c_{imp} is concentration of recharge water [mol m^{-3}]. A dimensionless concentration of one represents the initial solute concentration of the water in the conduit system and a dimensionless concentration of zero corresponds to the recharge concentration. Further, in the scenarios used for the model verification, the concentration of water in the fissured system is set equal to the initial concentration, i.e. the dimensionless concentration of water flowing from the fissured system into the conduit system is assumed to be one.

Knowing initial concentrations and inflow concentrations as well as the residence time of water in pipe 2 and pipe 3, the time-dependent concentration of the inflow to pipe 1 can be calculated by use of eq. (2.14). Taking further into account the residence time in pipe 1, eq. (2.14) can be applied to the outlet of the pipe network, where the conduit water is mixed with water from the fissured system, yielding the time-dependent outflow concentration.

Fig. 3.5 compares the concentrations at the outlet of the pipe network calculated numerically by the solute mass transport module and analytically as described above. The numerical computations were performed using different discretisations into pipe segments of length Δz. For each Δz the maximum time discretisation determined by the Courant criterion (eq. 3.4) was chosen as time step length in the simulation. Refining the discretisation of space, therefore, involved the usage of smaller time steps.

The concentration at the outlet decreases in two discrete steps, each of which marks

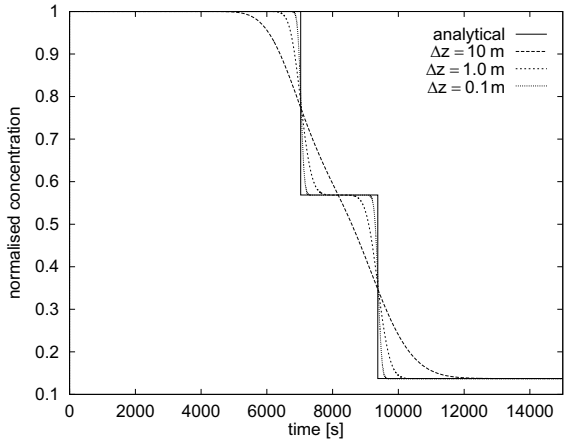

Figure 3.5: Verification of advective solute transport: Signal at the outlet of the pipe network shown in Fig. 3.4.

the arrival of recharge water from one injection point. Since purely advective transport is considered, a sharp concentration front as shown by the analytical calculation is expected. Yet, the numerically calculated breakthrough curves show a spreading. The spreading is an effect of the finite-difference scheme, which distributes the solute mass arriving in a pipe segment immediately over the entire volume of the segment. Since this spreading effect is similar to dispersion, it is termed numerical dispersion. The artificial dispersion coefficient resulting from this effect is given by Kinzelbach (1992) as

$$D_{dis} = \frac{v\Delta z - v^2\Delta t}{2} \qquad (3.29)$$

Both Fig. 3.5 and eq. (3.29) demonstrate that numerical dispersion can be reduced by refining the discretisation of space and time.

The numerical solution is exact if the Courant number $N_{Co} = v\Delta t/\Delta z$ equals one for each pipe segment (compare eq. 3.29). If the flow velocity is constant within the pipe network numerical dispersion can be avoided by adjusting the discretisation of space and time accordingly. Fig. 3.6 shows two pipe networks consisting of pipes of 0.1 m. Since there is only one injection point for recharge and no exchange with the fissured system, the flow velocities are constant within these systems. Therefore, the numerical calculation should

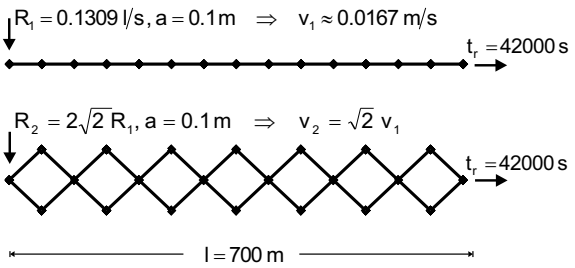

Figure 3.6: Pipe networks with identical tracer breakthrough times.

yield a sharp concentration front for both of the networks.

The recharge rates are chosen so that the residence times are identical for the two systems. Fig. 3.7 shows that the numerical calculation for the single conduit composed of 14 pipes and the analytical solution agree exactly. Moreover, the numerical result is identical for the two pipe networks as can be seen by comparing Fig. 3.7 and Fig. 3.8. The mixing of waters at the nodes of the network does not cause any deviation from the exact solution. In more complex systems, where flow velocities vary in space and time, the requirement $N_{Co} = 1$ is usually not met everywhere. Hence, numerical dispersion cannot be avoided completely if an upwind finite-difference scheme is employed.

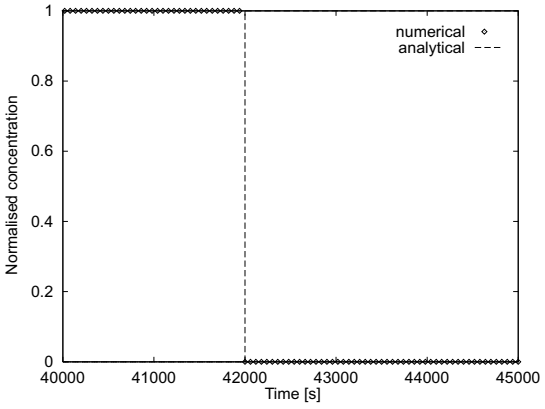

Figure 3.7: Verification of advective solute transport: Signal at the outlet of the single conduit shown in Fig. 3.6.

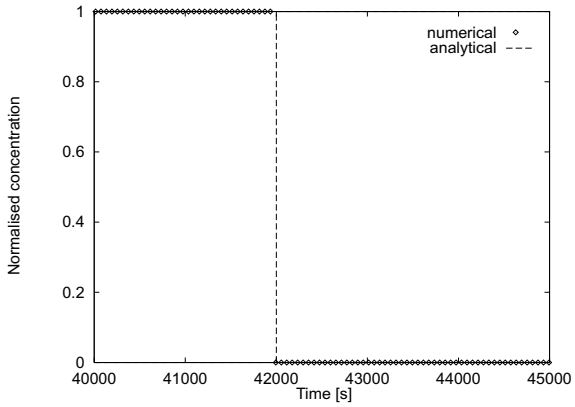

Figure 3.8: Advective solute transport: Signal at the outlets of the pipe network shown in the lower part of Fig. 3.6.

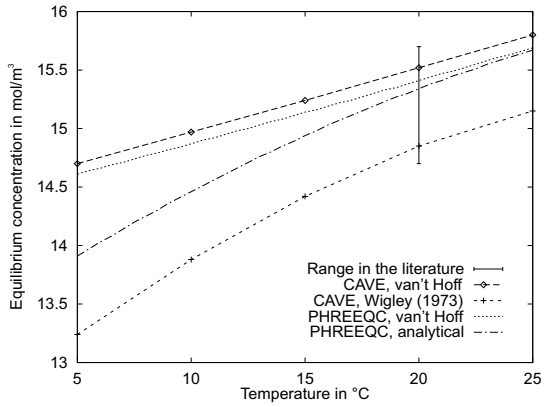

Figure 3.9: Equilibrium concentration for gypsum calculated by CAVE and by PHREEQC compared to the range found in the literature (see Tab. 3.2).

3.2.3 Gypsum dissolution

3.2.3.1 Chemical equilibrium

The gypsum dissolution module EDI calculates equilibrium concentrations of calcium and sulfate in pure water depending on the water temperature. The temperature dependence of the solubility product K_g is given either by the empirical equation (2.22) (Wigley, 1973) or by the van't Hoff equation (2.21). Input parameters used for the application of the two methods were taken from Appelo and Postma (1993) (see Tab. 3.1).

Table 3.1: Input parameters for the calculation of the equilibrium concentration. The values for gypsum are not used if the empirical equation given by Wigley (1973) is applied.

	$-\log K_g(25°\mathrm{C})$	ΔH [kJ mol^{-1}]
Gypsum	4.58	-0.456
$CaSO_4^0$	2.30	-6.90

The results obtained by CAVE were compared to results from the geochemical modelling program PHREEQC (Parkhurst, 1995). PHREEQC calculates temperature dependent values of the equilibrium constant using either the van't Hoff equation or an analytical expression. Fig. 3.9 shows the resulting equilibrium concentrations.

The values resulting from the application of the van't Hoff equation agree well between CAVE and PHREEQC. The empirical equation implemented in CAVE yields lower values than those calculated by PHREEQC. Nevertheless, the range in the literature is larger than the deviations between the calculations (Tab. 3.2 and Fig. 3.9).

Table 3.2: Equilibrium concentration for gypsum in contact with pure water at 20 °C.

Source	c_{eq} in mol m^{-3}
James (1992)	14.7
Christofferson & Chr. (1976)	15.3 ± 0.2
Liu & Dreybrodt (1997)	15.4
Jeschke et al. (2001)	15.5 ± 0.2

In the following calculations the equilibrium concentration has been set to 15 mol m^{-3}.

3.2.3.2 Dissolution kinetics

Dissolution kinetics of gypsum is assumed to be diffusion controlled. Therefore, the value of the joint diffusion coefficient of calcium and sulfate is an important parameter when calculating dissolution rates. Dreybrodt (1988) gives values for the diffusion coefficients of the single ions at 0 °C, 18 °C and 25 °C. Using these values as input for eq. (2.32) joint diffusion coefficients were calculated for each

temperature (Tab. 3.3, second column). In order to check the temperature correction of the diffusion coefficient implemented in CAVE (eq. 2.31), the joint diffusion coefficients at 0 °C and 25 °C were computed based on the values at 18 °C (Tab. 3.3, third column). Table 3.3 shows that the values computed by CAVE are close to those based on the data from the literature.

Table 3.3: Joint diffusion coefficients for calcium and sulfate ions in water calculated using values from Dreybrodt (1988) for the single ions at various temperatures. The values calculated by CAVE were based on the diffusion coefficients at 18 °C only.

	D in 10^{-10} m^2 s^{-1}	
T in °C	Dreybrodt (1988)	CAVE
0	4.27	4.24
18	*7.66*	*7.66*
25	9.11	9.28

In the following calculations the diffusion coefficient has been set to $6{\cdot}10^{-10}$ m^2 s^{-1}, which corresponds to a water temperature of 10 °C.

In order to verify the computation of gypsum dissolution rates and the coupling of dissolution reaction and advective transport, the pipe network shown in Fig. 3.4 is used to simulate reactive transport. The analytical calculation of the outflow concentrations is analogous as described for purely advective solute transport (section 3.2.2). Additionally, the increase in concentration due to gypsum dissolution is calculated by applying an analytical solution for the outflow concentrations. Like for a pipe segment in section 3.1.3.1, eq. (3.7) can be integrated from the conduit entrance to any position z along the conduit. Solving the resulting equation for the concentration at z yields

$$c(z) = c_{eq} - (c_{eq} - c_{in}) \exp\left(-\frac{\overline{N}_{Sh} D \pi}{Q} z\right) \tag{3.30}$$

where c_{in} is the concentration at the conduit entrance, and the mean Sherwood number is given by

$$\overline{N}_{Sh} = \frac{1}{z} \int_0^z N_{Sh} dz \tag{3.31}$$

Thus, the outflow concentration of a conduit of length l is obtained by setting $z = l$.

In turbulent flow the mean Sherwood number is given by eq. (2.37) or by eq. (2.38). In laminar flow far from the conduit entrance the diffusion boundary layer is fully developed and the Sherwood number is a constant of 3.66. Inserting eq. (2.36) into eq. (3.31), and replacing the velocity by the flow rate we find that in the entrance region the mean Sherwood number is given by

$$\overline{N}_{Sh} = 1.75 \left(\frac{Q}{Dz}\right)^{1/3} \tag{3.32}$$

Under the conditions considered in section 3.2.2 flow is turbulent in the pipe network. Fig. 3.10 shows the normalised concentrations if eq. (2.37) is applied for the calculation of the Sherwood number. The analytical and the numerical calculations agree well if a small discretisation Δz is chosen to reduce numerical dispersion (see section 3.2.2).

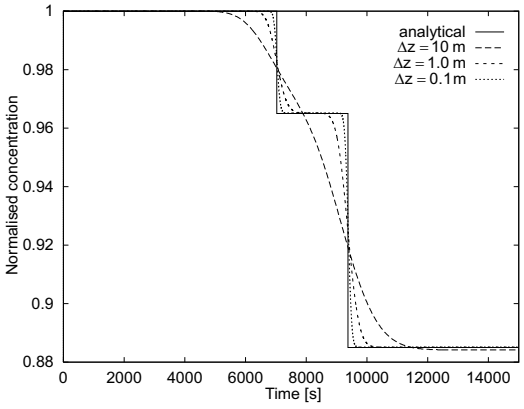

Figure 3.10: Verification of gypsum dissolution and transport in turbulent flow: Signal at the outlet of the pipe network shown in Fig. 3.4 using the Sherwood number given by eq. (2.37).

Fig. 3.11 shows the resulting concentrations if eq. (2.38) is applied. This equation includes the friction factor which depends on the

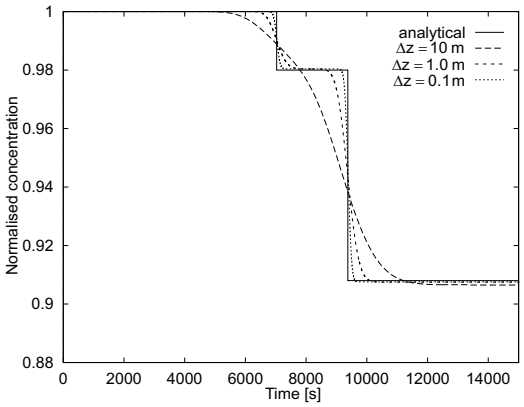

Figure 3.11: Verification of gypsum dissolution and transport in turbulent flow: Signal at the outlet of the pipe network shown in Fig. 3.4 using the Sherwood number given by eq. (2.38).

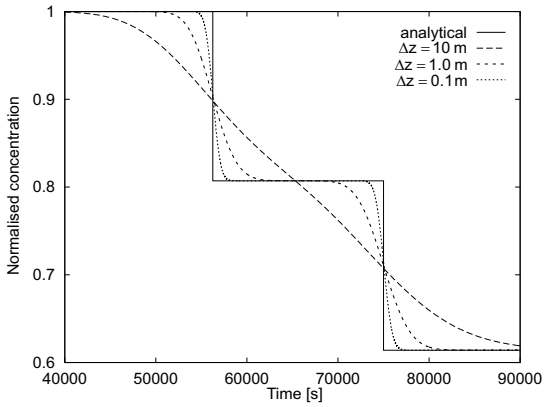

Figure 3.12: Verification of gypsum dissolution and transport in laminar flow: Signal at the outlet of the pipe network shown in Fig. 3.4 assuming a fully developed diffusion boundary layer.

roughness of the pipe wall via the Colebrook-White equation (2.6). The roughness of the pipe wall was set to 1% of the pipe diameters ($k = 0.01a$). Again the numerical calculation reproduces the expected concentrations well. A comparison of the two methods shows that the application of the more accurate equation (2.38) yields slightly higher concentrations. Yet, if the roughness of the pipe wall is not well known eq. (2.37) provides a reasonable approximation for the Sherwood number.

In order to check the calculation of the dissolution rates under laminar flow conditions, the recharge rates were reduced to 0.03927 l s^{-1}. Thus, the flow velocities are 1 cm s^{-1} in pipe 1, 2 cm s^{-1} in pipe 2 and 4 cm s^{-1} in pipe 3. In the first simulation (Fig. 3.12) a fully developed diffusion boundary layer was assumed ($N_{Sh} = 3.66$). Two further simulations were performed taking into account the incomplete development of the boundary layer in the entrance region. Firstly, a mean Sherwood number was computed for each pipe segment depending on the distance from the pipe entrance (eq. 3.11). Secondly, a mean Sherwood number for a pipe of 500 m length was used for the numerical calculation (eq. 3.32 with $z = 500\ m$), i.e. the same value as used for the analytical calculation. The two simulations yielded identical results which are shown in Fig. 3.13.

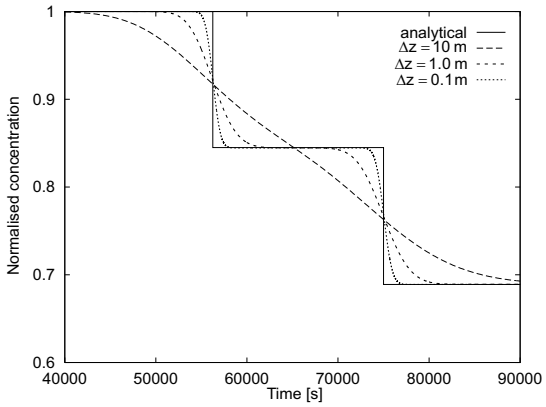

Figure 3.13: Verification of gypsum dissolution and transport in laminar flow: Signal at the outlet of the pipe network shown in Fig. 3.4 taking into account the incompletely developed diffusion boundary layer in the entrance region.

In any case the numerical and analytical calculations agree well if the length of the pipe segments Δz is sufficiently small. For all values of Δz the concentration at the outlet is considerably underestimated in this model scenario if a fully developed diffusion boundary layer is assumed. Flow velocities are too high to allow a full development of the diffusion boundary layer along the pipes. This results in higher concentrations, because a thinner boundary layer enhances the diffusion controlled dissolution reaction of gypsum. If the flow rates are lower or the conduits are longer the assumption of a fully developed boundary layer may be justified.

3.2.3.3 Conduit enlargement

In section 2.3.3 a relation between increase in conduit diameter and dissolution rate was derived (eq. 2.43). Replacing the dissolution rate by the first-order rate law eq. (2.29) yields a relation between the rate of conduit enlargement and the concentration

$$\frac{da}{dt} = \frac{2}{\rho_g} k(c_{eq} - c) \tag{3.33}$$

The mass transfer coefficient k can be replaced by eq. (2.34) yielding

$$\frac{da}{dt} = \frac{2}{\rho_g} \frac{N_{Sh} D}{a} (c_{eq} - c) \tag{3.34}$$

In the above equations c is the local concentration of the bulk solution at a distance z from the conduit entrance. Under steady-state flow conditions the concentration profile along the conduit can be calculated analytically by eq. (3.30) as a function of the mean Sherwood number for the conduit.

In turbulent flow the Sherwood number is empirically correlated to the Reynolds number (eq. 2.37, eq. 2.38), i.e. the Sherwood number depends on the conduit diameter. If the conduit is enlarged the concentration profile changes in time. In laminar flow, however, the mean Sherwood number is independent of the conduit diameter ($\overline{N}_{Sh} = 3.66$ or eq. 3.32, respectively). Under laminar and steady-state flow conditions, therefore, the concentration $c(z)$ does not change with time if the conduit is enlarged, and eq. (3.34) can be solved by integration

$$\int_{a_0}^{a(c,t)} a\,da = 2\rho_g \overline{N}_{Sh} D (c_{eq} - c) \int_0^t dt \tag{3.35}$$

yielding an analytical solution for the development of the conduit diameter in time

$$a(c,t) = \sqrt{a_0^2 + \frac{4\overline{N}_{Sh} D}{\rho_g} (c_{eq} - c) t} \tag{3.36}$$

where a_0 is the diameter at the time $t = 0$. Inserting eq. (3.30) yields the diameter as a function of the distance from the conduit entrance z and the time t

$$a(z,t) = \sqrt{a_0^2 + \frac{4\overline{N}_{Sh} D}{\rho_g} (c_{eq} - c_{in}) \exp\left(-\frac{\overline{N}_{Sh} D \pi}{Q} z\right) t} \tag{3.37}$$

This equation was employed for the calculation of the enlargement of a single conduit composed of 14 pipes (Fig. 3.6, upper part) under a steady-state flow rate of 0.1309 l s^{-1}. Fig. 3.14 shows the development of the numerically calculated hydraulic diameter of the pipe at the outlet. In one simulation a fully developed diffusion boundary layer was assumed. For the other simulation the mean Sherwood number was calculated taking into account the incomplete development of the boundary layer in the entrance region. In both cases, the numerical simulation fits very well the analytical solution for the conduit diameter at the outlet ($z = 700$ m).

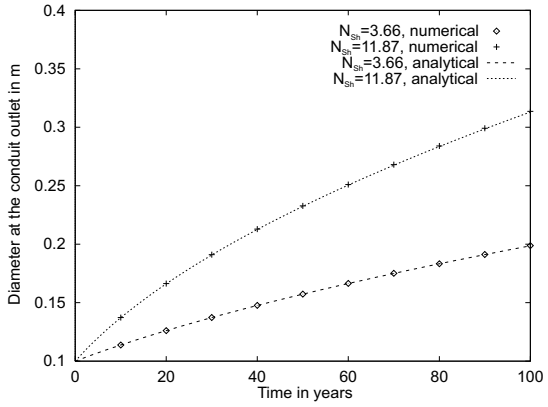

Figure 3.14: Development of the diameter at the outlet of a single conduit (Fig. 3.6) assuming a fully developed diffusion boundary layer ($N_{Sh} = 3.66$) or taking into account the entrance region ($N_{Sh} = 11.87$, i.e. using a mean Sherwood number for a conduit of 700 m length).

Fig. 3.15 shows the diameter as a function of the distance from the conduit entrance after a simulation time of 100 years. Again the numerical and analytical calculations agree very well. The diameter of the conduit is almost constant along the conduit axis in the case of the lower Sherwood number of $\overline{N}_{Sh} = 3.66$.

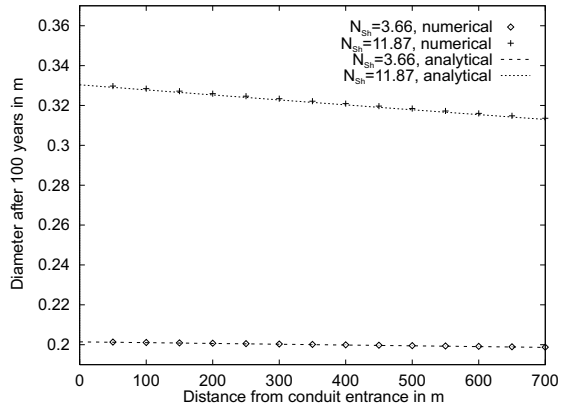

Figure 3.15: Diameters of a single conduit (Fig. 3.6) after 100 years of gypsum dissolution assuming a fully developed diffusion boundary layer ($N_{Sh} = 3.66$) or taking into account the entrance region ($N_{Sh} = 11.87$, i.e. using an average Sherwood number for a conduit of 700 m length).

Because of the low dissolution rates the concentration remains nearly constant at zero along the conduit. Hence, the rate of conduit enlargement is nearly constant too. In the case of the higher Sherwood number, however, the increase of the concentration along the conduit results in a marked decrease of dissolution rates and diameters.

The assumption of a fully developed boundary layer yields an underestimation of conduit diameters. As mentioned in the previous section, the effect of the entrance region may be negligible if conduits are much longer or flow rates much lower than in this scenario.

3.2.4 Heat transfer

The heat transport module HTM couples heat transport processes in the conduit to heat conduction in the rock. For verification purposes heat transfer in conduit flow is first considered separately. After that, the coupled processes are examined.

3.2.4.1 Heat transfer in conduit flow

If a constant wall temperature is assumed heat transfer in conduit flow is analogous to the diffusion controlled dissolution of gypsum. The corresponding analytical solution of eqs. (2.44) and (2.52) for the water temperature along a conduit under steady-state conditions reads:

$$T(z) = T_s - (T_s - T_{in}) \exp\left(-\overline{N}_{Nu} \kappa_w \frac{\pi z}{Q}\right) \tag{3.38}$$

where T_{in} is the water temperature at the conduit entrance, T_s is the temperature of the conduit wall, and the mean Nusselt number is given by

$$\overline{N}_{Nu} = \frac{1}{z} \int_0^z N_{Nu} dz \tag{3.39}$$

The temperature of the outflow from a conduit of length l is obtained by setting $z = l$.

In turbulent flow the mean Nusselt number is given by eq. (2.50) or by eq. (2.51). In laminar flow far from the conduit entrance the thermal boundary layer is fully developed and the Nusselt number is a constant of 3.66. Inserting eq. (2.48) in eq. (3.39), and replacing the velocity by the flow rate we find that in the entrance region the mean Nusselt number is given by

$$\overline{N}_{Nu} = 1.75 \left(\frac{Q}{\kappa_w z}\right)^{1/3} \tag{3.40}$$

The specific heat of water c_w is 4198 J kg^{-1} K^{-1}, and the thermal conductivity λ_w is 0.582 J m^{-1} K^{-1} (Incropera and DeWitt, 1996). With the density of water (999.7 kg m^{-3} at 10 °C) the thermal diffusivity of water $\kappa_w = 1.39 \cdot 10^{-7}$ m^2 s^{-1} results from eq. (2.49). This value is more than two orders of magnitude greater than the diffusion coefficient used for the calculation of dissolution rates of gypsum. Therefore, the water flowing in a conduit is much faster adjusted to the wall temperature than it is saturated with respect to gypsum. For that reason the pipe network shown in Fig. 3.4 was modified by reducing the length of the pipes by two orders of magnitude to 5 m (Fig. 3.16). The other flow parameters were

taken from the corresponding scenarios used for the verification of gypsum dissolution in section 3.2.3.2.

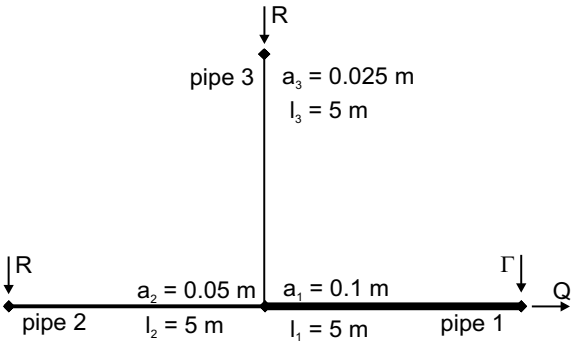

Figure 3.16: Pipe network for the verification of heat transfer in conduit flow.

The temperature of the recharge water was set to 6 °C. Rock temperature, initial temperature of the water as well as the water temperature in the fissured system were set to 8 °C. In the numerical simulation, the rock matrix is discretised into huge volume elements (Δr = 1000 m), so that the heat capacity of the volume elements representing the conduit wall is large enough to maintain a constant wall temperature over the entire simulation period. As previously seen for solute transport the temperature at the outlet is expected to drop in two steps, each of which marks the arrival of recharge water. The resulting temperatures $T(t)$ were normalised according to

$$T_{norm}(t) = \frac{T(t) - T_{imp}}{T_{ini} - T_{imp}} \tag{3.41}$$

where T_{imp} is the temperature of the recharge, and T_{ini} is the initial temperature of the conduit water. Thus, a normalised temperature of one corresponds to the initial conditions, whereas a normalised temperature of zero corresponds to the temperature of the recharge.

Fig. 3.17 and Fig. 3.18 show the normalised temperatures at the outlet of the network for turbulent flow conditions calculated using eq. (2.50) and eq. (2.51), respectively.

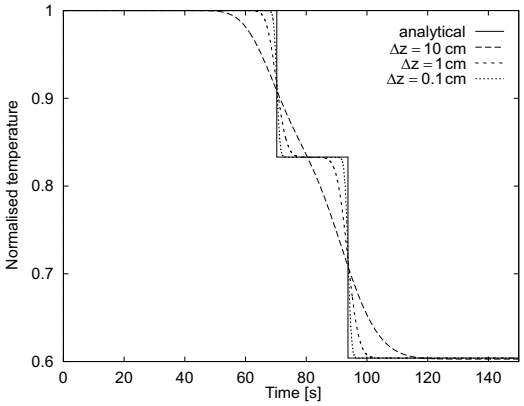

Figure 3.17: Verification of heat transfer in turbulent flow through conduits with a constant wall temperature: Signal at the outlet of the pipe network shown in Fig. 3.16 using the Nusselt number as given by eq. (2.50).

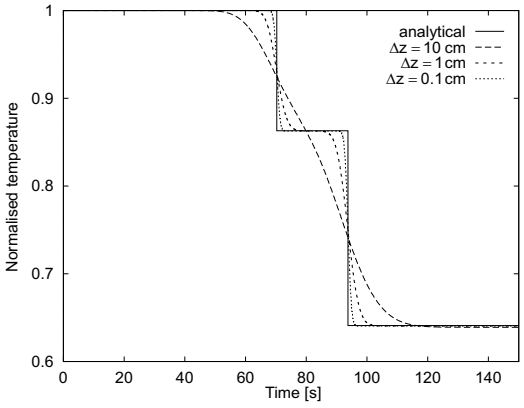

Figure 3.18: Verification of heat transfer in turbulent flow through conduits with a constant wall temperature: Signal at the outlet of the pipe network shown in Fig. 3.16 using the Nusselt number as given by eq. (2.51).

Fig. 3.19 shows the temperatures at the outlet of the network for laminar flow conditions, assuming a fully developed thermal boundary layer. In Fig. 3.20 the incomplete developed boundary layer near the conduit entrance was taken into account. The agreement between numerical calculation and analytical solution is reasonably well if the discretisation of the pipes into pipe segments of length Δz is sufficiently small. Simulation results depend on the selection of an empirical equation (i.e. eq. 2.50 or eq. 2.51) for the calculation of Nusselt numbers in turbulent flow (compare Fig. 3.17 and Fig. 3.18). For laminar flow conditions the assumption of a

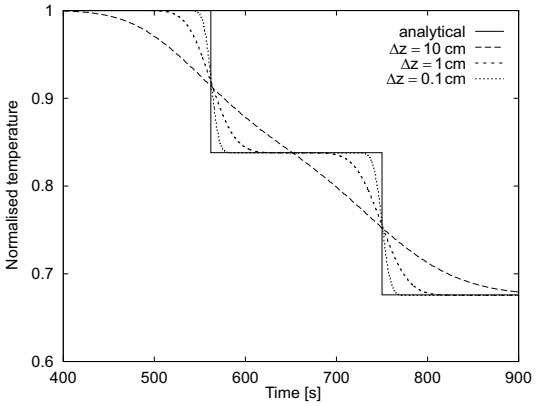

Figure 3.19: Verification of heat transfer in laminar flow through conduits with a constant wall temperature: Signal at the outlet of the pipe network shown in Fig. 3.16 assuming a fully developed diffusion boundary layer.

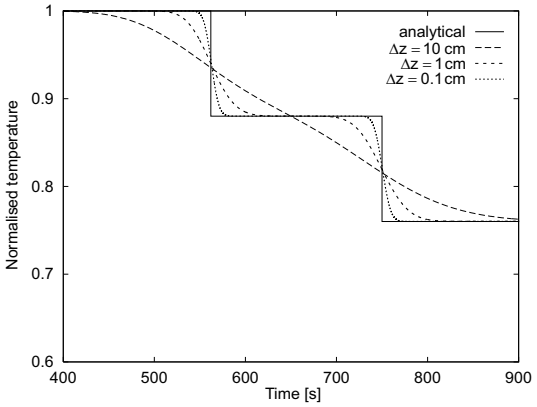

Figure 3.20: Verification of heat transfer in laminar flow through conduits with a constant wall temperature: Signal at the outlet of the pipe network shown in Fig. 3.16 taking into account the incomplete developed diffusion boundary layer in the entrance region.

fully developed thermal boundary layer yields lower water temperatures at the outlet than a simulation which takes into account that the boundary layer is not fully developed along the pipes. These results are very similar to those obtained by simulations of reactive solute transport (compare section 3.2.3.2).

3.2.4.2 Coupled heat transfer in conduit flow and rock

For the verification of the coupled processes in water and rock heat transport in a single conduit under steady-state flow conditions is simulated. Assuming that the water temperature equals the wall temperature (i.e. neglecting heat transfer between conduit wall and bulk water), Hückinghaus (1998) developed a semi-analytical method for the solution of this problem. In order to solve the governing partial differential equation a Laplace transformation is applied. However, the backward transformation has to be performed numerically using an algorithm by Stehfest (1970), which was implemented in a FORTRAN code by Häfner et al. (1992).

The assumption of equal water and wall temperature is most likely met for turbulent flow conditions, where the thermal boundary layer separating conduit wall and bulk water is very thin. Therefore, flow through a single conduit of 0.1 m diameter at a velocity of 1 m s^{-1} is considered. Inserting these values and the kinematic viscosity of water (1.3 m^2 s^{-1} at 10 °C) into eq. (2.2) yields a Reynolds number of approximately 70000. The specific heat of the gypsum rock was set to 1088 J kg^{-1} K^{-1}, and the thermal conductivity was 1.297 J m^{-1} K^{-1} (Marsh, 1999). With a density of 2320 kg m^{-3} a thermal diffusivity of $\kappa_r = 5.14 \cdot 10^{-7}$ m^2 s^{-1} results. Fig. 3.21 shows the temperature of the outflow from a conduit of 10000 m length calculated with different discretisations Δr of the rock matrix. The residence time of water in the conduit is 10000 s. After that time the temperature at the outlet decreases. The temperature does not drop in a sharp step like the concentrations in solute transport. Due to the slow heat conduction in the rock, the temperature of the conduit wall and the water temperature decrease over the entire simulation period. If the discretisation is sufficiently small the numerical calculation fits well to the results from the semi-analytical method by Hückinghaus (1998). Using a discretisation of $\Delta r = 10$ cm the deviation is not negligible, while results obtained for $\Delta r = 2$ cm and $\Delta r = 1$ cm are almost identical. The temperatures calculated with these discretisations are slightly below the semi-analytical solution. This is reasonable considering that

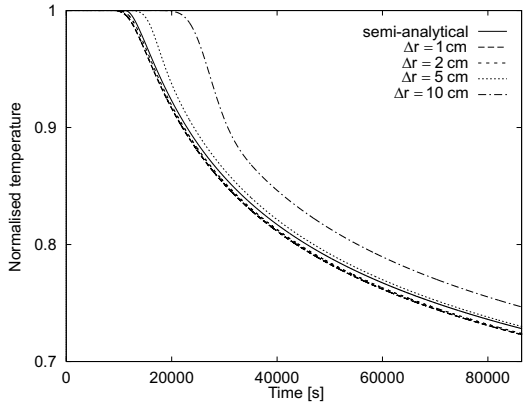

Figure 3.21: Comparison of semi-analytical calculation and numerical calculations with different discretisation of the rock matrix: Signal at the outlet of a single conduit of length 10000 m and diameter 0.1 m at a flow velocity of 1 m s^{-1}.

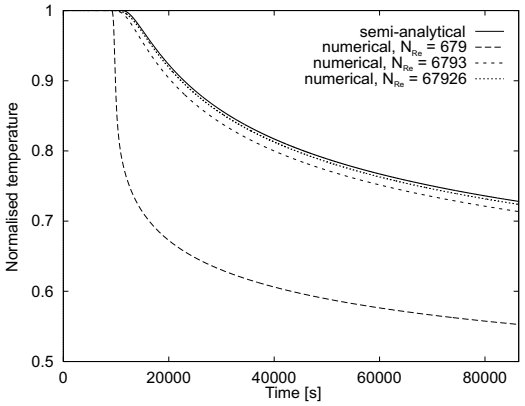

Figure 3.22: Comparison of semi-analytical calculation and numerical calculations: Signal at the outlet of single conduits of diameter 0.1 m. The flow velocity and the length of the conduits were adjusted, so that the residence time of water in the conduits is kept constant at 10000 s.

the implementation of the additional process of heat transfer between conduit wall and bulk water in the numerical method should yield a water temperature which is lower than the temperature calculated by the semi-analytical method. Thus, a discretisation of the rock into volume elements of 2 cm thickness appears to be sufficient and was used for the following simulations.

An interesting feature of the semi-analytical solution is its independence on the flow conditions in the conduit. The length of the conduit was varied and the flow velocity adjusted, so that the residence time was still maintained constant at 10000 s. Fig. 3.22 shows the results of the semi-analytical method and the numerical calculation for conduits of a length of 10000 m, 1000 m and 100 m, using a flow velocity of 1 m s^{-1}, 0.1 m s^{-1} and 0.01 m s^{-1}, respectively. As shown by the corresponding Reynolds numbers (67926, 6793 and 679, respectively) flow is laminar in the case of the lowest velocity. The result obtained by the semi-analytical method is identical in any case. While the numerically calculated outflow temperatures are close to the semi-analytical solution for turbulent flow conditions, they deviate considerably if flow is laminar. In laminar flow the heat transfer across the thermal boundary layer is slow enough to maintain a temperature difference between conduit water and rock surface. Thus, the assumption underlying the semi-analytical method is no longer justified and the semi-analytical method is not applicable.

Similar results were obtained for conduit diameters of 0.2 m (Fig. 3.23) and 0.05 m (Fig. 3.24). If flow conditions are turbulent the semi-analytical method and the numerical calculations agree well, the numerical values being slightly lower. Under laminar conditions the outflow temperatures are considerably lower, because heat transfer from the rock into the water is slower than in turbulent flow. It should be further noted that the temperature of the outflow decreases only slightly in the case of the smallest diameter (0.05 m, Fig. 3.24) used in the simulations. Hence, temperature variations at karst springs are probably mainly caused by heat transport in conduits of more than 5 cm in diameter (see also Hückinghaus, 1998).

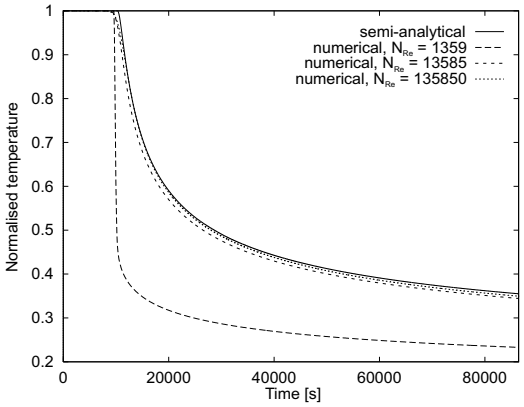

Figure 3.23: Comparison of semi-analytical calculation and numerical calculations: Signal at the outlet of single conduits of diameter 0.2 m. The flow velocity and the length of the conduits were adjusted, so that the residence time of water in the conduits is kept constant at 10000 s.

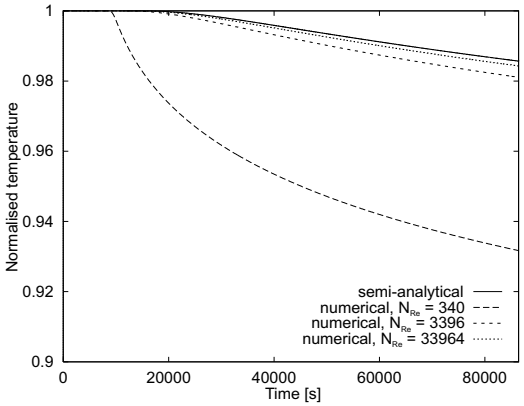

Figure 3.24: Comparison of semi-analytical calculation and numerical calculations: Signal at the outlet of single conduits of diameter 0.05 m. The flow velocity and the length of the conduits were adjusted, so that the residence time of water in the conduits is kept constant at 10000 s.

Chapter 4

Long-term karst genesis

This chapter describes the application of the newly developed modelling tool for the characterisation of gypsum karst aquifers by forward modelling of long-term karst genesis. The development of solution conduits is numerically simulated for a conceptual setting, which is based on field observations and speleogenetic concepts described in the following section.

4.1 Speleogenetic concepts

Speleogenetic concepts focus mainly on "common caves" (Ford and Williams, 1989) created by meteoric groundwater circulating in soluble rocks. These caves cover at least 90% of all known dissolutional caves longer than a few hundred metres (Ford, 2000). For this reason, caves created by waters ascending into soluble rocks from deeper strata are sometimes omitted in reviews on speleogenesis (e.g. Ford, 1998). Yet, this type of caves appears to be most important considering gypsum rocks.

The five longest gypsum caves are located in the Western Ukraine (Klimchouk, 2000b). World-wide, they account for more than half of the total known passage length of gypsum caves (Klimchouk, 1996c, 2000b). These huge Ukrainian maze caves developed under confined conditions with artesian flow from an underlying aquifer into a gypsum layer (Klimchouk, 2000b). Gypsum caves in England might be of similar origin (Cooper, 1998). Boreholes and mines have intersected gypsum caves in deep-seated settings (i.e. without an exposure of the soluble rock to the surface) under currently artesian conditions not only in the Western Ukraine but also in the Pre-Ural region of Russia and in the South Harz region of Germany (Klimchouk, 1996c). Thus, artesian speleogenesis appears to be a major mechanism of cavern genesis in gypsum.

The "classic concept of artesian flow" (Klimchouk, 2000c) implies slow lateral flow in separate aquifers. These conditions are considered to be very unfavourable for the evolution of extended maze caves (Palmer, 1991, 2000), because the groundwater becomes nearly saturated with respect to the soluble rock already near the recharge areas. The "non-classic concept" as suggested by Klimchouk (1997a, 2000c), however, takes into account that there is no true confinement, but only large permeability contrasts between different layers such that flow between the layers is not negligible. Fig. 4.1 illustrates the flow pattern in a typical artesian setting according to this concept.

In a typical artesian basin, the hydraulic heads increase with depth. The vertical hydraulic head gradient is maximised in areas of topographical lows. Thus, the flow system is characterised by upward cross-formational flow, preferentially discharging into the low elevated areas (e.g. into incised valleys). These discharge areas are most favourable for artesian speleogenesis.

Initially, soluble rocks like gypsum act as aquitards separating layers of higher permeability (i.e. aquifers). In the discharge ar-

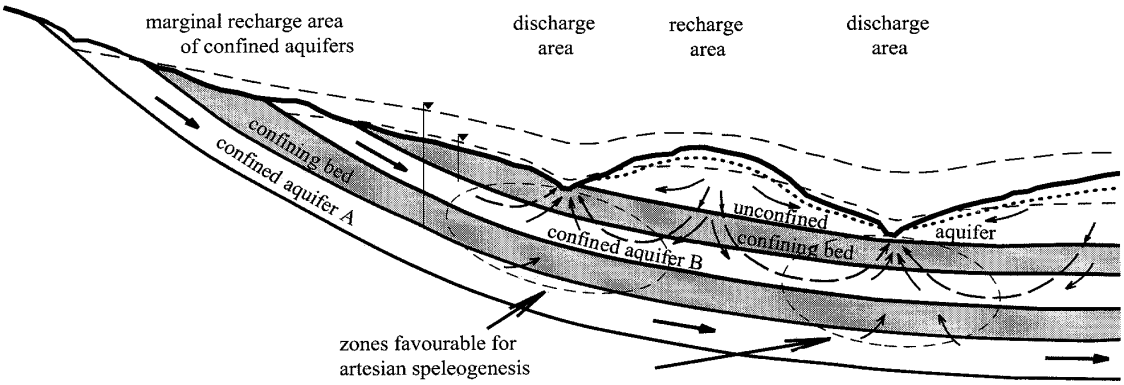

Figure 4.1: Flow pattern in a typical artesian basin (from Klimchouk, 1997a).

eas, upward flow of solutionally aggressive water from insoluble aquifers causes an enlargement of conduits in the overlying soluble units. When conduits have developed, the soluble units act as karst aquifers, which are sandwiched then between less permeable layers.

The following sections describe how this general speleogenetic concept has been transferred into a numerical model simulating the evolution of solution conduits under artesian conditions.

4.2 Model set-up

The upper part of Fig. 4.2 shows a typical artesian setting with two confined aquifers consisting of insoluble materials, e.g. sandstone, separated by an initially less permeable gypsum layer (compare Fig. 4.1). The topographic height at the left hand side acts as a recharge area. Discharge is mainly to the right. Additionally, a river cut into the confining layer drains the upper aquifer. This setup imposes a hydraulic head gradient between the aquifers and causes an upward directed flow component from the lower to the upper aquifer.

The lower part of Fig. 4.2 illustrates the translation of the conceptual setting into a numerical model. The model domain is a vertical 2D slice with a length of 506 m and a total thickness of 70 m subdivided into a gypsum layer of 22 m and two aquifers of 24 m thickness. In the numerical model the slice is represented by a vertical layer of the continuum model. The slice is vertically discretised by 35 rows of 2 m width. Laterally, it is subdivided into 95 columns. The width of the columns is set to 2 m in the centre of model domain and extended to a width of 10 m towards the left and right boundaries. The transmissivity is set to 10^{-5} m^2 s^{-1} for the aquifers and 10^{-8} m^2 s^{-1} for the gypsum. Thus, for a slice of 10 m width the hydraulic conductivities are 10^{-6} m s^{-1} for the aquifers and 10^{-9} m s^{-1} for the fissured system of the gypsum layer.

In confined aquifers, typical values for the storage coefficients are in the range from 0.005 to 0.00005 (Freeze and Cherry, 1979). In long-term karst genesis simulations with constant or slowly changing boundary conditions, storage does not significantly influence the simulation results. Therefore, the storage term in eq. 2.1 has been neglected in the model simulations presented here. Using the maximum value of the aforementioned range or neglecting the storage term yielded no significant deviation for test runs with the model scenario described in section 4.3.1.

At the left hand side and at the right hand

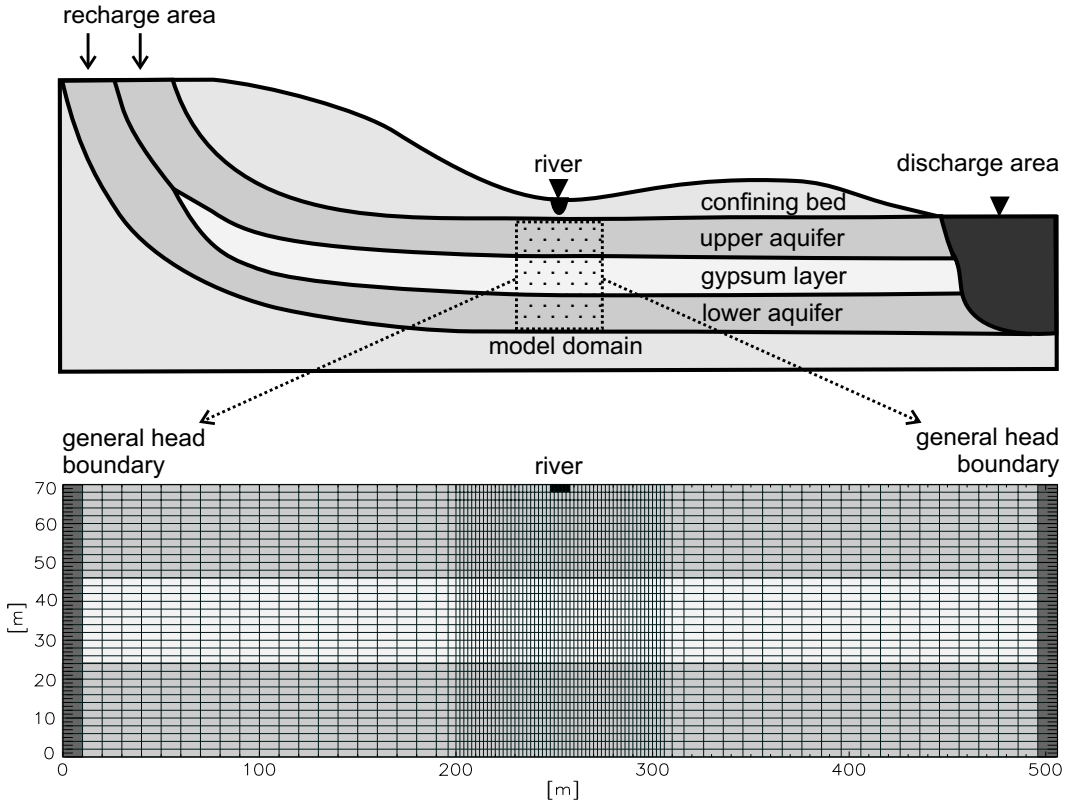

Figure 4.2: Conceptual model of an artesian setting and the corresponding numerical model.

side of the model domain general head boundaries (see section 3.1.1) with leakage factors of 10^{-8} m^2 s^{-1} for the aquifer cells and 10^{-11} m^2 s^{-1} for the cells of the gypsum layer represent recharge and discharge areas at a distance of 2 km. The elevation of the recharge area is 150 m, the discharge area is at a level of 70 m. The river draining the upper aquifer is represented by a river boundary (see section 3.1.1), which is applied to five cells at the top of the model domain. The water level of the river cells is set to 75 m, the leakage factor is $4 \cdot 10^{-8}$ m^2 s^{-1}. The bottom and top (apart from the river cells) of the model domain are no-flow boundaries.

The following sections examine the development of both single conduits (section 4.3) and conduit networks (section 4.4) in the gypsum layer beneath the river.

4.3 Single conduit development

In this section, a standard model scenario is defined, the results of which illustrate the basic principles of the concept of artesian speleogenesis (section 4.3.2). The standard parameters are varied to examine quantitatively the influence of the hydrogeological conditions on the karstification (sections 4.3.3 and 4.3.4).

4.3.1 Model scenario

Fig. 4.3 shows the central part of the model domain. Beneath the river a single conduit of 0.4 mm diameter intersects the gypsum layer. At four nodes, which subdivide the conduit into three pipes, an exchange of water between the conduit and the fissured system is allowed. The value of the exchange coefficient at the nodes, which couple the fissured systems of lower and upper aquifer to

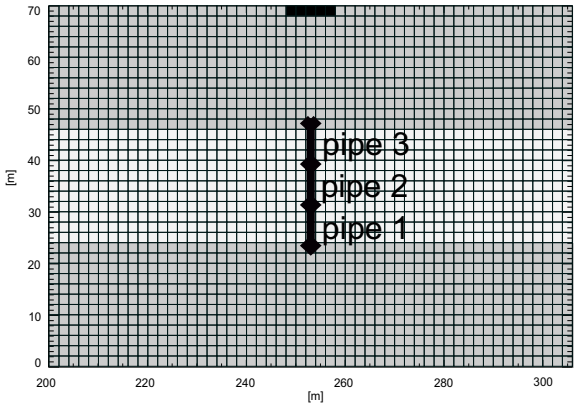

Figure 4.3: Implementation of a single conduit into the numerical model. The figure shows the middle part of the model domain only.

the conduit, was set to $2 \cdot 10^{-5}$ m^2 s^{-1}. By choosing this value the hydraulic resistance between the two aquifer nodes will be equal to the hydraulic resistance between two neighbouring cells within an aquifer if the hydraulic resistance of the conduit is negligible. It is generally believed that the exchange coefficient is proportional to the hydraulic conductivity of the fissured system (Bauer et al., 2000). Thus, the exchange coefficient at the nodes in the gypsum layer has to be smaller than that of the aquifer nodes by three orders of magnitude, i.e. an exchange coefficient of $2 \cdot 10^{-8}$ m^2 s^{-1} was chosen at the nodes in the gypsum layer.

Since flow is always directed from the lower aquifer into the gypsum layer and never reversed, the concentration of dissolved gypsum may be assumed to be zero in the lower aquifer. Thus, the conduit is supplied with aggressive water from the lower aquifer. If water transits from the gypsum layer into the conduit, however, it is assumed to be saturated with respect to gypsum. The equilibrium concentration is set to 15 mol m^{-3} ($\approx$ 2.6 g l^{-1} dissolved gypsum), and the joint diffusion coefficient of calcium and sulfate is $6 \cdot 10^{-10}$ m^2 s^{-1}. In section 3.2.3.2 these values have been shown to be reasonable at groundwater temperatures of 10 °C. The density of gypsum is set to 13600 mol m^{-3} ($\approx$ 2.3 g cm^{-3}), which is within the range given in the literature (e.g. Jubelt and Schreiter, 1980).

For laminar flow conditions a fully developed diffusion boundary layer is assumed, i.e. the Sherwood number is a constant ($N_{Sh} = 3.66$). Turbulence does not occur under the given boundary conditions. Inserting the initial diameter, the diffusion coefficient, and the Sherwood number in eq. (2.34) yields a maximum value of the mass transfer coefficient of $5.5 \cdot 10^{-6}$ m s^{-1}, which is almost two orders of magnitude smaller than the value of the surface reaction rate constant (see section 2.3.2.2). Thus, the assumption of a diffusion controlled dissolution process is justified for the given model scenario.

Using this model set-up a period of 1000 years was simulated using a time step length of one month.

4.3.2 Simulation results

Regarding pipe diameters and hydraulic heads, two stages of conduit development, separated by a short transition period, can be distinguished (Fig. 4.4). At the early stage the water flowing from the conduit into the upper aquifer is saturated with respect to gypsum. Therefore, the uppermost pipe is not enlarged and restricts the discharge through the conduit. Therefore, conduit growth is very slow and the hydraulic head gradient between the aquifers is maintained (Fig. 4.4a).

However, the inlet of the conduit is enlarged by the strongly undersaturated water entering the conduit. Thus, the hydraulic head of the lower aquifer propagates upward in time along the conduit, and the hydraulic head gradient along the upper part of the conduit (i.e. pipe 3) increases accordingly (Fig. 4.4b).

As a result the discharge through the conduit increases, and eventually the water emerging at the outlet of the conduit is undersaturated with respect to gypsum. In this situation a positive feedback mechanism triggers a rapid

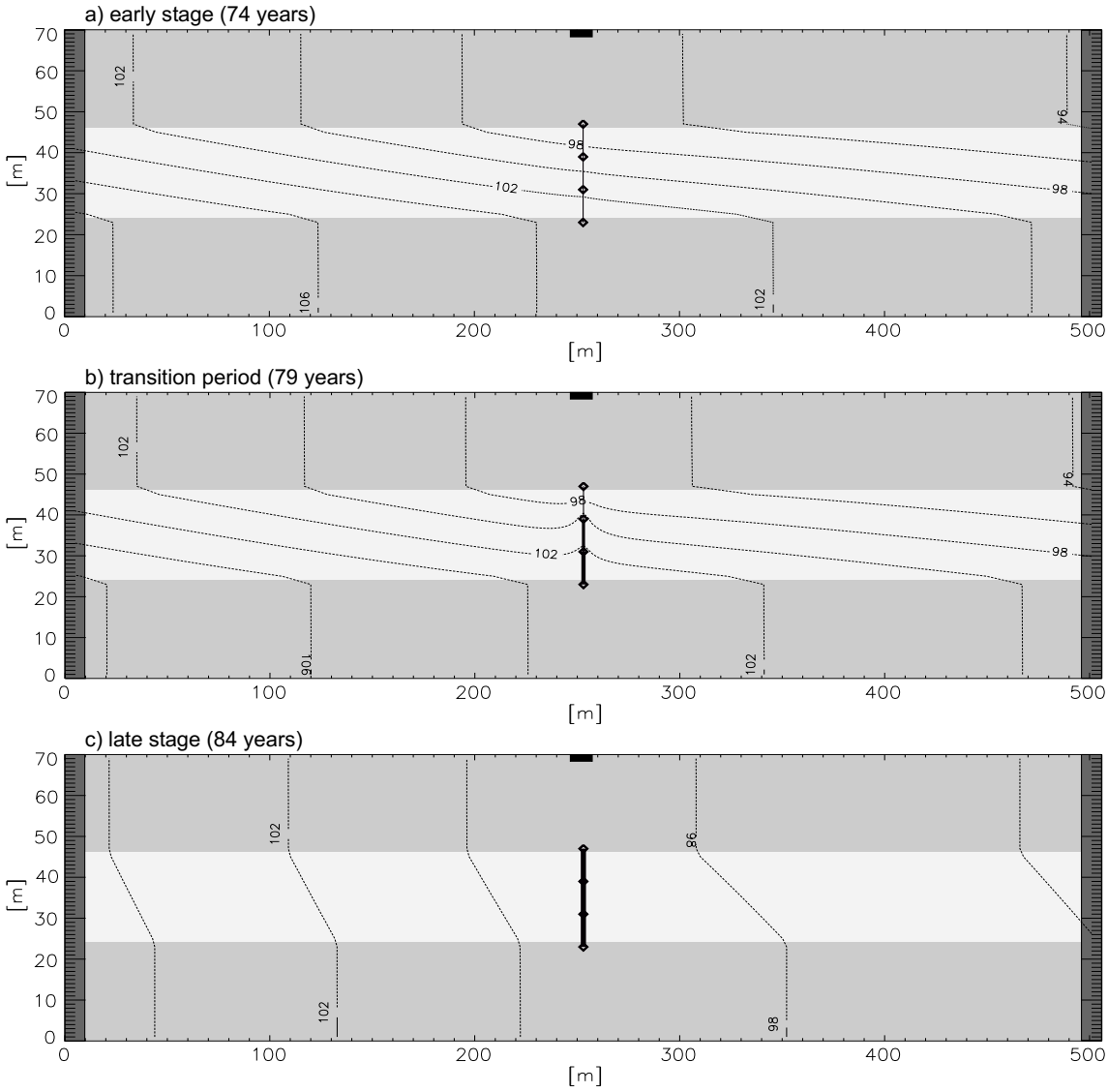

Figure 4.4: Different stages of conduit development. Dashed lines are the hydraulic heads in the fissured system (in m).

conduit growth (breakthrough), since the enlargement of the outlet due to gypsum dissolution causes increasing flow rates and decreasing concentrations and thus higher dissolution rates. Finally the hydraulic head gradient between the aquifers is diminished (Fig. 4.4c), because discharge through the conduit is now sufficiently high.

After breakthrough has occurred, the hydraulic resistance of the conduit is smaller than those of the aquifers. Discharge through the conduit is controlled by the boundary conditions and the hydraulic conductivity of the aquifers, but no longer by the diameter of the conduit as during the early stage. Thus, at the late stage of conduit development, the flow rate remains constant (Fig. 4.5).

Whereas exchange of water between the conduit and the fissured system of the gypsum layer is negligible at the late stage, it is an important factor of conduit development at the early stage (Fig. 4.5). Flow rates increase

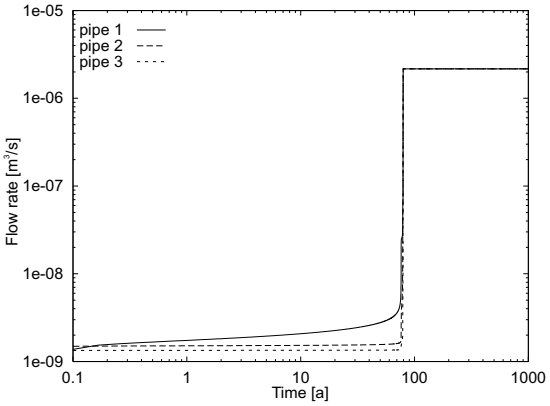

Figure 4.5: Flow rates in the pipes.

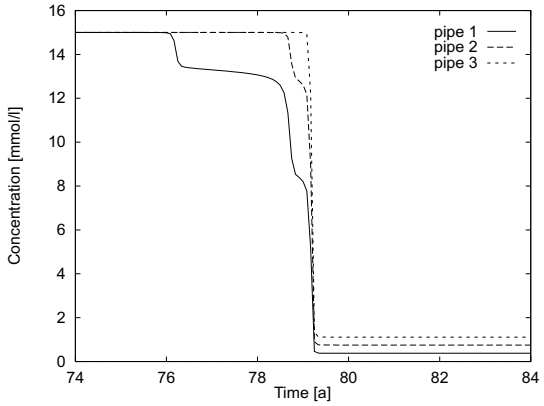

Figure 4.6: Concentrations at the outlets of the pipes.

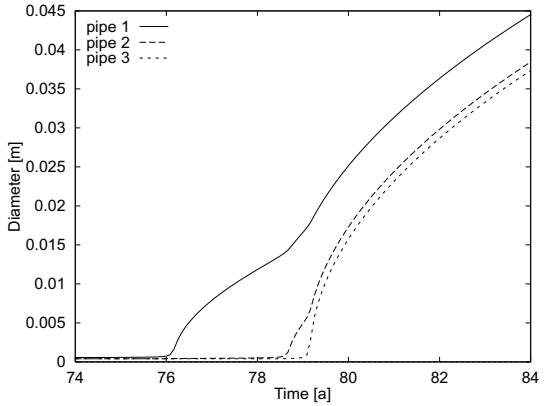

Figure 4.7: Diameters of the pipes.

in the lower part (pipe 1) of the conduit, although outflow into the upper aquifer is restricted by the small diameter of the outlet (pipe 3). The conduit drains into the gypsum layer and is supplied with additional aggressive water from the lower aquifer.

The positive feedback mechanism triggering breakthrough is illustrated in more detail in Fig. 4.6 and Fig. 4.7. At the early stage, outflow from all pipes is saturated with respect to gypsum. Due to the increasing flow rates aggressive water reaches the outlet of pipe 1 after 76 years (Fig. 4.6). At the same time enlargement of pipe 1 accelerates enormously (Fig. 4.7). From now on pipe 2 is supplied with aggressive water. After about 79 years the concentration drops at the outlet of pipe 2, and the diameter of pipe 2 increases. Soon after, the whole conduit is enlarged. Due to the increase of flow rates by several orders of magnitude (Fig. 4.5) concentrations drop to levels close to zero. Since flow rates remain constant, the concentrations stay constant from then on as well. As demonstrated by the analytical solution for the concentration in steady-state pipe flow (eq. 3.30), the concentration is unaffected from increasing conduit diameters, because the increase of the contact area available for gypsum dissolution is compensated by the increasing thickness of the diffusion boundary layer (compare eq. 2.33 and eq. 2.34).

The following sections examine the effects of parameter changes on the simulation results. Corresponding to the different stages of conduit development it is distinguished between the sensitivity of the breakthrough time, which characterises the time period of the early stage of conduit development (section 4.3.3), and the sensitivity of the conduit diameter, characterising the long-term conduit development (section 4.3.4).

4.3.3 Sensitivity of breakthrough time

In order to investigate the sensitivity of the breakthrough time to changes of model parameters, numerical simulations were conducted varying systematically the different parameters. The results of numerical simulations depend on the chosen model set-up and the discretisation of time and space. In addition to the hydrogeologic parameters, there-

fore, these parameters were included in the sensitivity analysis.

Within this section, the breakthrough time will be defined by the drop of the concentration at the outlet of the conduit to values of $c \leq 0.9c_{eq}$. Under certain conditions concentrations fall to values of $c > 0.9c_{eq}$ and remain constant afterwards. In these cases the breakthrough time will be defined by the time the concentration reaches the constant level. In most of the simulations conducted for sensitivity analysis, data output has been generated only for full years. Therefore, the breakthrough time of the standard scenario is referred to "80 years" instead of 79.25 years.

4.3.3.1 Model set-up and discretisation

In a sensitivity analysis for a model scenario of conduit development in carbonate rocks, Hückinghaus (1998) showed that the results of the numerical simulations were sensitive to the length of the time steps. However, for a time step length of a year or less, the influence of the time discretisation was negligible.

Considering the positive feedback mechanism which triggers the breakthrough (see section 4.3.2), a dependency of the simulation results on time discretisation is readily explained. During each time step the conduit diameter, the flow rates, and the dissolution rates remain constant. Only after the time step the conduits are enlarged, and the flow rates increase, causing a drop of concentrations and an increase of dissolution rates. In a time continuum these changes proceed continuously. The discrete time steps, however, cause a delayed change of the hydraulic and chemical conditions, i.e. the feedback mechanism is slowed down. Thus, the breakthrough time is expected to increase if the time step length increases. This effect might be generally more pronounced for the simulation of conduit development in gypsum than for that in carbonates, since gypsum is much more rapidly dissolved than carbonates.

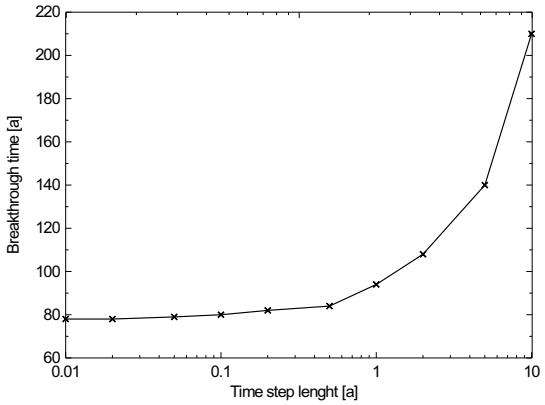

Figure 4.8: Sensitivity of breakthrough time to time discretisation.

Fig. 4.8 shows the relation between the breakthrough time and the discretisation of time for the model scenario described in section 4.3.1. For time steps of one year or more the breakthrough time increases significantly with increasing time step length. However, if the time step length is less or equal to 0.5 years the effect of time discretisation on the simulation result is negligible. Thus, for the given model scenario the chosen time step length of one month is sufficiently small.

Section 4.3.2 has shown that the flow rates decrease from the inlet (pipe 1) to the outlet (pipe 3) of the conduit in the period before the breakthrough occurs (Fig. 4.5). Flow from the conduit to the fissured system of the gypsum layer, therefore, has been considered as an important factor of conduit development at the early stage. The water exchange between the two flow systems may be influenced by the exchange coefficients at the nodes, but also by the number of nodes at which the pipe flow model is coupled to the continuum model. Therefore, both the exchange coefficient and the number of conduit nodes in the gypsum layer have been varied (Fig. 4.9).

In the standard scenario the conduit is coupled to the fissured system of the gypsum layer at two nodes. Without any node in the gypsum layer, no breakthrough is observed within a simulation period of 5 million years. With a single node in the gypsum layer the resulting breakthrough time is still

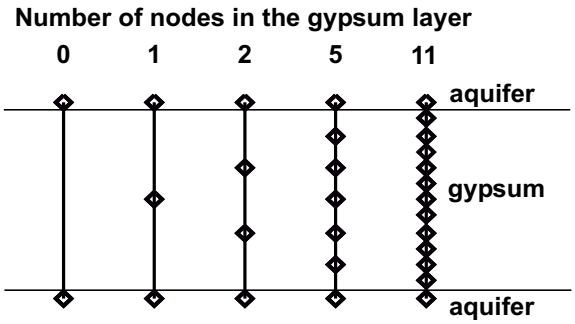

Figure 4.9: Discretisation of the conduit into pipes which are coupled to the continuum model at nodes. The number of nodes in the gypsum layer has been varied.

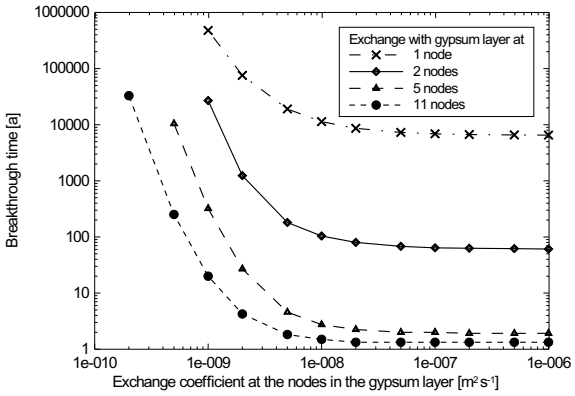

Figure 4.10: Sensitivity of breakthrough time to exchange coefficient and number of nodes in the gypsum layer.

two orders of magnitude larger than for the standard scenario (Fig. 4.10). Likewise, the breakthrough is considerably delayed if the exchange flow is restricted by reducing the exchange coefficient in the gypsum layer to less than 10^{-8} m^2 s^{-1}. Towards larger values of the exchange coefficient, the breakthrough time remains almost constant, since the maximum flow rate from the conduit into the fissured system is then limited by the hydraulic conductivity of the gypsum layer. However, the exchange between the two flow systems can be further enhanced by increasing the number of conduit nodes in the gypsum layer. With five or more nodes in the gypsum layer, breakthrough occurs almost instantaneously if exchange is not restricted by a low exchange coefficient (Fig. 4.10).

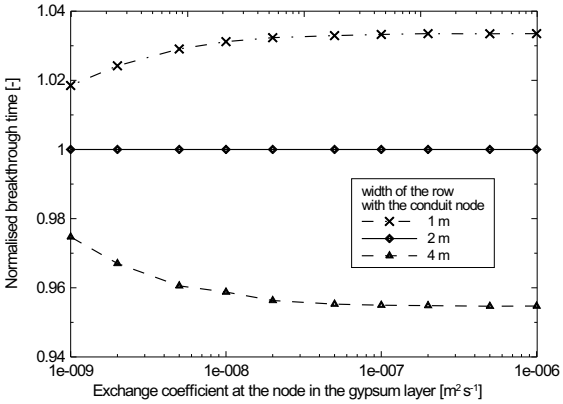

Figure 4.11: Sensitivity of the breakthrough time to the discretisation of the continuum model. In a model with only one conduit node in the gypsum layer, the width of the row containing the node has been varied. For each exchange coefficient, breakthrough times have been normalised by division through the corresponding breakthrough time for a cell width of 2 m.

In the modelling approach, the flow rate between the two hydraulic systems is assumed to depend linearly on the hydraulic head difference (eq. 2.10). Since flow in the fissured system is simulated by a finite-difference method, the heads of the fissured system are calculated at discrete cells. The width of these cells (i.e. the discretisation of the fissured system) possibly affects the head values, and thus the exchange flow between the two systems. Using the set-up with a single node in the gypsum layer, the width of the row containing the node was varied. The thickness of the gypsum layer was kept constant by adjusting the rows at the top and at the bottom of the layer accordingly. Fig. 4.10 shows the resulting breakthrough times normalised with respect to the breakthrough times obtained for a cell width of 2 m.

Reducing the cell width increases the breakthrough time slightly, larger cells shorten the breakthrough time. Once the lower part of the conduit has been enlarged, the hydraulic heads are higher in the conduit than in the adjacent fissured system. In this situation, the steep hydraulic head gradient near the conduit is better represented by a refined discretisation. With increasing cell width, the

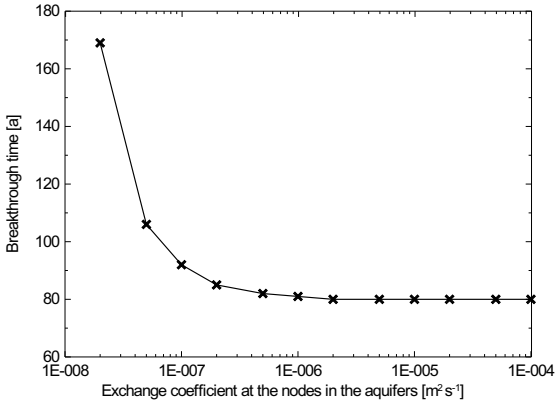

Figure 4.12: Sensitivity of breakthrough time to the exchange coefficient at the nodes in the aquifers.

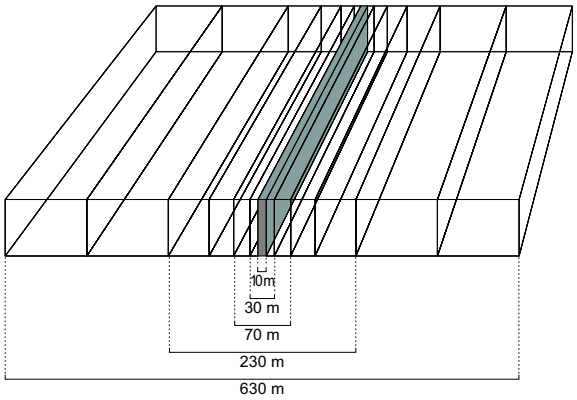

Figure 4.13: Extension of the 2D model (grey-coloured slice) to three dimensions.

heads represent average values over increasing areas. Therefore, the head difference (and thus the exchange flow rate) between the conduit and the fissured system increases with increasing cell width, causing an earlier breakthrough of the conduit. Yet, the discretisation of the fissured system is insignificant compared to the previously studied parameters.

Like the exchange flow between conduit and fissured system of the gypsum layer, the exchange coefficient at the nodes coupling conduit and aquifers may influence the breakthrough time of the conduit. However, Fig. 4.12 shows that the breakthrough time is constant as long as the exchange coefficient at the nodes is larger than 10^{-6} m^2 s^{-1}. Under these conditions, inflow to the conduit is not limited by the exchange coefficient but by the hydraulic resistance of the conduit. Using an exchange coefficient as low as $2 \cdot 10^{-8}$ m^2 s^{-1} (i.e. equal to the exchange coefficient in the gypsum layer) reduces the flow through the conduit so much that the concentration never drops below $0.9c_{eq}$ at the outlet of the conduit. Nevertheless, the breakthrough time (which has been defined here as the time period after which the outflow concentration remained constant) increases only by a factor of about two compared to the standard scenario.

Considering flow from the lower aquifer into the conduit and flow from the conduit into the fissured system of the gypsum layer and into the upper aquifer, the model set-up has to be examined critically. In a real aquifer, flow to and from the conduit is expected to be radial. The 2D model, however, does not allow for radial flow. Therefore, the flow rate in the conduit might be reduced in the model. In order to test whether or not a radial flow component increases the flow rates in the conduit and thus reduces the breakthrough time, the model was extended to three dimensions. For that, further vertical layers of the continuum model were added to the model set-up described in the previous section (Fig. 4.13).

The properties and the boundary conditions were chosen identically to the original 2D slice, but the widths of the slices (i.e. layers of the continuum model) were increased with increasing distance from the conduit. By that, the width of the model domain was successively increased from 10 m (i.e. a single slice) to 630 m. Increasing the width from 10 m to 30 m reduces the breakthrough time from 80 years to 76 years (Tab. 4.1). However, for model domains of larger width the breakthrough time remains constant at 75 years. Thus, the simplification inherent in the 2D model appears to cause only small errors with respect to the resulting breakthrough times.

Table 4.1: Breakthrough time for model domains of different width (see Fig. 4.13).

Width of model domain in m	10	30	70	230	630
Breakthrough time in a	80	76	75	75	75

4.3.3.2 Hydrogeologic parameters

The dissolutional removal of gypsum from the conduit walls evidently depends on the flow rate. Thus, the breakthrough time will be sensitive to parameters influencing flow through the conduit. The flow rate in a circular conduit is given for laminar flow conditions by the Hagen-Poiseuille equation (eq. 2.4). According to this equation, the flow rate is proportional to the fourth power of the conduit diameter, while it depends only linearly on other parameters like the hydraulic gradient.

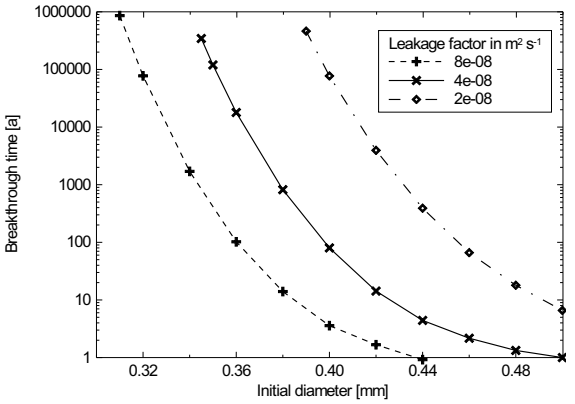

Figure 4.14: Sensitivity of the breakthrough time to the initial conduit diameter for various river leakage coefficients.

Fig. 4.14 shows that the breakthrough time is highly sensitive to changes of the initial conduit diameter (Fig. 4.14). The breakthrough occurs almost instantaneously if the diameter is increased by about 20% (i.e. $a_0 = 0.5$ mm) compared to the standard scenario (i.e. a river leakage coefficient of $4 \cdot 10^{-8}$ m^2 s$^-1$ and a diameter of 0.4 mm). If the diameter is reduced by 15% (i.e. $a_0 =$ 0.34 mm) no breakthrough is observed within one million years.

The leakage coefficient of the river affects the hydraulic gradient along the conduit (Fig. 4.14). Increasing the river leakage reduces the heads in the upper aquifer. Thus, the hydraulic head difference between lower and upper aquifer increases with increasing leakage coefficient. A variation of the leakage factor by a factor of two may change the breakthrough times by several orders of magnitude. Nevertheless, the simulation results are more sensitive to the initial diameter, as can be seen by comparing parameter combinations yielding identical breakthrough times. At a breakthrough time of about 100000 years, for instance, an increase of the leakage factor by 400% (i.e. from $2 \cdot 10^{-8}$ m^2 s^{-1} to $8 \cdot 10^{-8}$ m^2 s^{-1} is compensated by decreasing the initial conduit diameter only by 20% (i.e. from 0.4 mm to 0.32 mm).

The hydraulic gradient along the conduit is not only affected by the river leakage, but also by the conduit diameter. Therefore, the leakage factors cannot be easily transformed into values of the hydraulic gradient if different conduit diameters are compared (as in Fig. 4.14). In Fig. 4.15 the breakthrough times are plotted as a function of the hydraulic gradient for an initial conduit diameter of 0.4 mm (i.e. the value of the standard scenario). The axis at the top of the diagram shows the corresponding values of the leakage coefficient.

Under given hydraulic conditions conduit enlargement is controlled by the first-order rate law (eq. 2.29) for the dissolution of gypsum. Thus, the breakthrough time might be sensitive to the parameters included in eq. (2.29), i.e. the mass transfer coefficient k, the equilibrium concentration c_{eq}, and the concentration c in the conduit water. The concentration

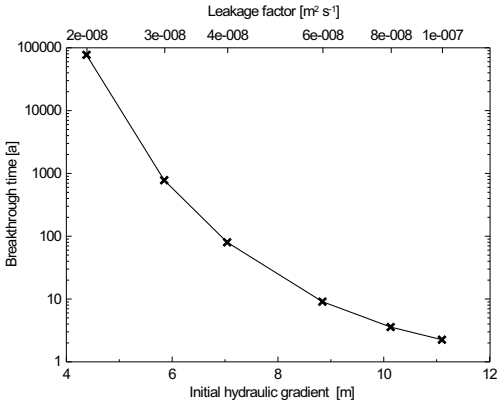

Figure 4.15: Sensitivity of the breakthrough time to the hydraulic gradient (and the river leakage factor).

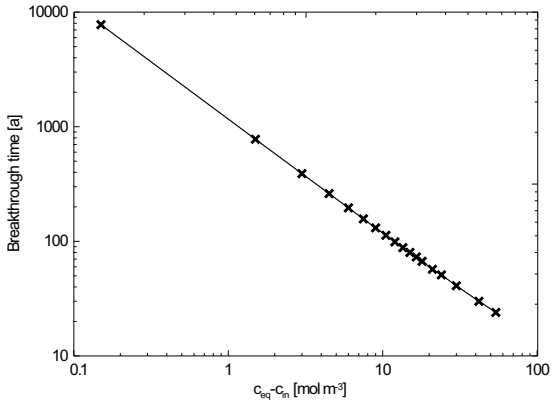

Figure 4.16: Sensitivity of the breakthrough time to the undersaturation with respect to gypsum.

profile along the conduit cannot be specified directly, but is a result of the numerical calculation. However, the concentration at the conduit inlet is specified as a boundary condition for the simulation.

In numerical simulations the breakthrough time was found to depend on both equilibrium concentration and inflow concentration. However, the simulations yielded identical breakthrough times if the undersaturation at the inlet, defined here as $(c_{eq} - c_{in})$, was kept constant. Thus, it is sufficient to examine the sensitivity of the breakthrough time to the undersaturation at the conduit inlet.

The undersaturation $(c_{eq} - c_{in})$ can vary over a wide range. According to Klimchouk (1996a) the solubility of gypsum (i.e. the equilibrium concentration) reaches a maximum of about 7.3 g l^{-1} (i.e. about 42 mol m^{-3}) in highly concentrated solutions of sodium chloride. Additionally, the equilibrium concentration depends on the water temperature (Fig. 3.9). Thus, a maximum increase of the equilibrium concentration (and thus of the undersaturation as defined above) by a factor of about three compared to the standard model scenario seems possible.

Plotting both breakthrough time and undersaturation on logarithmic axes (Fig. 4.16) yields an empirical correlation of the two parameters:

$$t_b \sim \frac{1}{c_{eq} - c_{in}} \tag{4.1}$$

where t_b denotes the breakthrough time. Thus, breakthrough occurs faster the lower the inflow concentration and the higher the equilibrium concentration with respect to gypsum.

The mass transfer coefficient k depends on the joint diffusion coefficient of calcium and sulfate, and on the thickness of the diffusion boundary layer, which separates the conduit wall from the bulk solution (see section 2.3.2.1). The diffusion coefficient depends on the water temperature, but variations of more than a factor of two are not reasonable due to temperature changes alone (see Tab. 3.3). Yet, Fig. 4.17 reveals that even smaller variations may change the breakthrough times by several orders of magnitude. Neglecting the simulation with a breakthrough time of two years (which might be affected by an insufficient time discretisation), the breakthrough times follow a power law. Since undersaturated water can penetrate deeper into the conduit if dissolution rates are low, the breakthrough is accelerated with decreasing mass transfer coefficients.

In the standard model scenario, a fully developed diffusion boundary layer has been assumed (i.e. $N_{Sh} = 3.66$). Taking into account that the diffusion boundary layer is not fully developed in the entrance region of a pipe (i.e.

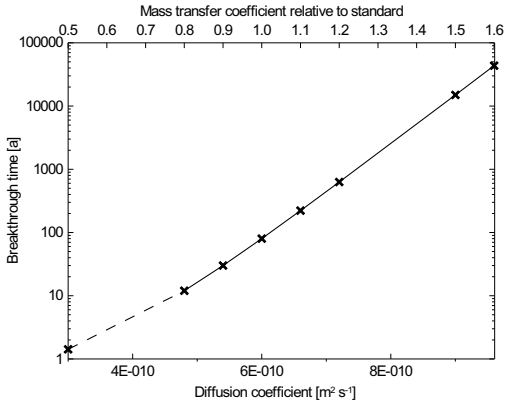

Figure 4.17: Sensitivity of the breakthrough time to the diffusion coefficient, which determines the mass transfer coefficient.

$N_{Sh} > 3.66$) yields larger mass transfer coefficients and thus higher dissolution rates. In a model run, the thickness of the diffusion boundary layer (given as the dimensionless Sherwood number N_{Sh}) for each pipe segment was calculated as a function of the distance from the pipe entrance using eq. (3.11). Compared to the standard scenario this modification led to a moderate increase of the breakthrough time from 80 years to 96 years. Taking into account the uncertainty of parameters like the initial conduit diameters, the error caused by the assumption of a fully developed diffusion boundary layer is negligible.

Fig. 4.18 summarizes the impact of the aforementioned hydraulic and chemical parameters on the breakthrough time. The initial conduit diameter is found to be the most influential parameter. The breakthrough times are also sensitive to both the hydraulic gradient and the mass transfer coefficient. The undersaturation of the inflow with respect to gypsum, however, is less important within the shown range of parameter variation.

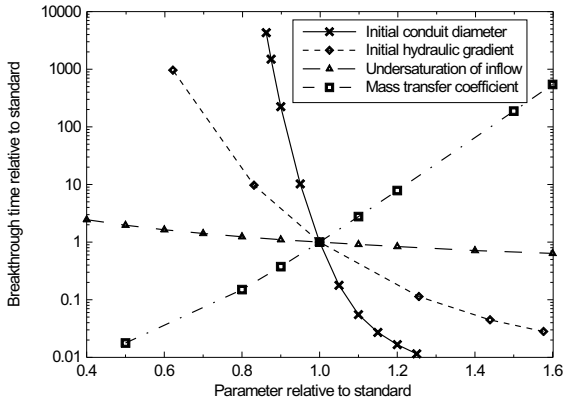

Figure 4.18: Sensitivity of the breakthrough time to variations of hydraulic and chemical parameters.

4.3.4 Sensitivity of long-term conduit development

In section 3.2.3.3 an analytical solution for the long-term development of the conduit diameter under steady-state flow conditions has been derived (eq. 3.36):

$$a(c,t) = \sqrt{a_0^2 + \frac{4N_{Sh}D}{\rho_g}(c_{eq} - c)t} \qquad (4.2)$$

Birk et al. (2000) showed that this equation applies to the long-term conduit development in the model scenario studied here. In this scenario flow rates are time-variant at the early stage of conduit development when they are controlled by the conduit diameter (Fig. 4.5). However, after the breakthrough flow rates remain constant, because the boundary conditions are constant in time[1]. Thus, the equation may be applied to calculate conduit diameters for times which are much larger than the breakthrough time.

In eq. (4.2) the concentration c depends on the flow rate and the position along the conduit axis. Replacing the concentration by eq. (3.30) yields a more general equation (section 3.2.3.3, eq. 3.37):

$$a(z,t) = \qquad (4.3)$$
$$\sqrt{a_0^2 + \frac{4\overline{N}_{Sh}D}{\rho_g}(c_{eq} - c_{in}) \exp\left(-\frac{\overline{N}_{Sh}D\pi}{Q}z\right) t}$$

It can be seen that the influence of the initial diameter a_0 is negligible for large times t. The same result may be obtained by conducting several numerical simulations using different

[1]The influence of time-variant boundary conditions on conduit development will be examined in section 4.4.2

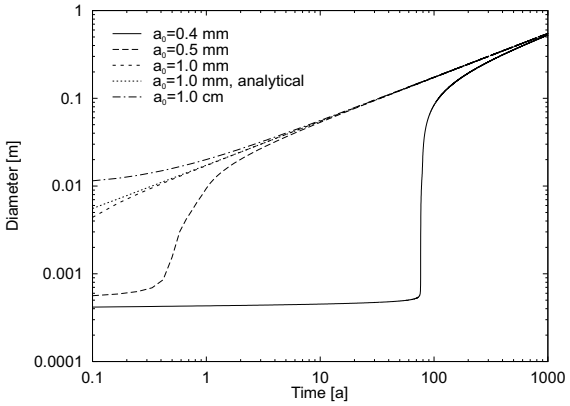

Figure 4.19: Numerically calculated diameters of pipe 1 for various initial diameters, and comparison with analytically calculated diameters (eq. 4.3).

initial diameters. Fig. 4.19 shows the development of the diameter of pipe 1 over a period of 1000 years. In addition to the numerically calculated results, the diameter at the outlet of pipe 1 has been plotted for an initial diameter of 1 mm using eq. 4.3. For smaller initial diameters eq. 4.3 yields the same straight line as for $a_0 = 1$ mm, while numerically and analytically calculated diameters are identical for $a_0 = 1$ cm. In the latter case the analytical solution is valid even for small times, because the flow rate through the conduit is constant from the beginning. Although the breakthrough times are highly sensitive to the initial diameter (see section 4.3.3), all numerical simulations approach the analytical solution if the simulation time is considerably larger than the breakthrough time.

Thus, *long-term* conduit development is insensitive to the initial conduit diameter. The initial diameter a_0 may be neglected in eq. (4.3) yielding

$$a(z,t) \approx \sqrt{\frac{4\overline{N}_{Sh}D}{\rho_g}(c_{eq}-c_{in})\exp\left(-\frac{\overline{N}_{Sh}D\pi}{Q}z\right)t} \tag{4.4}$$

The long-term conduit diameter is only controlled by the density of the rock ρ_g, by the undersaturation of the inflow with respect to gypsum ($c_{eq} - c_{in}$), by parameters describing the diffusion process of calcium and sulfate ions from the solid surface into the bulk solution (N_{Sh} and D), by the distance z from the conduit entrance, and by the flow rate Q.

Table 4.2: Standard parameter values and resulting conduit diameter after 1000 years.

Parameter	Standard value
$c_{eq} - c_{in}$	15 mol m^{-3} ($\approx$ 2.6 g l^{-1})
N_{Sh}	3.66
D	$6 \cdot 10^{-10}$ m^2 s^{-1}
ρ_g	13600 mol m^{-3} ($\approx$ 2.3 g cm^{-3})
z	8 m
Q	$2.166 \cdot 10^{-6}$ m^{-3} s^{-1}
a(1000 a)	54.6 cm

Eq. 4.4 was applied to examine quantitatively the sensitivity of long-term development of conduit diameters to the aforementioned parameters. Each parameter has been varied within a range of between 0.01 and 100 times the standard value listed in Tab. 4.2 (see also section 4.3.1). It is important to note that this range was chosen to elucidate the properties of the mathematical function rather than to define a sensible range in terms of natural conditions.

The resulting diameters (relative to the standard) at the outlet of pipe 1 ($z = 8$ m) are shown in Fig. 4.20. For the given standard parameters the exponential function is approximately one, because the exponent is very close to zero. If the absolute value of the exponent decreases further, therefore, the value of the exponential function remains almost unchanged. For this reason the conduit diameter is insensitive to a reduction of the distance from the conduit entrance.

The conduit diameter is hardly influenced by an increase of flow rates for the same reason. Only if the flow rate is reduced by an order of magnitude (i.e. the absolute value of the exponent increases) the conduit diameter is highly sensitive to the flow rate. In the mature karst system considered here, the flow rate in the conduit is governed by the hydraulic conductivities of the aquifers and by the regional head distribution. Thus, the flow

Table 4.3: Flow rates and diameters of pipe 1 calculated with different model domains (see Fig. 4.13).

Width of model domain in m	10	30	70	230	630
Flow rate in 10^{-5} m^{-3} s^{-1}	0.22	0.57	1.05	1.81	2.20
Diameter after 1000 a in cm (numerical)	52.9	53.2	53.2	53.3	53.3
Diameter after 1000 a in cm (analytical)	54.6	55.0	55.1	55.2	55.2

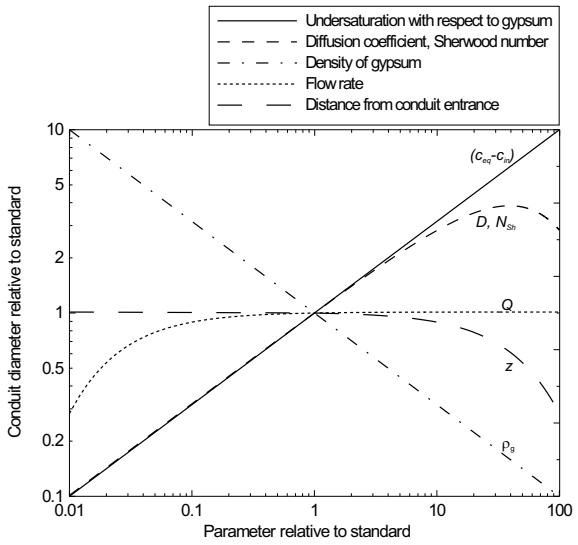

Figure 4.20: Sensitivity of the long-term development of the diameter at the outlet of pipe 1 calculated by eq. 4.4.

rate may generally vary over a wide range, depending on the local hydrogeologic conditions. As discussed in the previous section, the flow rate through the enlarged conduit may be underestimated in the model, since the real flow field is radial rather than two dimensional. In fact, when using a three dimensional model set-up with a total width of 630 m (see Fig. 4.13), the flow rate rises by an order of magnitude (Tab. 4.3). The conduit diameter after 1000 years, however, increases only by about 1% in both numerical simulation and analytical calculation. It may be noted that the numerically calculated diameters are slightly smaller than predicted by the analytical solution, because the breakthrough time of 80 years is not completely negligible with respect to the considered period of 1000 years.

The other parameters ($c_{eq}-c_{in}$, D, N_{Sh}, ρ_g) of the analytical solution do not (or not only) appear as an argument of the exponential function. The long-term conduit diameter is very sensitive to variations of these parameters. In general, the diameters decrease with increasing density of the rock, and increase with decreasing density. However, the density of gypsum rock is a fairly constant value. Jubelt and Schreiter (1980), for instance, give a range of between 2.2 g cm^{-3} and 2.4 g cm^{-3} for the density of gypsum, i.e. a variation of less than 10%.

As mentioned in section 4.3.3.2, the undersaturation of the inflow ($c_{eq} - c_{in}$) may vary over a wide range. Saturated inflow water prevents conduit development completely. The largest conduit diameter is obtained for high equilibrium concentrations in combination with inflow of concentration zero.

The diffusion coefficient may vary, for instance, due to changes in the water temperature (compare table 3.3). The Sherwood number is larger by several orders of magnitude if flow is turbulent. It may be also larger than 3.66 in laminar flow in the entrance region. Smaller values than 3.66, however, are physically not reasonable. For very large diffusion coefficients and/or Sherwood numbers the dissolution process may be surface reaction controlled (see section 2.3.2.2). Taking into account that the long-term conduit diameters are at least in the order of several tens of centimetres, however, the dissolution process is diffusion controlled over the entire parameter range shown in Fig. 4.20. Even in an entirely diffusion controlled dissolution process the long-term conduit diameter does not increase towards infinity if the diffusion

parameters are increased. The long-term diameter at the outlet of pipe 1 shows a maximum at large values of the diffusion parameters. A further acceleration of the dissolution process results in a decrease of conduit diameters, because the concentration at the outlet of pipe 1 approaches the equilibrium concentration.

As mentioned in section 4.3.3.1, a model run was performed, in which the Sherwood number was calculated depending on the distance from the pipe entrance (eq. 3.11). In this simulation a conduit diameter of 90 cm resulted after a simulation period of 1000 years (instead of 53 cm in the standard scenario). However, the model assumes that the diffusion boundary layer develops anew from the entrance of each pipe of 8 m length. Since the water exchange between conduit and fissured system is negligible after breakthrough (compare section 4.3.2), it is probably more realistic to assume that there is only one conduit of 24 m length. Using a mean Sherwood number for a conduit of 24 m length in the numerical simulation yielded a diameter of pipe 1 of 83 cm after 1000 years. Thus, the assumption of a fully developed diffusion boundary layer causes an underestimation of the long-term conduit diameter by nearly 40%.

4.4 Development of conduit networks

Section 4.4.1 defines model scenarios with a conduit network beneath the river (see model set-up shown in Fig. 4.2). The simulation results are described in section 4.4.2 focusing on the influence of structural preferences as well as on the effects of time-variant boundary conditions.

4.4.1 Model scenarios

In order to study the development of conduit networks in a gypsum layer under artesian conditions, a regular proto-conduit network, consisting of 63 pipes of 8 m length each, is incorporated into the continuum model (Fig. 4.21). The hydraulic and chemical boundary conditions for the pipe network are analogous to those of the scenario for single conduit development (section 4.3). The network is coupled to the fissured system (i.e. the continuum model) of the gypsum layer with an exchange coefficient of $2 \cdot 10^{-8}$ m^2 s^{-1} at each node linking several pipes. The lower and the upper aquifer are coupled to the conduit system with an exchange coefficient of $2 \cdot 10^{-5}$ m^2 s^{-1}.

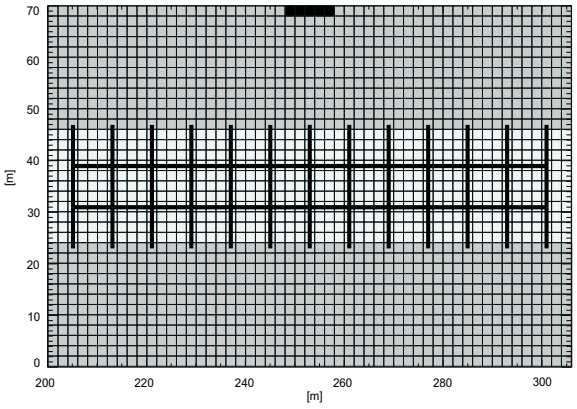

Figure 4.21: Implementation of a conduit network into the numerical model. The figure shows the middle part of the model domain only.

The concentration of dissolved gypsum is assumed to be zero in both lower and upper aquifer. Thus, if water transits from an aquifer into the pipe network the gypsum layer is supplied with solutionally aggressive water. Water flowing from the fissured system of the gypsum into the pipe network, however, is assumed to be saturated with respect to gypsum. The equilibrium concentration is set to 15 mol m^{-3} ($\approx$ 2.6 g l^{-1} dissolved gypsum), the joint diffusion coefficient of calcium and sulfate is $6 \cdot 10^{-10}$ m^2 s^{-1}, and the density of gypsum is 13600 mol m^{-3} ($\approx$ 2.3 g cm^{-3}).

Turbulence does not occur in the model scenarios described below. For laminar flow conditions a fully developed diffusion boundary layer is assumed, i.e. the Sherwood number is a constant ($N_{Sh} = 3.66$). As shown in section 4.3.4 the conduit diameters of the mature

karst system may be underestimated with this assumption. The diffusion boundary layer is probably not fully developed within the pipe length of 8 m if flow rates are high. On the other hand, the diffusion boundary layer may be built up over a larger distance if flow is dominated by a large single conduit with negligible exchange of water to the surrounding smaller conduits and to the fissured system. Therefore, we assume a fully developed diffusion boundary layer, keeping in mind that the resulting conduit diameters are lower estimates of the real diameters.

In a first scenario, the initial diameter of all pipes is set to 0.4 mm. The same pipe network is used in scenario 2, however, a layer (e.g. clay or mudstone) less permeable than the aquifers but more permeable than the fissured system of the gypsum is inserted at the top of the gypsum layer. The hydraulic conductivity of this layer is set to 10^{-8} m s^{-1} (for a 2D slice of 10 m width), and the value of the exchange coefficient at the conduit nodes in this layer is set to $2 \cdot 10^{-7}$ m^2 s^{-1}, which is in accordance with the alteration of the permeability. The thickness of the layer amounts to 2 m, and the thickness of the upper aquifer is reduced from 24 m to 22 m. In the third scenario the influence of irregular variations of the initial diameters is examined. For that, an initial diameter of 0.30 mm, 0.35 mm, or 0.40 mm is randomly assigned to each of the pipes. In the fourth and the fifth scenario the initial diameters of the uppermost vertical pipes are reduced to 0.3 mm and 0.25 mm, respectively, whereas the other pipe diameters are 0.4 mm.

4.4.2 Simulation results

Scenario 1

Fig. 4.22 (p. 60) illustrates the development of a conduit network consisting of pipes with a constant initial diameter of 0.4 mm. At the early stage of conduit development the flow rates in the conduits are limited by the narrow outlets at the top of the gypsum layer, which are not enlarged, because the water is already saturated with respect to gypsum when it reaches the upper part of the pipe network. However, beneath the river, where the hydraulic head gradient is steepest, a conduit starts to develop from the bottom of the gypsum layer (Fig. 4.22a, p. 60). Therefore, the higher hydraulic head of the lower aquifer propagates upward with time along the widened conduit. This causes an increase of flow through the conduit for two reasons. Firstly, the hydraulic head difference between the conduit and the fissured system of the surrounding gypsum increases, which causes a transfer of water from the conduit into the fissured system of the gypsum layer, and thus an increase of the flow rate in the lower part of the conduit. Secondly, the flow rate also increases in the upper part of the conduit due to the increased hydraulic head gradient. Since higher flow rates imply lower outflow concentrations, the water is more aggressive with respect to gypsum dissolution, so that it propagates further upward before it is saturated. Eventually, water emerging at the outlet to the upper aquifer is undersaturated with respect to gypsum (Fig. 4.22b, p. 60). As described in section 4.3.2 for a single conduit, a positive feedback mechanism triggers a rapid conduit growth, because the enlargement of an outlet causes a rapid increase of the flow rate through the conduit, and thus, decreasing concentrations and higher dissolution rates, which further accelerate the enlargement of the conduit.

After the breakthrough of a vertical conduit the hydraulic head gradient between the two aquifers is reduced and the flow rate does not increase further, since it is limited by the hydraulic resistances of the two aquifers. At this late stage of conduit development flow and gypsum dissolution are focused to the single conduit which has "broken through", whereas flow through the other parts of the pipe network is insignificant and will not induce any further enlargement of conduits. Therefore, the structure of the mature conduit systems does not change any more after breakthrough has occurred (Fig. 4.22b, c, p. 60), and the development of the pipe network results in the enlargement of a single vertical conduit

only. The processes governing conduit development in the network are similar to those described for a single conduit in section 4.3. The breakthrough time is slightly larger as compared to the single conduit, because the increased number of proto-conduits reduces the hydraulic head difference between lower and upper aquifer.

Scenario 2
This scenario examines how the presence of a low permeable layer like clay or mudstone at the top of the gypsum affects the development of the network of proto-conduits. Mudstone is found, for instance, at the top of the intensely karstified Permian gypsum in England (Cooper, 1995, 1998).

At the early stage, conduit development is similar to scenario 1. However, a second conduit is enlarged at the bottom of the gypsum (Fig. 4.23a, p. 61), because the intercalation of the low permeable layer ("clay layer") increases the initial hydraulic head difference between lower and upper aquifer. For the same reason the breakthrough of a vertical conduit occurs faster than in scenario 1 (Fig. 4.23b, p. 61).

In contrast to scenario 1, a considerable head difference between lower and upper aquifer is maintained after the breakthrough has occurred. Since there is also a lateral hydraulic head gradient within the gypsum layer, horizontal conduits are dissolutionally widened (Fig. 4.23c, p. 61). The presence of a clay layer at the top of the gypsum increases the spatial extension of karstification. At the late stage, solutional conduit enlargement is not focused to a single vertical conduit as in scenario 1, but proceeds laterally creating horizontal flow paths and several outlets at the top of the gypsum.

Scenario 3
In the scenarios considered so far, the initial aperture widths of the pipes were constant, i.e. the network of proto-conduits was homogeneous. This scenario examines the influence of unsystematic heterogeneities in the network of proto-conduits such as irregular variations of the initial diameters.

Fig. 4.24a (p. 62) shows that at the early stage several conduits are solutionally enlarged at the bottom of the gypsum layer. No conduit enlargement is initiated at places where the aperture width is less than 0.40 mm. Evidently, the locations of conduit development are related to the initial pipe diameters. At the following level (i.e. in the middle horizon of the gypsum layer) there is again a selection according to the initial diameter. Therefore, a solutionally enlarged pathway is first established at the right hand side of the network, where two vertical pipes of 0.40 mm initial diameter each succeed. Since the two pipes are vertically succeeded by one of small aperture width, a horizontal pathway is created. Eventually, one of the uppermost pipes is rapidly enlarged, i.e. a breakthrough occurs (Fig. 4.24b, p. 62). As in scenario 1 flow and gypsum dissolution are focused then to the solutionally enlarged pathway. Other conduits are not enlarged any further (Fig. 4.24b, c, p. 62).

In contrast to the scenarios with constant initial diameter, the breakthrough does not occur where the hydraulic gradient is steepest (i.e. beneath the river). Instead, the pathway of solutional conduit enlargement is predetermined by the random distribution of the initial diameters. Nevertheless, the general structure of the resulting conduit system is similar to the case of a constant initial diameter (scenario 1). Apart from a short horizontal passage there is only one single vertical pathway connecting lower and upper aquifer. Thus, unsystematic heterogeneities such as randomly distributed initial aperture widths are not sufficient to induce the development of long horizontal passages or even maze caves in an artesian setting. However, they may influence breakthrough time and location of the enlarged conduit.

Scenario 4
In order to examine the effect of systematic heterogeneities of the conduit system, the initial diameters of the uppermost vertical pipes

were reduced to 0.3 mm. Thus, the vertical conductivity of the pipe network is reduced as compared to its lateral conductivity. A similar structural and textural differentiation of the gypsum layer is observed, for instance, in the gypsum karst of the Western Ukraine (Klimchouk, 2000b).

Due to the small aperture widths, flow rates through the uppermost pipes are diminished and breakthrough is slowed down compared to the homogeneous network of scenario 1. Horizontal conduits are widened beneath the low permeable horizon (Fig. 4.25a, p. 63), but this lateral growth of conduits stops after the breakthrough of a vertical conduit has occurred (Fig. 4.25b, c, p. 63). Like in scenario 1 and scenario 3, flow and gypsum dissolution are focused to the highest conductive vertical flow path. Unlike the clay layer at the top of the gypsum (scenario 2), the systematic heterogeneity examined in scenario 4 increases the spatial extension of solutional conduit enlargement at the early stage of conduit development only.

Scenario 5

In this scenario, the initial diameters of the uppermost pipes are reduced further to 0.25 mm, i.e. the pipe network is more heterogeneous than in scenario 4. The breakthrough of the vertical conduit is even more slowed down and the horizonzal development of the conduit network is more extensive than for the other scenarios (Fig. 4.26a, p. 64). Moreover, at the left edge of the network a second conduit is enlarged. Eventually, the two growing conduits are connected by a breakthrough event (Fig. 4.26b, p. 64). Since no vertical breakthrough occurs during the simulation period, the hydraulic head gradient is maintained across the gypsum layer, and the enlargement of horizontal conduits continues, because of the continuing supply with undersaturated water from the lower aquifer (Fig. 4.26c, p. 64).

Comparison of dissolution rates

Fig. 4.27 compares dissolution rates and total dissolved mass of gypsum for the scenarios considered above. In all scenarios a considerable increase of dissolution rates is observed after about 100 years. During this period one or more vertical conduits are enlarged in the lower part of the gypsum layer, causing an increase of flow rates in parts of the conduit system and thus higher total dissolution rates. However, the increase of dissolution rates is generally terminated when the lower and upper aquifer are hydraulically connected by the solutional enlargement of a vertical flow path, which reduces the hydraulic gradient across the gypsum layer. Only in scenario 2, where the low-permeability layer at the top of the gypsum maintains a considerable hydraulic head difference between the aquifers, dissolution rates increase further after the breakthrough of a vertical conduit.

Total mass of gypsum dissolved is smallest in scenario 1, but the values for scenario 3 and scenario 4 are similarly low. In these scenarios, gypsum dissolution at the late stage of conduit development is focused only to the flow path connecting lower and upper aquifer, whereas the other parts of the conduit system remain largely unaffected from dissolution. Therefore, dissolution rates stay constant at a comparably low level. Remarkably, dissolution rates are even higher at the early stage than at the late stage in scenario 4. In this scenario conduit enlargement proceeds laterally until the breakthrough of a vertical conduit focuses flow to a single vertical flow path. Therefore, the area of gypsum exposed to solutionally aggressive water is larger at the early stage than later on.

Significantly more gypsum is dissolved in scenario 2 and in scenario 5. In both of these scenarios conduit enlargement proceeds laterally over the entire simulation period, because flow into the upper aquifer is restricted either by a low permeable layer (scenario 2) or by small aperture widths at the top of the gypsum (scenario 5). In the latter case it is important that the aperture widths are small enough to prevent the solutional enlargement of vertical outlets to the upper aquifer. Otherwise lateral conduit enlargement will stop

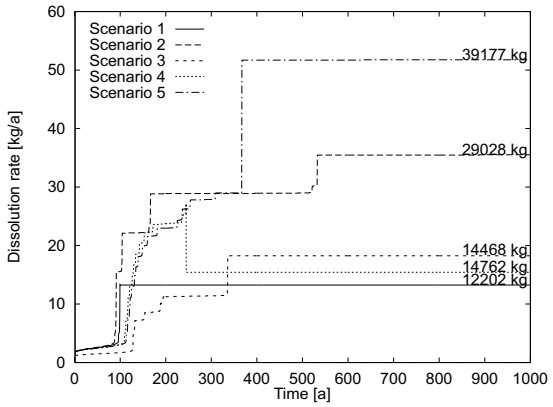

Figure 4.27: Dissolution rates (in kg a^{-1}) and dissolved masses after 1000 years (in kg) in the entire conduit system.

and dissolution rates will drop to a lower level as demonstrated by scenario 4. In the following section it will be examined how a vertical breakthrough might occur even if the aperture widths at the top of the gypsum are very small.

Time-variant boundary conditions
Conduit development in an artesian setting is driven by the hydraulic gradient between a lower and an upper aquifer which are separated by a soluble gypsum layer. In the conceptual setting shown in Fig. 4.2 the hydraulic head difference between the aquifers is induced by a river draining the upper aquifer. In geological times neither the river head nor the thickness of the layer separating the river from the upper aquifer are constant. Rather, the river incises, i.e. both river head and thickness of the uppermost confining layer, in which the river is incising, decrease with time.

In order to examine the influence of river incision on the development of a conduit network, the river boundary condition was changed in the scenario 5 after 1000 years (Fig. 4.28, p. 65, compare Fig. 4.2). The river head was reduced from 75 m to 73 m, and the leakage factor was doubled, which corresponds to halving the thickness of the layer separating the river from the aquifer. After 2000 years the separating layer was again halved (i.e. the leakage factor was again doubled) and the river head was reduced to 72 m.

Incision of the river causes a decrease of hydraulic heads in the upper aquifer and thus an increase of the hydraulic gradient across the gypsum layer. Due to the increased hydraulic gradient undersaturated water penetrates deeper into the conduit network causing an enlargement on the right of the model domain (Fig. 4.28b, p. 65).

A further incision of the river after 2000 years increases the hydraulic gradients even more and initiates the development of further conduits at the bottom of the gypsum (Fig. 4.29a, p. 66). After breakthrough the two aquifers are connected by a highly conductive conduit which reduces the head difference between lower and upper aquifer (Fig. 4.29b, p. 66). The resulting structure includes three vertical conduits at the bottom of the gypsum, which are connected by a large horizontal passage to a vertical outlet to the upper aquifer. Closer examination of the water budget at the conduit nodes reveals that only the left and the middle vertical conduits at the bottom of the gypsum are supplied with aggressive water from the lower aquifer. At the right hand side the solutionally enlarged conduit acts as an outlet to the lower aquifer like the vertical conduit at the top acts as an outlet to the upper aquifer. Thus, the flow direction, which was initially only upward, has changed in parts of the conduit system.

Note that breakthrough did not occur immediately beneath the river but further to the right. The location of the vertical outlet of the conduit system to the upper aquifer is determined by the hydraulic gradient. Before evolution of a horizontal conduit, the hydraulic gradient across the gypsum layer is steepest beneath the river. Subsequent to the lateral enlargement of a conduit, the location of the highest hydraulic gradient at the top of the gypsum moves to the right. Thus, breakthrough occurs to the right of the river.

4.5 Discussion

The model simulations demonstrate that conduit development under artesian condi-

tions may be subdivided into two stages, which are separated by a breakthrough event hydraulically connecting the aquifers below and above the gypsum. At the early stage, flow from the lower aquifer through the conduit system into the upper aquifer is limited by the small aperture widths of the conduits. On the other hand, flow rates rise due to the solutional enlargement of the conduits until flow is limited by the hydraulic resistance of the aquifers. The latter situation arises when a vertical flow path across the gypsum layer has been rapidly enlarged in the breakthrough event.

In the sensitivity analysis (sections 4.3.3 and 4.3.4), early conduit development (characterised by the breakthrough time) was found to be very different from long-term conduit development at the late stage (characterised by the conduit diameter after a period much larger than breakthrough time).

Long-term development of a single conduit under constant boundary conditions may be predicted by an analytical solution (eq. 4.2 or eq. 4.3) of the model equations. The analytical solution agrees well with the numerical calculation, giving confidence in the numerical model, which has to be used if more complex systems like conduit networks are studied or if boundary conditions are time-variant. Most of the parameters influencing long-term conduit development can be measured or are known from the literature. The necessary assumptions on the development of the diffusion boundary layer along the conduit walls, however, imply some uncertainty in the Sherwood number. Nevertheless, the long-term conduit diameters may be predicted reasonably well if the hydrogeologic conditions are known.

Early conduit development cannot be easily predicted. This is demonstrated by the analysis of the sensitivity of the breakthrough time, yielding a great influence of specific parameters like exchange coefficient and spatial discretisation of the pipe network, which are hardly related to measurable physical properties. Although breakthrough times cannot be quantitatively predicted, the model simulations prove useful for the characterisation of the early development of gypsum karst aquifers, as the sensitivity analysis yields an assessment of the relative influence of hydrogeologic parameters (Fig. 4.20).

In contrast to long-term conduit development, which is independent from the initial diameter of the conduit, the breakthrough time is highly sensitive to this parameter. The initial conduit diameter is even found to be the most influential hydrogeologic parameter during early karstification (Fig. 4.18).

The high sensitivity of the breakthrough time to the initial conduit diameter implies some interesting speleogenetic consequences. In the sensitivity analysis, breakthrough occurred either almost instantaneously or virtually never (i.e. after a period which is geologically unreasonable) when the initial diameters were slightly varied. Thus, it is generally very unlikely to encounter a situation, in which a breakthrough occurs under constant boundary conditions. The natural evolution of the landscape, which includes the erosion of confining layers and the incision of valleys, however, increases the hydraulic gradients at least locally. Under natural conditions breakthrough events are probably induced due to time-variant hydraulic boundary conditions, which slowly change breakthrough times (of a corresponding scenario with constant boundary conditions) from “virtually never” to “almost instantaneously”. Nowadays, human impacts such as water abstraction may also increase hydraulic gradients imposed on conduit systems.

The model scenarios dealing with the development of conduit networks in an artesian setting reveal that the structure of the mature conduit system is mainly determined at the early stage of conduit development, which ceases with breakthrough of a vertical conduit. At later times, dissolution of gypsum is mainly focused to the single flow path, where breakthrough has occurred.

Without any structural preferences vertical

shafts develop rather than horizontal cave systems, because the breakthrough occurs vertically along the direction of the hydraulic gradient before any lateral conduit development is initiated (scenario 1). Scenario 3 demonstrates that taking into account unsystematic heterogeneities like randomly distributed initial aperture widths will change the position of the breakthrough locally. The general cave pattern, however, is not significantly different from the structure resulting from a simulation without heterogeneity.

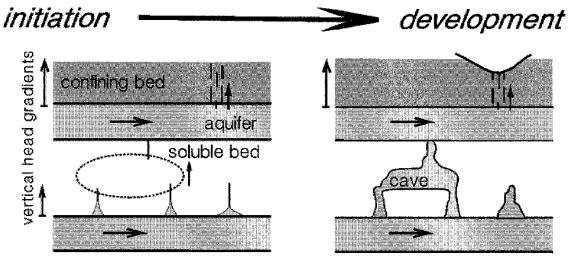

Figure 4.30: Initiation and development of conduits according to Klimchouk (2000c, slightly modified).

Horizontal conduits may develop if systematic structural preferences favour lateral flow (scenarios 2, 4, 5). However, if a vertical breakthrough connects the two aquifers the hydraulic gradient across the gypsum layer is reduced, and flow is focused towards the vertical flow path (scenario 4). Under these conditions a further development of horizontal conduits is found to cease, except for the case of a low-permeability layer at the top of the gypsum restricting vertical flow (scenario 2). The degree of karstification is generally higher if breakthrough times are larger. This result is opposing the popular view that the breakthrough time may be considered "as a measure of the intensity of karstification" as stated by Dreybrodt and Gabrovšek (2000) for limestone terrains. A similar view is expressed by naming the period after the breakthrough the "main stage of artesian development" (Klimchouk, 2000c). This term should be replaced by the more neutral expression "late stage of artesian development", since total dissolution rates in a conduit network may be higher before breakthrough occurs than later on (compare scenario 4).

Scenario 5 demonstrates that the variation of boundary conditions in time plays an important role for the evolution of maze caves under artesian conditions. In this scenario the karstification of the gypsum layer was most intensive, because the initial diameters of the vertical pipes at the top of the gypsum were small enough to prevent breakthrough, thus inducing lateral conduit development. As demonstrated by the sensitivity analysis for a single conduit (compare Fig. 4.18), a breakthrough of the vertical pipes at the top of the gypsum would only occur within a reasonable time if the values of initial aperture widths were within a narrow range. Thus, it is more likely that the breakthrough is induced by an increase of the hydraulic gradient. The structure of the conduit network, resulting from a simulation with time-variant boundary conditions, is found to be very similar to the conceptual model developed by Klimchouk (2000c) as depicted in Fig. 4.30 (compare Fig. 4.29c, p. 66).

It is characteristic for this structure that the number of vertical conduits is larger at the bottom of the gypsum than at the top. The number of conduits enlarged at the top of the gypsum is restricted, since conduit development generally ceases after an outlet to the upper aquifer has been enlarged. Klimchouk (2000c) termed the conduits at the bottom "feeder conduit", implying that the conduits act as inlets for the water from the lower aquifer. Yet, the model simulation presented in the previous section demonstrates that these conduits may also act as an outlet for the conduit water (though initially all conduits at the bottom of the gypsum received water from the lower aquifer).

In the numerical simulation a systematic heterogeneity of initial conduit diameters was required to generate a similar structure of the mature conduit system as shown in Fig. 4.30. This agrees very well with field observations from the Western Ukraine suggesting that the

structure of the maze caves is predetermined by laterally extended fissure networks, which are vertically poorly connected (Klimchouk, 2000b).

The model predicts the evolution of maze caves of different structure if the vertical flow is restricted by a low permeable layer at the top of the gypsum rather than by systematic heterogeneities of aperture widths. As demonstrated by scenario 2, horizontal passages may develop in the gypsum beneath the low permeable layer. In contrast to scenario 5, however, the number of vertical conduits is predicted to be lower at the bottom of the gypsum unit than at the top. Scenario 2 is similar to the hydrogeologic setting found in gypsum karst terrains of England , where Permian gypsum (Edlington Formation) is overlain by mudstone (Cooper, 1995, 1998). The presence of extended cave systems in the subsurface is proven there by frequently occurring subsidence and collapses. The subsidence-prone areas appear to be related to the margins of a buried valley (Cooper, 1998), which may locally induce an increase of hydraulic gradients similar to the river boundary of the model scenarios presented here. Yet, the actual structure of the cave systems is not precisely known.

The application of the karst genesis model has proven useful for the characterisation of karst conduit systems. The long-term conduit diameters evolving in mature karst systems can be reasonably well predicted if the required parameters are known (compare eq. 4.2 or eq. 4.3). Moreover, the model helps to infer the general structure of cave systems developing under given hydrogeologic conditions. Simulation results are highly sensitive to several hydrogeologic parameters (e.g. aperture width, hydraulic boundary conditions). In particular these parameters, therefore, have to be adequately quantified by field investigations and subsequently transferred into comprehensive conceptual models. Note that not only present aquifer properties but also hydrogeologic conditions of the geologic past have to be determined. In order to cope with uncertainties in the data, possible ranges for most influential parameters have to be covered by sensitivity analyses or parameter studies. In addition to hydrogeologic parameters, model-specific parameters (e.g. spatial discretisation of conduits into pipes) influence the simulation results, because the exchange of water between the conduit system and the fissured system depends on them. At present, however, the relation of these parameters to aquifer properties is rather unknown.

Due to both uncertainty of model parameters and high sensitivity of simulation results, forward modelling of long-term karst genesis predicts general cave patterns rather than precise location and geometry of conduits. In order to characterise highly complex karst systems more quantitatively, additional methods are required.

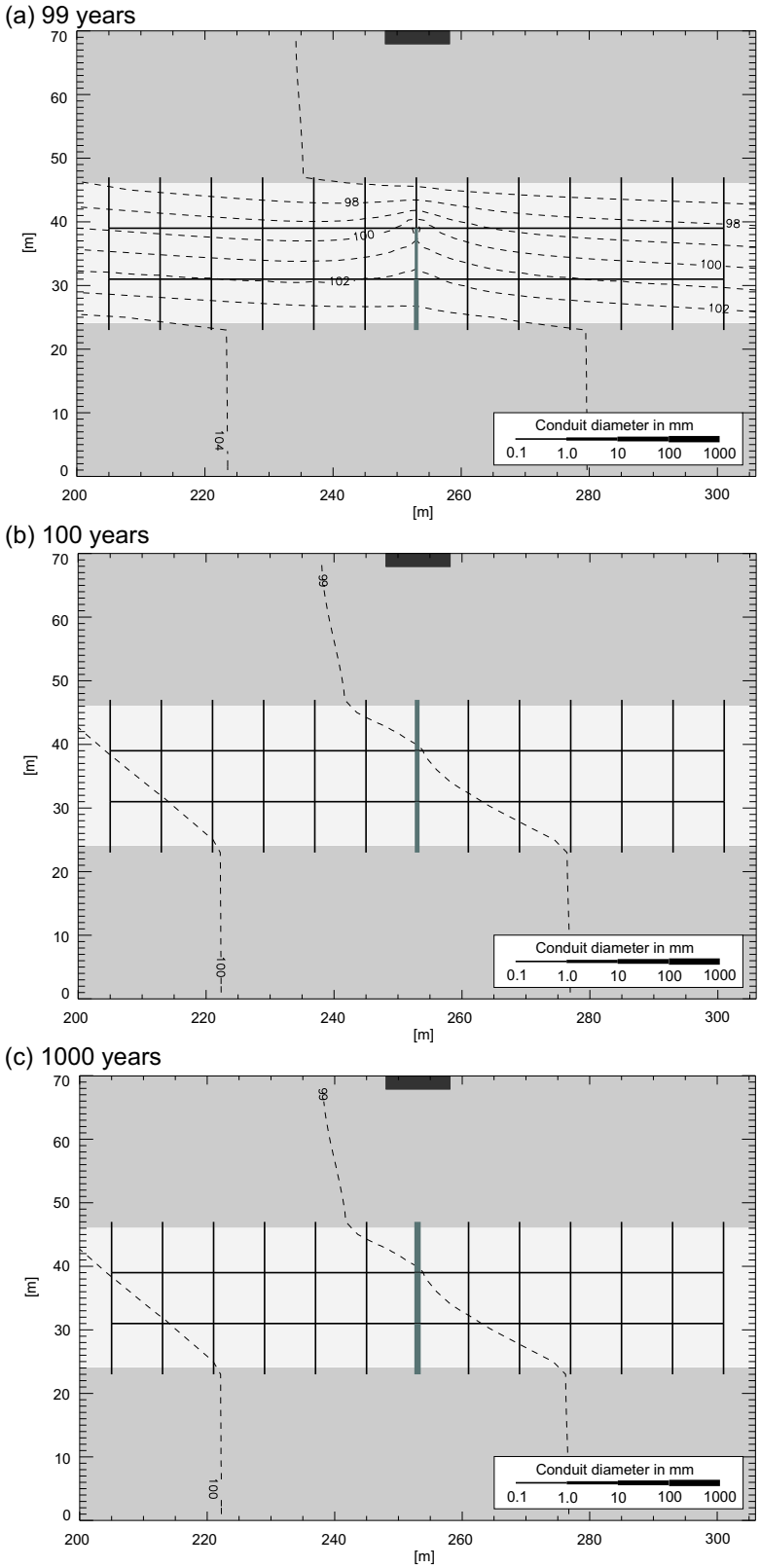

Figure 4.22: Scenario 1: Conduit diameters and hydraulic heads of the fissured system in m (dashed lines). Grey coloured pipes indicate that outflow is less than 90% saturated with repect to gypsum. The initial diameters of all pipes were 0.4 mm.

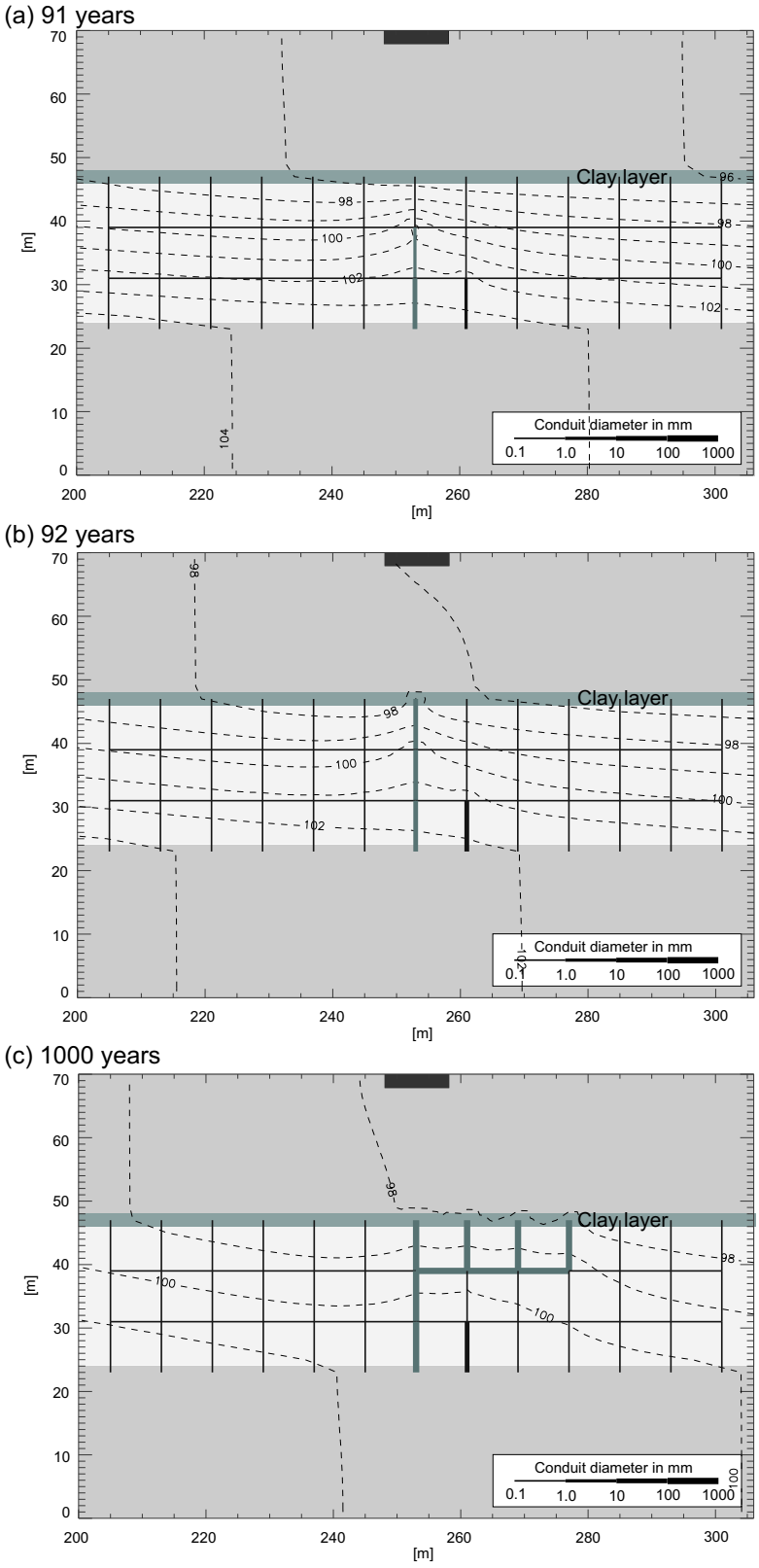

Figure 4.23: Scenario 2: Conduit diameters and hydraulic heads of the fissured system in m (dashed lines). Grey coloured pipes indicate that outflow is less than 90% saturated with repect to gypsum. The initial diameters of all pipes were 0.4 mm. At the top of the gypsum layer is a clay layer of 2 m thickness.

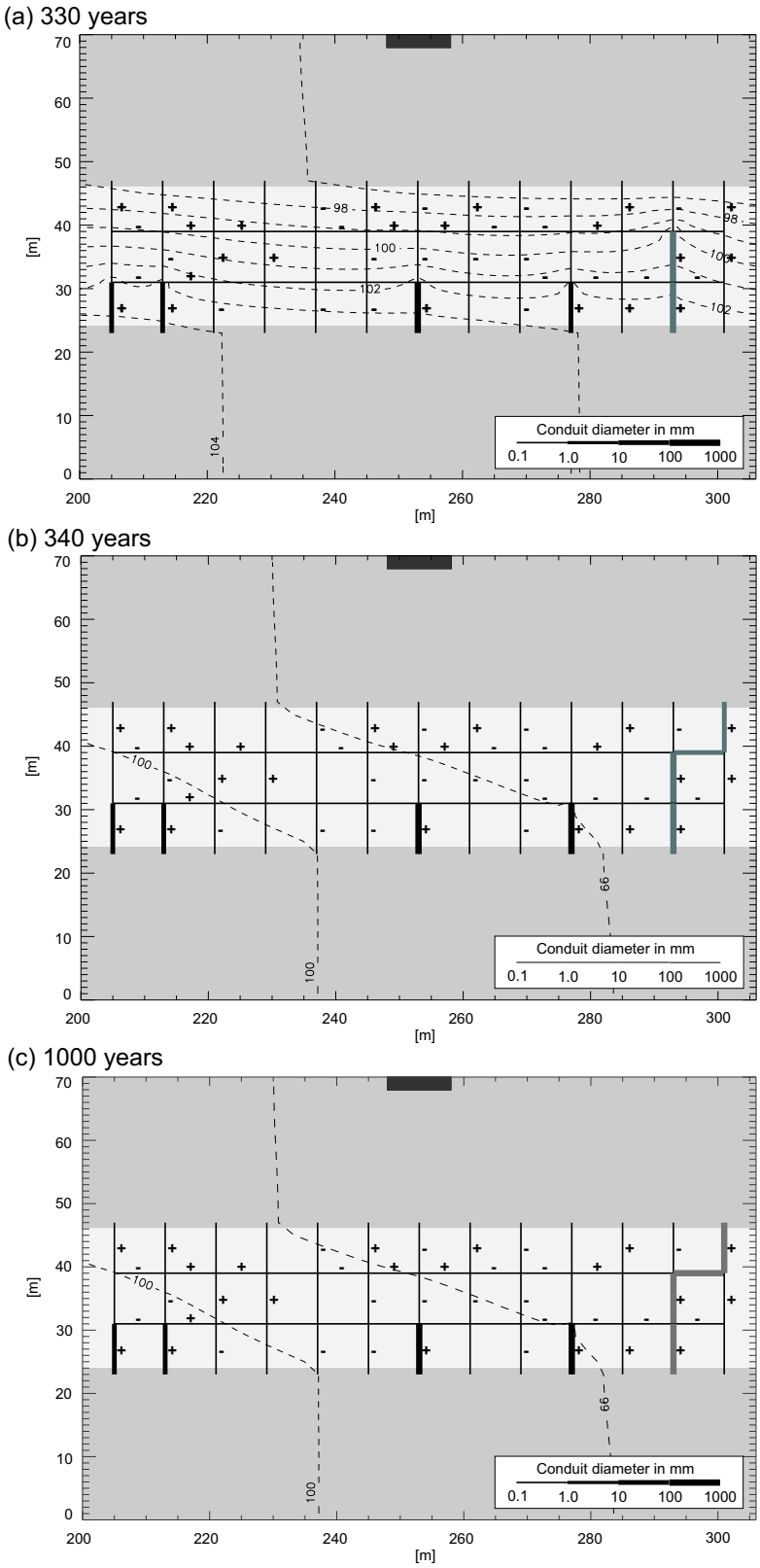

Figure 4.24: Scenario 3: Conduit diameters and hydraulic heads of the fissured system in m (dashed lines). Grey coloured pipes indicate that outflow is less than 90% saturated with repect to gypsum. Initial diameters of 0.30 mm (-), 0.35 mm, and 0.4 mm (+) were randomly assigned to the pipes.

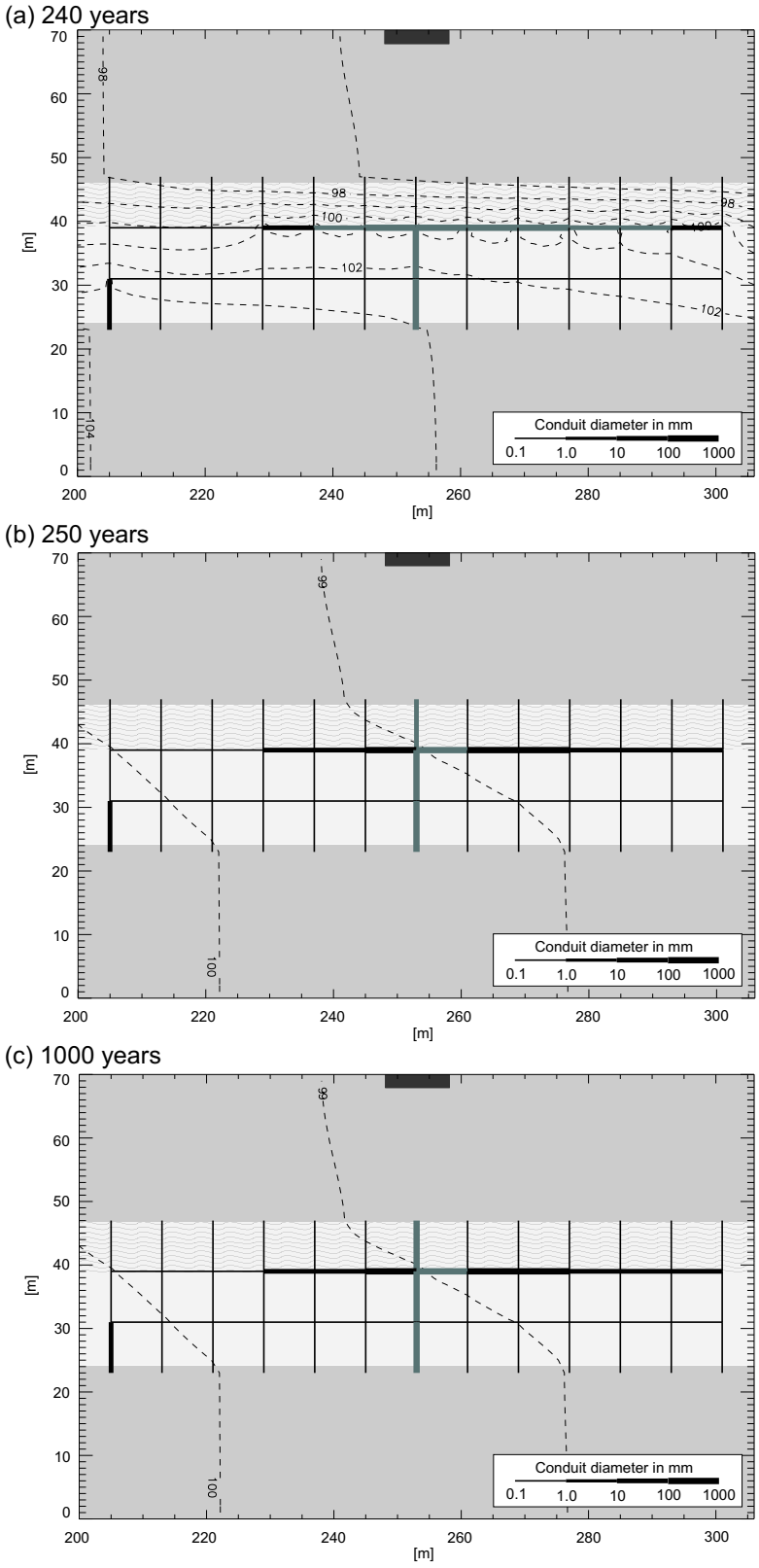

Figure 4.25: Scenario 4: Conduit diameters and hydraulic heads of the fissured system in m (dashed lines). Grey coloured pipes indicate that outflow is less than 90% saturated with repect to gypsum. The initial diameters of the vertical pipes in the upper part of the gypsum layer (wavy lines) were 0.3 mm, all other initial diameters were 0.4 mm.

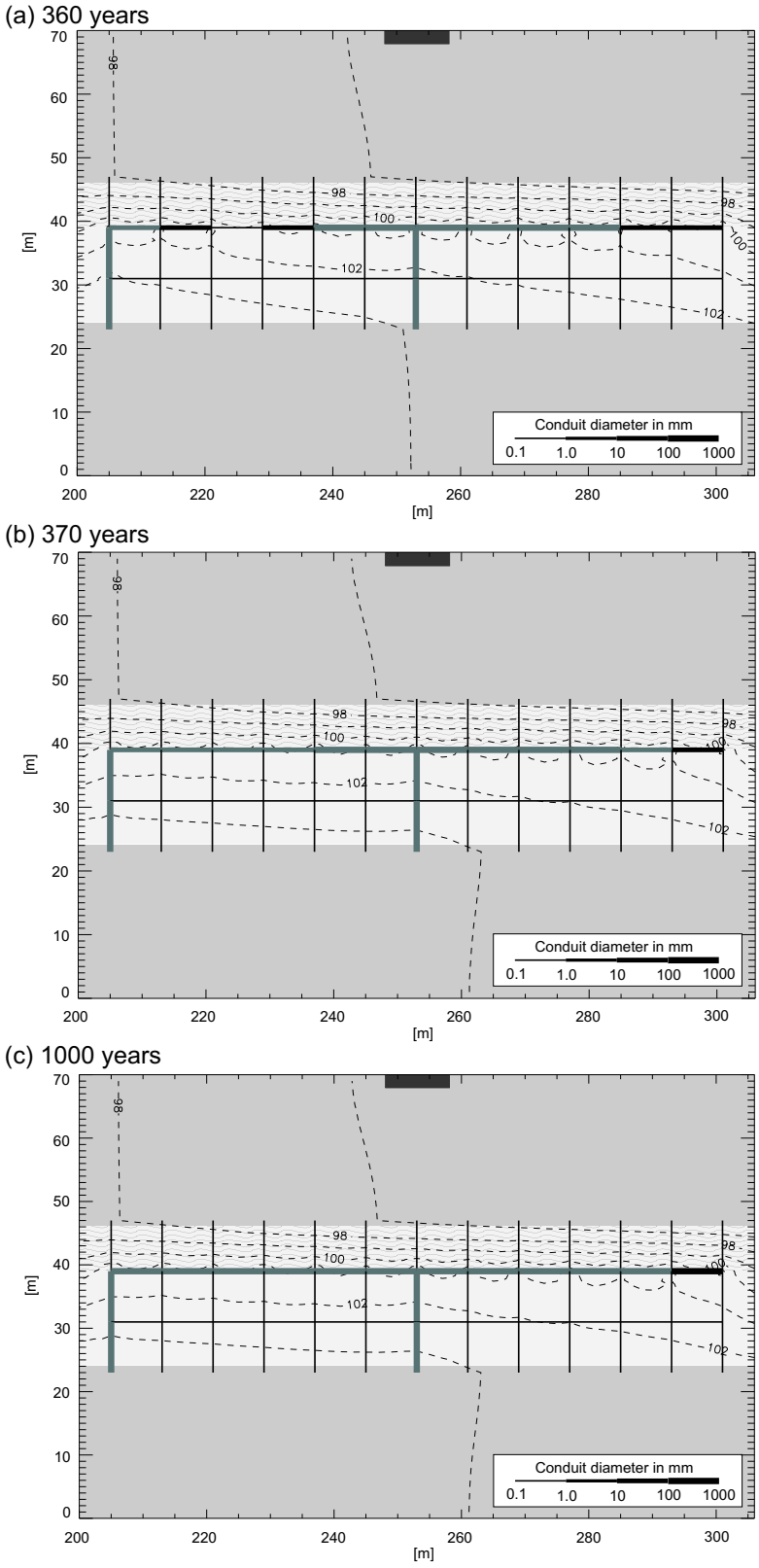

Figure 4.26: Scenario 5: Conduit diameters and hydraulic heads of the fissured system in m (dashed lines). Grey coloured pipes indicate that outflow is less than 90% saturated with repect to gypsum. The initial diameters of the vertical pipes in the upper part of the gypsum layer (wavy lines) were 0.25 mm, all other initial diameters were 0.4 mm.

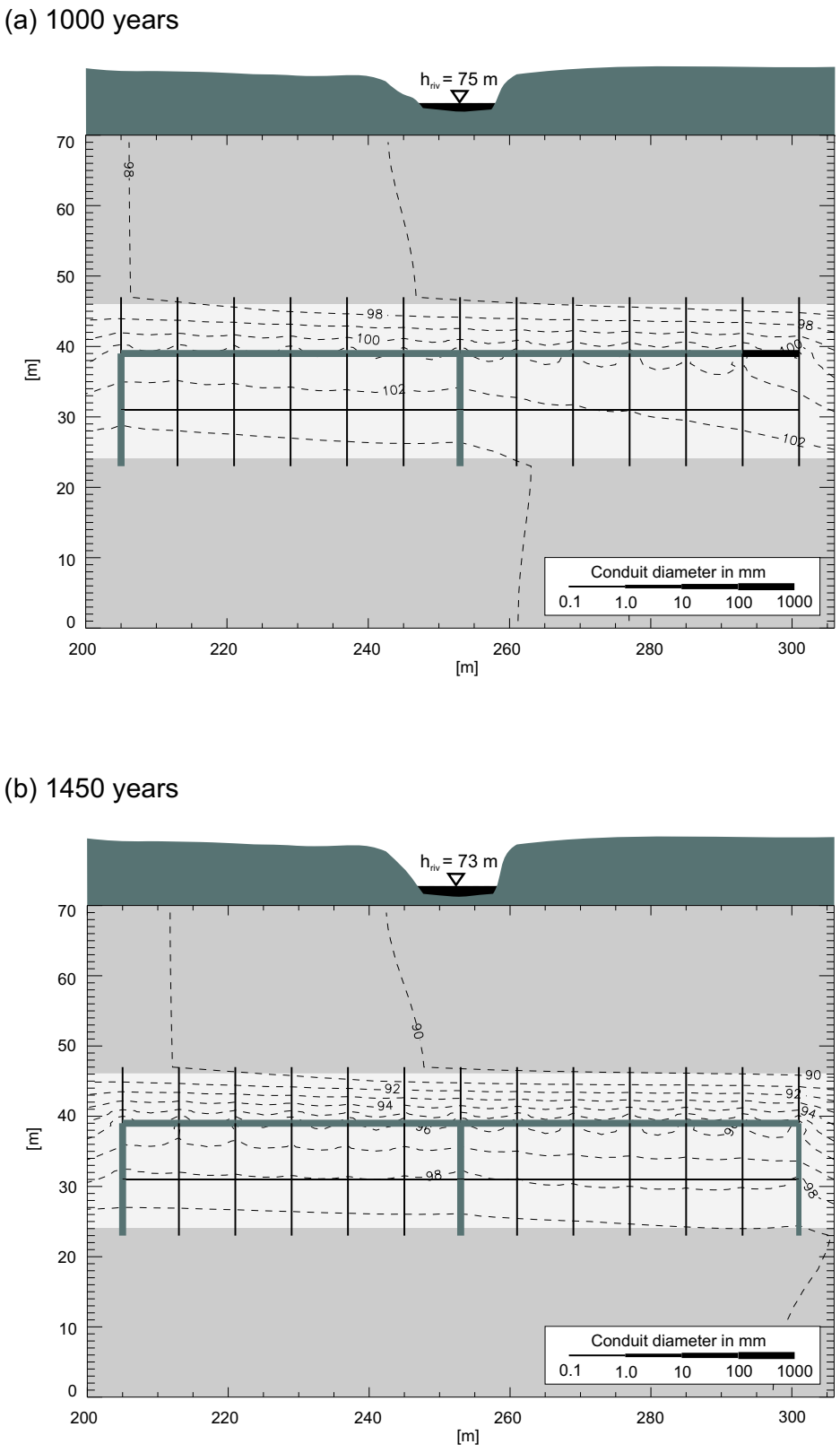

Figure 4.28: Scenario 5: Conduit diameters and hydraulic heads of the fissured system in m (dashed lines). Grey coloured pipes indicate that outflow is less than 90% saturated with repect to gypsum. After 1000 years, the river head was lowered and the leakage factor of the river boundary condition was doubled, corresponding to a incision of the river which halves the thickness of the low permeable layer in between river and upper aquifer.

(a) 2090 years

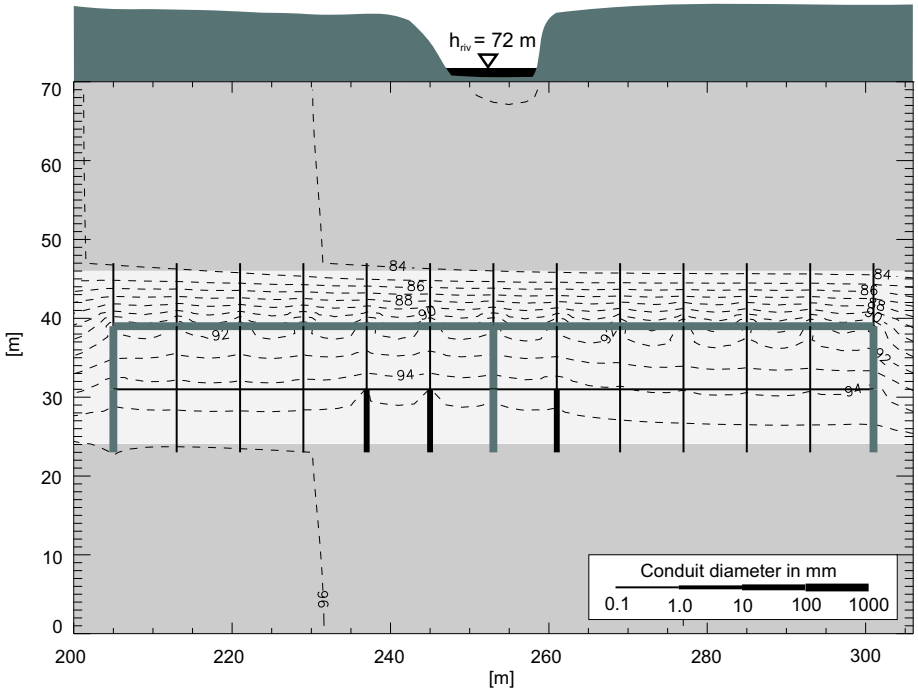

(b) 2100 years

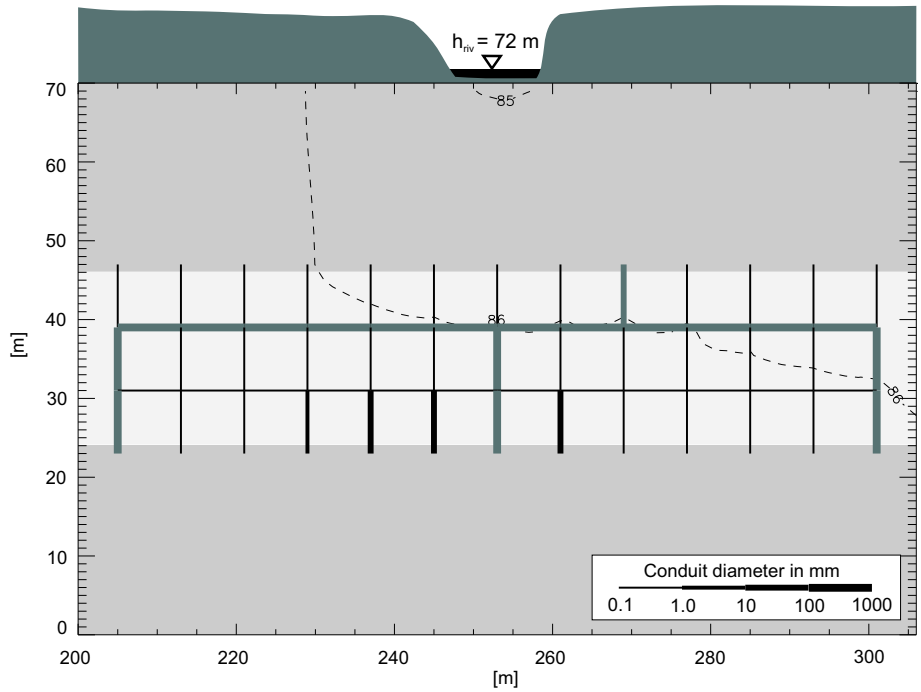

Figure 4.29: Scenario 5: Conduit diameters and hydraulic heads of the fissured system in m (dashed lines). Grey coloured pipes indicate that outflow is less than 90% saturated with repect to gypsum. After 2000 years, the river head was lowered further and the leakage factor of the river boundary condition was doubled again.

Chapter 5

Short-term karst spring response

The previous chapter dealt with the *early* karstification of gypsum under artesian conditions. Such *deep-seated karst* (i.e. not evident at the surface and without exposure of soluble rock) is probably an initial stage of many present karst systems. Klimchouk and Ford (2000) identify various stages of karst evolution succeeding the deep-seated setting. Firstly, *subjacent karst* evolves if the soluble rock is locally breached by erosion. Secondly, an *entrenched karst* develops where the entire thickness of the soluble rock is cut by valleys. Eventually, the removal of the cap rocks leads to *denuded karst* settings. Thus, karst evolution results in *mature* systems characterised by surface karst features such as dolines, sinkholes and karst springs. Due to their surface exposure these systems are much better accessible than the previously considered deep-seated settings. In addition to karst genesis modelling, therefore, other methods, such as tracer tests or analysis of spring hydrograph recession, may be applied to characterise mature karst systems. The following sections present the application of a modelling approach, supporting the characterisation of mature karst systems based on the analysis of short-term karst spring responses to recharge events.

5.1 Approach

Fig. 5.1 illustrates the basic idea of simulating short-term karst spring responses to recharge events using a process-based modelling tool. Aim of the numerical simulations is to infer the unknown geometry of the karst conduit system, thus supporting the characterisation of karst aquifers at the catchment scale.

The right hand side of Fig. 5.1 schematically depicts how a karst spring responds to a recharge event. Due to rapid localised recharge into the conduit system, discharge soon increases after precipitation. Spring discharge decreases when direct infiltration into the conduit ceases. The decrease of spring discharge is usually much slower than the increase, since recharge into the fissured system is slow and often delayed, for instance, due to the buffering effect of an epikarstic horizon (Williams, 1983). Moreover, the fissured system provides a high storage capacity for the recharge water. Thus, after a recharge event the fissured system is able to release water into the conduits and to supply the karst spring over a large period even when direct infiltration has completely stopped.

In phreatic (i.e. completely water filled) conduits the increase of hydraulic pressure due to infiltration of water into a sink is instantaneously transmitted to the spring, thus inducing a rise in spring discharge. The infiltrated water arrives later at the spring, because flow velocities are generally slower than the transmission of hydraulic pressure. Therefore, a time lag between rising spring discharge and variation of physico-chemical parameters, like solute concentration and water temperature, is frequently observed at karst springs.

The upper right diagram of Fig. 5.1 depicts the solute concentration at a spring as it is typically observed after a recharge event.

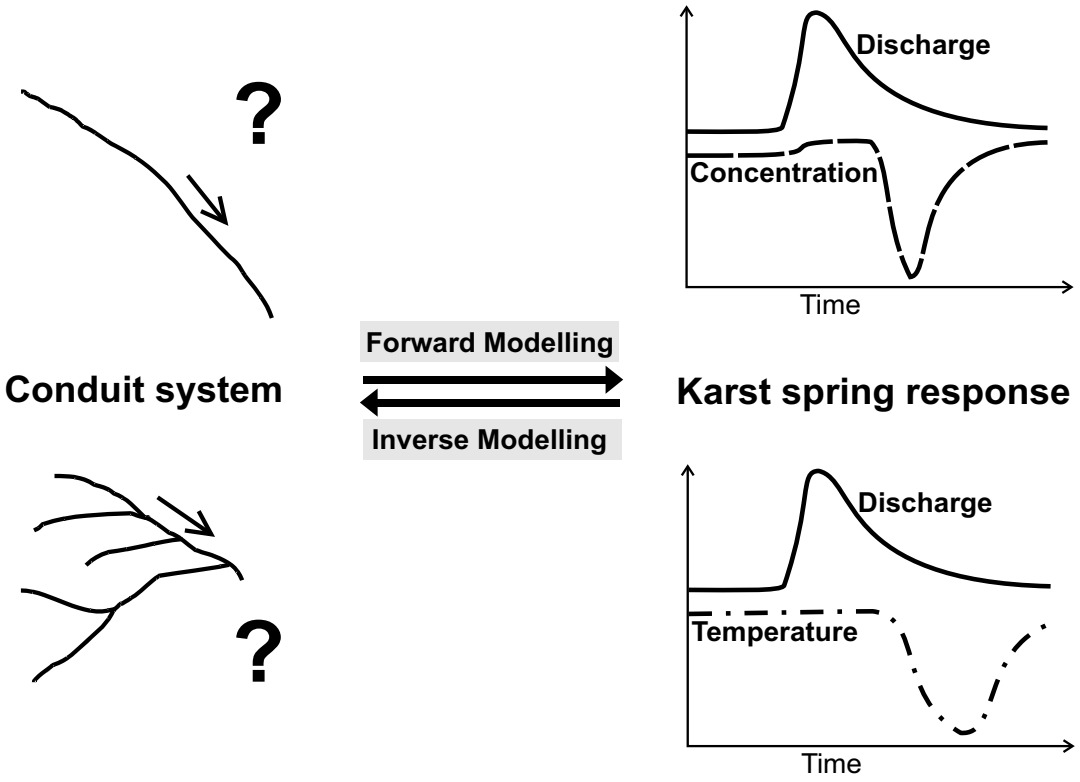

Figure 5.1: Schematic diagram illustrating the approach of inferring the geometry of the conduit system from karst spring signals using a process-based modelling tool.

Soon after the rise of spring discharge an increase of solute concentration is observed, which is evidence for the displacement of highly mineralised water previously stored in the phreatic zone or in an epikarstic horizon (Williams, 1983). When recharge water arrives at the spring the concentration drops, because recharge water is usually much less mineralised than karst groundwater. Later on, highly mineralised water from the fissured system largely supplies the karst spring, thus causing an increase of concentrations to about the pre-event level.

The lower right diagram of Fig. 5.1 shows that a similar variation may be observed for spring water temperature. If recharge temperature is lower than groundwater temperature the arrival of recharge water at the spring will cause a temperature drop. However, the temperature signal is often delayed compared to the concentration signal. This is observed, for instance, at the carbonate karst spring *Gallusquelle* (Sauter, 1992) and at the gypsum karst spring *Urenbrunnen* (Reichel, 1989; Bundschuh, 1997; compare also section 5.3) both situated in Southern Germany.

As mentioned in section 1.2.2, variations of both solute concentration and water temperature at karst springs are known to reflect the geometry of the karst conduit system. The different behaviour of the two parameters suggests that they probably do not contain the same but complementary information about the karst flow system. Therefore, the process-based modelling tool introduced in chapter 3 can be applied to examine how solute concentration and spring water temperature depend on the structure and geometry of the conduit system in a gypsum karst aquifer.

At first, parameter studies are conducted (section 5.2), in order to examine by forward modelling how spring signals depend on conduit geometry. The parameter studies concentrate on the different behaviour of solute concentration and water temperature as well as on the influence of the hydraulic interaction of fissured system and conduit system.

The model is then applied to characterise the karst aquifer supplying the aforementioned gypsum karst spring *Urenbrunnen* (section 5.3). Aim of the field application of the modelling tool is to find out whether it is possible to infer the geometry of a real conduit system from inverse modelling of karst spring signals.

5.2 Parameter studies

One of the objectives of this work is to examine whether the combined analysis of short-term variations of temperature and solute concentration at a karst spring helps to reduce the ambiguity in the aquifer characterisation. Therefore, the parameter studies aim to find out the differences between heat and solute transport in karst aquifers.

Differences in short-term variations are probably more significant in a system dominated by fast transport in conduits than in coupled systems, where fast conduit flow interacts with a slow flow component. Therefore, pure conduit systems will be considered first, i.e. flow in the fissured system is switched off in the model simulations (section 5.2.1). After that, transport simulations in coupled systems will be presented, in order to examine the influence of the interaction between conduit system and fissured system on karst spring signals (section 5.2.2).

5.2.1 Conduit flow systems

5.2.1.1 Single conduits of variable aperture width

Renner (1996) and Hückinghaus (1998) simulated heat transport in fractures and conduits, respectively. In their simulations, the aperture width along the flow path was varied, while both fracture/conduit volume and area of rock exposed to water remained constant. By that, they demonstrated that temperature signals at the outlet of fractures or

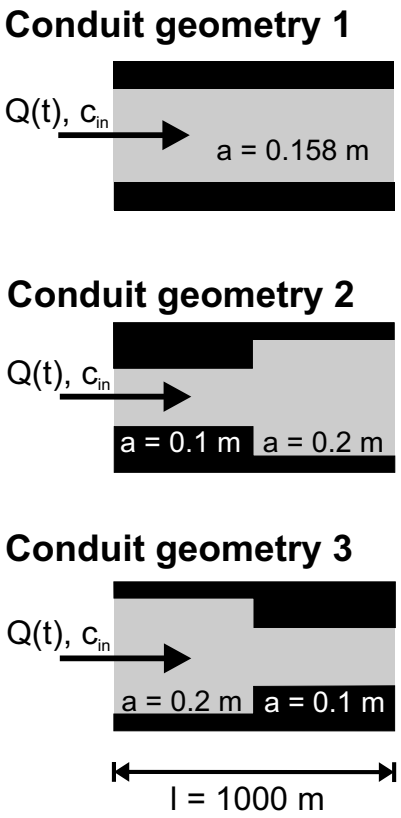

Figure 5.2: Three model set-ups with different conduit geometry. Residence times for the different conduits are identical if flow rates are equal.

conduits of different geometry may be identical for steady-state flow conditions, but can be distinguished if flow is transient.

In order to examine whether a similar result is obtained for hydrochemical signals, gypsum dissolution and solute transport are simulated in conduits of different geometry. Conduit volumes are identical for the three conduits depicted in Fig. 5.2. Therefore, residence times are identical if flow rates in the conduits are equal. The area of rock exposed to water, however, is identical only for the two conduits with geometry 2 and geometry 3. For the conduit with geometry 1 the contact area is larger than for the other conduits. Note that this parameter would be identical in any case if fractures with identical volumes were used instead of circular conduits.

Over a period of three hours, a flow rate of 2 l s^{-1} is applied to the conduits. Then the flow rate is reduced to 1 l s^{-1}. Hydro-

chemical parameters are identical to those of the model verification (section 3.2.3) and the karst genesis simulations (section 4), i.e. the equilibrium concentration is set to 15 mol m^{-3} ($\approx$ 2.6 g l^{-1} dissolved gypsum), and the joint diffusion coefficient of calcium and sulfate is $6 \cdot 10^{-10}$ m^2 s^{-1}. Water initially in the conduit is assumed to be saturated with respect to gypsum, whereas recharge concentration is zero. With the given discharge and conduit diameters, flow is always turbulent. Therefore, Sherwood numbers are calculated using one of the empirical correlations given by eq. (2.37) and eq. (2.38). In combination with eq. 2.34, the first equation allows a direct calculation of diffusion mass transfer coefficients. With a maximum flow rate of 2 l s^{-1} and a minimum diameter of 0.1 m, a maximum value of about $6 \cdot 10^{-6}$ m s^{-1} results for the mass transfer coefficient occurring in the model scenarios. Since this value is more than an order of magnitude smaller than the surface reaction rate constant (compare section 2.3.2.2), gypsum dissolution is diffusion controlled under the given conditions. The resulting concentrations at the conduit outlets were normalised using eq. (3.28) as described in section 3.2.2, i.e. a normalised concentration of one is equivalent to complete saturation while recharge concentration is zero.

At first, eq. (2.37) was used for the calculation of Sherwood numbers. As shown in Fig. 5.3, the recharge water emerges at the outlets of the three conduits at the same time, marked by a significant drop of concentrations. Before the flow rates are varied the concentrations are identical for conduit geometry 2 and 3. In the simulation with conduit geometry 1, the concentration, however, drops to a lower level. At first glance, this might be surprising, because the contact area available for gypsum dissolution is larger for this geometry than for the others. Yet, the increase in diameter results also in an increase of diffusion boundary layer thickness, which slows down the dissolution process. In the karst genesis simulations (section 4.3.2), eq. (3.30) has demonstrated that the two effects compensate each other if the boundary layer is fully developed, i.e. the solute concentration in the conduit is independent of the conduit diameter. If for turbulent flow diffusion boundary layer thickness is parameterised using eq. (2.37) the variation of contact area is even outweighed by the increasing boundary layer thickness. For a conduit with constant aperture width a, this may be demonstrated by replacing the Sherwood number in eq. (3.30) by eq. (2.37), eq. (2.2), and eq. (2.11), yielding a quantitative relationship between conduit diameter a and concentration c at the distance z from the conduit entrance:

$$c(a,z) = c_{eq} - (c_{eq} - c_{in}) \cdot \exp\left(-0.10 D^{2/3} \nu_w^{-7/15} Q^{-1/5} a^{-4/5} z\right) \tag{5.1}$$

Thus, in turbulent flow outflow concentrations decrease with increasing conduit diameters.

Likewise, eq. 5.1 predicts an increase of outflow concentrations for decreasing flow rates Q as it is observed in the simulations after three hours. However, after reducing the flow rate it takes about five hours until a constant concentration level is reached. During this transition period, which is equivalent to the residence time of water in the conduit, the water emerging at the outlet has been flowing at two different flow rates through the conduit. Fig. 5.3 reveals that the outflow concentration during the transition period depends on the sequence of the different conduit diameters. The rise of concentration is faster for the case that the smaller diameter is closer at the outlet of the conduit (i.e. conduit geometry 3). Thus, if the calculation of diffusion boundary layer thickness is based on eq. (2.37) simulations of reactive solute transport yield similar results as heat transport simulations conducted by Renner (1996) and Hückinghaus (1998). Conduits of different geometry can be distinguished if flow is transient.

Whereas the roughness of conduit walls is not taken into account in the above employed eq. (2.37), the more accurate eq. (2.38) includes this parameter. Since both equations

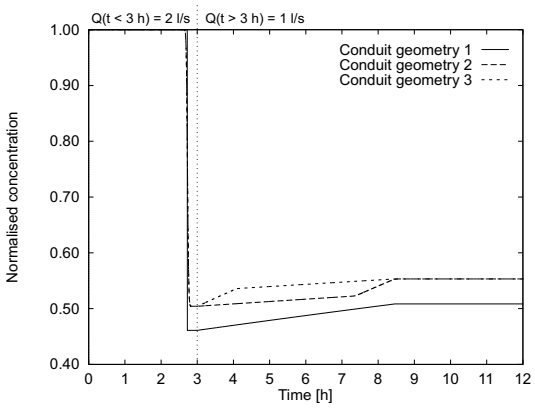

Figure 5.3: Normalised outflow concentrations for the three conduits of different geometry shown in Fig. 5.2 using eq. (2.37) for the calculation of Sherwood numbers.

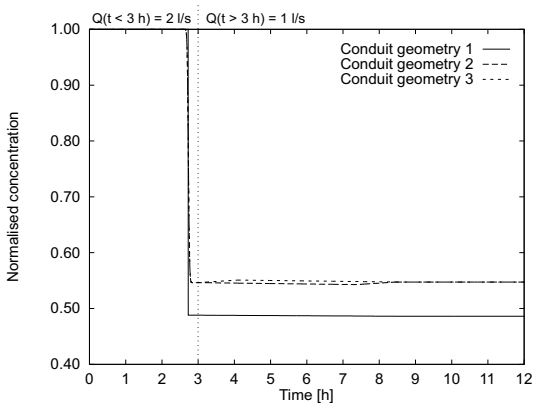

Figure 5.4: Normalised outflow concentrations for the three conduits of different geometry shown in Fig. 5.2 using eq. (2.38) for the calculation of Sherwood numbers.

are empirical correlations for smooth pipes only, a small value for the surface roughness of 0.0001 m was used in simulations with eq. (2.38). Fig. 5.4 shows the solute concentration at the conduit outlet resulting from these simulations. As in the above discussed simulations, gypsum dissolution and solute transport were simulated for conduits of different geometry depicted in Fig. 5.2. As before, the arrival of recharge water at the spring is marked by a drop of concentrations to values which are equal for conduits of geometry 2 and geometry 3, while a lower concentration distinguishes conduit geometry 1 from both of the other conduits. In contrast to the simulations based on eq. (2.37), no significant difference in concentration is observed between geometry 2 and 3 during the transition period after the reduction of flow rates. Hence, geometry 2 and 3 cannot be distinguished when the more accurate eq. (2.38) is employed for calculation of Sherwood numbers in conduits with smooth walls. Based on this equation, solute transport simulations yield a result different from that obtained by Renner (1996) and Hückinghaus (1998) for heat transport. Even if flow is transient conduits of different geometry may not always be distinguished by solute concentrations at the spring.

Both methods used for the quantification of mass transfer across the diffusion boundary layer depend on the assumption of smooth conduit walls. Yet, in a real karst aquifer conduit walls are characterised by high surface roughness. Although the validity of eq. (2.38) is not proven for these conditions, Incropera and DeWitt (1996) suggest to use it as a first approximation. Thus, using eq. (2.38) the surface roughness was varied for the case of conduit geometry 1, in order to examine the influence of rough conduit walls on the simualtion result. Fig. 5.5 reveals that concentrations at the conduit outlet increase with increasing surface roughness. Concentrations are generally lower if eq. (2.37) is used instead of eq. (2.38). This was previously observed in the model simulations conducted for model verification (section 3.2.3.2). Note that in the case of rough conduit walls the simulations predict a decrease of concentrations for decreasing flow rates, which opposes the predication based on usage of eq. (2.37) (compare also eq. 5.1).

The simulations thus reveal a dependency between concentration signals at gypsum karst springs and roughness of conduit walls. Simulation results, however, are based on mass transfer correlation for smooth pipes, because equations for the parameterisation of mass transfer across the diffusion boundary layer are not yet established for conduit walls of high surface roughness. Therefore, the predictive capability of reactive solute transport simulations is reduced if reactions are diffu-

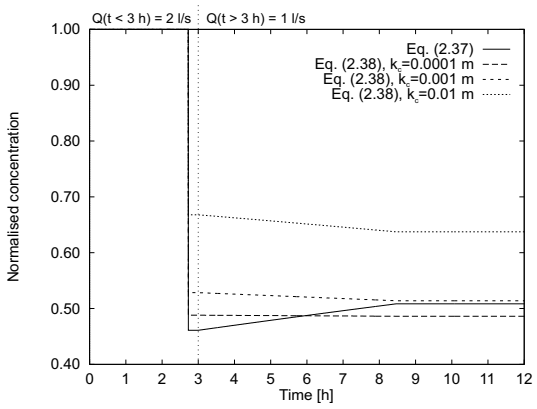

Figure 5.5: Concentration at the outlet of a conduit of geometry 1 (Fig. 5.2) using two different empirical equations for the calculation of Sherwood numbers, one of which takes surface roughness into account, whereas the other does not.

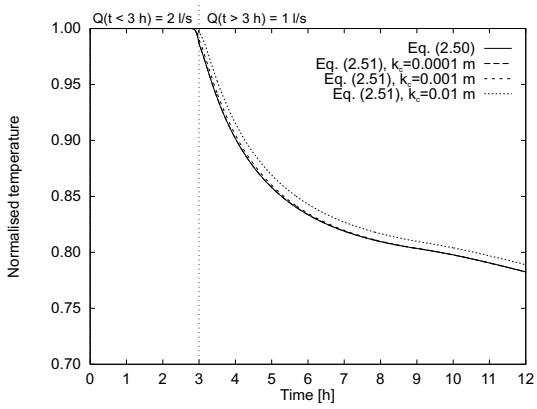

Figure 5.6: Temperatures at the outlet of a conduit of geometry 1 (Fig. 5.2) using two different empirical equations for the calculation of Nusselt numbers, one of which takes surface roughness into account, whereas the other does not.

sion controlled (e.g. gypsum dissolution).

In order to examine whether or not water temperatures are affected in a similar way by the formula selected for calculation of Nusselt numbers, heat transport was simulated for conduit geometry 1 using both eq. (2.50) and eq. (2.51). In addition, the influence of surface roughness on water temperatures was examined when the latter was used. Parameters were chosen like in section 3.2.4. The specific heat of water is 4198 J kg^{-1} K^{-1}, and the thermal conductivity of water is 0.582 J m^{-1} K^{-1}, yielding a thermal diffusivity of $\kappa_w = 1.39 \cdot 10^{-7}$ m^2 s^{-1}. The specific heat of gypsum rock is set to 1088 J kg^{-1} K^{-1}, and the thermal conductivity of gypsum is 1.297 J m^{-1} K^{-1}. With a density of 2320 kg m^{-3} a thermal diffusivity of $\kappa_r = 5.14 \cdot 10^{-7}$ m^2 s^{-1} results for the rock. The initial rock temperature, which is identical to the temperature of the water initially in the conduit, is set to 8 °C. The temperature of recharge water is 6 °C.

Fig. 5.6 demonstrates that the water temperature at the outlet remains almost unaffected from changes of surface roughness. This is because heat transfer from the rock into the conduit water is controlled by slow conduction in the rock rather than by heat transfer across the thermal boundary layer at the conduit wall (compare section 3.2.4.2). For the same reason, the choice between eq. (2.50) and eq. (2.51) does not significantly influence the result of heat transport simulation. Thus, in contrast to solute concentration, water temperature is insensitive to surface roughness of conduit walls. On the one hand, therefore, water temperatures do not provide any information about surface roughness. On the other hand, heat transport simulations are not affected by uncertainties originating from the difficulties connected with quantifying the boundary layer thickness in turbulent flow through rough pipes.

Since heat transport in turbulent flow is not controlled by heat transfer across the thermal boundary layer, the simpler eq. (2.50) is used for the calculation of water temperatures at the outlets of the conduits shown in Fig. 5.2.

Fig. 5.7 depicts the temperatures at the conduit outlets, normalised using eq. (3.41) as described in section 3.2.4.1. Due to fast heat transfer across the thermal boundary layer, temperatures remain almost unchanged even after the first recharge water has emerged at the outlet. Water temperatures decrease after about three hours when temperatures at the conduit walls have fallen as a consequence of slow heat conduction in the rock. The effect of varying flow rates cannot be seen very well

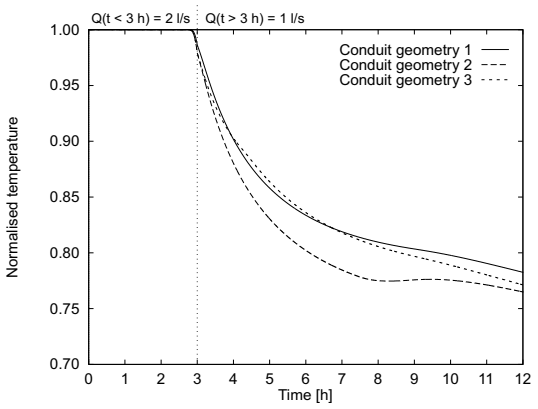

Figure 5.7: Normalised outflow temperature for the three conduits of different geometry shown in Fig. 5.2.

in Fig. 5.7, because the effect of conduit walls cooling down is superimposed.

This example demonstrates that a combined analysis of solute concentrations and water temperatures yields more information than the analysis of a single parameter. On the one hand, temperatures behave very similarly during the first eight hours for geometry 1 and geometry 3, though later on the differences increase. Thus, for these two conduits solute concentrations are more different than water temperatures. On the other hand, using solute concentrations, geometry 2 and geometry 3 can hardly be distinguished, whereas water temperatures for the two conduits differ distinctly over a large period.

Comparison of Fig. 5.3/5.4 and Fig. 5.7 reveals a further difference between solute concentration and water temperature. Whereas the drop of concentration indicates the first arrival of recharge water at the spring, the variation of water temperature may be delayed. Thus, residence time of water in the conduit may be overestimated if considering water temperature only.

5.2.1.2 Single conduit *vs.* pipe network

While the above simulations dealt with single conduits only, the following scenarios address the question of whether single conduits and dendritic pipe networks can be distinguished by combined analysis of solute concentration and water temperature at a karst spring. As shown by the model scenarios above, the results of reactive solute transport simulations are affected by the choice of an empirical equation for the Sherwood number. Since we are interested here in examining the principles of heat and solute transport rather than in an accurate quantification of concentrations and temperatures, the simplest eq. (2.37) and eq. (2.50) were employed for the calculation of Sherwood numbers and Nusselt numbers, respectively. Note that in the following simulations the maximum value for the diffusion mass transfer coefficient given by eq. (2.34) is approximately $6.5 \cdot 10^{-6}$ m s^{-1}, which is much less than the surface reaction rate constant for gypsum dissolution (about 10^{-4} m s^{-1}). Like in the simulations before, therefore, gypsum dissolution is diffusion controlled.

As a first scenario we compare temperatures and concentrations of spring water emerging from a single conduit of 1200 m length with spring signals resulting from heat and solute transport in a pipe network (Fig. 5.8). Both conduit systems consist of 24 pipes, each of a diameter of 0.2 m and a length of 50 m. Thus, both the conduit volume and the area of rock exposed to conduit water are equal for the two systems. Moreover, the pipe network is arranged such that the distance between the individual injection points and the outlet is always identical. Therefore, the residence time of water is the same in both systems provided the total recharge, which is applied to only one point of the single conduit, is distributed equally on the eight inlets of the pipe network.

The water initially in the pipes has equilibrium concentration with respect to gypsum (15 mol m^{-3}) and is in equilibrium of temperature with respect to the rock (8 °C). Recharge with both lower concentration (0 mol m^{-3}) and lower temperature (6 °C) is injected at the nodes marked in Fig. 5.8. The total recharge amounts to 12 l s^{-1} during the first six hours (21600 s)

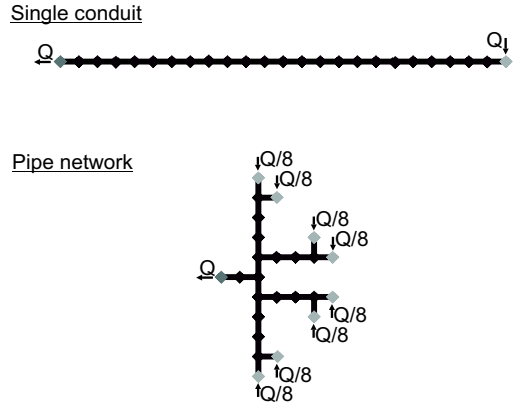

Figure 5.8: Geometry of a single conduit and a dendritic pipe network, both of which have identical conduit volume and identical surface area exposed to water. All pipes are 0.2 m in diameter and 50 m in length.

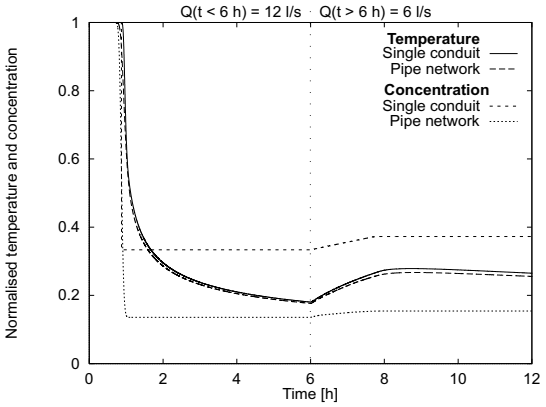

Figure 5.9: Normalised concentration and temperature at the outlets of the conduit systems shown in Fig. 5.8.

and is reduced then to 6 l s^{-1}, i.e. each inlet of the pipe network is supplied with 1.5 l s^{-1} and 0.75 l s^{-1}, respectively. Under these conditions flow in the pipes is always turbulent.

The resulting solute concentrations and water temperatures at the spring were normalised using eq. (3.28) as described in section 3.2.2. A normalised concentration or temperature of one is equivalent to complete saturation or initial rock/water temperature, respectively, whilst normalised recharge concentration and recharge temperature are zero.

Fig. 5.9 shows that the normalised water temperature at the spring obtained by the heat transport simulation is virtually the same for both the single conduit and the pipe network. At a flow rate of 12 l s^{-1} the water takes approximately 52 minutes (3142 s) to flow from the inlet to the spring. Thus, after that time the water temperature falls below its initial value. Since the rock is permanently cooled by recharge water, the temperature keeps falling as long as the flow rate remains constant. When the flow rate is decreased to 6 l s^{-1} the residence time of water in the conduit system increases. Due to the lengthened contact time of water and rock surface, the water temperature rises. At first, however, water emerging at the spring has been mainly flowing with the higher flow rate through the conduit system. Therefore, water temperatures increase as long as emerging spring water has been flowing through the whole conduit system with the lower flow rate. After this transition period, the cooling of the rock matrix and the consequentially decreasing heat flux from the rock eventually causes the water temperature to decrease again. Since the temperature signals of single conduit and pipe network are more or less identical during the whole simulation period, it is not possible in this case to distinguish between the different conduit structures by analysing spring water temperatures only. We will look therefore at the second parameter, i.e. the solute concentration of water emerging at the spring.

Although the solute concentration basically shows a similar behaviour in either case, the values obtained for the single conduit are higher than those of the pipe network (Fig. 5.9). When recharge water appears at the spring, the solute concentration drops below saturation reaching temporarily a constant normalised concentration of 0.33 at the outlet of the single conduit and a value of 0.14 at the outlet of the pipe network. These values may be also obtained using the above derived eq. (5.1). For steady-state conditions this equation can be directly applied to the single conduit. In the pipe network steady-state concentrations can be calculated in downstream direction using the average of

the outlet concentrations of upstream pipes as inflow concentration for each downstream pipe.

Eq. (5.1) demonstrates that spring water concentrations increase with decreasing flow rate. Therefore, the change in flow rates after six hours (21600 s) initiates a transition period, in which the concentration of the spring water increases. After that period water emerging at the spring has been flowing with a constant flow rate through the whole conduit system. Therefore, the normalised concentration again reaches constant values of 0.37 at the outlet of the single conduit and 0.15 at the outlet of the pipe network. Thus, the solute concentration of the spring water emerging from the single conduit is clearly different from the concentration at the outlet of the pipe network even under steady-state flow conditions, i.e. it is possible to distinguish both conduit systems by analysing the spring water concentrations.

This result reflects the different controlling processes of heat and solute transport in a gypsum aquifer. Heat transfer from the rock to the turbulently flowing water is not limited by heat transfer across the thermal boundary layer between rock surface and bulk water, but by heat conduction in the rock matrix. Since the latter does not depend upon the flow conditions in the pipe, conduit systems with identical pipe volume, identical surface area and the same residence time of water in the system will show identical water temperatures at the spring even if flow velocities differ. Gypsum dissolution, however, is controlled by mass transfer across the diffusion boundary layer between pipe wall and bulk water. The thickness of this boundary layer and the mass transfer across it are influenced by the flow velocity in the pipe. Therefore, if flow conditions are not the same in two conduit systems, which are equal with respect to all other properties, solute concentrations will be different at the outlets of the systems. Within the branches of the pipe network shown in Fig. 5.8 flow rates are obviously smaller than in the pipes of the single conduit. Thus, the

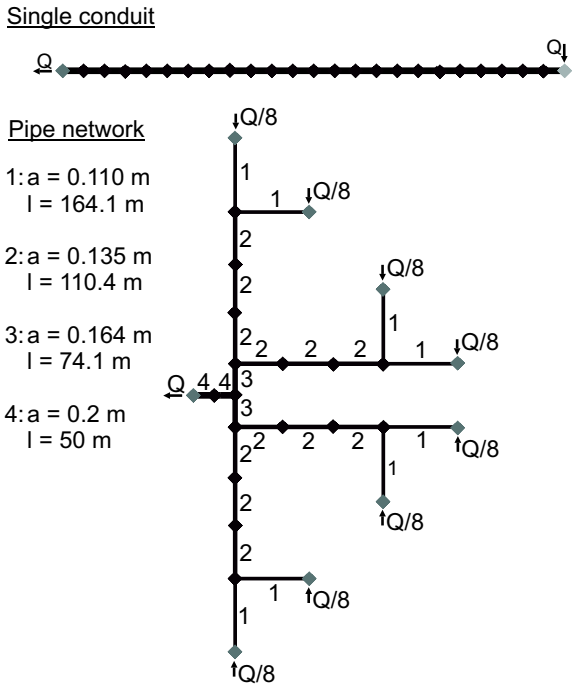

Figure 5.10: Geometry of a single conduit and a dendritic pipe network, both of which have identical conduit volume but different surface area. The single conduit consists of pipes of 0.2 m in diameter and 50 m in length.

diffusion boundary layer is thinner in the single conduit, i.e. the diffusion process is faster and the solute concentration of the spring water is larger as compared to the pipe network.

From the above discussion the question arises, whether a pipe network exists, which shows the same solute concentration at the outlet as the single conduit considered before. In fact, eq. (5.1) reveals, that it is possible to compensate for different flow rates by changing pipe length and pipe diameter. However, if changing these parameters the total volumes of the two conduit systems still have to be equal, since otherwise the residence times of water would be different in the two systems. Fig. 5.10 shows an appropriate pipe network and the corresponding single conduit, which is the same as in scenario one.

The resulting solute concentrations of the spring water (Fig. 5.11) are now the same for

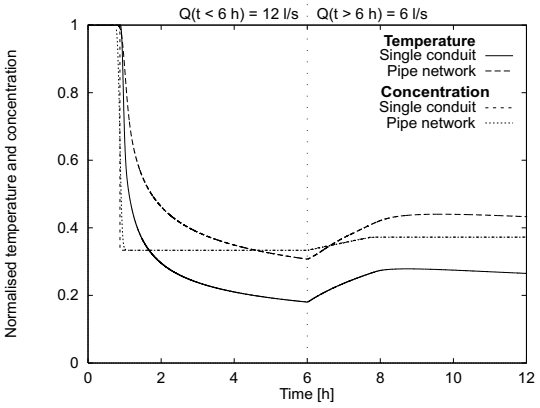

Figure 5.11: Normalised concentration and temperature at the outlets of the conduit systems shown in Fig. 5.10.

the two conduit systems. However, the temperatures of water emerging at the outlet of the pipe network are larger than those of the single conduit. In order to make the pipe network equivalent to the single conduit with respect to solute concentration, the area of rock exposed to water had to be increased as compared to the single conduit. Under these conditions heat transfer between rock and flowing water, which is limited by heat conduction in the rock rather than by velocity-dependent heat transfer across the thermal boundary layer, is faster in the pipe network than in the single conduit, thus accounting for larger temperatures of water emerging from the pipe network.

5.2.2 Coupled flow systems

In this section the single conduit with a length of 1200 m, which has been considered in the previous section, is coupled to a fissured system, in order to examine the effects of a hydraulic interaction of the two flow systems on short-term karst spring response. Fig. 5.12 shows the model domain and the discretisation of the fissured system coupled to the conduit. The width of both rows and columns is generally set to 50 m. In the centre of the domain the conduit is situated in a row of 1 m width, and the width of rows adjacent to this row is successively increased to 50 m (1 m, 1.5 m, 2.5 m, 5 m, 10 m, 20 m, 35 m, 50 m). This central refinement of the model grid aims at a better representation of the steep hydraulic gradients near the conduit.

The aquifer is assumed to be unconfined. The whole model domain is supplied with recharge of 10^{-8} m s^{-1} (316 mm per year). The aquifer drains to a fixed head boundary at the left, which is set to 1 m, while the bottom of the aquifer is set to a height of 0 m. This set-up may be interpreted as a river on the left hand side of the model domain, incised to 1 m above the bottom of a gypsum layer. The hydraulic conductivity of the fissured system is 10^{-5} m s^{-1}.

At first, a conduit of 0.2 m in diameter is coupled to the fissured system with an exchange coefficient of 0.1 m^2 s^{-1} at all nodes. At the fixed head boundary the conduit node is set to a hydraulic head of 1 m. Fig. 5.13 shows the resulting steady-state flow field for the given parameters. The hydraulic heads in the fissured system decrease from the right hand side to the fixed head boundary on the left. There is also a steep hydraulic gradient near the conduit indicating flow from the fissured system into the conduit. In accordance with this observation, the total outflow from the fissured system via the fixed head cells amounts to only about 1.6 l s^{-1}, whereas the outflow from the conduit (i.e. the spring discharge) amounts to 11.6 l s^{-1}. Thus, the model domain is mainly drained by the conduit.

Starting with the steady-state flow field, direct recharge is injected at the right hand end of the conduit with a rate of 5 l s^{-1} over a period of 6 hours (21600 s). The recharge to the fissured system remains unchanged. Water flowing from the fissured system into the conduit is assumed to be saturated with respect to gypsum, while the solute concentration of direct recharge is zero. The temperature of water flowing from the fissured system into the conduit is set to a constant value of 8 °C. The initial temperature of both conduit water and rock temperature is also 8 °C, while the temperature of direct recharge

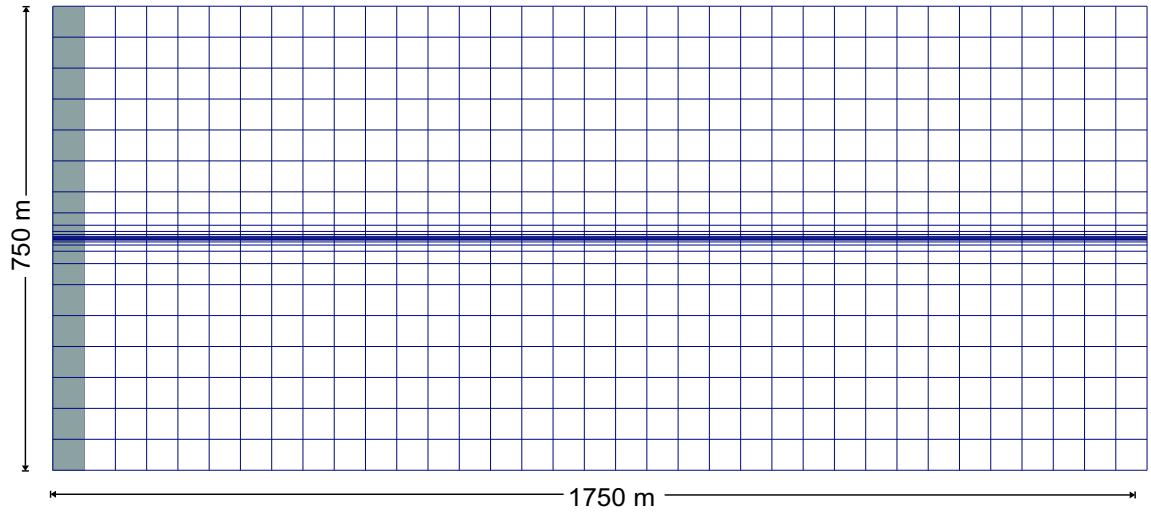

Figure 5.12: Model domain with discretisation of the fissured system. Grey coloured cells are fixed head boundaries, other boundaries are no-flow boundaries.

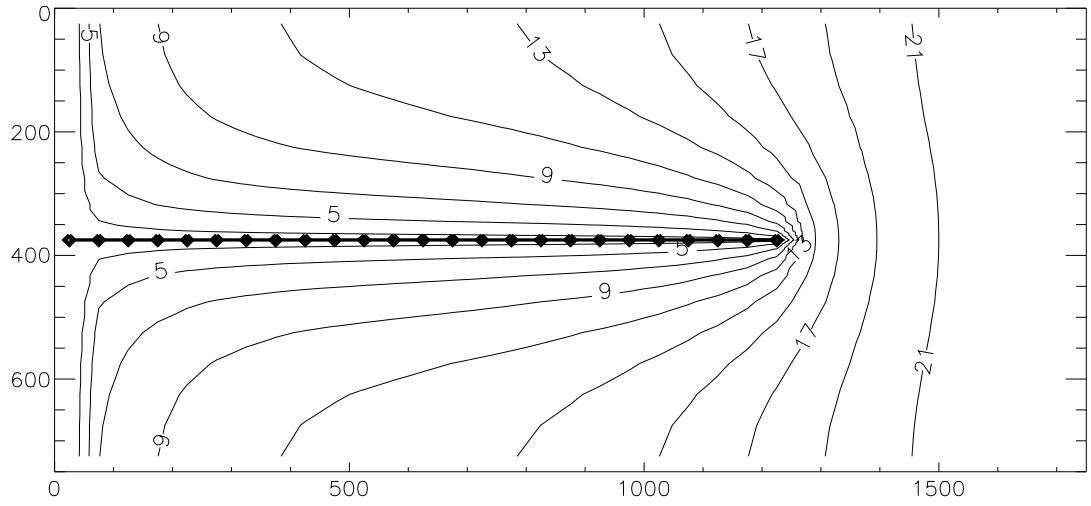

Figure 5.13: Steady-state flow field (hydraulic heads in the fissured system) with a single conduit of 0.2 m in diameter coupled to a fissured system.

is only 6 °C. All other parameters determining heat and solute transport remain unchanged as compared to the above studied model scenarios.

In contrast to karst genesis simulations, where the storage term could safely be neglected in eq. 2.1, storage in the fissured system might play an important role in transient short-term simulations of recharge events. In the first model run the specific yield of the fissured system S_f is set to 0.01. Later on, it is varied. The time step length for the flow simulation is set to 600 s.

Model results of the first scenario ($S_f = 0.01$, $\alpha = 0.1$ m^2 s^{-1}, $a = 0.2$ m) are illustrated in Fig. 5.14. The upper part of the figure shows the total spring discharge as well as the rates of flow from the fissured system into the conduit and of direct recharge into the conduit. Flow from the fissured sys-

tem and direct recharge always sum up to the total spring discharge, because no storage is assumed in the conduit. Although direct recharge rises immediately (i.e. after one time step in the diagram) at the beginning of the simulation, total spring discharge increases slowly due to storage of water in the fissured system. Direct infiltration of water into the conduit causes an increase of hydraulic heads in the conduit system. This reduces the head difference between fissured system and conduit system. Thus, less water flows from the fissured system into the conduit. Since the model domain is mainly drained by the conduit, the obstruction of exchange flow between the two flow systems causes storage of water by an increase of hydraulic heads in the fissured system. As the simulation proceeds, the increase of heads in the fissured system leads to an increase of flow from the fissured system into the conduit, and thus to an increase of spring discharge. When direct recharge to the conduit stops after 6 hours (21600 s) the head difference (and thus the exchange flow) between the two flow systems rises suddenly. Since the conduit is then supplied by water previously stored in the fissured system, the spring discharge decreases slowly to approach the steady-state flow rate (compare Fig. 5.14).

The lower part of Fig. 5.14 illustrates the physico-chemical response of the karst spring. Solute concentration and water temperature have been normalised using eq. (3.28). After about one hour the drop of both concentration and temperature indicates that recharge water directly infiltrated into the conduit emerges at the spring. The concentration decreases immediately to a minimum value of about 0.73 and increases slowly afterwards until after direct recharge is switched off it rises quickly to pre-event values. The slow increase of concentration in a period with constant direct recharge is induced by the coupling of the two flow systems. As can be seen from the upper diagram in Fig. 5.14, the ratio of direct recharge and flow from the fissured system into the conduit is shifted towards the latter during the recharge event.

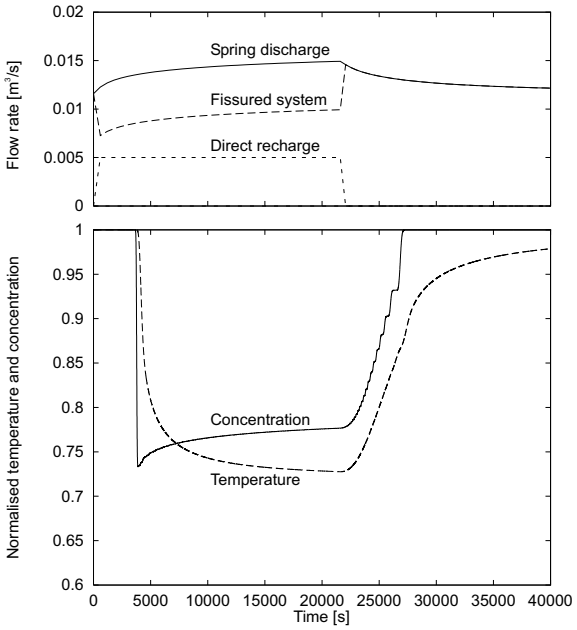

Figure 5.14: Spring signals for a conduit of 0.2 m diameter, a specific yield in the fissured system of 0.01, and an exchange coefficient of 0.1 $m^2\ s^{-1}$.

This change of mixing ratio causes an increase of solute concentrations at the spring, because the portion of gypsum saturated water increases. The low concentration values indicate that direct recharge water still emerges at the spring for more than one hour (about 5000 s) after recharge has stopped. This corresponds to the time the water needs to flow from the inlet at the right hand end of the conduit to the outlet at the left. Concentration increases for two reasons after direct recharge is switched off. Firstly, more water from the fissured system is mixed to the direct recharge water due to the pressure drop in the conduit, thus shifting the mixing ratio of waters from the two flow systems towards the highly saturated water from the fissured system. Secondly, the flow rate decreases in the conduit, causing an increase of residence time in the conduit, and thus higher concentrations (compare eq. 5.1). Temperature decreases more slowly and decreases further until direct recharge stops. The latter has been explained in the previous section by the permanent cooling of conduit walls during the recharge event. In contrast to solute concentration, the water temperature does not reach

its pre-event level during the period shown in Fig. 5.14, but remains colder even if concentration values indicate that spring discharge is composed of water from the fissured system only (i.e. after about 27000 s). The delayed increase of temperature values is an effect of heat transfer from the conduit water to the conduit walls which have been cooled down during the recharge event. Because of this heat transfer and due to conduction within the rock, temperatures of the conduit walls slowly recover to the pre-event rock temperature. Therefore, the conduit water will slowly approach the rock temperature if it is solely supplied by water from the fissured system.

The following scenarios will be used to examine the influence of several parameters on the response of the karst spring. Evidently, some characteristics of spring response are affected by the storage and subsequent release of water in the fissured system. A parameter describing the storage is the specific yield S_f, which has been set to 0.01 in the above scenario. Fig. 5.15 illustrates the hydraulic and physico-chemical spring response resulting for a specific yield of 0.1 while the other parameters remain unchanged. Compared to the previous scenario the spring discharge is less influenced by the injection of direct recharge into the conduit. Due to the higher storage capacity (specific yield of 0.1 as compared to 0.01 in the previous scenario) hydraulic heads in the fissured system increase only slightly and more slowly when exchange flow is obstructed by a pressure increase in the conduit. Therefore, flow from the fissured system into the conduit is reduced nearly by the same amount as is injected into the conduit via direct recharge. For this reason the spring water contains less water released from the fissured system than in the above scenario. Therefore, both concentration and temperature decrease to lower levels if specific yield is increased, i.e. the properties of spring water are shifted closer to those of direct recharge.

Fig. 5.16 depicts the spring response for a fissured system with a low specific yield of 0.001 only. If exchange flow is restricted by a

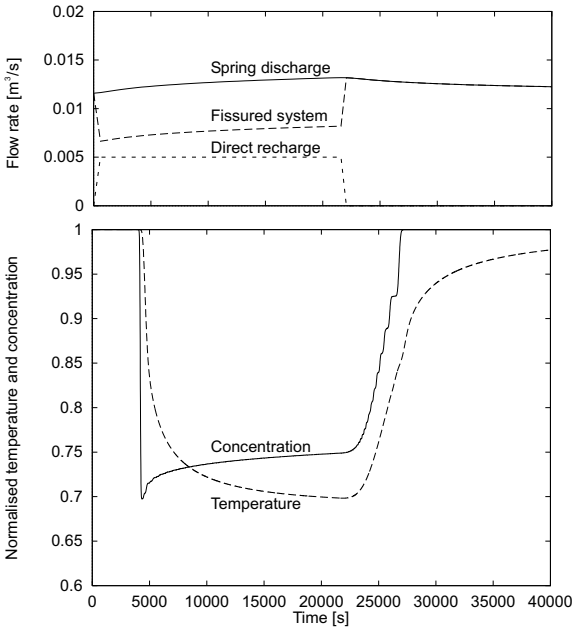

Figure 5.15: Spring signals for a conduit of 0.2 m diameter, a specific yield of the fissured system of 0.1, and an exchange coefficient of 0.1 $m^2\ s^{-1}$.

pressure increase in the conduit the hydraulic heads in the fissured system rise faster than in the previous scenarios. Therefore, flow from the fissured system into the conduit and thus total spring discharge increase faster and reach higher values than before. Compared to the above scenarios the spring water is composed of more water released from the fissured system and less direct recharge. Hence, solute concentration and water temperature increase (i.e. get closer to the properties of the fissured system) with decreasing specific yield of the fissured system. Yet, the principle behaviour of the karst spring is the same in any case, and the differences between the three scenarios are small compared to the large variation of specific yield.

The above explanations demonstrate that the hydraulic interaction of the two coupled flow systems not only determines the hydraulic but also the physico-chemical response of a karst spring after a recharge event. Thus, simulation results may be expected to be sensitive to the exchange coefficient α coupling the two systems. However, model simulations reveal that an increase of the selected exchange coefficient does not affect the simulation re-

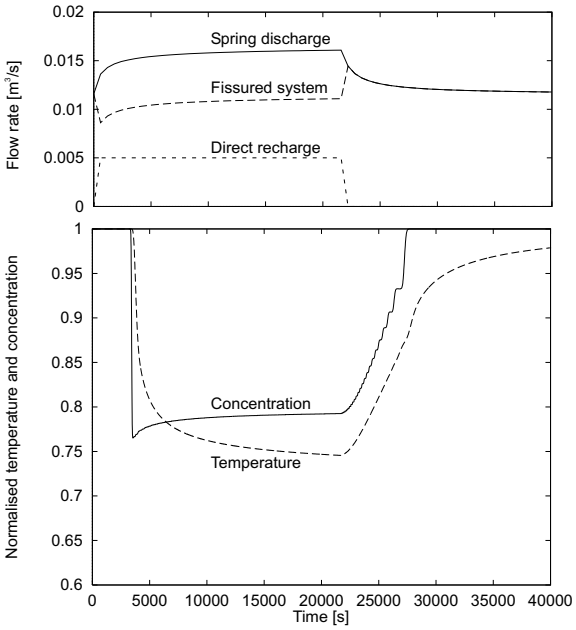

Figure 5.16: Spring signals for a conduit of 0.2 m in diameter, a specific yield of the fissured system of 0.001, and an exchange coefficient of 0.1 $m^2\ s^{-1}$.

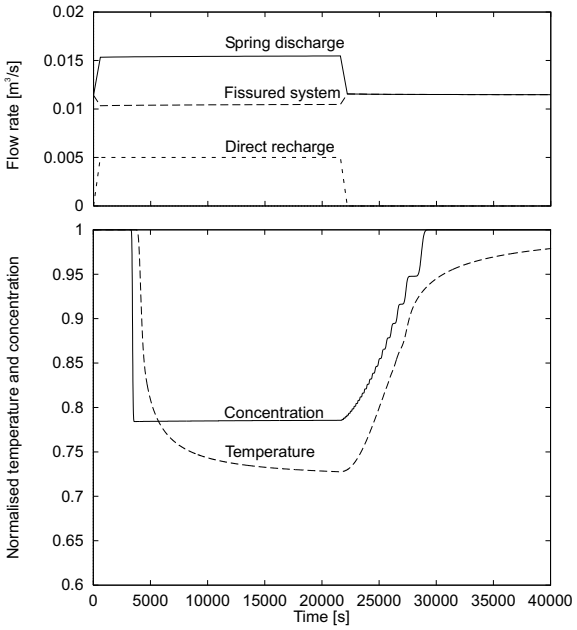

Figure 5.17: Spring signals for a conduit of 0.2 m diameter, a specific yield of the fissured system of 0.01, and an exchange coefficient of 0.0001 $m^2\ s^{-1}$.

sults. The same is found if the exchange coefficient is only moderately decreased. Yet, it is evident that a further decrease will yield similar results as the scenarios shown in section 5.2.1 when the exchange coefficient approaches zero.

Fig. 5.17 shows the results of a model run with a considerably reduced exchange coefficient of 0.0001 $m^2\ s^{-1}$ and a specific yield of 0.01. Remarkably, the steady-state spring discharge which is only provided by the fissured system is nearly the same as with an exchange coefficient of 0.1 $m^2\ s^{-1}$ (11.4 $l\ s^{-1}$ instead of 11.6 $l\ s^{-1}$). Thus, the hydraulic head difference between both flow systems is much higher in the scenario with the small exchange coefficient (compare eq. 2.10). In this situation, an increase of pressure in the conduit, induced by the injection of direct recharge, causes a relatively small change of the hydraulic head difference between the two flow systems. The rate of flow from the fissured system into the conduit, therefore, is much less influenced by the recharge event than in the above scenarios. Since exchange flow from the fissured system remains nearly on pre-event level, the total spring discharge rises rapidly to more than 15 $l\ s^{-1}$ when direct recharge is applied to the conduit. When direct recharge water emerges at the spring solute concentrations decrease to values higher than in the above scenarios, because of the large portion of highly saturated water from the fissured system contained in the spring discharge. Due to the weak interaction of both flow systems the concentration remains on an almost constant level during the recharge event. The water temperature, however, decreases because of the continuously cooling conduit walls.

As a final scenario of the parameter studies, a conduit diameter of $a = 0.5\ m$ is used. Fig. 5.18 shows the simulation results. Note that the simulation time is increased compared to the other model runs. Hydraulic response of the karst spring is similar to the above scenario with a small exchange coefficient. Evidently, the pressure increase in the conduit due to injection of direct recharge is smaller if the conduit diameter is larger. Thus, the rate of flow from the fissured system into the conduit remains nearly constant. The physico-chemical response of the karst spring, however, is different compared to the

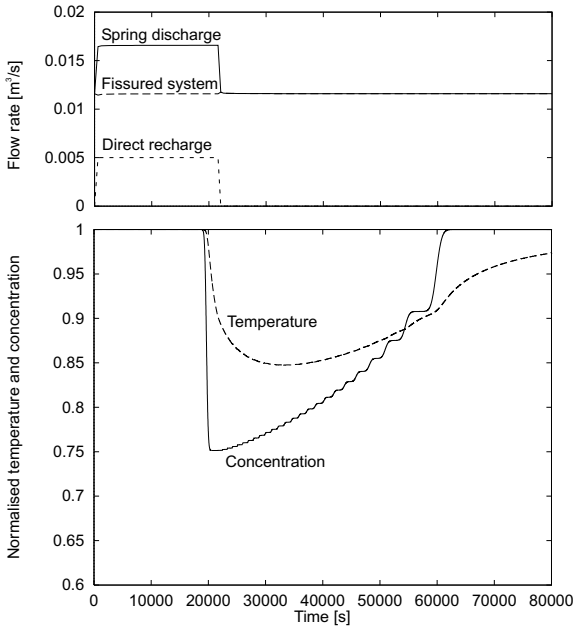

Figure 5.18: Spring signals for a conduit of 0.5 m diameter, a specific yield of the fissured system of 0.01, and an exchange coefficient of 0.1 $m^2\ s^{-1}$.

previously studied scenarios. As a consequence of the larger conduit diameter, the flow velocity is lower and the residence time of water in the conduit is larger than before. Therefore, both solute concentration and water temperature decrease after more than five hours (18000 s). More importantly, the temperature drop is much weaker than in the scenarios with a small conduit diameter, whereas the concentration values are within the previously observed range. Both of these parameters are influenced by the lengthened residence time which brings the water closer to equilibrium with the surrounding rock (i.e. equilibrium concentration and rock temperature, respectively). Yet, in the case of solute transport this effect is superimposed by the increase of diffusion boundary layer thickness with increasing conduit diameter, which slows down the diffusion controlled dissolution of gypsum. Boundary layer thickness, however, is not a controlling process of heat transport in the aquifer. In contrast to solute concentrations, therefore, temperatures increase due to the lengthened residence time of water in the conduit. Thus, temperature is found to be more sensitive to changes in conduit diameter than solute concentration.

5.3 Field application

In the above parameter studies the hydraulic and physico-chemical response of a karst spring to recharge events was simulated for a given conduit structure. This forward modelling is certainly useful to deepen the understanding of the relation between aquifer properties and karst spring response. The final objective of the model application, however, is to infer aquifer properties such as conduit geometry from signals measured at a karst spring, i.e. inverse modelling. In this section the inverse approach is applied to a field site, aiming at the development of a general methodology to be followed for the model application rather than at the site characterisation itself.

Modelling of flow and transport requires an adequate knowledge of geologic and hydrogeologic conditions at the field site. Aquifer properties were partly known from site-specific literature (section 5.3.1). In addition, recession of discharge measured at the spring (section 5.3.2.1) and results of a combined tracer and recharge test conducted at the field site (section 5.3.2.2) were used to define several possible model set-ups (section 5.3.3). The models were then calibrated to spring discharge and solute concentration measured after a recharge event using recharge as calibration parameter (section 5.3.4). In order to validate the calibrated models, the measured spring water temperatures were simulated by heat transport modelling (section 5.3.5). Finally, the sensitivity of heat transport simulations was examined (section 5.3.6).

5.3.1 Field site

The field site is situated approximately 50 km south-west of Tübingen in the *Gäu* region of Southern Germany (Fig. 5.19). Among several gypsum karst springs, the *Urenbrunnen*

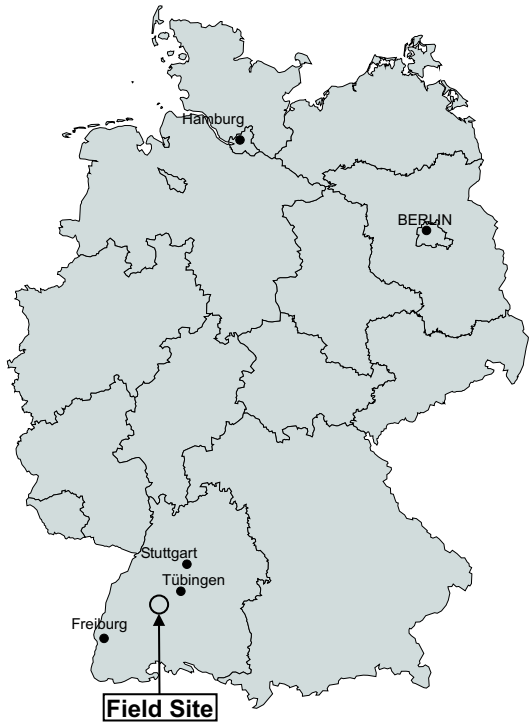

Figure 5.19: Location of field site.

in the south of the town of Vöhringen discharges the highest flow rates in this area. More importantly, the spring exhibits short-term variations of both solute concentrations and water temperatures after substantial recharge events (Reichel, 1989; Bundschuh, 1991, 1997). The *Urenbrunnen* catchment, therefore, was selected as a field site for the application of the numerical model.

Fig. 5.20 shows a geological cross-section through the area south of the *Urenbrunnen*. The spring discharges from Triassic gypsum layers (*Grundgipsschichten*) of about 20 m thickness. Gypsum alternates with clays and marls in the upper part of these layers. The lower part, however, is almost free from clay/marl-intercalations, thus allowing the evolution of karst conduits (Reichel, 1989). The gypsum layers crop out in a SW-NE striking belt, the width of which ranges between several hundreds of metres and about one kilometre.

Hydraulic conductivies of the gypsum layer are not available for the area of the field site. The results of pumping tests conducted in the same stratigraphic layer in the area of Stuttgart (Ufrecht, 1998) may serve as first approximation. There, the transmissivity of the karstified gypsum layer ranges from $1 \cdot 10^{-3}$ to $5 \cdot 10^{-3}$ m^2 s^{-1}, though in areas, where gypsum has been almost completely dissolved, transmissivities are much lower due to the relative enrichment of clays and marls. Assuming that only the lower part of the gypsum is karstified (since the upper part is rich of clay and marl), the aquifer thickness amounts to about 10 m, yielding hydraulic conductivities from $1 \cdot 10^{-4}$ to $5 \cdot 10^{-4}$ m s^{-1}. Yet, these values may only provide an order of magnitude estimate for the field site considered here.

The catchment area of the spring is not known precisely. Estimates about the size of the area may be derived from water budget calculations. During the hydrologic year 1987 Reichel (1989) measured both spring discharge (41 l s^{-1} at average) of the spring and precipitation (989 mm per year, corresponding to 31.3 l s^{-1} km^{-2}) at a station close to the spring. Moreover, he calculated potential evapotranspiration with the method of Haude (1955) using air temperature and air humidity data from a station situated about 25 km south of the *Urenbrunnen* catchment. Temperature values were corrected based on the known difference of mean annual temperatures between the locations. Taking into account the field capacity of soils, the method of Renger et al. (1974) yielded an actual evapotranspiration of approximately 590 mm per year (18.7 l s^{-1} km^{-2}). Subtracting actual evapotranspiration from precipitation as given by Reichel (1989) yields a maximum recharge (i.e. assuming that no surface runoff occurred) in 1987 of 12.6 l s^{-1} km^{-2}. Comparing maximum recharge (12.6 l s^{-1} km^{-2}) and spring discharge (41 l s^{-1}) reveals that the catchment comprises an area of at least 3 km^2, though the area within the orographic water divide is considerably smaller.

In order to determine flow direction and subsurface catchment area, Reichel (1989) measured the strike of fractures, conduits and

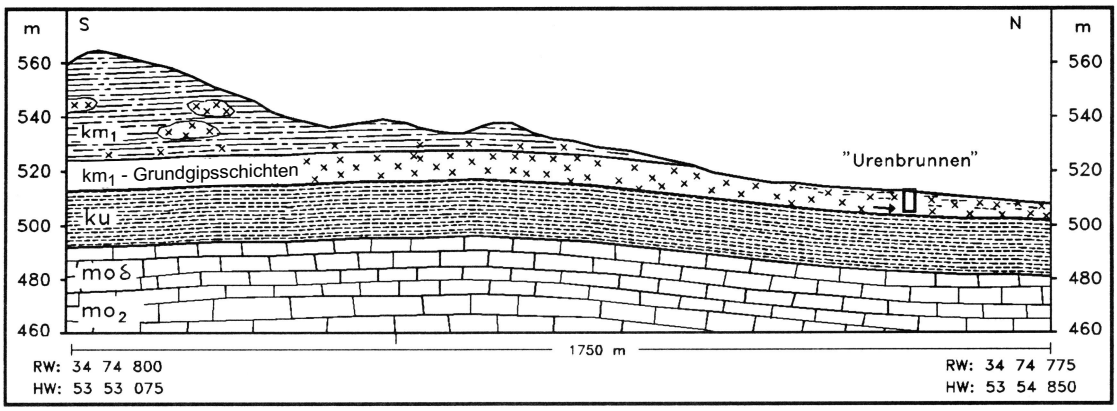

Figure 5.20: Geological cross-section through the *Urenbrunnen* catchment (from Bundschuh, 1991, slightly modified). km1: *Gipskeuper* (including *Grundgipsschichten*), ku: *Lettenkeuper*, mo: *Oberer Muschelkalk*.

caves. In addition, he analysed scallops in a cave south of Vöhringen. These field observations indicate a dominant flow direction from SSW to NNE, which approximately corresponds to the dip of layers (approximately 3° to 4° to NE).

Two tracer tests conducted in 1980 confirmed a flow direction from SSW to NNE (Münzing, 1980). In the first experiment, a tracer was injected into a sink (*Grangärten*) situated about 170 m SSE of the *Urenbrunnen* spring. About three hours later the tracer was detected at the spring, yielding a linear velocity of 53 m h^{-1}. In the second test, a tracer was injected into a borehole situated about 1 km south of the spring. The tracer emerged at several points east of the spring, but not at the spring itself.

Reichel (1989) measured discharge, water temperature, electrical conductivity and solute content of water at the *Urenbrunnen* spring in 1986 and 1987. The measuring and sampling frequency varied from weekly to monthly. The modelling approach to be applied here, however, is based on the analysis of short-term variations in the order of hours or days only. Therefore, additional field work was required to provide data for model set-up, calibration and validation.

5.3.2 Field work

As demonstrated by the previous section, the hydrogeologic characterisation of the field site is still incomplete. Therefore, additional field work was conducted. Time series of hydrological and physico-chemical parameters were measured at the *Urenbrunnen* spring (section 5.3.2.1). Moreover, a combined tracer and recharge test was conducted, in order to examine effects of water infiltration at a sink on discharge and physico-chemical parameters at the spring (section 5.3.2.2).

5.3.2.1 Time series of hydrological and physico-chemical parameters

In order to measure short-term variations of hydraulic and physico-chemical parameters, an automatic digital data logger (PHYTEC PRODATA) was installed at the *Urenbrunnen* spring. Spring water level, spring water temperature and electrical conductivity of spring water were measured at 30 minute intervals. In addition, spring discharge was measured at intervals of about one month using a flow meter. Correlation of discharge and water level yielded a stage-discharge relation (see appendix A), which was employed then to transform the automatically recorded spring water levels into spring discharge rates. Note that

the highest measured discharge was 89 l s^{-1}. Flow rates above this value are based on extrapolation of the stage-discharge relation and thus have to be considered as estimates only. In addition to discharge measurement, water samples were taken and analysed for major cations (using AAS) and major anions (using Ionchromatography) in the hydrogeochemistry laboratory of the Center for Applied Geoscience, University of Tübingen (appendix B). Sulfate concentrations measured in these samples were linearly correlated to electrical conductivities recorded at the spring (appendix C).

Fig. 5.21 (p. 88) shows the measured time series of discharge, electrical conductivity and water temperature from October, 1999 to October, 2000. Daily precipitation was provided by the *Deutscher Wetterdienst* for the station Haigerloch, which is about 10 km ENE of Vöhringen situated at about the same topographic height as the *Urenbrunnen* spring.

The most distinct karst spring response was observed in December, 1999 when both heavy precipitation and snow melt increased the spring discharge to nearly 120 l s^{-1}. At the same time electrical conductivity and water temperature decreased. However, the minimum electrical conductivity was observed almost six days earlier than the minimum temperature. Electrical conductivity may be considered as a measure of solute content of spring water. Thus, the measured response of the *Urenbrunnen* spring corresponds to the typical behaviour of a coupled fissured-conduit system as revealed by the parameter studies in section 5.2.2. Electrical conductivity reached its minimum value even before the maximum spring discharge was measured.

This behaviour has been explained in section 5.2.2 by the temporal variation of the composition of inflow into the conduit system, i.e. highly mineralised water released from the fissured system and low mineralised direct recharge into conduits. At the beginning of a recharge event hydraulic heads rise rapidly in the conduit system, whereas heads increase more slowly in the fissured system. Flow from the fissured system into the conduit system, therefore, is obstructed, and there might be even flow from conduits into the fissured system. Since the ratio of direct recharge and flow from the fissured system into the conduit system is highest at the beginning of a recharge event, electrical conductivity drops sharply when the first recharge water emerges at the spring. With increasing duration of the recharge event flow from the fissured system into the conduit system increases as compared to direct recharge. This causes an increase of solute concentrations (measured as electrical conductivity) at the spring as well as a further increase of spring discharge. As demonstrated by the parameter studies in section 5.2.2, water temperature may decrease as long as the conduit walls are cooled down by the direct infiltration of cold recharge water into conduits. The end of the recharge event is indicated by an increase of water temperature. Both minimum of water temperature and maximum of spring discharge, therefore, occur at about the same time.

As indicated by the duration of both temperature decrease and increase of spring discharge, the total length of the recharge event in December 1999 amounted to about three weeks. Yet, the fluctuations of discharge and temperature, and even more clearly the occurrence of several electrical conductivity peaks, demonstrate that several discrete recharge events followed each other during this period. The superposition of several events makes this period difficult to analyse. For a first application of the numerical model a discrete single event is better suited.

Such a single recharge event was observed at the end of May 2000 when a precipitation of 55.5 mm was measured on a single day (Fig. 5.22). About five and a half hours after discharge had begun to rise, the electrical conductivity started to drop to the lowest value of the whole observation period. At the same time the temperature increased by approximately 0.25 °C. Compared to the above mentioned winter event, temperature increase

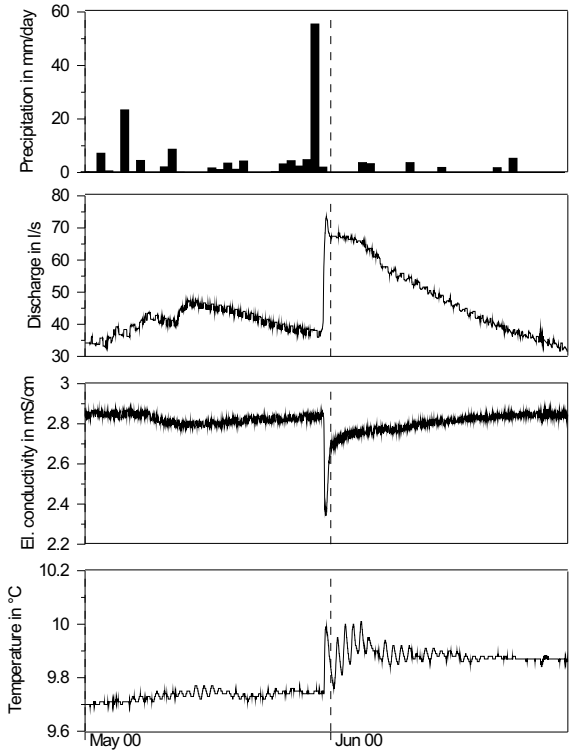

Figure 5.22: Time series of hydrological and physico-chemical parameters at the *Urenbrunnen* spring in May and June 2000.

thus was considerably less. Moreover, the maximum temperature peak occurred almost at the same time as the minimum of electrical conductivity, which may be explained by the short duration of the recharge event. In the days after the event, when electrical conductivity had risen again, a daily variation of water temperature was still observed. On June 7, 2000 a flow measurement in a drain ending in the aforementioned *Grangärten* sink yielded flow rates of approximately 5 l s^{-1}. Electrical conductivity of water in the drain was almost identical to the value measured at the spring, thus indicating that the groundwater level had risen above the bottom of the drain. Water temperature in the drain, however, showed an increase during the day from 11.0 °C at 9:45 to 12.2 °C at 12:10 and 14.0 °C at 16:00 (Central European Summer Time). All of these temperature values were above spring water temperature. It may be concluded from these observations that the temporal variations observed at the *Urenbrunnen* spring after recharge, are probably mainly caused by water infiltrating at the *Grangärten* sink.

5.3.2.2 Tracer and recharge test

In order to better understand the relation between infiltration at the *Grangärten* sink and response of the *Urenbrunnen* spring a combined tracer and recharge test was conducted on June 27, 2000. 600 g of Uranin were dissolved in 100 l of demineralised water and injected into the sink at a distance of approximately 170 m from the spring. In between five and ten minutes later 6.9 m^3 of water with a temperature of 14.8 °C and an electrical conductivity of 0.70 mS cm^{-1} (at 25 °) were injected. After about 45 minutes, 7.0 m^3 of water (temperature: 11.9 °C; electrical conductivity: 0.68 mS cm^{-1}) were injected once more. Even after the second injection there was still some Uranin visible at the edges of the drain which ends in the sink. Since the natural flow rate in the drain was very low (less than 1 l s^{-1}), a part of the tracer remained in the sink.

Water level, electrical conductivity and water temperature were measured at the spring every minute using a data logger (Phytec Prodata). Spring discharge was measured using a flow meter. Uranin concentrations were measured fluorometrically (Turner Field Fluorometer 10-AU-005) and integrated over intervals of one minute. In addition, water samples were taken from a small spring about 300 m NW of the *Urenbrunnen* and fluorometrically analysed in the laboratory (Perkin-Elmer LS-3B).

Fig. 5.23 (p. 89) shows the response of the *Urenbrunnen* spring to tracer and water injection. The water level measurement was disturbed by a periodical abstraction of spring water over a period of 10 minutes with a subsequent break of 20 minutes, which could not be stopped during the tests. Water levels which were recorded at one minute intervals (thin line), therefore, were plotted as a

moving average over 30 minutes (thick line). During the night the withdrawal of water was interrupted, which caused a higher water level until pumping started again at the next morning. In spite of the disturbance of water level measurements, the moving average shows clearly that the water level rose rapidly after water injection but decreased slowly over a period of several hours. The rapid rise of water levels at the spring indicates that sink and spring are connected by a phreatic (i.e. water filled) conduit system which is able to transmit the pressure impulse rapidly.

Using the aforementioned stage-discharge relationship (see appendix A), the water levels can be transformed into spring discharge rates yielding approximately 34 l s^{-1} previous to water injection, approximately 37 l s^{-1} as maximum discharge, and a recession to slightly less than 35 l s^{-1} 9 hours after tracer injection. However, using a flow meter a spring discharge of only 32 l s^{-1} was measured during recession. More importantly, integrating discharge rates (determined using the stage-discharge relation) over time yields a water volume of nearly 34 m^3 after 9 hours, i.e. a volume too large by a factor of 2.5 compared with the injected water volume. This clearly demonstrates that the stage-discharge relation derived from measurements ranging between 13 l s^{-1} and 89 l s^{-1}, which were probably sometimes affected by water withdrawal, measurement errors (data logger or hydrometer) etc., is not well suited to determine small variations of spring discharge. Applying the stage-discharge relation to the water levels measured during the night, which were not affected by water withdrawal, yields a discharge of between 36 l s^{-1} and 37 l s^{-1}. The difference to the spring discharge during the day is roughly in accordance with estimates of the rate of water withdrawal (about 1 l s^{-1}, personal communication with Mr. Treinen, Town of Vöhringen).

While no Uranin was detected at the small spring 300 m NW of the *Urenbrunnen*, a tracer recovery of 73% after 24 hours (57% after 10 hours) is determined at the *Urenbrunnen* based on an average spring discharge of approximately 35 l s^{-1}. The Uranin concentration started to rise rapidly at about 200 minutes after tracer injection (Fig. 5.23, p. 89). This time of initial arrival corresponds to a maximum linear velocity of 51 m h^{-1}. The peak concentration was measured after 332 minutes, yielding a dominant linear velocity of 31 m h^{-1}. Analysing the shown Uranin curve with the method of moments as described by Field (1999) yields a mean tracer residence time of 503 minutes and a mean tracer velocity of 20 m h^{-1}. Using the method of moments a longitudinal dispersivity of 21 m results for the shown curve. A much smaller dispersivity of 2 m results from an adaptation of the analytical solution for a Dirac impulse (Käss, 1992) to the rising limb of the curve. These differences reflect the strong asymmetry of the tracer breakthrough curve, as it is frequently observed at karst springs (compare section 2.2.2).

Using an average spring discharge of about 35 l s^{-1}, the conduit volume can be estimated from the tracer residence time (Field, 1999), yielding 426 m^3 (initial arrival), 703 m^3 (peak) and 1107 m^3 (method of moments). Dividing the conduit volume by the distance sink-spring yields an estimate for the cross-sectional area of flow (initial arrival: 2.5 m^2; peak: 4.1 m^2; method of moments: 6.5 m^2), which can be easily transformed into the corresponding diameter of a circular conduit (initial arrival: 1.8 m; peak: 2.3 m; method of moments: 2.9 m). The same parameters may be estimated using the analytical solution for a Dirac impulse, which was adapted to the rising limb of the tracer breakthrough curve, yielding a conduit volume of 585 m^3, a flow cross-section of 3.4 m^2, and a conduit diameter of 2.1 m.

At about the same time when the Uranin emerged at the spring the electrical conductivity of the spring water was reduced by approximately 2% (Fig. 5.23), because the injected water was less mineralised than the aquifer water. Taking into account the electrical conductivity of both injected water and

aquifer water, a recovery of 90% is determined after 24 hours (84% after 10 hours). The values recorded every minute (thin line) show fluctuations which were smoothed by calculating moving averages over 10 minutes (thick line). Yet, the results of the recharge test must be considered less reliable than those of the tracer test, since the signal is very week compared to the amplitude of fluctuations. Nevertheless, the curve of electrical conductivity can be analysed similarly to a tracer breakthrough curve. Neglecting that electrical conductivity decreases slightly from the beginning, the kink after about 260 minutes indicates the first arrival of the injected water, yielding a maximum linear velocity of 39 m h^{-1}. The peak was recorded after 367 minutes, yielding a dominant linear velocity of 28 m h^{-1}. Applying the method of moments yields a mean residence time of 485 minutes and a mean velocity of 21 m h^{-1}. Like for the tracer test conduit volumes (initial arrival: 470 m^3; peak: 661 m^3; method of moments: 895 m^3), cross-sectional area of flow (initial arrival: 2.7 m^2; peak: 3.9 m^2; method of moments: 5.2 m^2) and corresponding diameter of a circular conduit (initial arrival: 1.9 m; peak: 2.2 m; method of moments: 2.6 m) may be estimated from the recharge test. Thus, the results of the recharge test are similar to those of the tracer test. This indicates that solute concentrations did not considerably increase due to gypsum dissolution, since otherwise an apparently lower recovery of the injected water would have occurred.

The injected recharge was not only of different mineralisation but also of higher temperature than the aquifer water. Nevertheless, the water temperature at the spring did not increase, but a slight decrease of temperature was observed significantly earlier than the initial tracer arrival at the spring. Before water injection water temperature at the spring was nearly constant. Thus, the measured variation is probably caused by the water injection. A possible explanation relies on the assumption of various water temperatures in different parts of the aquifer. Due to the injection of water the flow field might have changed then, so that more water of lower temperature emerged at the spring, while flow from warmer parts was temporarily obstructed. Yet, this explanation remains rather speculative. Moreover, the variations are so small that measurement errors cannot be excluded. Temperature values, therefore, were not used for the design of the numerical model for the *Urenbrunnen* catchment.

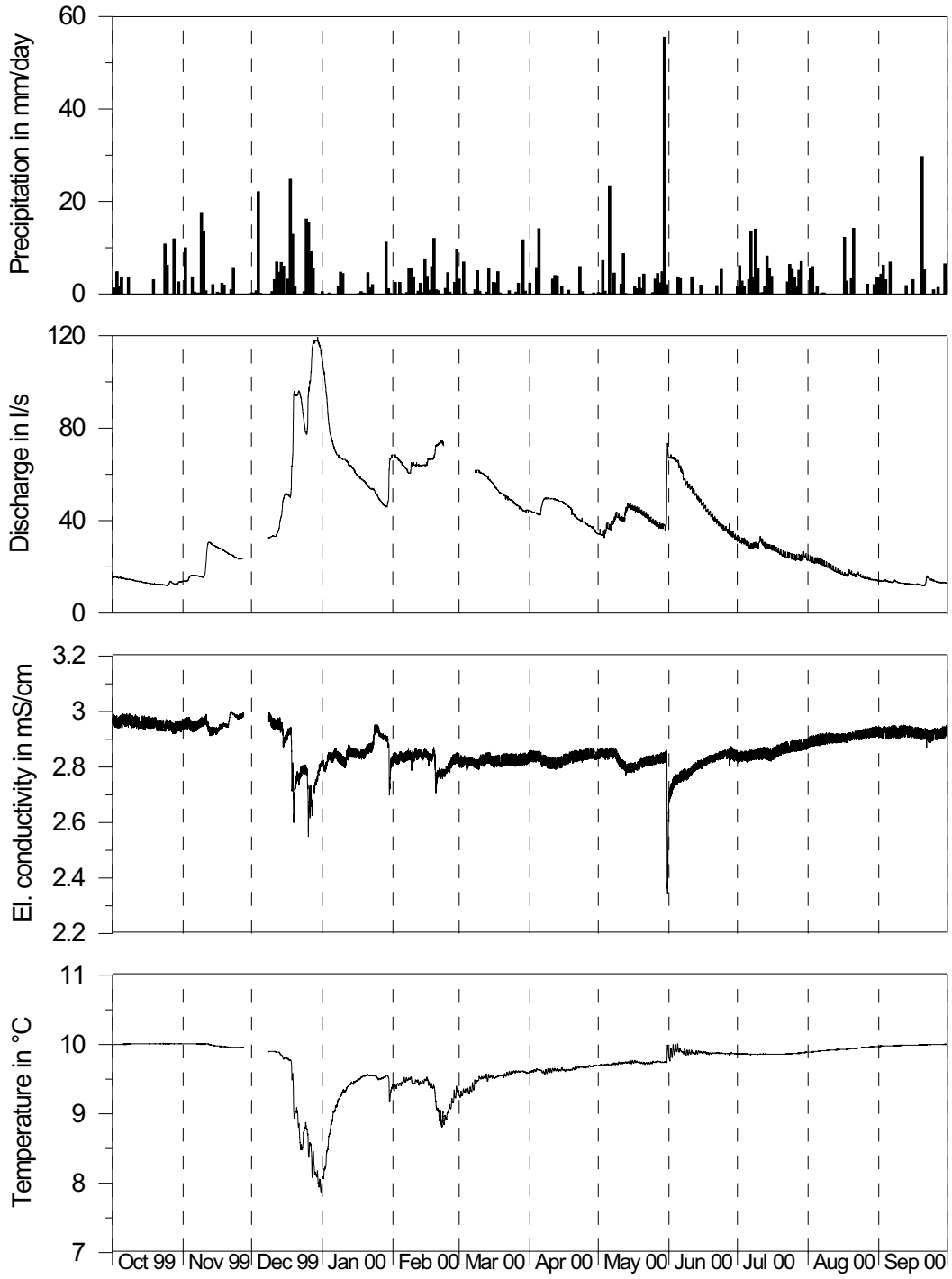

Figure 5.21: Time series of hydrological and physico-chemical parameters at the *Urenbrunnen* spring, Vöhringen, Germany.

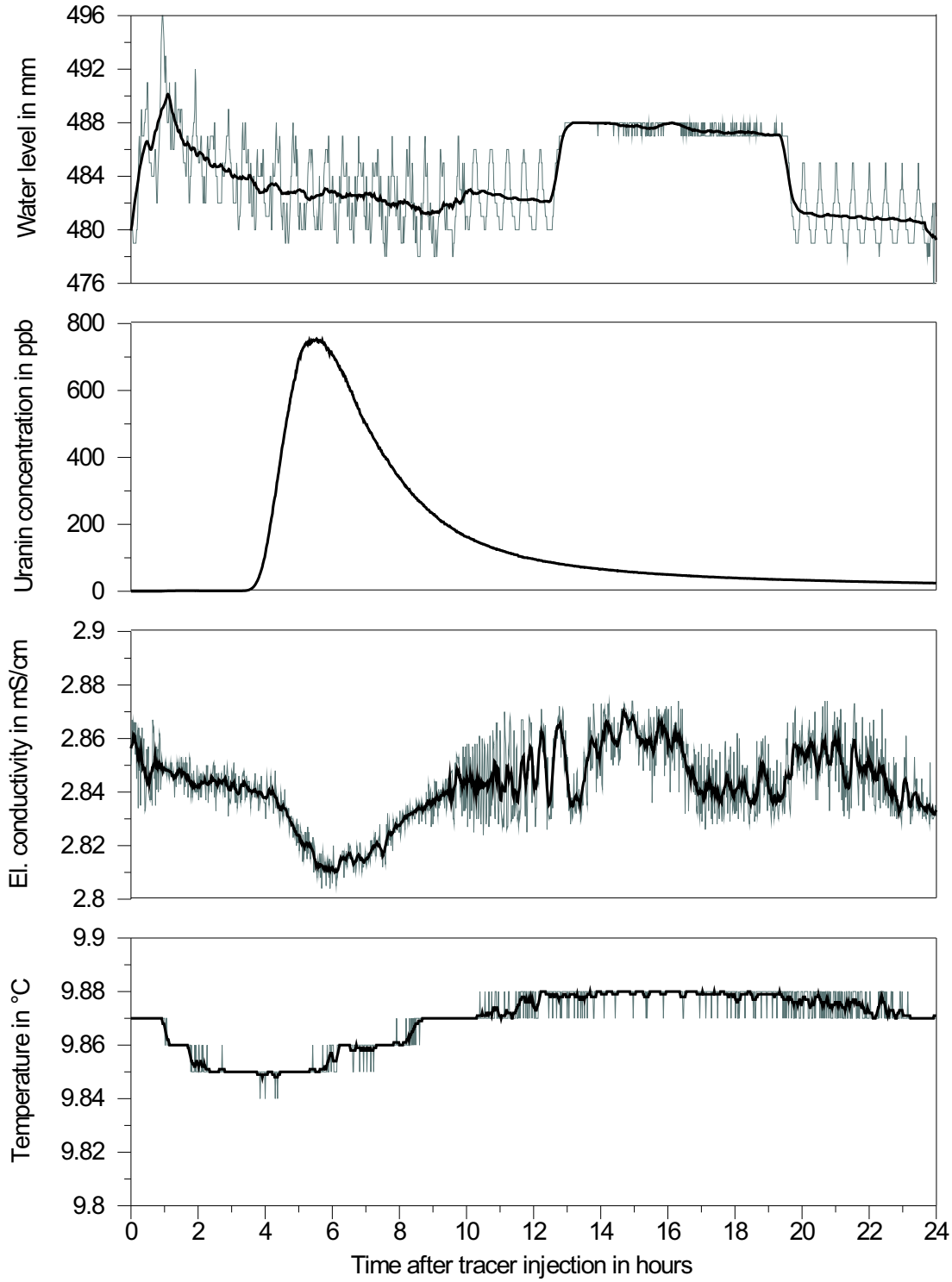

Figure 5.23: Response of the *Urenbrunnen* spring to tracer and water injection at the *Grangärten* sink.

5.3.3 Model set-up

This section describes the development of a model set-up for the numerical simulation of flow and transport at the field site. At first, the general methodology and its adaptation to the present case are outlined. After that, four possible model set-ups are presented, all of which are mainly based on results of the combined tracer and recharge test.

5.3.3.1 Methodological aspects

Setting up a transient flow model for a field site requires data such as

- aquifer geometry,
- hydraulic properties of the aquifer,
- recharge distribution in time and space,
- hydraulic boundary conditions,
- inital hydraulic heads.

Neither hydraulic heads nor recharge were measured in the area of the *Urenbrunnen* catchment. For the other parameters rough estimates exist at best. However, the results of the combined tracer and recharge test provide a basis for the design of the numerical model. In addition, the recession of spring discharge previous to the tracer/recharge test may be used to infer aquifer properties, though the results may not be unambiguous.

At first, aquifer geometry and boundary conditions were defined using the results of hydrogeological investigations described in section 5.3.1. Based on the postulated aquifer geometry, properties of both fissured system and conduit system were defined by the following steps, some of which include assumptions on initial hydraulic heads as well as on recharge distribution:

1. Define a conduit system.
2. Compute a steady-state flow field by adjusting uniformly distributed recharge to the fissured system to yield spring discharge 20 days before the tracer/recharge test was conducted.
3. Switch off recharge to simulate the recession of discharge over a period of 20 days by adjusting hydraulic conductivity, (unconfined) specific yield and (confined) storage coefficient of the fissured system.
4. Simulate the tracer/recharge test based on the hydraulic head distribution obtained by the previous step. Modify the conduit system to reproduce the observed
   - hydraulic response of the spring,
   - tracer breakthrough at the spring,
   - variation of electrical conductivity at the spring.

The described procedure is an iterative process, because any changes of the conduit system possibly affect steady-state flow field and recession previous to the tracer/recharge test.

Note that in contrast to karst genesis simulations, the fissured system may include here not only parts of the aquifer, in which solutional enlargement is negligible. In parts of the aquifer, which are karstified but do not influence the karst spring signals (e.g., due to a large distance), the geometry of the conduit system cannot be identified due to the lack of information, though some assumptions about the conduit structure might be derived from field observations. Thus, these parts of the aquifer may better be modelled using a continuum approach, i.e. “the fissured system”.

As for the recession period, it was assumed that the natural recharge to the fissured system was negligible during the tracer/recharge test. Some additional assumptions were necessary to define the distribution of the injected water in space (i.e. between conduit and fissured system) and time.

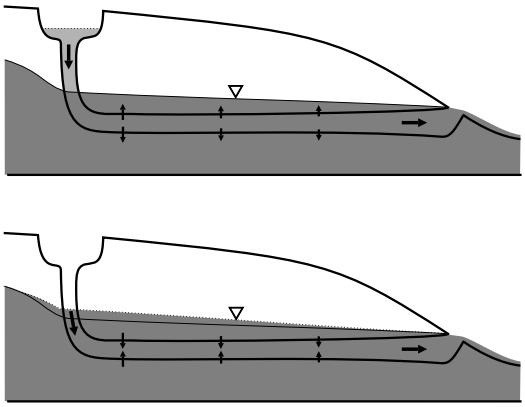

Figure 5.24: Conceptual model 1 for a delayed hydraulic karst spring response: Interaction of fissured system and conduit system.

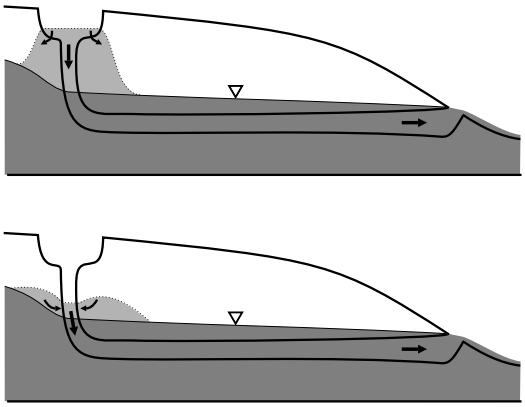

Figure 5.25: Conceptual model 2 for a delayed hydraulic karst spring response: Delayed transfer of recharge to conduit.

The simplest approach (termed "conceptual model 1") is to inject the total water volume over a period corresponding to the time actually needed for the injection of water in the experiment and to adjust the distribution between fissured system and conduit system according to the measured karst spring response. With this assumption, the delayed hydraulic response of the karst spring (see Fig. 5.23) has to be explained by storage of water in the fissured system (compare Fig. 5.24). This would be also in accordance to the parameter studies with coupled flow systems (section 5.2.2).

A different approach ("conceptual model 2") possibly accounts as well for the observed delayed hydraulic response of the karst spring. Water which is injected into the sink will not only infiltrate directly into the conduit but also into the adjacent unsaturated zone (compare Fig. 5.25). Thus, part of the recharge is stored above the original water table and arrives only delayed at the conduit. This conceptual idea may be transferred into the numerical model by adjusting the temporal distribution of recharge to the measured hydraulic response of the spring.

In order to test both of these ideas in model scenarios, the measured spring water level had to be transformed into spring discharge rates. However, the stage-discharge relation derived from long-term time series was found to be not accurate enough to quantify the small changes of discharge occurring after the water injection (compare section 5.3.2.2). It was assumed therefore that the discharge above a constant base flow rate (i.e. spring discharge before injection of water) sums up to the injected water volume (14 m^3). With the additional assumption that the relation between water level and spring discharge is approximately linear within the considered range of values, water levels can be transferred then into discharge rates as illustrated by Fig. 5.26.

For the simulation of advective transport of Uranin from the sink to the spring, the Uranin concentration of recharge into the sink has to be specified. Probably the tracer (600 g Uranin in 100 l water) was mixed to the water which was added after tracer injection (13.9 m^3). Therefore, a constant concentration of 42.9 ppb was used, i.e. equivalent to a solution of 600 g Uranin in the total injected water volume of 14 m^3. Uranin concentration of water flowing from the fissured system into the conduit system was assumed to be zero.

Likewise the electrical conductivity of recharge water was averaged, yielding a value of 0.69 mS cm^{-1}. For the calculation of reactive transport, it was assumed that this value corresponds to a solution free of dissolved gypsum (concentration zero), while the initial value of spring water (about 2.85 mS cm^{-1}) was assigned to water in the

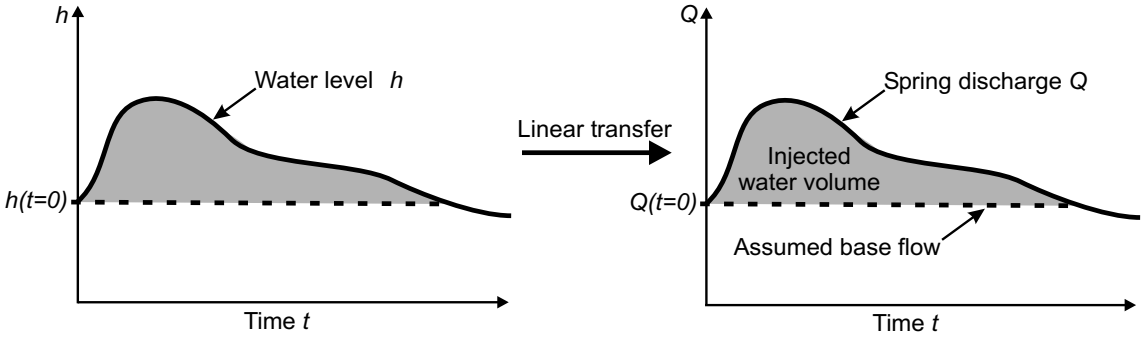

Figure 5.26: Linear transfer of water levels into rates of spring discharge.

fissured system, which was assumed to be in equilibrium with respect to gypsum. The real hydrogeochemical processes, however, are much more complex, since the injected water, though almost free of sulfate, contained calcium ions (probably from the dissolution of limestone). This, however, is of minor importance, since the field data suggest that the dissolution reaction did not significantly increase the solute concentration of the injected water (compare section 5.3.2.2).

5.3.3.2 Model scenarios

In this section, four different model set-ups are presented, all of which were able to simulate the tracer/recharge test reasonably well. Following the above outlined methodology, an aquifer geometry (identical for all scenarios) was defined based on results of hydrogeological field investigations. In accordance with water budget calculations, the model domain covers an area of 3.5 km in length and 1 km in width. The aquifer thickness is set to 10 m, i.e. the lower part of the gypsum layer which is free of clay/marl intercalations. The aquifer is assumed to be unconfined if hydraulic heads are lower than the aquifer top. If hydraulic heads are above the aquifer top, the aquifer is confined by the low permeable clay layers in and above the upper part of the *Grundgipsschichten*. The long side of the model domain strikes about SSW-NNE, corresponding to the flow direction in the area. At the narrow northern end of the model domain, where the *Urenbrunnen* is situated, a fixed head boundary condition is defined with a hydraulic head of 5 m above aquifer bottom.

As in the parameter studies presented in section 5.2.2, a conduit system is incorporated into the fissured system using an exchange coefficient of 0.1 $m^2\ s^{-1}$. This value is large enough to assure that exchange flow is not limited by the exchange coefficient, i.e. a further increase of the exchange coefficient does not affect simulation results.

Fig. 5.27 shows the finite-difference grid of the model domain representing the fissured system and the structure of the conduit system for the first scenario. Model 1 is based on the assumption that the injected water rapidly passed the unsaturated zone (Fig. 5.24). The total water volume of 14 m^3 is equally distributed over a period of one hour, i.e about the time actually needed to inject the water into the sink.

A single conduit could not reproduce the observed asymmetric tracer breakthrough curve. Therefore, an anisotropic pipe network is inserted between sink and karst spring. Apart from conduits close to the sink, the diameters of conduits parallel to the model boundary are set to 0.92 m, while the diameters of the diagonal conduits amount to 0.68 m. The roughness of the conduit walls is set to one tenth of the conduit diameter in this and all following

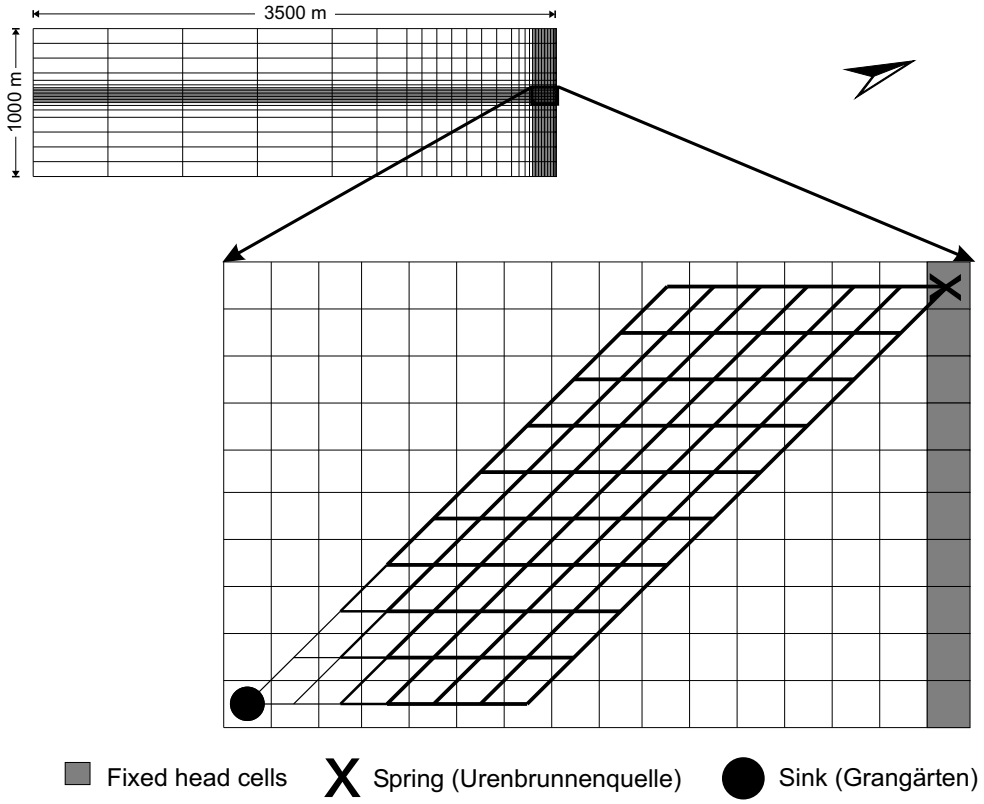

Figure 5.27: Model 1: Pipe network connecting sink and spring.

models. To reproduce the delayed hydraulic response of the karst spring, water has to be stored in the fissured system. As shown in section 5.2.2, this requires small conduit diameters, since otherwise the pressure increase in the conduit system is too small to induce any significant interaction of conduit system and fissured system. In the present example, the diameters of the two conduits starting at the sink are set to 0.04 m only. The diameters of the following conduits increase successively (0.1 m, 0.25 m) to the aforementioned 0.68 m or 0.92 m, respectively. Parameters characterising the fissured system have much less influence on the simulation of the tracer/recharge test, though they determine the recession of spring discharge. Among these are the specific yield, which is set to 0.05, and the confined storage coefficient, which is set to $6 \cdot 10^{-4}$. The hydraulic conductivity of the fissured system is set to $4 \cdot 10^{-5}$ m s^{-1} at distances of more than 1 km from the fixed head boundary. At distances of less than 1 km from the fixed head boundary, the hydraulic conductivity is increased in the central part of the model domain to $4 \cdot 10^{-4}$ m s^{-1} and reduced near the boundaries ($1 \cdot 10^{-5}$ m s^{-1}), in order to focus flow to the pipe network. This corresponds to the reasonable assumption of a more intense karstification close to both karst spring and sink.

Model 2 is depicted by Fig. 5.28. This model is based on the assumption of a delayed transfer of injected water to the conduit as illustrated in Fig. 5.25. Thus, the distribution of recharge in time was adjusted to the measured hydraulic response of the karst spring. Since the resulting recharge period amounts to six hours, the model is able to simulate the observed tailing of the tracer breakthrough curve reasonably well without including any dispersion processes. Therefore, sink and spring are connected only by a single conduit of 1.65 m diameter. In addition, the storage coefficient of the fissured system was slightly increased ($7 \cdot 10^{-4}$), whereas specific yield and hydraulic conductivity were identical to model 1.

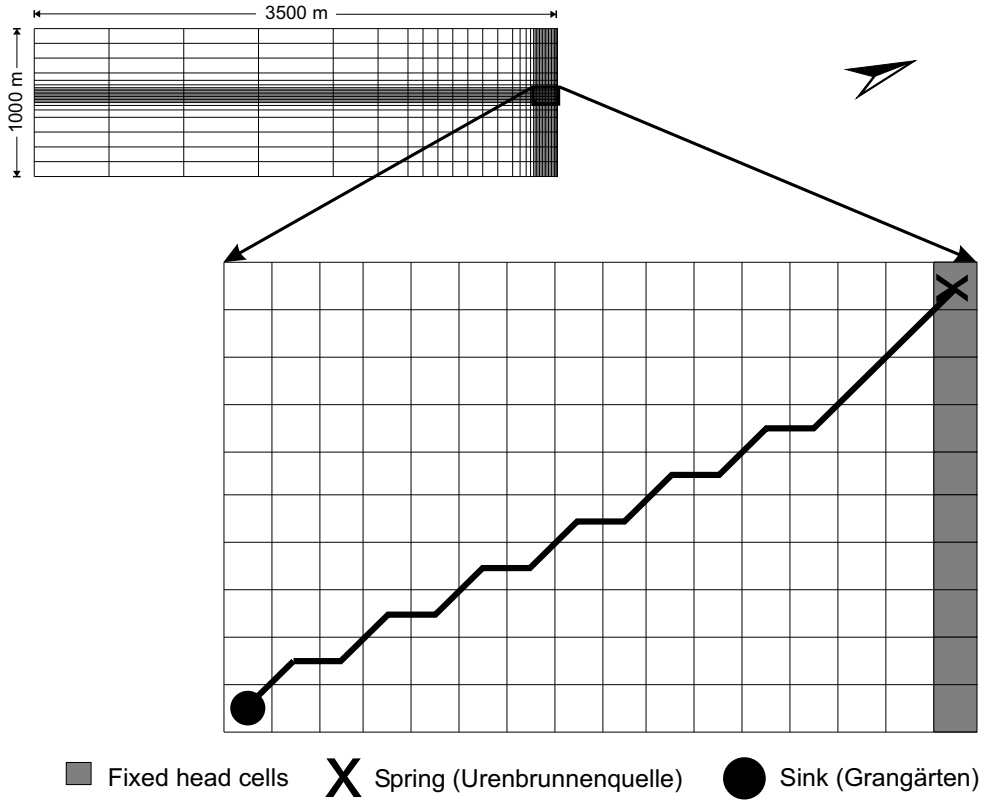

Figure 5.28: Model 2: Single conduit connecting sink and spring.

Like model 2, both model 3 (Fig. 5.29) and model 4 (Fig. 5.30) are based on the assumption of a delayed water transfer from the sink to the conduit. In addition, some assumptions about the drainage of the catchment were introduced. In the previous models regional flow was focused to the sink and the karst spring by adjusting the hydraulic conductivity distribution of the fissured system accordingly. Now the catchment is mainly drained by a discrete conduit, whereas the hydraulic conductivity of the fissured system is constant over the whole model domain ($4 \cdot 10^{-5}$ m s^{-1}). Existence and location of such conduits are indicated, though not proven, by a group of sinkholes about 1 km SSW of the *Urenbrunnen* spring.

In model 3 a conduit of 2.2 m in diameter is directly linked to the spring. Since the conduit connecting sink and spring captures much less water than in model 2, a much smaller conduit diameter of 0.4 m is required to adjust the model to the observed tracer residence time. Specific yield and storage coefficient of the fissured system were 0.09 and $4 \cdot 10^{-4}$, respectively.

In model 4 the catchment is drained by a conduit of 1.9 m in diameter, which is connected to the sink. Since the conduit linking sink and spring thus receives more water than in model 2, the diameter had to be increased to 1.9 m as well. Storage coefficient of the fissured system is identical to model 3 ($4 \cdot 10^{-4}$), whilst specific yield was slightly increased (0.1).

Even though the parameter combinations are by no means unambiguous, the four models represent the characteristics of the karst aquifer exhibited in both recession of spring discharge and spring response to tracer and water injection. This will be demonstrated comparing measurements and simulation results.

Fig. 5.31 shows measured and simulated spring discharge during the recession period before the combined tracer and recharge test

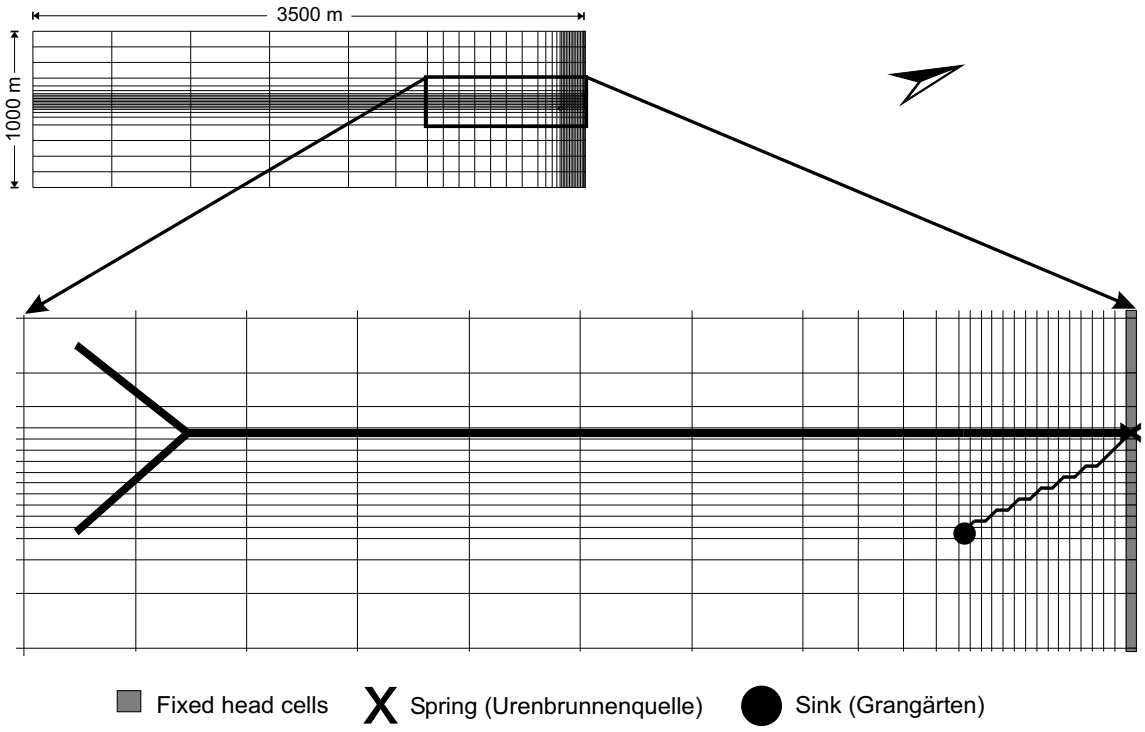

Figure 5.29: Model 3: Single conduit connecting sink and spring. Catchment is drained by a preferential flow path to the spring (simple dendritic conduit system).

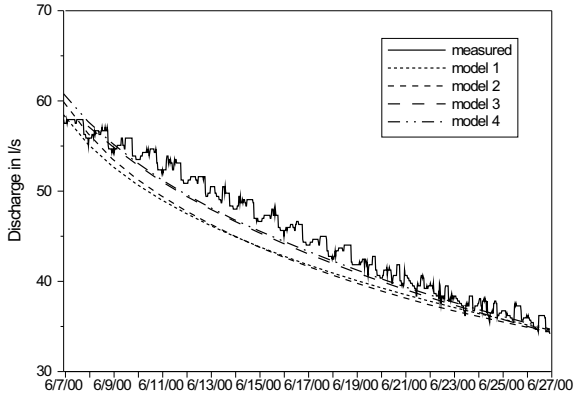

Figure 5.31: Comparison of measured and simulated recession of the discharge at the *Urenbrunnen* spring before the tracer/recharge test was conducted.

was conducted. The simulated values are slightly below the measured spring discharge. This is reasonable, considering that actually there might have been some recharge (from heavy rainfall on May 30/31 and small events in June) during the period, whereas no recharge was applied to the model domain. The flow field resulting from the simulation of the recession period served as initial condition for the simulation of the hydraulic response of the karst spring to water injection into the sink. Therefore, initial spring discharges are slightly different for the four model scenarios. Nevertheless, the simulated karst spring responses agree well with the measurement in each case (Fig. 5.32). For models 2, 3 and 4 an even better fit could easily be obtained by adjusting recharge distribution in time. This, however, appears to be unreasonable, considering the accuracy of the water level measurements which were disturbed by time-variant water withdrawal from the spring.

Fig. 5.33 compares simulated and measured Uranin concentrations at the karst spring. None of the models yields a tailing as extended as actually observed at the spring. In the field, Uranin was still visible at the sink after the injection of both tracer and water. Since there was natural flow of water through a drain into the sink, the Uranin was proba-

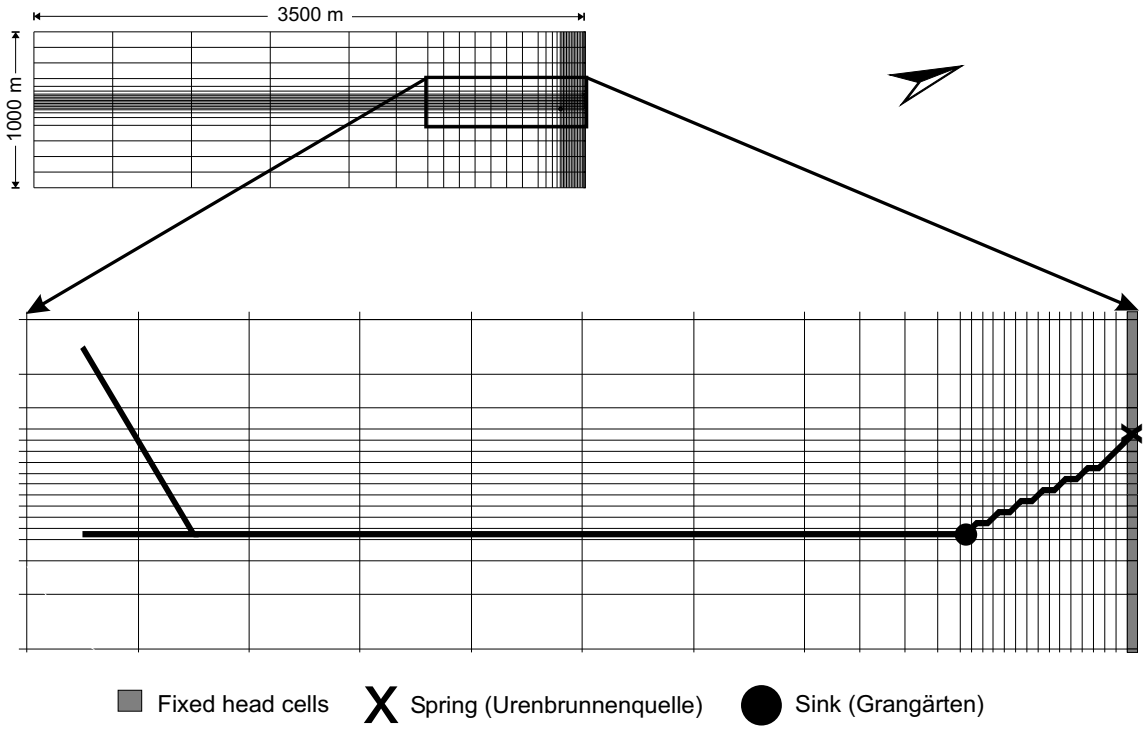

Figure 5.30: Model 4: Single conduit connecting sink and spring. Catchment is drained by a preferential flow path to the sink (simple dendritic conduit system).

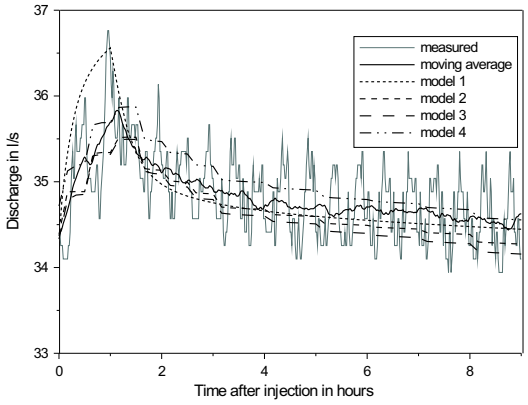

Figure 5.32: Comparison of measured and simulated discharge at the *Urenbrunnen* spring after the combined injection of tracer and water at the *Grangärten* sink.

bly slowly injected into the subsurface over a large period. This process is not included in the models as recharge is only applied over a period of one (model 1) or six hours (model 2, 3, 4). Nevertheless, model 1, 2 and 4 fit the observed curve very well, whereas the concentrations simulated by model 3 are too high for the falling limb of the curve. In model 3 flow from the sink to the spring is controlled by recharge into the sink, because regional flow is mainly captured by a large conduit draining directly to the spring. During water injection into the sink flow velocities are high, causing a rapid spreading of the tracer. When recharge ceases flow velocities decrease significantly. The tracer, which has spread all along the conduit between sink and karst spring, is then only slowly transported to the spring, thus emerging there over a large period. In the other models regional flow is mainly drained by the conduit linking sink and spring. Therefore, flow velocities in the conduit are mainly controlled by regional flow, but almost independent of water injection into the sink, i.e. flow velocity remains nearly constant. Thus, the signal at the karst spring is not expanded in time as observed in model 3.

A similar result is obtained for electrical conductivity. Fig. 5.34 shows electrical conductivities calculated by the reactive trans-

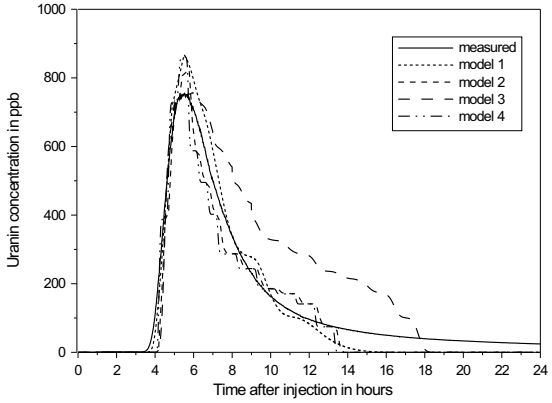

Figure 5.33: Comparison of measured and simulated tracer breakthrough curve at the *Urenbrunnen* spring after tracer injection at the *Grangärten* sink.

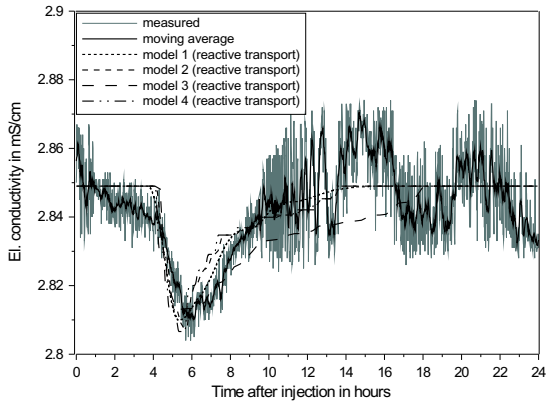

Figure 5.34: Comparison of measured and simulated electrical conductivity at the *Urenbrunnen* spring after tracer and water injection at the *Grangärten* sink, taking into account the dissolution reaction of gypsum.

port model, which includes gypsum dissolution and advective transport. Model 3 well reproduces the measurements during the first eight hours, but deviates strongly afterwards. In contrast, the other three models approximate the measurement well over the whole period. Although model 3 fits the field data less well than the other scenarios, it is further used for comparison in model calibration (section 5.3.4) and validation (section 5.3.5).

Fig. 5.35 shows electrical conductivities resulting from the simulation of purely advective transport, i.e. neglecting the increase of solute content due to gypsum dissolution.

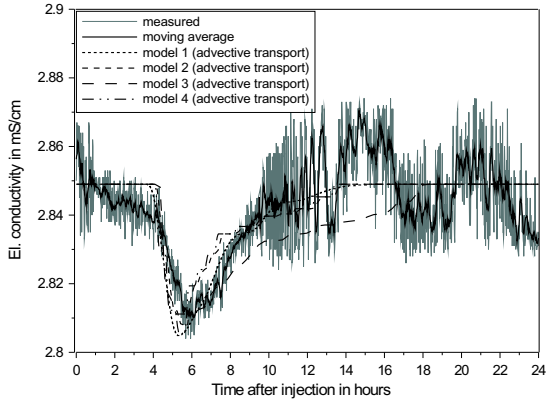

Figure 5.35: Comparison of measured and simulated electrical conductivity at the *Urenbrunnen* spring after tracer and water injection at the *Grangärten* sink, assuming purely advective transport.

Comparison with Fig. 5.34 reveals that effects of gypsum dissolution are indeed negligible. Only in the case of model 1 the curves differ noticeably, though the differences are still small. Model 1 includes some pipes of small diameter. In these pipes flow velocities are high and diffusion boundary layers therefore are thin. Thus, the diffusion controlled dissolution process of gypsum is not completely negligible in model 1.

5.3.4 Calibration

This section describes how the four model set-ups, which are mainly based on field data originating from the combined tracer and recharge test, were calibrated to the recharge event on May 30/31. Firstly, the methodology is outlined. Secondly, the results for the four different scenarios are presented.

5.3.4.1 Methodological aspects

The model set-ups developed in the previous section represent combinations of the hydrogeologic parameters, which are in agreement with the available field data. However, model 3 is less satisfactory than the other

models. Although other parameter combinations might agree just as well or even better with the field data, each of the model scenarios is treated in this section like the "true set-up". The parameters describing aquifer properties, therefore, remained unchanged. Recharge was considered to be the only calibration parameter and had to be adjusted to the observed karst spring response.

The methodology to be followed was:

1. Simulate the recession period previous to the recharge event:
   - Compute a steady-state flow field at the beginning of the recession period by adjusting recharge into the fissured system to the measured spring discharge.
   - Adjust recharge into the fissured system according to the observed recession of discharge.
2. Use the resulting flow field as initial condition for the simulation of the recharge event:
   - Adjust direct recharge (mineralisation differs from aquifer water) to the observed hydrochemical response of the karst spring.
   - Adjust recharge into the fissured system to the observed spring discharge.

The adjustment of direct recharge and recharge into the fissured system is an iterative process. The hydrochemical signal measured at the karst spring is determined by the ratio of direct recharge and flow from the fissured system into the conduit system (compare parameter studies in section 5.2.2). Thus, on the one hand the hydrochemical signal at the spring changes if recharge into the fissured system is modified. On the other hand, the adjustment of direct recharge to the measured hydrochemical signal changes the simulated spring discharge, so that recharge into the fissured system has to be modified again.

Direct recharge into the conduit system was only applied to the *Grangärten* sink which is known to cause physico-chemical responses of the *Urenbrunnen* spring. Recharge into the fissured system was uniformly applied to the whole catchment area. With these two assumptions the above outlined procedure yields a unique distribution of recharge in space. In addition, it was assumed that the distribution of recharge in time has only a single peak or plateau.

The sulfate concentration was selected as a characteristic hydrochemical parameter, which clearly distinguishes recharge water and pre-event aquifer water. Due to the presence of other ions in solution the equilibrium concentration of sulfate with respect to gypsum is higher in the aquifer water than in pure water. Therefore, the equilibrium concentration was calculated using the geochemical modelling software PHREEQC (Parkhurst, 1995). Based on solute concentrations measured in a spring water sample taken on June 5, 2000 (see appendix B) an equilibrium concentration of 15.7 mol m^{-3} was obtained for sulfate. Electrical conductivities measured at the spring were transformed into sulfate concentrations by a linear correlation (appendix C), yielding a pre-event sulfate concentration of 14.4 mol m^{-3}, i.e. $c/c_{eq} = 0.92$. The pre-event concentration was assumed to be the sulfate concentration of water flowing from the fissured system into the conduit system. The sulfate concentration of direct recharge was assumed to be zero.

5.3.4.2 Results

Fig. 5.36 shows the measured and simulated recession of spring discharge before the recharge event on May 30, 2000. As previously mentioned, the measurement was disturbed by water withdrawal during the day, but the fluctuation thus caused is still within the accuracy of the employed stage-discharge

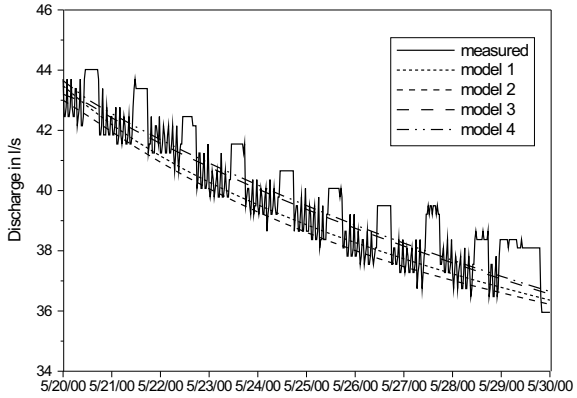

Figure 5.36: Measured and simualted recession of spring discharge at the *Urenbrunnen* from May 20, 2000 to May 30, 2000.

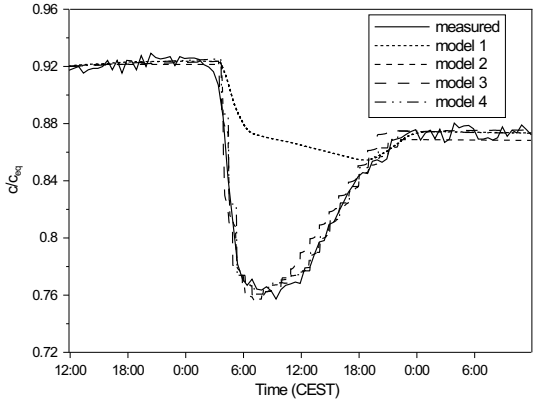

Figure 5.37: Measured and simulated sulfate concentration (normalised with respect to equilibrium concentration) at the *Urenbrunnen* from May 30, 2000 to June 1, 2000.

relation (compare appendix A). In May 2000, spring discharge decreased more slowly than within the period of June 2000, which was taken for the adjustment of aquifer properties of the model scenarios (compare section 5.3.3). In order to slow down recession in the models, recharge had to be applied to the fissured system. The highest recharge rates were applied to model 2 ($6.5 \cdot 10^{-9}$ m s^{-1} = 205 mm a^{-1}) and model 1 ($6 \cdot 10^{-9}$ m s^{-1} = 189 mm a^{-1}). Both model 3 and model 4 required a lower rate of $5 \cdot 10^{-9}$ m s^{-1} = 158 mm a^{-1}. Based on the flow field resulting from the simulation of the recession period, the recharge event of May 30/31 was simulated. Direct recharge and recharge into the fissured system were iteratively adjusted until the measured sulfate concentrations were obtained. However, model 1 could not be adjusted to the measured concentrations, whereas the other models fit the measurement very well (Fig. 5.37).

The sulfate concentrations resulting from model 1 (Fig. 5.37) were based on the simulated flow rates shown in Fig. 5.38. Note that Fig. 5.37 and the corresponding figures for the other models include both direct recharge and flow from the fissured system into the conduit system, but not recharge into the fissured system. The latter, therefore, is tabulated in appendix D. The total spring discharge is mainly composed of highly mineralised water from the fissured system, even though the maximum rate of less mineralised direct recharge amounts to 12 l s^{-1}, i.e. about 20% of the maximum discharge. The abundance of water from the fissured system is due to the transfer of direct recharge from the conduit system into the fissured system, caused by the pressure increase in the conduit system in the narrow pipes near the sink. Small diameters were needed in this part of the pipe network to adjust the model to the results of the combined tracer and recharge test (compare section 5.3.3). Yet, the recharge event of May 30/31, 2000 cannot be simulated with this model set-up, because a further increase of direct recharge is compensated by an increase of flow from the conduit system into the fissured system. In addition, the simulated gypsum dissolution rates prove model 1 inappropriate. During the recharge event the two pipes starting from the sink are solutionally enlarged from initial diameters of 4 cm to nearly 6 cm at the end of the simulation. This change in conduit geometry, which causes a slow decrease of sulfate concentrations during the recharge event (compare Fig. 5.37), would have occurred long before due to similar events in the past, i.e. the suggested conduit geometry is unstable with respect to present hydrologic conditions.

Fig. 5.39 shows the calibrated flow rates of model 2. Both direct recharge and recharge to the fissured system were identical to those

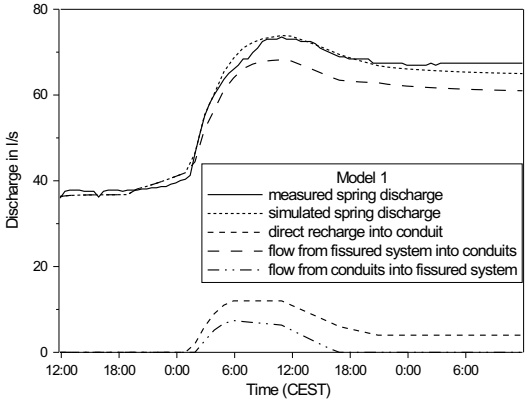

Figure 5.38: Model 1: Measured and simulated spring discharge at the *Urenbrunnen* from May 30, 2000 to June 1, 2000.

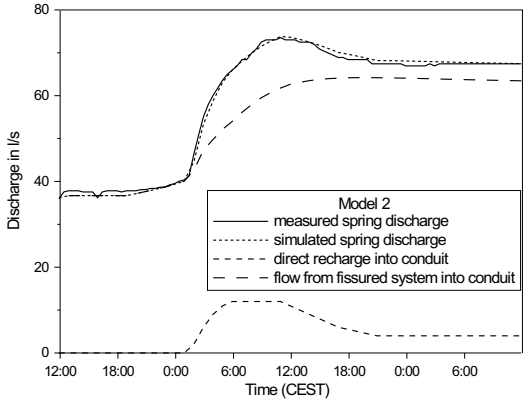

Figure 5.39: Model 2: Measured and simulated spring discharge at the *Urenbrunnen* from May 30, 2000 to June 1, 2000.

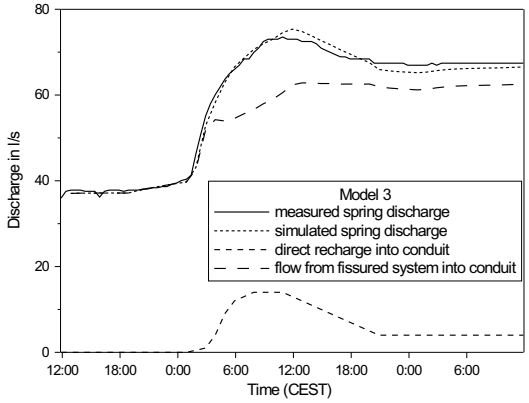

Figure 5.40: Model 3: Measured and simulated spring discharge at the *Urenbrunnen* from May 30, 2000 to June 1, 2000.

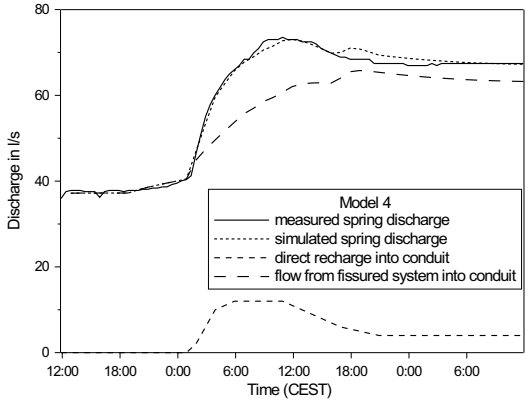

Figure 5.41: Model 4: Measured and simulated spring discharge at the *Urenbrunnen* from May 30, 2000 to June 1, 2000.

used for the above discussed simulation with model 1. Yet, in the simulation with model 2 the pressure increase in the conduit system was too small to cause any flow from the conduit system into the fissured system, which is why the model could be adjusted to the measured sulfate concentrations (Fig. 5.37). Fig. 5.39 demonstrates that the initial increase of spring discharge is mainly caused by direct recharge into the conduit system. In addition, an increase of flow from the fissured system into the conduit system is needed to account for the observed discharge. Like in the parameter studies shown in section 5.2.2, the composition of the spring water is shifted towards larger portions of flow from the fissured system during the recharge event. Note, however, that the "fissured system" as defined in section 5.3.3 may include karstified parts of the aquifer if they do not effect physico-chemical responses of the karst spring.

The incorporation of conduits draining the catchment via the sink (i.e. model 4), however, yields flow rates similar to model 2, as can be seen by comparing Fig. 5.41 to Fig. 5.39. Fig. 5.40 demonstrates that the incorporation of large conduits, draining the catchment directly to the spring changes the results of model calibration. In model 3, the initial increase of spring discharge is solely caused by flow from the fissured system into the conduit system, since otherwise the sulfate concentrations would drop earlier than actually observed. Though not proven wrong, this assumption appears to be unrealistic, as it corresponds to the assumption that diffuse

infiltration into the fissured system is faster than surface runoff and subsequent focused infiltration into the sink. To summarise the results of the model calibration, models 2 and 4 appear to be more appropriate than models 1 and 3.

5.3.5 Validation

This section examines if and how the calibrated models can be validated using the measured spring water temperatures.

5.3.5.1 Methodological aspects

Spring water temperature was measured at the *Urenbrunnen* spring, but not used for model set-up and calibration. This parameter may be employed for model validation by simulation of heat transport. In doing so, aquifer properties and recharge distribution of the calibrated models remain unchanged. A basic problem, however, originates from the unknown temperature of direct recharge. Whereas the assumption of a negligible solute content of recharge is certainly reasonable, recharge temperatures may vary over a wide range. Thus, based on spring water temperatures, the only possibility of a true validation would be to measure temperatures of water infiltrating at the sink. Though in principle feasible, this requires considerable expenses and was not carried out in the present study, as the outstanding importance of the sink was not initially recognised.

As a hypothesis it was assumed that recharge temperature remains constant during the recharge event. Although this was proven wrong by field observations conducted about one week after the recharge event (compare section 5.3.2), the assumption is probably justified at the initial stage of the event. Based on this hypothesis, the recharge temperature was adjusted so that the amplitude of the simulated spring water temperatures agreed with the measured amplitude if temperature

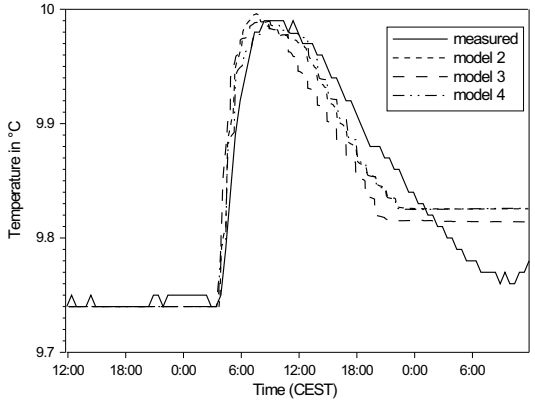

Figure 5.42: Measured and simulated water temperatures at the *Urenbrunnen* from May 30, 2000 to June 1, 2000.

of water flowing from the fissured system into the conduit system and initial temperature of rock and conduit water were set to pre-event temperature of spring water (9.74 °C). In addition, heat transport simulations require the specification of parameters characterising the thermal properties of rock and water. Here, the same values were taken as for model verification (section 3.2.4) and parameter studies (section 5.2).

5.3.5.2 Results

Since model calibration has proven model 1 definitely wrong, heat transport simulations were only conducted for the other model set-ups. The adjustment of recharge temperatures yielded a value of 11.20 °C for both model 2 and 4, but a lower value of 11.05 °C for model 3. Fig. 5.42 shows the resulting spring water temperatures, all of which fit the measurement reasonably well. Only the late values deviate strongly, probably due to the effect of time-variant recharge temperatures. This might also account for the smaller early deviations between simulated and measured temperatures, considering that the simulated values are too high (i.e. actual recharge temperature was probably lower) at night, but too low (i.e. actual recharge temperature was probably higher) during the day. Although the differences between the three models are small, model 3 fits the measurement slightly

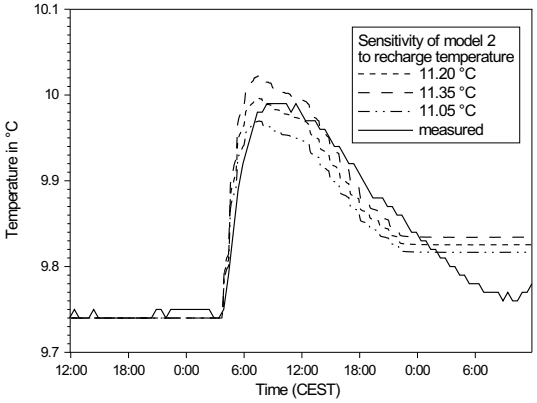

Figure 5.43: Sensitivity of spring water temperatures to recharge temperature in model 2.

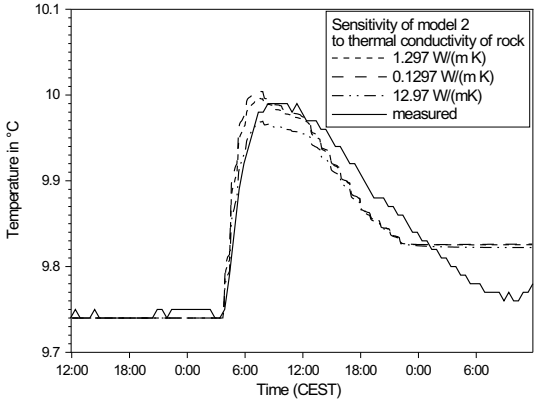

Figure 5.44: Sensitivity of spring water temperatures to thermal conductivity of rock in model 2.

less well than the two other models, which confirms the result of the model calibration. Thus, validation by heat transport simulation gives confidence in the calibrated models, though additional measurements are required to truly validate the models.

5.3.6 Sensitivity

In the previous section, measurement of recharge temperature was suggested as a possibility for model validation. Yet, whether this approach is feasible depends on the sensitivity of the simulation results to the measured parameter. Therefore, the influence of recharge temperature on spring water temperature was examined using the example of model 2.

Fig. 5.43 shows results of simulations, in which the adjusted recharge temperature was varied by about 10% of the difference between recharge temperature and pre-event temperature of spring water. Note that the lower temperature (11.05 °C) corresponds to the value of model 3 (compare section 5.3.4). Simulated spring water temperatures vary by about the same amount as recharge temperature. Considering the accuracy of data loggers, these temperature differences are measurable.

Simulation results may further be affected by false estimates of thermal properties of both rock and water. Whereas the thermal properties of water are well known, the properties of rock may vary for different types of rock. As an example, the thermal conductivity of rock was varied in simulations with model 2. Fig. 5.44 reveals that the model is almost insensitive to decreasing thermal conductivities even by an order of magnitude. Even if the standard value is used heat conduction is evidently too slow to dampen the temperature signal. Thus, a further reduction of thermal conductivity remains inefficacious. However, an increase of thermal conductivity results in lower spring water temperatures, as heat conduction is then fast enough to dampen the signal significantly.

5.4 Discussion

In the previous sections of this chapter hydraulic and physico-chemical karst spring responses to recharge events were examined using the newly developed solute and heat transport modules, which were implemented into the karst modelling tool CAVE. On the one hand, karst spring responses were predicted by forward modelling of flow and transport in synthetic conduit systems. On the other hand, field data from a karst spring in Southern Germany (*Urenbrunnen*, Vöhringen) were used as input parameters for the inverse approach, aiming at inferring the conduit geometry from the measured karst spring response.

The parameter studies presented in section 5.2.1 demonstrate that conduit systems of different geometry can be distinguished by different solute concentrations or different temperatures of the outflow. Liedl et al. (1998) concluded from heat transport simulations with single fractures (Renner, 1996) or single conduits (Hückinghaus, 1998) that unsteady flow conditions are required for that. Some simulations of both reactive solute transport and heat transport presented in this work confirm this conclusion. A sequence of conduits of variable diameter but identical total volume and total surface area can only be identified if flow is transient. However, in many cases transient flow conditions are not required. Circular conduits of constant diameter and such of variable diameter are different in both solute concentration and temperature of the outflow even for steady-state conditions. The same is generally true for single conduits and dendritic conduit networks, though certain configurations cannot be distinguished by using only one of the two parameters, i.e. either solute concentrations or water temperature. Yet, single conduits and dendritic networks, which are equivalent with respect to one parameter, are different with respect to the other one. Thus, it should be theoretically possible to infer the geometric structure of conduit systems from the physicochemical response of the outflow.

However, the relation of conduit geometry and solute concentration is only poorly defined in the case of turbulent flow through conduits with high surface roughness, which are probably the most frequently met conditions in mature karst systems. If dissolution of rock is controlled by diffusion of ions from rock into water the solute concentration depends on the thickness of the diffusion boundary layer separating rock surface and bulk solution. In the parameter studies two different empirical equations were tested for the quantification of boundary layer thickness, both of which predict a different behaviour of outflow concentrations. More importantly, both are valid for smooth pipes only. Considering further that the diffusion boundary layer is influenced by the roughness of conduit walls, solute concentrations cannot be accurately predicted. In the case of the aforementioned conduits, the differences in concentration, caused by differences in conduit geometry, are smaller than the uncertainty arising from an unknown roughness length of conduit walls (compare Figs. 5.3, 5.4, 5.5). Even if surface roughness is well defined the employed equations are a first approximation for rough conduit walls only.

As demonstrated by Fig. 5.5, it is even difficult to predict whether solute concentrations decrease or increase due to changing flow rates. Using the most simple empirical approach (eq. 2.37, Beek and Muttzall, 1975) for the quantification of boundary layer thickness, a decrease of flow rates results in increasing concentrations, whereas the more complex equation (2.38) (Incropera and DeWitt, 1996) yields almost constant concentrations for smooth pipes, but decreasing concentrations for rough conduit walls. Although the examples presented in this work refer to gypsum, the same difficulties arise for solute transport simulations in carbonate aquifers under conditions in which the dissolution process is diffusion controlled. Grasso (1998) empirically examined the relation of spring discharge and solute content of spring water for a number of carbonate karst springs. As he employed the empirical eq. (2.37), his model simulations could only explain the increase of concentration for decreasing flow rates, which was actually observed at most of the karst springs. However, at two springs concentrations were found to decrease for decreasing flow rates. This observation agrees well with results of parameter studies presented in this work, in which solute transport in rough conduits was simulated (compare Fig. 5.5).

Whereas the dissolution of gypsum is usually diffusion controlled under natural conditions, heat transfer is controlled by a different process, namely conduction in the rock. Only in laminar flow, heat transfer from rock surface into water is slow enough to affect the overall heat transport in karst aquifers (compare

section 3.2.4.2). Yet, after recharge events flow conditions are frequently turbulent in the large conduits of mature karst systems. Due to the different controlling processes the aforementioned difficulties, arising from the empirical quantification of boundary layer thickness, are of minor importance in heat transport simulations. In turbulent flow, the simulated outflow temperatures are insensitive to the selected empirical equation as well as to the roughness of the conduit walls (compare Fig. 5.6). Thus, spring water temperatures can be predicted more accurately than solute concentrations if the required input parameters are known for both heat and solute transport simulations.

Both heat and solute transport are influenced by the hydraulic interaction of the two flow systems of a karst aquifer, i.e. the conduit system and the fissured system. If coupled flow systems are used (section 5.2.2) the modelling tool is in principle able to simulate both the hydraulic and the physico-chemical response of a karst spring as observed, for instance, at the *Urenbrunnen* spring in Southern Germany. Typically, solute concentrations rapidly drop after recharge events and increase soon afterwards, whereas the temperature responds more slowly. The process-based approach followed in this thesis helps to identify reasons for the different temporal variation of the two parameters.

In earlier work the time lag between hydrochemical and temperature response was attributed to "the excellent solubility of gypsum" (Bundschuh, 1997) or to the "high heat capacity of the water" (Sauter, 1992). Though these reasons might account for a different behaviour of solute concentration and water temperature in batch experiments, they do not apply to karst systems. If the residence time in the aquifer is about the same for both early and late recharge water emerging at the spring the increase of solute content due to gypsum dissolution remains constant. However, the composition of spring water is likely to change during recharge events. Initially, the portion of direct recharge into the conduits is highest, while it decreases afterwards when flow from the fissured system into the conduit system increases. Since flow from the fissured system is generally much higher mineralised than direct recharge, the time-variant ratio of the two flow components is reflected in the hydrochemical response of the karst spring, i.e. the lowest solute concentration is usually observed immediately after the first arrival of recharge water. As demonstrated by the parameter studies, varying solute concentrations at the spring might also be caused by strongly changing flow rates. In contrast to mass diffusion, heat transfer between rock surface and turbulently flowing conduit water is very fast. Therefore, conduit water rapidly assimilates to the temperature of conduit walls. For this reason, spring water temperatures only decrease after conduit walls have cooled down[1]. Conduit walls are permanently cooled during the recharge event if the recharge water is colder than the rock. Therefore, spring water temperatures decrease over a large period until the infiltration of cold recharge water ceases or until a flow component of higher temperature (i.e. flow from the fissured system) outweighs the colder flow component (i.e. direct recharge). Whereas solute concentration is thus a better indicator of the initial arrival of recharge at the spring, water temperature is better suited to indicate the presence of a direct recharge component at the late stage of the event.

The different behaviour of solute content and temperature of spring water is perfectly illustrated by time series measured at the *Urenbrunnen* spring (Fig. 5.21). On the one hand, solute concentration drops immediately when direct recharge water emerges at the spring, but rises again soon. A short event of high intensity like in May 2000, therefore, causes the largest drop of electrical conductivity at the *Urenbrunnen*, whereas events of lower intensity induce only lower hydrochemical variations at the spring even if they last

[1] Only the case of recharge water being colder than rock is considered here. The corresponding case of recharge water being warmer than rock may also occur as demonstrated by time series of spring water temperatures at the *Urenbrunnen*.

over several weeks like in December 1999. On the other hand, water temperature changes more slowly during the recharge event. The most distinct variation of water temperature, therefore, may be expected for recharge events of long duration like in December 1999. Thus, the results of the parameter studies agree qualitatively with field observations at the *Urenbrunnen* spring.

In order to achieve quantitative agreement of model results and field data, inverse modelling is required. A general methodology for the site-specific application of the newly developed karst modelling tool includes the following steps:

1. Develop a conceptual model of the karst aquifer based on field data such as
   - geometry of the karstified unit,
   - surface karst features (sinkholes, dolines),
   - hydraulic heads,
   - hydrological data,
   - hydrochemical data,
   - results of tracer tests,
   - results of hydraulic tests.
2. Transfer the conceptual model into one or several numerical models which are in accordance to the field data. Considering several model set-ups serves to examine the ambiguity contained in the field data.
3. Calibrate the numerical models to one ore more recharge events using recharge distribution as calibration parameter, while aquifer properties remain unchanged. The calibrated models have to be in accordance with both spring discharges and solute concentrations observed at the spring.
4. Validate the numerical models by heat transport simulations using aquifer properties and recharge distribution of the calibrated models. The validated models have to be in accordance with water temperatures measured at the spring.

In the case of the *Urenbrunnen*, available field data were limited to information about aquifer geometry, surface karst features and some hydrological and hydrochemical data. In addition, a combined tracer and recharge test was conducted. Nevertheless, field data remain incomplete compared to the list given above. Therefore, four different model set-ups were tested. Among these, model 1 (i.e. a conduit network) could be definitely proven wrong during calibration to the recharge event of May 2000. Though not clearly wrong, model 3 (i.e. single conduit linking sink and spring, while regional flow is drained directly to the spring) fitted the results of the tracer test less well than the other model set-ups. More importantly, some unrealistic assumptions were required to calibrate the model to the recharge event in May, 2000. The remaining model set-ups (model 2 and 4) are rather similar. Both include a single conduit linking sink and spring. In addition, model 4 includes a large conduit focusing regional flow to the sink.

The diameters of the conduit connecting the sink with the spring are slightly different in the two models. Model 2 receives a part of the regional flow in between sink and conduit, whereas a great part of the regional flow is directly focused to the sink in model 4. Therefore, the flow rate near the sink is smaller in model 2 than in model 4. Hence, model 2 requires smaller conduit diameters (1.65 m) than model 4 (1.90 m). The larger diameter agrees well with those calculated from the first arrival of both tracer and low mineralised water injected into the sink (compare section 5.3.2). The diameters calculated from tracer/water residence times represent a flow cross-section for the total spring discharge. Therefore, the values are closer to that of model 4 than to that of model 2. Based on the peaks of Uranin concentration or electrical conductivity, diameters of 2.2 m and 2.3 m, respectively, are obtained. The method

of moments (Field, 1999) yields even larger diameters of 4.1 m and 2.6 m, respectively, because the long tailing of the curve is taken into account, i.e. the diameters represent a flow cross-section corresponding to the mean residence time of the total recovered tracer mass. Since the tailing is not caused by linear advective transport as assumed in this calculation, the resulting conduit diameters are too large. In general, the tailing of tracer breakthrough curves is caused by additional dispersion and retardation processes, some of which were mentioned in section 2.2.2. Both model 2 and model 4 account for the whole dispersion and retardation observed at the spring by a delayed transfer from the sink to the phreatic conduit (i.e. retardation in the unsaturated zone). Thus, in the present case other dispersion or retardation mechanisms do not significantly influence solute transport between the sink and the spring. As the most obvious explanation for the similar shape of hydraulic response and tracer breakthrough curve at the spring (compare Fig. 5.23), this is already suggested by the field data.

Although the numerical models represent well the behaviour of the karst aquifer exhibited in the response of the karst spring, the results are not unambiguous, because site-specific field data were rather limited. Above all, more information about the fissured system is required. This includes values for hydraulic properties as well as measurements of hydraulic heads. In addition, data on direct recharge into the sink would be helpful to validate the numerical model. Surface runoff into the sink could probably be measured directly. Although the direct infiltration into the conduit could be smaller than the measured flow rate, this would provide estimates of the rates of direct recharge. As suggested in section 5.3.5, temperature of direct recharge should also be recorded, because the simulated spring water temperature was found to be very sensitive to this parameter.

A further possibility to check the model would be the simulation of additional recharge events. In this work, a short event of high intensity has been simulated. Therefore, the additional simulation of a long recharge event would probably be most useful. For that, much higher computational efforts are required. More importantly, the present modelling approach assumes that both temperature and solute concentration of water flowing from the fissured system into the conduit system remain constant during the recharge event. This assumption, however, may be wrong for long-lasting recharge events. Thus, the modelling concept underlying the karst modelling tool CAVE will have to be further extended for the simulation of karst spring responses during long recharge events.

Chapter 6

Summary and conclusions

This work deals with the development of a process-based numerical karst modelling tool and its exemplary application to gypsum aquifers. The model is designed to support the characterisation of karst aquifers using two complementary approaches: Firstly, the simulation of solutional conduit enlargement, which aims at predicting the geometry of the fast conduit flow system by forward modelling of long-term aquifer genesis; secondly, the simulation of heat and solute transport processes, which aims at inferring aquifer properties from the observed short-term karst spring response to recharge events using both forward and inverse modelling.

In order to be able to simulate conduit enlargement in gypsum rocks, the existing karst modelling tool CAVE was extended by a gypsum dissolution module, taking into account both literature data and experimental results about gypsum dissolution kinetics. In addition, reactive solute transport and heat transport were implemented in two transport modules, yielding a process-based modelling tool for the simulation of short-term karst spring response. Both gypsum dissolution and reactive solute transport modules were verified by analytical solutions, whereas an existing semi-analytical method was employed to verify heat transport.

The newly developed karst modelling tool was applied to simulate conduit development in deep-seated artesian settings. Field observations in the Western Ukraine suggest that the development of large gypsum maze caves starts in this type of setting. A typical conceptual model, consisting of an initially low permeable gypsum layer separating two insoluble confined aquifers, was translated into a numerical model. Employing the numerical model, two different stages of conduit development were identified. The early stage is characterised by a large vertical hydraulic head gradient across the gypsum layer which induces ascending flow of solutional aggressive water from the lower aquifer into the gypsum layer. Vertical flow, however, is limited by the initially small diameters of the proto-conduits incorporated in the gypsum. Flow rates rise considerably if a conduit is enlarged over the whole thickness of the gypsum layer. Since increasing flow rates accelerate solutional conduit enlargement while conduit enlargement induces increasing flow rates, a positive feedback loop is active then, causing rapid conduit enlargement. This so-called "breakthrough" initiates the late stage of conduit development, which is characterised by much lower hydraulic gradients and flow rates limited by the hydraulic resistance of the insoluble aquifers rather than by that of solution conduits in the gypsum.

Considering a single conduit, a sensitivity analysis was conducted for both early conduit development in the period before the breakthrough and long-term conduit development over periods much longer than breakthrough times. Early development was examined by numerical simulations, whereas an analytical solution of the model equations was derived for long-term conduit diameters. On the one hand, the initial diameter of proto-conduits was identified as the most influential parameter at the early stage of conduit devel-

opment, though simulation results are also very sensitive to other parameters such as the hydraulic gradient and the diffusion mass transfer coefficient. Long-term conduit diameters, on the other hand, were shown to be almost insensitive to initial conduit diameters, whereas other parameters, such as the undersaturation of water with respect to gypsum, are found to be more influential.

By numerical simulations with pipe networks it was demonstrated that the structure of mature conduit systems is already determined at the early stage of conduit development. Since the diameters of the proto-conduits are most influential at this stage, the geometry of mature conduit systems is guided by structural preferences caused, for instance, by heterogeneous distributions of initial aperture widths. Under artesian conditions solution conduits are laterally enlarged beneath a horizon less prone to karstification until the early stage of conduit development is terminated by the enlargement of a vertical conduit across the gypsum layer. This breakthrough event is most likely triggered by increasing hydraulic gradients due to the incision of valleys into the confining layers above the upper aquifer. The results of the model simulations agree with field observations from the Western Ukraine, suggesting that the structure of huge maze caves is predetermined by laterally extended fissure networks which are vertically only poorly connected. The numerical simulations predict lateral conduit networks of different structure for settings where upward flow across the gypsum layer is restricted by low permeable insoluble materials such as clay at the top of the gypsum. This type of setting is found in gypsum karst areas in England, where karstification in the subsurface is proven by surface karst features like sinkholes.

The model simulations show that karst genesis modelling is a useful method for the prediction of general cave patterns. The application of the numerical model has to be preceded by the development of a conceptual model based on extensive field data. Thus, model simulations do not replace conventional field investigations, but prove helpful for the interpretation of field data. Moreover, the conception of field investigations may be supported by parameter studies and sensitivity analyses identifying relevant parameters. Due to the high sensitivity of model results, the structure and location of conduit systems cannot be predicted precisely. Great carefulness in defining boundary conditions and model parameters is required even if only general cave patterns are of interest. Hence, the uncertainty resulting from highly influential parameters like initial diameters always has to be taken into account by conducting parameter studies which cover the possible range of variation. In contrast to general spatial cave patterns, which are determined at the early stage of conduit development, the prediction of long-term conduit diameters by numerical or analytical calculation is less difficult, because most of the required parameters can be either measured or taken from the literature.

As an additional method, which may help to infer the structure of karst conduit systems, the process-based simulation of short-term karst spring responses is suggested in this work. Parameter studies demonstrate that different controlling processes of heat and solute transport (i.e. heat conduction in the rock and diffusion mass transfer from rock surface into bulk solution, respectively) account for the frequently observed different behaviour of water temperatures and solute concentrations at karst springs. Forward modelling of water temperatures and solute concentrations shows that conduit systems of different geometry, which are equivalent with respect to one parameter, can be distinguished by taking into account the other parameter. The results of solute transport simulations, however, are affected by uncertainties originating from the insufficient knowledge of diffusion boundary layer thickness in turbulent flow through rough pipes. Nevertheless, conduit systems may be in principle characterised by analysing variations of both water temperatures and solute concentrations.

Real karst systems are frequently characterised by dualistic flow systems, consisting

of a highly conductive conduit system coupled to a less permeable fissured system. The karst spring response following recharge events is mainly induced by fast flow and transport in the conduit system. The major part of groundwater, however, is stored in the fissured system. As demonstrated by parameter studies, the rapid infiltration of recharge into the conduit system may influence flow between the two systems. Thus, the interaction of conduit system and fissured system must not be neglected in short-term transport simulations.

After recharge events, spring water is composed of varying portions of direct recharge into the conduit system and flow from the fissured system into the conduit system. The ratio of the two flow components is mainly determined by the spatial distribution of recharge and surface runoff, which may focus the water into sinks. It is further influenced by properties of both conduit system (e.g. conduit diameters) and fissured system (e.g. specific yield). Model simulations suggest that temporal variations of solute concentrations are mainly caused by varying ratios of the two flow components, though varying dissolution rates may also play a role if spring discharge varies strongly. As shown by field observations, solute concentrations often rapidly drop to the minimu and increase more slowly afterwards. This suggests that the ratio of direct recharge and flow from the fissured system is highest at the beginning of the recharge event and decreases afterwards. Spring water temperatures, however, are strongly influenced by the slow assimilation of conduit walls to the temperature of conduit water. Therefore, water temperatures may apparently indicate an increasing portion of direct recharge even if solute concentrations prove the opposite. Although less easily employed for the quantification of the two flow components, water temperatures are helpful for the identification of direct recharge at late stages of recharge events when spring discharge is mainly composed of flow from the fissured system. The temperature assimilation of conduit walls the “intensifies” the otherwise weak signal at the spring.

Forward modelling has been proven to be helpful for the identification of processes and controlling parameters governing heat and solute transport in karst aquifers. Karst spring signals can be interpreted in terms of physical parameters characterising the conduit system, and the combination of temperature and concentration data may help to reduce the ambiguity of the interpretation. A major practical problem, however, arises from the usually unknown distribution of recharge, which infiltrates either locally into the conduit system (i.e. direct recharge) or diffusely into the fissured system from where it is only slowly released into the conduit system.

In order to test the practical feasibility of the suggested approach, the model was applied to the field site Vöhringen in Southern Germany, where the *Urenbrunnen* spring rises from karstified gypsum layers. Based on literature data and results of a combined tracer and recharge test, conducted at the *Grangärten* sink near the karst spring, four alternative model set-ups were developed. Using time series of discharge and solute concentration recorded at the spring, the model set-ups were calibrated to the measured karst spring response after a recharge event. Direct recharge and flow from the fissured system were considered as calibration parameters for the simulation of transient flow and reactive solute transport. By that, one of the models could be clearly proven wrong, while another model required unreasonable assumptions about the recharge distribution and fitted the results of the combined tracer and recharge less well than the other models.

The remaining two models could be calibrated very well to the measured spring discharge and solute concentration. Moreover, both of them could reasonably well reproduce the observed variation of water temperatures using the calibrated recharge distribution. Thus, none of the two remaining model set-ups could be proven wrong by the heat transport simulation. Both models are similar in that they include a single conduit in between the sink and

the spring. The conduit diameters, however, differ slightly (1.90 m *vs.* 1.65 m), because in one of the models regional flow is focused to the sink, whereas in the other model it is more diffusely released from the fissured system into the conduit between sink and spring. Both models account for the tailing of the tracer breakthrough curve and the delayed hydraulic response, observed in the combined tracer and recharge experiment, solely by a delayed transfer of tracer and water to the sink. Hence, dispersion and retardation between sink and spring are caused by infiltration processes rather than by mechanisms in the phreatic zone. Moreover, as already suggested by the similar recovery of conservative tracer and water which is subjected to dissolution reactions, the model simulations demonstrate that gypsum dissolution does not significantly influence solute transport along the small distance of only 170 m between the sink and the spring. Thus, advection is the dominating solute transport mechanism along the flow path from the *Grangärten* sink to the *Urenbrunnen* spring.

The field application of the modelling tool demonstrates that the suggested inverse approach, which aims at inferring aquifer properties from karst spring signals, is in principle feasible under realistic conditions. Above all, the combination of tracer test data and time series recorded after recharge events has been proven to reduce the ambiguity in the aquifer characterisation. Model calibration was based on measured spring discharge and solute concentrations, while spring water temperatures were employed for model validation. The field application could not demonstrate that a combined simulation of heat and solute transport reduces the ambiguity in the model calibration, though this is suggested by the aforementioned parameter studies. The similar behaviour of solute concentration and water temperature in the examined recharge event may be attributed to the minor role of rock-water interactions in heat and solute transport at the field site. This is caused by the small flow distance and the large conduit diameter, both of which reduce the ratio of surface area to water volume as compared to the parameter studies. Both field data and model simulations further suggest that the differences between solute and heat transport are probably better exhibited in recharge events over longer time periods, the simulation of which requires not only higher computational efforts but also the critical evaluation of the employed modelling concept, which assumes that physico-chemical properties of water flowing from the fissured system into the conduit system are constant in time.

Future work will have to focus on site-specific application of the modelling tool, combining the two presented methods for one field site. This will require extensive geological and hydrogeological field work focusing on the most influential parameters. In long-term karst genesis modelling these include, for instance, initial diameters and possible locations of proto-conduits as well as information about hydraulic boundary conditions and their variation in the geologic past. Compared to the data available for the presented field application, more information about volumetric rates and physico-chemical properties of direct recharge as well as about hydraulic properties of the fissured system could serve to reduce the ambiguity in the process-based simulation of short-term karst spring responses. In order to account for uncertainties in the data, it is further recommended to conduct parameter studies covering possible ranges for the most influential parameters.

Bibliography

Appelo, C. A. J. and D. Postma (1993). *Geochemistry, groundwater and pollution.* Balkema, Rotterdam.

Aris, R. (1956). On the dispersion of a solute in a fluid flowing through a tube. *Proceedings of the Royal Society of London, Series A* 235: 67–77.

Ashton, K. (1966). The analysis of flow data from karst drainage systems. *Transactions of the Cave Research Group of Great Britain* 7: 161–203.

Atkinson, T. C. (1977). Diffuse flow and conduit flow in limestone terrain in the Mendip Hills, Sommerset (Great Britain). *Journal of Hydrology* 35: 93–110.

Barenblatt, G. I., I. P. Zheltov, and I. N. Kochina (1960). Basic concepts in the theory of seepage of homogeneous liquids in fissured rocks. *Journal of Applied Mathematics and Mechanics* 24: 1286–1303.

Barton, A. F. M. and N. M. Wilde (1971). Dissolution rates of polycristalline samples of gypsum and orthorhombic forms of calcium sulphate by a rotating disc method. *Trans. Faraday Soc.* 67: 3590–3597.

Bauer, S., R. Liedl, and M. Sauter (2000). Modelling of karst development considering conduit-matrix exchange flow. In Stauffer, F., W. Kinzelbach, K. Kovar, and E. Hoehn, editors, *Calibration and reliability in groundwater modelling: Coping with uncertainity - Proceedings of the ModelCARE'99 conference, IAHS Publ. no. 265*, pp. 10–15.

Beek, W. J. and K. M. K. Muttzall (1975). *Transport Phenomena.* Wiley, London.

Benderitter, Y. and B. Roy (1993). Flow characterization through heat transfer evidence in a carbonate fractured medium: first approach. *Water Resources Research* 29: 3741–3747.

Benito, G., A. Pérez-González, F. Gutiérrez, and M. J. Machado (1998). River response to Quarternary subsidence due to evaporite solution (Gállego River, Ebro Basin, Spain). *Geomorphology* 22: 243–263.

Berkowitz, B., C. Naumann, and L. Smith (1994). Mass transfer at fracture intersections: An evalution of mixing models. *Water Resources Research* 30(6): 1765–1773.

Birk, S., R. Liedl, and M. Sauter (2000). Characterization of gypsum aquifers using a coupled continuum-pipe flow model. In Stauffer, F., W. Kinzelbach, K. Kovar, and E. Hoehn, editors, *Calibration and reliability in groundwater modelling: Coping with uncertainity - Proceedings of the ModelCARE'99 conference, IAHS Publ. no. 265*, pp. 16–21.

Bundschuh, J. (1991). *Der Aquifer als thermodynamisches System - Untersuchungen zum Wärmetransport in oberflächennahen Grundwasserleitern unter besonderer Berücksichtigung von Quellwassertemperaturen (Modellversuche und Geländebeispiele)*, Vol. 11 of *Tübinger Geowissenschaftliche Arbeiten, Reihe C.* Institut und Museum für Geologie und Paläontologie der Universität Tübingen, Tübingen.

Bundschuh, J. (1993). Modeling annual variations of spring and groundwater temperatures associated with shallow aquifer systems. *Journal of Hydrology* 23: 427–444.

Bundschuh, J. (1997). Temporal variations of spring water temperatures in relation to the extents of the heat transport modes occurring in the karstified lower gypsum-keuper aquifer (karnian, southern germany. In *Proceedings of the 12^{th} International Congress of Speleology, La Chaux-de-Fonds, Switzerland, Volume 2*, pp. 129–132.

Carslaw, H. S. and J. C. Jaeger (1959). *Conduction of heat in solids*. Oxford University Press, Oxford, second edition.

Christofferson, J. and M. R. Christofferson (1976). The kinetics of calcium sulphate dihydrate in water. *J. Crystal Growth* 35: 79–88.

Clark, M. M. (1996). *Transport modeling for environmental engineers and scientists*. Wiley, New York.

Clemens, T. (1998). Simulation der Entwicklung von Karstaquiferen. Ph.D. diss., Eberhard-Karls-Universität Tübingen, Tübingen.

Clemens, T., D. Hückinghaus, R. Liedl, and M. Sauter (1999). Simulation of the development of karst aquifers: role of the epikarst. *International Journal of Earth Sciences* 88: 157–162.

Clemens, T., D. Hückinghaus, M. Sauter, R. Liedl, and G. Teutsch (1996). A combined continuum and discrete network reactive transport model for the simulation of karst development. In *Calibration and reliability in groundwater modelling - Proceedings of the ModelCARE 96 conference held at Golden, Colorado, September 1996, IAHS Publ. no. 237*, pp. 309–318.

Clemens, T., D. Hückinghaus, M. Sauter, R. Liedl, and G. Teutsch (1997a). Modelling the genesis of karst aquifer systems using a coupled reactive network model. In *Hard rock hydrosystems - Proceedings of Rabat Symposium S2, IAHS Publ. no. 241*, pp. 3–10.

Clemens, T., D. Hückinghaus, M. Sauter, R. Liedl, and G. Teutsch (1997b). Simulation of the evolution of maze caves. In *Proceedings of the 12^{th} International Congress of Speleology, La Chaux-de-Fonds, Switzerland, Volume 2*, pp. 65–68.

Clemens, T., D. Hückinghaus, M. Sauter, R. Liedl, and G. Teutsch (1998). Simulation of the evolution of maze caves. *Bulletin d'Hydrogéologie* 16: 201–210.

Cooper, A. H. (1986). Foundered strata and subsidence resulting from the dissolution of Permian gypsum in the Ripon and Bedale areas, North Yorkshire. In Harwood, G. M. and D. B. Smith, editors, *The English Zechstein and related topics*, pp. 127–139. Geological Society, London.

Cooper, A. H. (1988). Subsidence resulting from the dissolution of Permian gypsum in the Ripon area; its relevance to mining and water abstraction. In Bell, F. G., M. G. Culshaw, J. C. Cripps, and M. A. Lovell, editors, *The Engineering geology of underground movements*, pp. 387–390. Geological Society, London.

Cooper, A. H. (1995). Subsidence hazards due to the dissolution of Permian gypsum in England: investigation and remediation. In Beck, B. F., editor, *Karst geohazards - engineering and environmental problems in karst terrane*, pp. 23–29, Rotterdam. Balkema. Proceedings of the fifth multidisciplinary conference on sinkholes and the ebvironmental impacts of karst, Gatlinburg, Tennesse, 2-5 April 1995.

Cooper, A. H. (1998). Subsidence hazards caused by the dissolution of Permian gypsum in England: geology, investigation and remediation. In Maund, J. G. and M. Eddleston, editors, *Geohazards in engineering geology*, pp. 265–275. Geological Society, London.

Cvijić, J. (1918). Hydrographie souterraine et évolution morpholique du Karst. *Recueil des Travaux de l'Institute de Géographie Alpine* 4: 375–426.

de Marsily, G. (1986). *Quantitative hydrogeology - Groundwater hydrology for engineers*. Academic Press, Orlando.

Dreiss, S. J. (1982). Linear kernels for karst aquifers. *Water Resources Research* 18(4): 31–44.

Dreiss, S. J. (1983). Linear unit-response functions as indicators of recharge areas for large karst springs. *Journal of Hydrology* 61: 31–44.

Dreiss, S. J. (1989a). Regional scale transport in a karst aquifer: 1. Component separation of spring flow hydrographs. *Water Resources Research* 25(1): 117–125.

Dreiss, S. J. (1989b). Regional scale transport in a karst aquifer: 2. Linear systems and time moment analysis. *Water Resources Research* 25(1): 126–134.

Dreybrodt, W. (1988). *Processes in Karst Systems - Physics, Chemistry, and Geology*. Springer, Berlin.

Dreybrodt, W. (1990). The role of dissolution kinetics in the development of karst aquifers in limestone: a model simulation of karst evolution. *Journal of Geology* 98: 639–655.

Dreybrodt, W. (1992). Dynamics of karstification: a model applied to hydraulic structures in karst terranes. *Applied hydrogeology* 3: 20–32.

Dreybrodt, W. (1996). Principles of early development of karst conduits under natural and man-made conditions revealed by mathematical analysis of numerical models. *Water Resources Research* 32(9): 2923–2935.

Dreybrodt, W. and F. Gabrovšek (2000). Dynamics of the evolution of single karst conduits. In Klimchouk, A. B., D. C. Ford, A. N. Palmer, and W. Dreybrodt, editors, *Speleogenesis - evolution of karst aquifers*, pp. 184–193. National Speleological Society, Huntsville.

Eisenlohr, L., M. Bouzelboudjen, L. Kiraly, and Y. Rossier (1997a). Numerical versus statistical modelling of natural response of karst hydrogeological system. *Journal of Hydrology* 202: 244–262.

Eisenlohr, L., L. Kiraly, M. Bouzelboudjen, and Y. Rossier (1997b). Numerical simulation as a tool for checking the interpretation of karst spring hydrographs. *Journal of Hydrology* 193: 306–315.

Field, M. S. (1999). Quantitative analysis of tracer breakthrough curves from tracing tests in karst aquifers. In *Karst modeling - Proceedings of the symposium held February 24 through 27, 1999, Charlottesville, Virginia*, pp. 163–171.

Ford, D. C. (1998). Perspectives in karst hydrogeology and cavern genesis. *Bulletin d'Hydrogéologie* 16: 9–29.

Ford, D. C. (2000). Speleogenesis under unconfined settings. In Klimchouk, A. B., D. C. Ford, A. N. Palmer, and W. Dreybrodt, editors, *Speleogenesis - evolution of karst aquifers*, pp. 319–324. National Speleological Society, Huntsville.

Ford, D. C. and P. W. Williams (1989). *Karst geomorphology and hydrology.* Unwin Hyman, London.

Freeze, R. A. and J. A. Cherry (1979). *Groundwater.* Prentice Hall, Englewood Cliffs.

Gabrovšek, F. and W. Dreybrodt (2000). Role of mixing corrosion in calcite-aggressive H_2O-CO_2-$CaCO_3$ solutions in the early evolution of karst aquifers in limestone. *Water Resources Research* 36(5): 1179–1188.

Gale, S. J. (1984). The hydraulics of conduit flow in carbonate aquifers. *Journal of Hydrology* 70: 309–327.

Gnielinski, V. (1976). New equations for heat and mass transfer in turbulent pipe and channel flow. *International Chemical Engineering* 16(2): 359–368.

Grasso, D. A. (1998). Interprétation des réponse couplées hydrauliques et chimiques des sources karstiques (Essai d'inférence de la structure des système karstiques). Ph.D. diss., Université de Neuchâtel, Neuchâtel.

Groves, C. G. and A. D. Howard (1994a). Early development of karst systems: 1. Preferential flow path enlargement under laminar flow. *Water Resources Research* 30(10): 2837–2846.

Groves, C. G. and A. D. Howard (1994b). Minimum hydrochemical conditions allowing limestone cave development. *Water Resources Research* 30(3): 607–615.

Grund, A. (1903). Die Karsthydrographie - Studien aus Westbosnien. *Geographische Abhandlungen* 7: 103–200.

Gutiérrez, F. (1996). Gypsum karstification induced subsidence: effects on alluvial systems and derived geohazards (Calatayud Graben, Iberian Range, Spain). *Geomorphology* 16: 277–293.

Häfner, F., D. Sames, and H.-D. Voigt (1992). *Wärme- und Stofftransport - Mathematische Methoden.* Springer, Berlin.

Harbaugh, A. W. and M. G. McDonald (1996). *Programmer's documentation for MODFLOW-96 - an update to the US Geological Survey modular finite-difference groundwater model*, Vol. 96-486 of *USGS Open-File Report.* USGS.

Hartmann, R. (1998). Zur Empfindlichkeit von Karstgrundwasserleitern, erläutert am Beispiel eines Schadensfalles mit halogenierten Lösungsmitteln. *NNA-Berichte* 11(2): 87–92.

Haude, W. (1955). Zur Bestimmung der Verdunstung auf möglichst einfache Weise. *Mitt. d. Dt. Wetterdienstes* 2(11): 24 S.

Hauns, M., P.-Y. Jeannin, and O. Atteia (2001). Dispersion, retardation and scale effect in tracer breakthrough curves in karst conduits. *Journal of Hydrology* 241: 177–193.

Hauns, M., P.-Y. Jeannin, and F. Hermann (1998). Tracer transport in karst underground rivers: tailing effect from channel geometry. *Bulletin d'Hydrogéologie* 16: 123–141.

Horlacher, H.-B. and H.-J. Lüdecke (1992). *Strömungsberechnung für Rohrsysteme*. Expert Verlag, Ehningen.

Howard, A. D. and C. G. Groves (1995). Early development of karst systems: 2. Turbulent flow. *Water Resources Research* 31(1): 19–26.

Hückinghaus, D. (1998). *Simulation der Aquifergenese und des Wärmetransports in Karstaquiferen*, Vol. 42 of *Tübinger Geowissenschaftliche Arbeiten, Reihe C*. Institut und Museum für Geologie und Paläontologie der Universität Tübingen, Tübingen.

Huyakorn, P. S., B. H. Lester, and C. R. Faust (1983). Finite element techniques for modeling groundwater flow in fractured aquifers. *Water Resources Research* 19(4): 1019–1035.

Incropera, F. P. and D. P. DeWitt (1996). *Fundamentals of heat and mass transfer*. Wiley, New York, 4^{th} edition.

James, A. N. (1992). *Soluble materials in civil engineering*. Ellis Horwood, Chichester.

James, A. N. and A. R. R. Lupton (1978). Gypsum and anhydrite in foundations of hydraulic structures. *Geotechnique* 28: 249–272.

Jeannin, P.-Y. and M. Sauter (1998). Analysis of karst hydrodynamic behaviour using global approaches: a review. *Bulletin d'Hydrogéologie* 16: 31–48.

Jeschke, A. A., K. Vosbeck, and W. Dreybrodt (2001). Surface controlled dissolution rates of gypsum in aqueous solutions exhibit nonlinear dissolution kinetics. *Geochimica et Cosmochimica Acta* 65(1): 27–34.

Jubelt, R. and P. Schreiter (1980). *Gesteine:Sammeln, Bestimmen, Vorkommen, Merkmale*. Enke, Stuttgart.

Käss, W. (1992). *Geohydrologische Markierungstechnik*. Borntraeger, Berlin.

Katzer, F. (1909). *Karst und Karsthydrographie*, Vol. 8 of *Zur Kunde der Balkaninsel - Reisen und Beobachtungen*. Kajon, Sarajevo.

Kaufmann, G. and J. Braun (1999). Karst aquifer evolution in fractured rocks. *Water Resources Research* 35(11): 3233–3238.

Kaufmann, G. and J. Braun (2000). Karst aquifer evolution in fractured, porous rocks. *Water Resources Research* 36(6): 1381–1391.

Kemper, W. D., J. Olsen, and C. J. DeMooy (1975). Dissolution rate of gypsum in flowing water. *Soil Sci. Amer. Proc.* 39: 458–463.

Kinzelbach, W. (1992). *Numerische Methoden zur Modellierung des Transports von Schadstoffen im Grundwasser*, Vol. 21 of *Schriftenreihe gwf Wasser, Abwasser*. Oldenbourg, München, second edition.

Kiraly, L. (1998). Modelling karst aquifers by the combined discrete channel and continuum approach. *Bulletin d'Hydrogéologie* 16: 77–98.

Klimchouk, A. B. (1992). Large gypsum caves in the Western Ukraine and their genesis. *Cave Science* 19(1): 3–11.

Klimchouk, A. B. (1996a). The dissolution and conversion of gypsum and anhydrite. *International Journal of Speleology* 25(3-4): 21–36.

Klimchouk, A. B. (1996b). Gypsum karst of the Western Ukraine. *International Journal of Speleology* 25(3-4): 263–278.

Klimchouk, A. B. (1996c). Speleogenesis in gypsum. *International Journal of Speleology* 25(3-4): 61–82.

Klimchouk, A. B. (1997a). Artesian speleogenetic setting. In *Proceedings of the 12th International Congress of Speleology, La Chaux-de-Fonds, Switzerland, Volume 1*, pp. 157–160.

Klimchouk, A. B. (1997b). The role of speleogenesis in the Miocene gypsum in the Western Ukraine in groundwater circulation in the multi-storey artesian system. In Günay, G. and A. I. Johnson, editors, *Karst waters and environmental impacts*, pp. 281–291. Balkema, Rotterdam.

Klimchouk, A. B. (2000a). Speleogenesis in gypsum. In Klimchouk, A. B., D. C. Ford, A. N. Palmer, and W. Dreybrodt, editors, *Speleogenesis - evolution of karst aquifers*, pp. 431–442. National Speleological Society, Huntsville.

Klimchouk, A. B. (2000b). Speleogenesis of great gypsum mazes in the Western Ukraine. In Klimchouk, A. B., D. C. Ford, A. N. Palmer, and W. Dreybrodt, editors, *Speleogenesis - evolution of karst aquifers*, pp. 261–273. National Speleological Society, Huntsville.

Klimchouk, A. B. (2000c). Speleogenesis under deep-seated and confined settings. In Klimchouk, A. B., D. C. Ford, A. N. Palmer, and W. Dreybrodt, editors, *Speleogenesis - evolution of karst aquifers*, pp. 244–260. National Speleological Society, Huntsville.

Klimchouk, A. B. and V. Andrejchuk (1996). Environmental problems in gypsum karst terrains. *International Journal of Speleology* 25(3-4): 145–156.

Klimchouk, A. B. and D. C. Ford (2000). Types of karst and evolution of hydrogeologic settings. In Klimchouk, A. B., D. C. Ford, A. N. Palmer, and W. Dreybrodt, editors, *Speleogenesis - evolution of karst aquifers*, pp. 45–53. National Speleological Society, Huntsville.

Krauskopf, K. B. (1982). *Introduction to geochemistry*. McGraw-Hill, Singapore, second edition.

Krešić, N. (1997). *Hydrogeology and groundwater modeling*. CRC Press, Boca Raton.

Lamont-Black, J., P. L. Younger, R. A. Forth, A. H. Cooper, and J. P. Bonniface (1999). Hydrogeological monitoring strategies for investigating subsidence problems potentially attributable to gypsum karstification. In Beck, B. F., A. J. Pettit, and J. G. Herring, editors, *Hydrogeology and Engineering Geology of Sinkholes and Karst*, pp. 141–148. Balkema, Rotterdam.

Lauritzen, S.-E., N. Odling, and J. Petersen (1992). Modelling the evolution of channel networks in carbonate rocks. In Hudson, J. A., editor, *ISRM Symposium, Eurock92*, pp. 57–62. Thomas Telford, London.

Lebedev, A. L. and A. V. Lekhov (1990). Dissolution kinetics of natural gypsum in water at 5-25 °C. *Geochemistry International* 27: 85–94.

Liedl, R., S. Renner, and M. Sauter (1998). Obtaining information about fracture geometry from heat flow data in karst systems. *Bulletin d'Hydrogéologie* 16: 143–153.

Liedl, R. and M. Sauter (1998). Modelling of aquifer genesis and heat transport in karst systems. *Bulletin d'Hydrogéologie* 16: 185–200.

Liedl, R. and M. Sauter (2000). Charakterisierung von Karstgrundwasserleitern durch Simulation der Aquifergenese und des Wärmetransports. *Grundwasser* 1: 9–16.

Liersch, K. M. (1987). Zur Wasserbilanz der Rhumequelle und ihres Einzugsgebiete, des Pöhlder Beckens. *Neues Archiv für Niedersachsen* 36(3): 293–305.

Liu, S. T. and G. H. Nancollas (1971). The kinetics of dissolution of calcium sulphate dihydrate. *J. Inorg. Nucl. Chem.* 33: 2295–2311.

Liu, Z. and W. Dreybrodt (1997). Dissolution kinetics of calcium carbonate minerals in H_2O-CO_2 solutions in turbulent flow: The role of the diffusion boundary layer and the slow reaction $H_2O + CO_2 = H^+ + HCO^{3-}$. *Geochimica et Cosmochimica Acta* 61: 2879–2889.

Lowe, D. J. (1992). A historical review of concepts of speleogenesis. *Cave Science* 19(3): 63–90.

Lowe, D. J. (2000). Development of speleogenetic ideas in the 20th century - the early modern approach. In Klimchouk, A. B., D. C. Ford, A. N. Palmer, and W. Dreybrodt, editors, *Speleogenesis - evolution of karst aquifers*, pp. 30–38. National Speleological Society, Huntsville.

Maloszewski, P., P. Harum, and R. Benischke (1992). Mathematical modeling of tracer experiments in the karst of Lurbach System. *Steirische Beiträge zur Hydrogeologie* 43: 116–136.

Marsh, A. (1999). Material properties. The Fridge - Architectural Science Lab, School of Architecture and Fine Arts, University of Western Australia - Online Information and Course Notes (http://fridge.arch.uwa.edu.au/materials/MaterialProperties.html). Website visited on March 9, 2000.

Martel, E. A. (1921). *Nouveau traité des eaux souterraines.* Delagrave, Paris.

McDonald, M. G. and A. W. Harbaugh (1988). *A modular three-dimensional finite-difference groundwater model*, Vol. 83-875 of *USGS Open-File Report.* USGS.

Moreno, L., I. Neretnieks, and T. Eriksen (1985). Analysis of some laboratory tracer runs in natural fractures. *Water Resources Research* 19(2): 951–958.

Münzing, K. (1980). Hydrogeologisches Gutachten zu Färbeversuchen im Gebiet des Urenbrunnens auf Gemarkung Vöhringen, Lkr. Rottweil (TK 25, Blätter 7617 Sulz am Neckar und 7618 Haigerloch). Unpublished report of the Geological Survey of Baden-Wuerttemberg (Geologisches Landesamt Baden-Württemberg).

Neretnieks, I. (1983). A note on fracture flow dispersion mechanisms in the ground. *Water Resources Research* 19(2): 364–370.

Opdyke, B. N., G. Gust, and J. R. Ledwell (1997). Mass transfer from smooth alabaster surfaces in turbulent flows. *Geophys. Res. Lett.* 14: 1131–1134.

Padilla, A., A. Pulido-Bosch, and A. Mangin (1994). Relative importance of baseflow and quickflow from hydrographs of karst spring. *Ground Water* 32(2): 267–277.

Palmer, A. N. (1988). Solutional enlargement of openings in the vicinity of hydraulic structures in karst regions. Paper presented at 2nd Conference on Environmental Problems in Karst Terranes and Their Solutions, Assoc. of Groundwater Sci. and Eng., Nashville, Tenn., Nov. 16-18,1988.

Palmer, A. N. (1991). Origin and morphology of limestone caves. *Geological Society of America Bulletin* 103: 1–21.

Palmer, A. N. (1998). Modelling the evolution and morphology of limestone caves. *Bulletin d'Hydrogéologie* 16: 157–166.

Palmer, A. N. (2000). Hydrogeologic control of cave patterns. In Klimchouk, A. B., D. C. Ford, A. N. Palmer, and W. Dreybrodt, editors, *Speleogenesis - evolution of karst aquifers*, pp. 77–90. National Speleological Society, Huntsville.

Parkhurst, D. L. (1995). *User's guide to PHREEQC - a computer program for specification reaction-path, advective-transport, and inverse geochemical calculations*, Vol. 95-4227 of *Water-Resources Investigations Report.* USGS, Lakewood, Colorado.

Press, W. H., B. P. Flannery, S. A. Teukolsky, and W. T. Vetterling (1986). *Numerical recipes.* Cambridge University Press, New York.

Qingchun, Y., S. Jifang, W. Junwei, and O. Yuzo (1999). Some investigations on early organization of karst system. *Journal of China Univerity of Geosciences* 10(4): 314–321.

Raines, M. A. and T. A. Dewers (1997). Mixed transport/reaction control of gypsum dissolution kinetics in aqueous solutions and initiation of gypsum karst. *Chemical Geology* 140(1-2): 29–48.

Raven, K. G., K. S. Novakowski, and P. A. Lapcevic (1988). Interpretation of field tracer tests of a single fracture using a transient solute storage model. *Water Resources Research* 24(12): 2019–2032.

Reichel, T. (1989). Hydrogeologische und hydrochemische Untersuchungen in einem Gipskeupergebiet im Vorland der Südwest-Alb. Diplom thesis, Institut für Geologie und Paläontologie, Eberhard-Karls-Universität Tübingen.

Renger, M., O. Strebel, and W. Giesel (1974). Beurteilung bodenkundlicher, kulturtechnischer und hydrologischer Fragen mit Hilfe von klimatischer Wasserbilanz und bodenphysikalischen Kennwerten. *Z. Kulturtechn. Flurberein.* 15: 148–160, 206–221, 263–271, 353–366.

Renner, S. (1996). *Wärmetransport in Einzelklüften und Kluftaquiferen - Untersuchungen und Modellrechnungen am Beispiel eines Karstaquifers*, Vol. 30 of *Tübinger Geowissenschaftliche Arbeiten, Reihe C.* Institut und Museum für Geologie und Paläontologie der Universität Tübingen, Tübingen.

Renner, S. and M. Sauter (1997). Heat as a natural tracer: Characterisation of a conduit network in a karst aquifer using temperature measurements of spring water. In Günay, G. and A. I. Johnson, editors, *Karst waters and environmental impacts*, pp. 423–429. Balkema, Rotterdam.

Sauter, M. (1992). *Quantification and forecasting of regional groundwater flow and transport in a karst aquifer (Gallusquelle, Malm, SW. Germany)*, Vol. 13 of *Tübinger Geowissenschaftliche Arbeiten, Reihe C.* Institut und Museum für Geologie und Paläontologie der Universität Tübingen, Tübingen.

Sauter, M. and R. Liedl (2000). Modeling karst aquifer genesis using a coupled continuum-pipe flow model. In Klimchouk, A. B., D. C. Ford, A. N. Palmer, and W. Dreybrodt, editors, *Speleogenesis - evolution of karst aquifers*, pp. 212–219. National Speleological Society, Huntsville.

Shuster, E. T. and W. B. White (1971). Seasonal fluctations in the chemistry of limestone springs: a possible means for characterizing carbonate aquifers. *Journal of Hydrology* 14: 93–128.

Siemers, J. (1998). *Simulation von Karst-Aquiferen - Eine numerische Untersuchung zur Bildung von zweidimensionalen Höhlensystemen durch Verkarstungsprozesse*, Vol. 30 of *Abhandlungen zur Karst- und Höhlenkunde.* Verband der deutschen Höhlen- und Karstforscher, München.

Siemers, J. and W. Dreybrodt (1998). Early development of karst aquifers on percolation networks of fractures in limestone. *Water Resources Research* 34(3): 409–419.

Singhal, B. B. S. and R. P. Gupta (1999). *Applied hydrogeology of fractured rocks.* Kluwer Academic Publishers, Dordrecht.

Skelland, A. H. P. (1974). *Diffusional mass transfer.* Wiley, New York.

Stehfest, H. (1970). Numerical inversion of Laplace transforms. *Communications of the ACM* 1: 47–49.

Ströbel, W. (1973). Der Grundgips im Raum Stuttgart als Modell für Gipsauslaugung und Bildung von Erdfällen. In *Proceedings of a symposium on sinkholes and subsidence, Hannover*, pp. T1–G 1–8. Deutsche Gesellschaft für Erd- und Grundbau.

Svensson, U. and W. Dreybrodt (1992). Dissolution kinetics of natural calcite minerals in CO_2-water systems approaching calcite equilibrium. *Chemical Geology* 100: 129–145.

Taylor, G. I. (1953). Dispersion of soluble matter in solvent flowing slowly through a pipe. *Proceedings of the Royal Society of London, Series A* 219: 186–203.

Taylor, G. I. (1954). The dispersion of matter in turbulent flow through a pipe. *Proceedings of the Royal Society of London, Series A* 223: 446–468.

Teutsch, G. (1988). Grundwassermodelle im Karst: Praktische Ansätze am Beispiel zweier Einzugsgebiete im Tiefen und Seichten Malmkarst der Schwäbischen Alb. Ph.D. diss., Eberhard-Karls-Universität Tübingen, Tübingen.

Ufrecht, W. (1998). Hydrogeologisches System-Modell Stuttgart. Report of the Environmental Department of the City of Stuttgart (Amt für Umweltschutz, Landeshauptstadt Stuttgart).

Vierneisel, B. (2000). Lösungskinetik von Gips in durchströmten Röhren. Diplom thesis, Institut für Geologie und Paläontologie, Eberhard-Karls-Universität Tübingen.

Weast, R. C., editor (1979). *CRC handbook of chemistry and physics - A ready-reference book of chemical and physical data.* CRC Press, Boca Raton, 60^{th} edition.

Werner, A., H. Hötzl, and W. Käss (1997). The interpretation of a high water tracer test in the Danube-Aach-system (Western Swabian Alb, Germany). In *Proceedings of the 12^{th} International Congress of Speleology, La Chaux-de-Fonds, Switzerland, Volume 2*, pp. 187–190.

Werner, A., H. Hötzl, W. Käss, and P. Maloszewski (1998). Evaluation of a tracer test in the Danube-Aach-System Western Swabian Alb, Germany. *Bulletin d'Hydrogéologie* 16: 111–122.

Whitaker, S. (1977). *Fundamental principles of heat transfer*. Pergamon Press, New York.

White, W. B. (1969). Conceptual models for carbonate aquifers. *Ground Water* 7(3): 15–21.

White, W. B. (1988). *Geomorphology and hydrology of karst terrains*. Oxford University Press, New York.

Wigley, T. M. L. (1973). Chemical evolution of the system calcite-gypsum-water. *Canadian Journal of Earth Sciences* 10: 306–315.

Williams, P. W. (1983). The role of the subcutaneous zone in karst hydrology. *Journal of Hydrology* 61: 45–67.

Wittke, W. and H. Hermening (1997). Grouting of cavernous gypsum rock underneath the foundation of the weir, locks and powerhouse at Hessigheim on the river Neckar. In *Dix-neuvièm Congrès des Grand Barrages, Florence, 1997*, pp. 613–626. Commission Internationale des Grands Barrages.

Wollrath, J. and R. Helmig (1992). *Strömungsmodell für inkompressible Fluide: ROCKFLOW, Version 2*. Institut für Strömungsmechanik und elektronisches Rechnen im Bauwesen, Universität Hannover.

Appendix A

Stage-discharge relation

The stage-discharge relation shown in Fig. A.1 is based on discharge measured in the period from September, 1999 to September, 2000 using a flow meter (Ott). Corresponding spring water levels were recorded by an automatic data logger (Phytec Prodata).

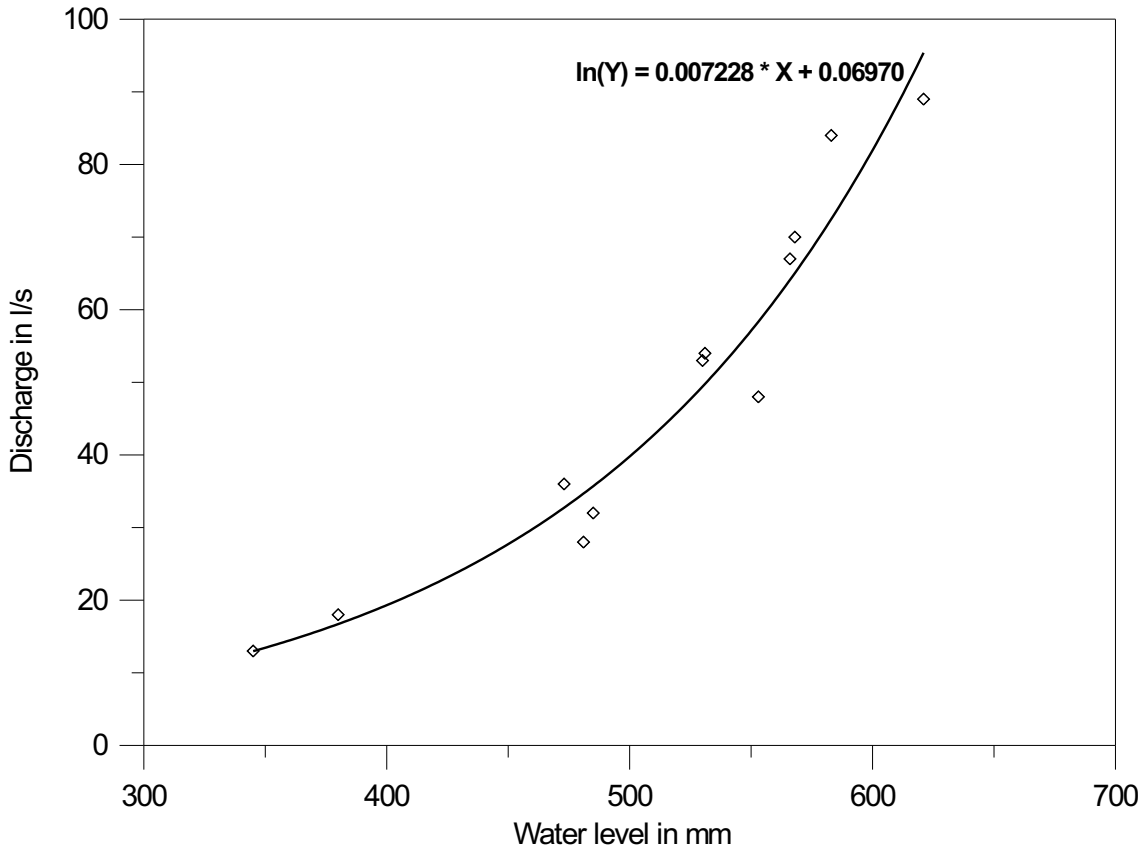

Figure A.1: Stage-discharge relation for the *Urenbrunnen* spring.

Appendix B

Solute content of spring water

Table B.1: Solute content of water samples taken from the *Urenbrunnen* spring. Hydrochemical analysis were conducted at the Center for Applied Geoscience, University of Tübingen, by Renate Riehle (cations, using AAS) and Anne Hartmann-Renz (anions, using Ionchromatography).

Date	Calcium	Magnesium	Sodium	Potassium	Sulfate	Chloride	Nitrate
	mol m^{-3}	mol m^{-3}	mol m^{-3}	mol m^{-3}	mol m^{-3}	mol m^{-3}	mol m^{-3}
04/30/99	18.5	3.3	3.0	0.24	14.3	2.0	0.30
06/11/99	13.9	3.3	3.6	0.26	14.6	2.0	0.28
07/09/99	13.4	3.5	3.5	0.27	14.9	2.0	0.26
07/30/99	12.5	3.5	4.0	0.29	15.1	2.2	0.28
09/17/99	13.1	3.7	4.1	0.28	15.2	2.0	0.25
09/28/99	13.6	3.7	3.9	0.29	15.3	2.0	0.24
10/20/99	17.3	3.9	3.8	0.29	15.1	1.9	0.25
11/10/99	13.5	3.7	4.0	0.30	15.3	2.1	0.26
12/08/99	13.6	3.7	4.5	0.28	14.9	2.8	0.27
12/21/99	12.0	3.1	3.6	0.27	14.1	2.1	0.32
01/12/00	12.9	3.3	3.6	0.21	14.4	2.3	0.31
01/26/00	13.3	3.5	3.4	0.24	14.4	2.4	0.31
02/09/00	12.6	3.5	3.6	0.23	14.2	2.1	0.31
02/23/00	13.6	3.3	3.4	0.22	14.2	1.9	0.30
03/22/00	13.4	3.5	3.0	0.22	13.5	2.0	0.32
04/10/00	13.1	3.3	2.8	0.22	13.9	1.9	0.29
05/08/00	12.9	3.5	2.8	0.23	14.4	1.8	0.28
05/22/00	13.9	3.5	2.7	0.23	13.9	1.6	0.27
06/05/00	14.4	3.3	2.5	0.23	14.5	1.3	0.26
06/07/00	14.8	3.3	3.0	0.24	14.5	1.6	0.28

Appendix C

Correlation of sulfate concentration and electrical conductivity

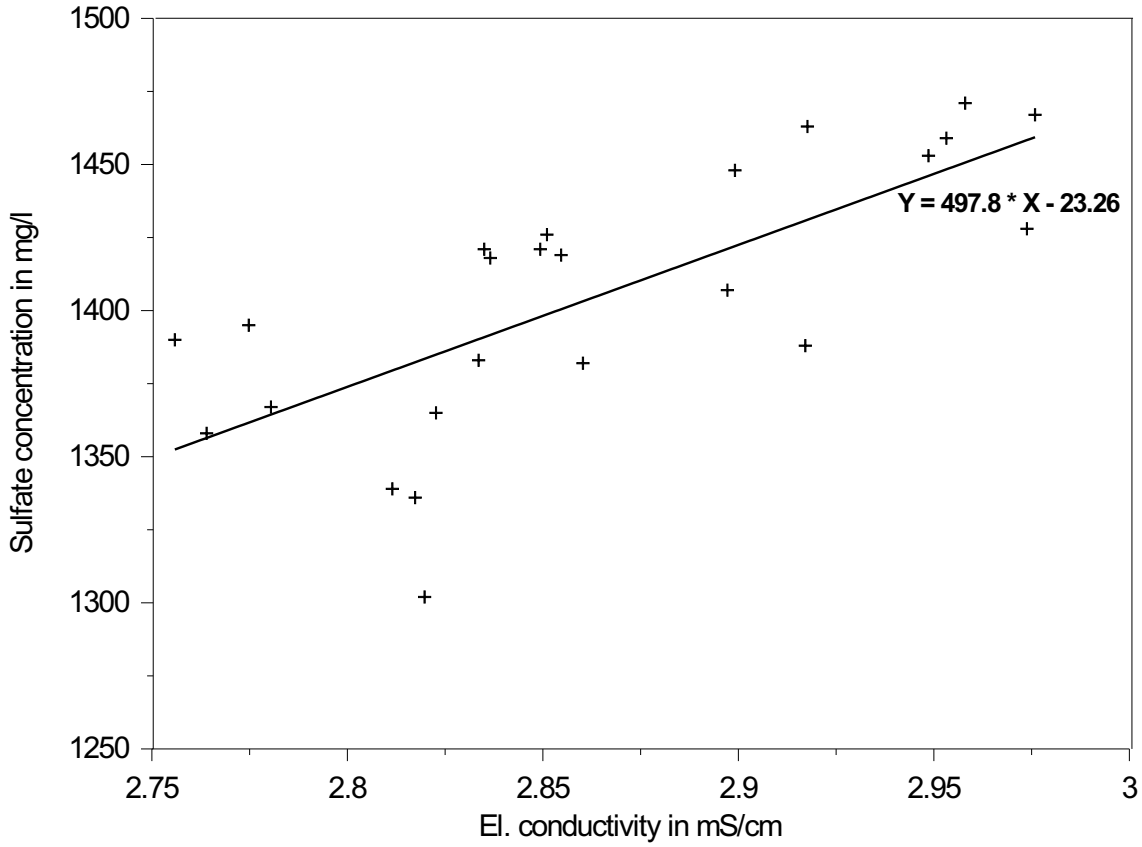

Figure C.1: Correlation of sulfate concentration and electrical conductivity at the *Urenbrunnen* spring.

Appendix D

Calibrated time distribution of recharge into fissured system

Table D.1: Calibrated time distribution of recharge into the fissured system for the event on May 30/31, 2000 at the field site Vöhringen, Southern Germany. Recharge was distributed uniformly in space over the whole model domain. For the simulation of short-term flow and transport on the field site four different model set-ups were used as described in section 5.3. (CEST = Central European Summer Time; dates refer to the day, on which the period starts.)

Date	Time	Recharge into fissured system			
	CEST	$[10^{-9}$ m $s^{-1}]$			
		Model 1	Model 2	Model 3	Model 4
05/30/2000	12:00-19:00	10	10	10	10
05/30/2000	19:00-1:00	150	150	80	100
05/31/2000	1:00-2:00	400	400	250	400
05/31/2000	2:00-3:00	800	800	750	400
05/31/2000	3:00-4:00	600	600	600	400
05/31/2000	4:00-5:00	400	400	400	400
05/31/2000	5:00-6:00	200	200	340	400
05/31/2000	6:00-7:00	150	150	310	400
05/31/2000	7:00-8:00	100	100	290	350
05/31/2000	8:00-9:00	80	80	280	350
05/31/2000	9:00-10:00	60	60	270	300
05/31/2000	10:00-11:00	60	60	180	300
05/31/2000	11:00-12:00	60	60	90	300
05/31/2000	12:00-13:00	35	35	90	250
05/31/2000	13:00-14:00	35	35	90	150
05/31/2000	14:00-15:00	35	35	90	80
05/31/2000	15:00-16:00	35	35	90	40
05/31/2000	16:00-17:00	35	35	90	40
05/31/2000	17:00-18:00	35	35	90	30
05/31/2000	18:00-19:00	35	35	90	30
05/31/2000	19:00-20:00	35	35	90	30
05/31/2000	20:00-12:00	35	35	50	30